Australian Government
Bureau of Meteorology

The Centre for Australian Weather and Climate Research
A partnership between CSIRO and the Bureau of Meteorology

CSIRO

Atmospheric Stability Environments and Fire Weather in Australia – extending the Haines Index

Graham A. Mills and Lachlan McCaw

CAWCR Technical report No. 20

March 2010

www.cawcr.gov.au

Atmospheric Stability Environments and Fire Weather in Australia – extending the Haines Index

Graham A. Mills [1,2] and Lachlan McCaw [2,3]

[1] *Centre for Australian Weather and Climate Research*
[2] *Bushfire Cooperative Research Centre*
[3] *Department of Environment and Conservation, Manjimup. Western Australia*

CAWCR Technical Report No. 020

March 2010

ISSN: 1835-9884

National Library of Australia Cataloguing-in-Publication entry

Title: Atmospheric Stability Environments and Fire Weather in Australia – extending the Haines Index [electronic resource] / Graham A. Mills and Lachlan McCaw.

ISBN: 978-1-921605-550

Series: CAWCR technical report ; 20.

Enquiries should be addressed to:
Dr Graham A. Mills
Centre for Australian Weather and Climate Research:
A partnership between the Bureau of Meteorology and CSIRO
GPO Box 1289, Melbourne
Victoria 3001, Australia

G.Mills@bom.gov.au

Copyright and Disclaimer

All images reproduced in greyscale. A colour version of CAWCR Technical Report No.020 is available online: http://www.cawcr.gov.au.

Contents

ABSTRACT

The characteristics of the Haines Index, used to link vertical atmospheric stability and humidity with erratic fire behaviour, are examined for locations covering the majority of the areas of southern Australia that are subject to bushfires. It is shown that the index, originally developed for conditions in the north-west of the United States, is not configured to identify the most extreme conditions in Australia due to the different temperature lapse and humidity climatology of the two continents. An alternative extended version of the index is proposed, and along with a number of other measures of atmospheric stability, is compared with the fire danger index on a number of days of extreme or unexpected fire activity, and also for a number of days on which marked pyrocumulus cloud development was noted. While more quantitative comparison with fire behaviour data is required, the results suggest that the use of this extended Haines Index, C-HAINES, may provide additional and independent information to that provided by the traditional fire danger indices, particularly in conditions where unexpected night-time flare-ups of going fires have occurred, as well as in a number of cases of prescribed burns where fire behaviour was unexpectedly active. A number of case studies are presented in Appendix 2.

1 INTRODUCTION

It has long been believed amongst fire behaviourists that low- to mid-tropospheric atmospheric instability affects fire behaviour. The simplest conceptual model of this hypothesis is the "plume dominated" fire, where, in low wind conditions, a less stable atmosphere allows a deep convective column to develop, with the stronger updrafts in this column leading to stronger low-level inflow to the fire providing a positive feedback to fire activity (Byram 1954,1959, Luke and McArthur 1978, Rothermel 1991). Rothermel (1991) also proposed that pyrocumulus clouds, more likely in an unstable atmosphere, can lead to abrupt changes in fire behaviour due to downbursts triggered by evaporation of precipitation from those clouds, while other authors have proposed more direct circulation linkages between pyrocumulus clouds and fire behaviour (eg Tolhurst and Chatto 1999). In the most extreme circumstances pyrocumulus clouds can even trigger tornadoes (Cunningham and Reeder 2009). Pyrocumulus clouds can also form in the smoke columns downstream of a wildfire, and lightning from these storms trigger further fire ignitions.

Other studies have suggested that a deeply unstable lower troposphere may affect fire behaviour through the mixing of high momentum and/or low humidity air from the mid-troposphere to the surface, (e.g. Mills 2005, 2008a,b, Zimet et al. 2007, Kaplan et al. 2008). Other stability effects that may impact on fire behaviour or occurrence are increased spotting (lofting of firebrands downwind) distances (Ellis 2003), and the chance of local intense fire-induced vortices developing. Most of these effects are not, at least explicitly, encapsulated in the standard fire danger indices that are used in operational practice, such as the Australian McArthur Forest/Grassland Fire Danger Indices (FFDI/GFDI, Luke and McArthur 1978), the United States Forest Fire Danger Rating System (Deeming et al. 1977) or the Canadian Fire Weather Index (deGroot et al. 2005), as all these combine measures of antecedent rainfall and observations or forecasts of near-surface wind speed, temperature, and humidity data to estimate fire danger for fires that are primarily wind-driven.

The desire to provide some quantitative indication of the effects of atmospheric stability on fire behaviour led Haines (1988) to develop the Haines Index (HI): this has integer values from two to six, with six representing the most severe conditions. In Haines' data set the HI took a value of six on only around five percent of occasions, and thus a value of six did indicate unusual conditions. The inputs to the HI comprise two components, one representing lower-tropospheric humidity and one representing low-to-mid tropospheric lapse rate. While developed on a limited data set based in the United States, the HI is widely applied, and a number of studies in the United States (e.g. Werth and Ochoa 1993, Saltenberger and Barker 1993, Potter and Goodrick 2003, Goodrick 2003) have shown some positive correlation of the HI with fire behaviour/area burnt. Bally (1995) showed that a large proportion of fire activity in Tasmania occurs on days with a Haines Index $\geq$5, and that this provides information independent of and complementary to the FFDI. In Tasmania the HI is used in combination with the FFDI in determining the need to issue a fire weather warning (Bureau of Meteorology 2008a).

Other studies, though, (Werth and Werth 1998, Long 2006, and McCaw et al. 2007) indicate that the HI does not provide sufficient discrimination of exceptional days in regions with typically hot, dry Mediterranean or arid climates. In such climates, which include large parts of Southern Australia, a large proportion of days during the fire seasons have HI $\geq$5, and thus this index does not discriminate days on which exceptional fire danger due to atmospheric instability might occur. These varied results suggest that while the HI may be a useful adjunct to

fire weather forecasting in some regions, it is less useful in others as it "saturates", with a large proportion of high-range environments.

There have been a number of discussion papers attempting to improve understanding of the HI, and to diagnose reasons for its greater or lesser utility in different areas. Potter et al. (2002) discussed the relationship between the choice of levels for components of the HI and the depth of the mixed layer, and argued that there was no unique choice for all conditions, although he did suggest that the "Haines layer" should include the entrainment layer that lies above the mixed layer. Potter (2002, 2005) presented dynamically-based arguments to propose some stability indicators that were argued to have a stronger physical basis than the HI, although the relationship between these indicators and fire activity is as yet un-documented. Jenkins (2002, 2004) conducted some idealised numerical experiments to analyse the relationship between modelled fire activity and lower atmospheric stability, and one conclusion of that study, in common with Potter et al. (2002), was that the HI may benefit from some refinement.

In this paper the climatology of the HI over Southern Australia is analysed in terms of the climate of its lapse rate and humidity ingredients. Based on this analysis, a modification to the HI that increases the discrimination of extreme conditions for a given location is proposed, and other potential diagnostic indicators of atmospheric stability effects on fire behaviour are discussed. Using six-hourly NWP model data, an eight-year climatology of these diagnostic quantities has been generated. These values are compared for a number of events over Australia for which fire agencies have reported unexpectedly or unusually active fire behaviour, and for a number of events during which large pyrocumulus clouds have been observed, this being a superficial indicator of deep vertical circulations associated with the fire. These statistical analyses are complemented by a summary of the main points from a number of case studies, which are presented in more detail in Appendix 2. Finally, the potential usefulness of these diagnostic forecast products and the means by which such products might be incorporated into fire weather forecast practice will be discussed.

2 DATA

2.1 FIRE EVENTS

When relating atmospheric parameters to fire behaviour there is always the problem of determining the particular influence of the atmospheric parameters of the day on that fire, given that vegetation (fuel) characteristics, topography, and mitigation efforts all have significant effect on the net fire activity or area burnt, and that a controlled field experiment changing atmospheric parameters is impossible. Further, atmospheric conditions may be conducive to extreme fire behaviour but if there is no ignition on that day, there is no fire activity. In this study events have been compiled from a variety of sources to assess the association between extrema of the various stability measures calculated and fire activity. Some of these are wildfire or prescribed fire events where unusual fire activity has been noted, either anecdotally or in a documented sense, and where speculations about stability effects on the behaviour of that fire have been made. Others are days during recent major fire events when active convective development has been observed in association with extreme fire behaviour. These events are listed in Table 1, with a very brief description of the location and characteristics of the event, and an acknowledgement of the source of the information

Table 1 - Fire activity events.

EVENT	Critical Dates	Comments	Reference/Source	Seq. No / Case Study
Berringa Fire	25 Feb 1995	Major fire spread after weak wind change, with large pyrocumulus cloud	Tolhurst and Chatto 1999	25 Y
Denbarker Block	12 Dec 2002	Major wind-driven fire run on 13 December	McCaw, personal communication	46 Y
Big Desert Fire	17 Dec 2002 18 Dec 2002 19 Dec 2002 20 Dec 2002 21 Dec 2002	Lightning ignition in north-west Victoria Large area burnt Large area burnt Large area burnt Large area burnt	http://www.dse.vic.gov.au	39a Y 39b Y 39c Y 39d Y 39e Y
Lake Tay fire	10 Feb 2003	Lightning ignition 100km north of Ravensthorpe. Major fire run on 10 Feb, with ~ 150000ha burnt that day.	McCaw, personal communication	47 Y
Wangary fire	10 Jan 2005 11 Jan 2005	Ignition Major fire run	Bureau of Meteorology (2005)	31a 31b
Pickering Brook (Darling Ranges) fire	17 Jan 2005	Massive pyrocumulus cloud afternoon 17 Jan	Cheney (2009)	12 Y
Bluegum Plantation	23 Mar 2005	Unusually active fire behaviour in bluegum plantation	McCaw and Smith (2008)	32 Y
Randall Block (Perth Hills)	15 Oct 2005	Unusually active fire behaviour in Darling Ranges	McCaw, personal communication	36 Y
Hovea fire	17 Dec 2005	Unexpected crown scorching in prescribed burn	Chandler (2005)	38 Y
Murray-Sunset NP	19 Sep 2006	273 fires started by lightning, massive pyrocumulus	Smith (2007)	40/15 Y
Grose Valley Fires	20 Nov 2006 21 Nov 2006 22 Nov 2006	Major fire activity and pyrocumulus development Major fire activity and pyrocumulus development Major fire activity	www.rfs.nsw.gov.au – (major fire updates) www.blackheathweather.com	51b 51c 51d
Little Desert Fires	20 Nov 2006	10800 ha burnt	Smith (2007)	41 Y
Casterton Complex	21 Nov 2006	12500 ha burnt	Smith (2007)	42 Y
Billo Road Fire Mt David Fire	10 Dec 2006 11 Dec 2006 19 Dec 2006	Unexpectedly active fire behaviour in pine plantation	Cruz and Plucinski (2007)	33 Y 34 Y 35 Y
Eastern Victorian fires 2006-2007	10 Dec 2006 14 Dec 2006 11 Jan 2007	Tawonga Gap fire run (33500 ha) Coopers Creek fire day Tatong (33000 ha)	Smith (2007) Smith (2007), Smith (2007)	44 Y 44a Y 45 Y
Scamander/St Mary's fire	10 Dec 2006 11 Dec 2006 14 Dec 2006	Fire ignition Major fire run and house loss (Scamander) Major fire run and house loss (Four Mile Creek)	Tasmania Fire Service (2007)	61a Y 61b Y 61c Y
Boorabbin	30 Dec 2007	Major fire runs before and after wind change	Bureau of Meteorology (2008b)	50

Table 2. Pyrocumulus events. Highlighted events are also included in the fire activity events listed in Table 1.

EVENT	Critical Dates	Comments	Reference/Source	Seq. No
Berringa Fire	25 Feb 1995	Major fire spread after weak wind change, with large pyrocumulus cloud	Tolhurst and Chatto 1999	25
Upper South-east SA	2 Jan 2001	Pyrocumulus	http://au.geocities.com/auswxchaser/2Dec01	1
Dundas Nature Reserve	18 Jan 2001	Pyrocumulus and particulate transport into statosphere	A. Tupper/ M.Fromm (personal communication)	2
Richmond, NSW	22 Sep 2001	Pyrocumulus	http://australiasevereweather.com/gallery2/v/pyrocumulus	3
Woodburn, NSW	22 Dec 2001	Pyrocumulus	http://australiasevereweather.com/gallery2/v/pyrocumulus	4
Castlereagh, NSW	25 Dec 2001	Pyrocumulus	http://australiasevereweather.com/gallery2/v/pyrocumulus	5
Rooty Hill, NSW	5 Dec 2002	Pyrocumulus	http://australiasevereweather.com/gallery2/v/pyrocumulus	6
Canberra	17 Jan 2003	Pyrocumulus and aerosol injection to statosphere	R. McRae/M. Fromm personal communication	8a
Canberra	18 Jan 2003	Canberra fire day	Fromm et al. (2006)	8
Eastern Vic	30 Jan 2003	Alpine fires breakout day – pyrocumulus development on smoke plume	Bureau of Meteorology (2003)	9
NE Vic	24 Feb 2003	Cumulus development on smoke plumes from prescribed burns	DSE photo / A.Wain personal communication	10
Dorrigo, NSW	1 Dec 2004	Huge pyrocumulus	http://downunderchase.com/stormchasing04-05/01_12_04ac.html	11
Pickering Brook	17 Jan 2005	Massive pyrocumulus on afternoon of 17 Jan	Cheney (2009)/Bureau Weather Calendar Dec 2006)	12
South-east WA	5 Feb 2005	Pyrocumulus development/stratospheric particulate injection	M. Fromm (personal communication)	
Brisbane Ranges	22 Jan 2006	Convection/lightning ignition on smoke plume from Brisbane Ranges fire	ABC (2006) – “Bushfire Summer”	14
Murrayville, VIC	19 Sep 2006	Pyrocumulus above lightning ignited fires	Bureau of Meteorology Library VCMB fires055a	40/15
Blackheath NSW	21 Nov 2006	Pyrocumulus above Grose Valley fires	www.blackheathweather.com/generalphotos.html	51c
Blackheath NSW	22 Nov 2006	Pyrocumulus above Grose Valley fires	www.blackheathweather.com/generalphotos.html (also R. McCrae / M. Fromm personal communication)	51d
Pilliga forest NSW	29 Nov 2006	Pyrocumulus	http://narrabriweather.net/events/PilligaNov06.html	18
Eastern Vic	14 Dec 2006	Pyrocumulus	A. Tupper (personal communication)	19
Pilliga forest NSW	15 Dec 2006	Pyrocumulus	http://narrabriweather.net/events/PilligaNov06.html	20
Buchan, Vic	6 Jan 2007	Pyrocumulus	Bureau of Meteorology Library VCMB 08february	21
Yarrangobilly	6 Feb 2007		R. McRae/A.Tupper (personal communication)	22
Tanami Desert	13 Sep 2007		http://australiabushfiremonitor.blogspot.com/2007/09/tanami-derert-flareup.html	23
Bribie Island	22 May 2007	Pyrocumulus above prescribed burn	http://www.schools.ash.org.au/paa2/mediagallery	24

One easily perceptible association of atmospheric instability and a fire is the development of a pyrocumulus cloud over the fire. While there is no requirement that the atmosphere has affected the fire behaviour in order for such a pyrocumulus cloud to develop, there is at least the joint requirement that the atmosphere be sufficiently unstable that the development of a convective cloud can be supported, and also that the fire is sufficiently active that the heat, and perhaps more importantly the moisture (Potter 2005), release from that fire modify the environmental conditions sufficiently to allow the development of the pyrocumulus cloud. Some of these events were brought to the authors' attention via email discussions, two from their documentation (the Berringa fire: Tolhurst and Chatto 1999, and the Canberra fire: Fromm et al. 2006)), and a number by searching the web for "pyrocumulus". These events are listed in Table 2, together with fire location, brief comment, and attribution.

Some of these events are not mutually exclusive, in that, for example, on some days lightning ignitions occur from pyrocumulus that develop in the smoke plume downstream from an existing active fire, as occurred in Victoria on 30 January 2003 and 22 January 2006. For other events, such as the day of the Canberra fires of 18 January 2003, several days during the Grose Valley (NSW) fires of November 2006, and several days during the north-east Victorian fires of 2006-7 there were both extreme fire behaviour and massive pyrocumulus development.

2.2 Meteorological Data

Previous analyses of the HI in Australia (Bally 1995, Long 2006, and McCaw et al. 2007) have used radiosonde data, which in Australia is available at 0000 UTC at some 30 sites, and at a lesser number of stations at 1200 UTC1. These data thus have two significant limitations when comparing with fire events – fire activity is generally greatest near the time of maximum temperature, and most bushfires (both planned and unplanned) occur at locations remote from the radiosonde location. Numerical Weather Prediction (NWP) model fields, be they forecasts or assimilated analyses, have greater time resolution and also wide spatial resolution, but can suffer from model error or inhomogeneities in the data set when changes to the NWP system take place. In this study the primary atmospheric profile data used are derived from the Australian Bureau of Meteorology's (the Bureau) operational limited area data assimilation system, LAPS (Puri et al. 1998). Since late 1999 this system has had a horizontal grid spacing of 0.375o latitude/longitude. The number of vertical levels increased from 29 to 51 on 3 May 2006, and again from 51 to 61 on 30 October 2007. These latter vertical resolution changes were accompanied by analysis changes. Most of the analyses of instability indices presented in this paper are based on the 6-hourly LAPS analyses, available at 0000, 0600, 1200 and 1800 UTC, although forecasts are used in some of the case studies (see Appendix 2) to provide greater spatial or temporal detail. Data for 8 years (2000-2007) inclusive were used, and stability indices were calculated at the 0000, 0600, 1200, and 1800 UTC analysis times every 1.5 degrees over land south of 20oS to reduce the size of the data sets. All indices described in the next section were calculated on this grid.

For the events that occurred before 2000, or for which it was thought higher spatial and temporal resolution fields might provide greater insight, slightly different approaches were taken. For events prior to 2000, the ERA40 global reanalysis data (Kallberg et al. 2005) were used as initial and boundary conditions to run LAPS model simulations of the events, while in other cases high resolution (0.05o grid spacing, hourly output) LAPS forecasts, using LAPS analyses as initial and boundary conditions, were used.

[1] UTC is 11 hours earlier than Eastern Australian Daylight Savings Time (EDST)

For comparison with events, data from the closest of these gridpoints to each fire event location were used. Contoured fields (at the full NWP model resolution) of the various stability indicators were also produced for each of the events listed in Tables 1 and 2 to subjectively assess the representativeness of conditions at the fire location at 0600 UTC. Where it was considered that highly mobile meteorological systems, such as cold fronts, made the point values unrepresentative, a nearby value was used. Having first developed the set of fire events, a wide scatter of gridpoints across southern Australia, but biased to forested areas, resulted, and after inspection a few further gridpoints were added to fill in some glaring gaps. The resulting distribution of gridpoints is shown in Fig. 1, with "location numbers" cross-referenced to the events listed in Tables 1 and 2 in Table 3.

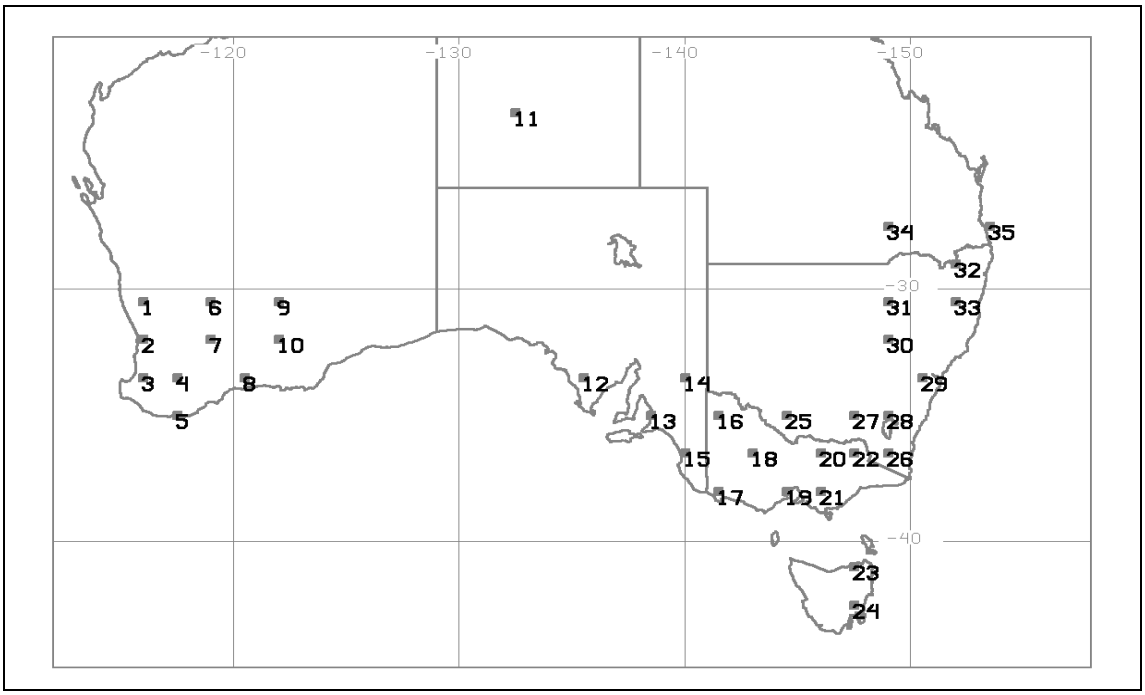

Figure 1. Map of Australia showing gridpoints for which statistical analysis of index values are calculated. Event locations can be cross-referenced using the numbers and the listings in Tables 1, 2 and 3.

3 FIRE WEATHER STABILITY INDICES – THE HAINES INDEX

In common meteorological practice, the use of stability indices is generally applied to the discrimination of thunderstorm environments. Most such indices are based on parcel theory, whereby the temperature of a parcel lifted, with no mixing with its environment, from some (lower) level to a higher level is compared with the temperature of the environment at that higher level to estimate parcel buoyancy. These indices generally incorporate low-level moisture and temperature, together with some mid-tropospheric temperature component, and assume that at some point a lifted parcel will cool to condensation, and subsequently ascend along a saturated adiabat. Indices may indicate some measure of buoyancy between two levels (e.g. the Surface Lifted Index) or provide a more integrated measure through a depth of the atmosphere (e.g. Convective Available Potential Energy, CAPE). For fire weather applications the atmosphere is usually very dry, so moist convection is less of an issue, at least until after a pyrocumulus cloud has formed.

Table 3. List of locations shown in Fig. 1, together with its location number and geographic mnemonic used in this paper

Location number (Fig. 1)	Geographic Memonic (Tables A1 and A2)	Latitude/Longitude	Event Numbers (Tables 1 and 2)
1	Dalwallinu	30.5S 116.0E	
2	Perth	32.0S 116.0E	12, 36
3	Bridgetown	33.5S 116.0E	32, 38
4	Katanning	33.5S 117.5E	
5	Mt Barker	35.0S 117.5E	46
6	Southern Cross	30.5S 119.0E	50
7	Hyden	32.0S 119.0E	
8	Ravensthorpe	33.5S 120.5E	47
9	Kalgoorlie	30.5S 122.0E	
10	Dundas NR	32.0S 122.0E	2, 13
11	Tanami	23.0S 132.5E	23
12	Cummins	33.5S 135.5E	31a, 31b
13	Mt Lofty	35.0S 138.5E	
14	Riverland	33.5S 140.0E	1
15	South-east SA	36.5S 140.0E	
16	Murraylands	35.0S 141.5E	39a-e, 40/15, 16
17	Casterton	38.0S 141.5E	
18	Horsham	36.5S 143.0E	41, 42
19	Sheoaks	38.0S 144.5E	14, 25
20	Wangaratta	36.5S 147.5E	
21	West Gippsland	38.0S 146.0E	45
22	North-east Vic	36.5S 147.5E	10, 21, 44, 44a
23	North-east Tas	41.0S 147.5E	61a,b,c
24	Hobart	42.5S 147.5E	
25	Hay	35.0S 144.5E	
26	South-east Coast	36.5S 149.0E	9
27	Wagga	35.0S 147.5E	
28	Canberra	35.0S 149.0E	8, 8a, 22, 33, 34
29	Wollemi	33.5S 150.5E	3, 4, 5, 6, 51b,c,d
30	Dubbo	32.0S 149.0E	
31	Pilliga	30.5S 149.0E	18, 19
32	Glen Innes	29.0S 152.0E	
33	Dorrigo	30.5S 152.0E	11
34	St George	27.5S 149.0E	
35	Bribie Island	27.5S 153.5E	24

3.1 The mid-level Haines Index

Haines (1988) proposed three variants of the HI, one for low elevation sites, one for medium elevations, and one for higher elevations over the United States. For each there are two components – a temperature lapse rate between a lower and an upper level, and the dewpoint depression at the lower level. Depending on specified thresholds each component contributes 1, 2 or 3 to the index. Summing these two components gives the value of the HI, which can thus range from 2 to 6, with the higher values indicating greater fire danger. Haines based his thresholds on data for two radiosonde stations over a one year period, requiring that any threshold developed should identify climatologically unusual atmospheric conditions. He found that some 51% of fires in his data set occurred when the Haines Index was 6, but the Haines Index was 6 on only some 5% of days during the fire season.

In its Australian applications the mid-level HI has been used (Bally 1995, Long 2006, McCaw et al. 2007), and the calculation of this form is summarised in Table 4. Potter et al. (2002) argued that the Haines layer should span the entrainment layer, and that the interpretation of the HI might be questioned in cases of deep mixed layers. However, given the relatively low relief of most of Australia, the high-level Haines variant is perhaps not a suitable choice for local conditions, it was decided to focus on the mid-level version in this study.

Table 4: Components of the mid-level Haines Index, following McCaw et al. (2007).

Stability Term: 850-700 hPa Temperature Difference	Stability Score	Moisture term: 850 hPa Dewpoint Depression	Moisture Score
< 6C	1	< 6C	1
6-10C	2	6-12C	2
>10C	3	>12C	3

The HI has been shown to provide very useful indications of enhanced fire activity in Tasmania (Bally 1995) and in its area of development in the north-western mountain states of the USA (Werth and Ochoa 1993). However, less discrimination of extreme days has been shown over the mainland Australian states (Long 2006, McCaw et al. 2007), although these analyses have not included a systematic comparison with fire activity data.

Figure 2a,b shows the percentage of days when, at 0600 UTC (mid afternoon in eastern Australia), the mid-level HI exceeds 5 and 6 respectively for the period September-April inclusive (the winter months have been excluded in the analysis to be presented here). If it is considered that a 5% level is needed in order for a HI=6 to identify the "unusual" events, then only the south-west of Western Australia (WA), Southern Victoria, and Tasmania approximate this frequency, while 20-30% of days reach this threshold for most of the inland stations.

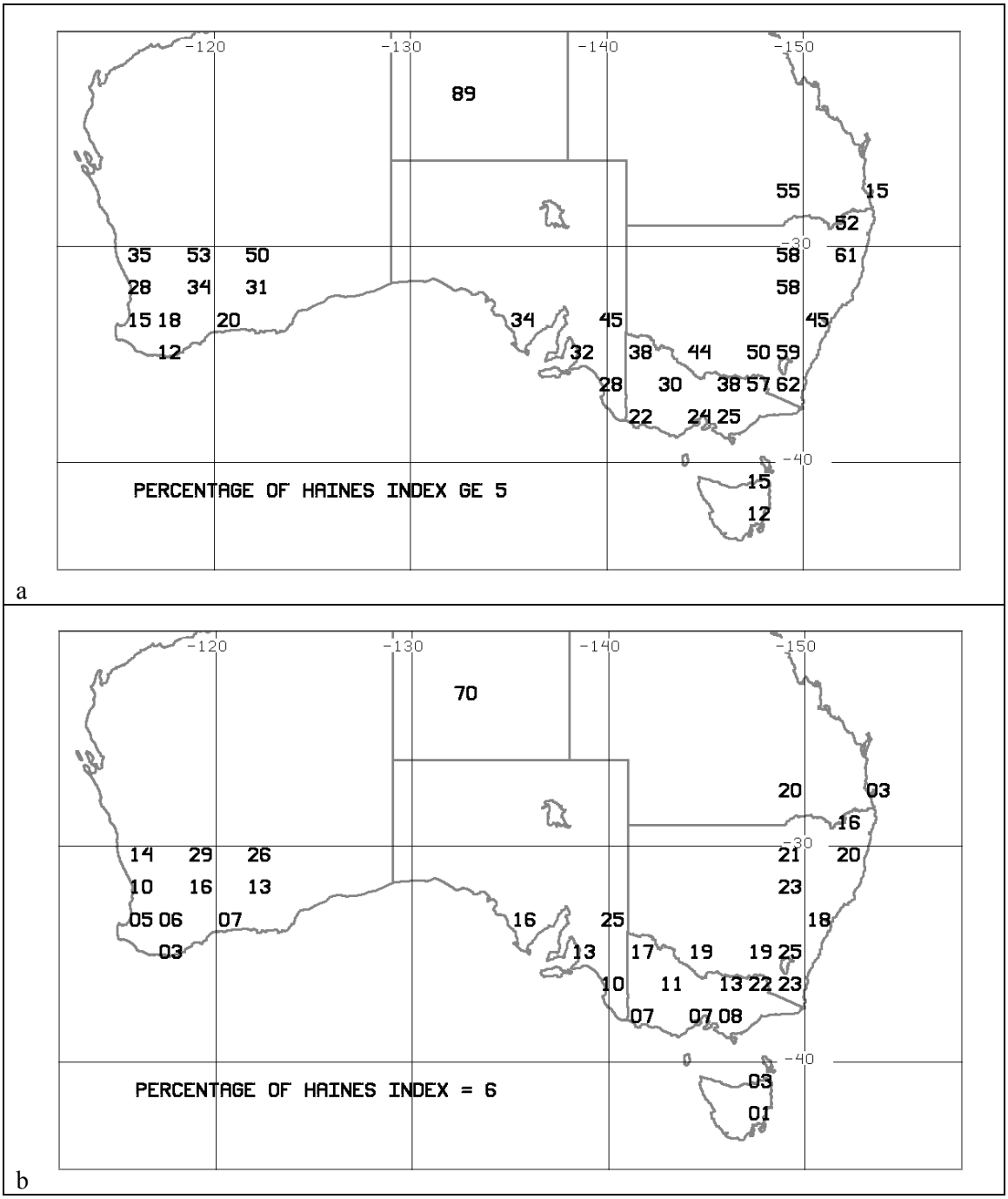

Figure 2. Percentage of days between September 1 and 30 April for the years 2000-2007 inclusive for which the mid-level Haines Index is greater or equal to 5 (upper panel), and equal to 6 (lower panel) at the selected locations.

Obviously, the climate of the HI is a function of the climate of the 850-700 hPa temperature lapse (TL) and 850 hPa dewpoint depression (DPD) ingredients that are input to the calculation. For the 850-700 hPa layer the dry-adiabatic lapse rate is of the order of 14-17C, depending on the temperature, while dewpoint depression is essentially unbounded, although highly non-linear as the mixing ratio becomes very small. Figure 3a,b shows the percentage of days (for the same 8-month period) on which TL and DPD exceed the upper Haines bounds of 10C and 12C respectively.

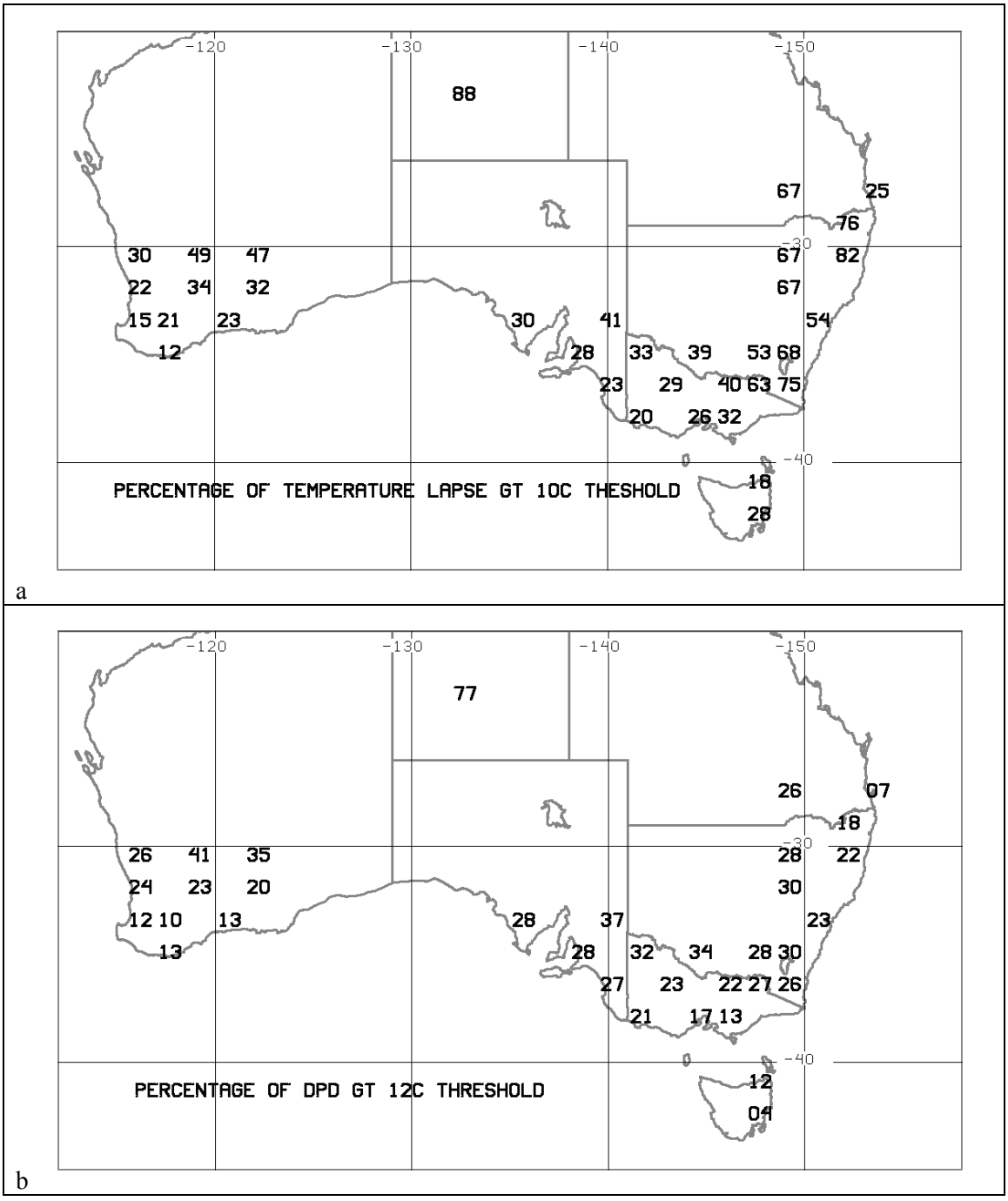

Figure 3. Percentage of days between September 1 and 30 April for the years 2000-2007 inclusive for which the 850-700 hPa temperature lapse is greater than 10C (upper panel) and for which the 850 hPa dewpoint depression is greater than 12C (lower panel) at the selected locations.

There is a strong correspondence between the percentage of HI=6 (Fig. 2) and the percentage of days exceeding the thresholds of both TL and DPD (Fig. 3). Scatterplots (Fig. 4) demonstrate the strong relationship between the percentages of HI=6 and the percentages exceeding the bounds of the lapse and humidity thresholds, with correlations of 0.74 and 0.89 respectively. Note the outlier point in both plots is that of Tanami (11) which has a strong inland desert climate, and this datum has been excluded from the regression and straight line fitting, but left in the plots for completeness. The cluster of points for the dewpoint depression plot is particularly close to the fitted line (Fig. 4b), but there is essentially no relationship between the percentages of TL and DPD exceeding the respective upper Haines thresholds for each station (Fig. 4c), suggesting that these two parameters do provide some independent information.

Figure 3 also reveals some interesting differences in climatology between south-western and south-eastern Australia. In the south-west, the percentage of days exceeding the lapse rate threshold of 10°C is similar to that for the percentage exceeding the dewpoint depression threshold of 12°C. In contrast, for many of the grid points in the south-east (other than South Australia) the percentage exceeding the lapse rate threshold is more than double that exceeding the dewpoint depression threshold.

It might be argued that those physical factors encapsulated in the HI are intrinsic to the fire weather climates of those locations with large percentages of days with HI=6, and that more active fire behaviour is the norm in those areas. However, there is no particular justification for this argument, with the Haines thresholds being determined by the characteristics of Haines' development data set, and it might equally well be argued that there is attraction in being able to discriminate the days on which the 5-10% of instability extremes occurs at any individual location. Given that both the TL and DPD distributions over Australia frequently exceed the upper Haines bounds, the development of a more open-ended "continuous" index that represents this climatological distribution of TL and DPD is described in the next section.

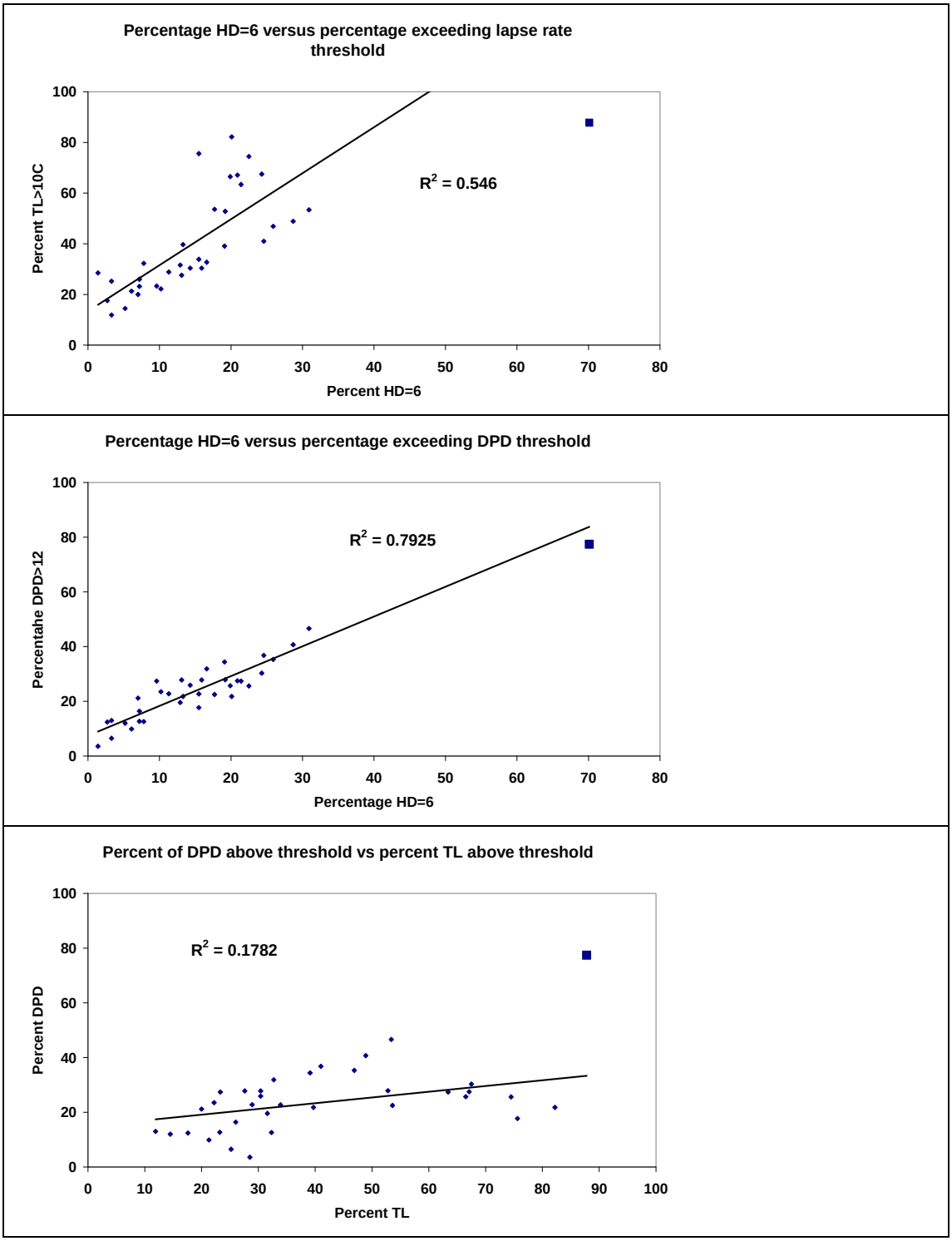

Figure 4. Scatterplot showing the percentage of days for which mid-level Haines Index (HD) equals 6 versus the percentage of days exceeding the 10C 850-700 hPa temperature lapse threshold (top), and versus the percentage of days exceeding the 12C 850 hPa dewpoint depression threshold (middle). In the lower panel the percentage of days exceeding the dewpoint depression threshold is plotted against the percentage of days exceeding the lapse rate threshold. In all three plots, the outlier (large square) is that for the Tanami gridpoint, which has been excluded from the regressions.

3.2 A continuous Haines Index

If the Stability Score and the Humidity Score (Table 4) components of the HI are referred to as HA and HB, then linear functions of TL and DPD (respectively) for these components can be derived by requiring that these functions match the (TL, HA) points (6,1) and (10,3) and the (DPD, HB) points (6,1) and (12,3):

$$CA = 0.5 (T850 - T700) – 2. \quad (1)$$

$$CB = 0.3333 (T850 - DP850) – 1. \quad (2)$$

where CA (CB) is the continuous form of HA (HB), and adding the two provides a "continuous Haines Index", hereafter C-HAINES

$$CH = CA + CB \quad (3)$$

In practice it has been found that occasional very large dewpoint depressions in the LAPS analysis data set, together with the non-linearities of the hypsometric equations, occasionally caused the CB term to become disproportionately large, and so the following two conditions were applied:

$$\text{if } (T850 - DP850) > 30C, \text{ then } (T850 - DP850) = 30C \quad (4)$$

and

$$\text{if } CB > 5., \text{ then } CB = 5. + (CB - 5.) / 2. \quad (5)$$

The latter condition reduces the slope of the DPD relationship for dewpoint depressions greater than 18C, while the former limits the upper value of CB.

There is no a priori physical reasoning to justify this formulation, apart from the desire to provide greater discrimination at the higher end of the range. The CA and CB terms are each 1 at the threshold between 1 and 2 for the standard Haines index, and are each 3 at the thresholds between 2 and 3. There is a natural upper limit of ~6 imposed by the dry-adiabatic lapse rate, which is between 14 and 17C for the range of temperatures usually experienced in Australia, on the range of CA. For CB the arbitrary limits set in Eqs 4 and 5 result in an upper bound of CB of 7. Thus the upper bound of the proposed C-HAINES is ~13. There is no specified lower bound, but this is not the range of interest, and in the data sets developed in this study values are limited to be not less than zero.

Calculating C-HAINES at each point shown in Fig. 1 allows statistical properties of its distribution to be calculated. Figure 5a shows the spatial representation of the 95th percentile of C-HAINES for the September-April period at the analysis points chosen in this study. Comparing these with the percentage of days on which HI=6 (Fig. 2) suggests that there is some positive relationship between the two, and this is supported by the scatterplot of Fig. 5b, although the relationship is not linear.

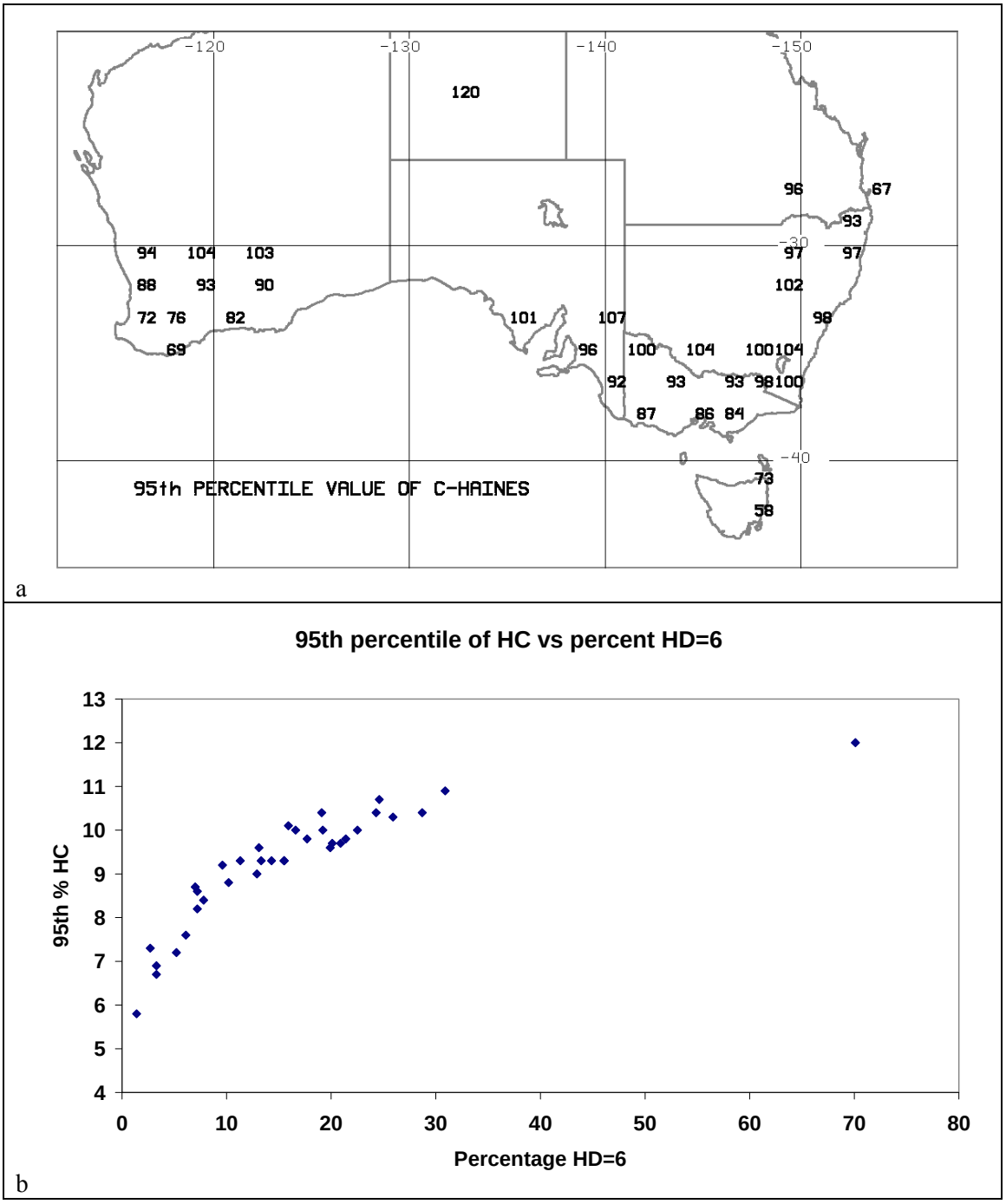

Figure 5. Upper panel – 95th percentile value of C-HAINES (multiplied by 10) at the sampled gridpoints. Data is at 0600 UTC for the months of September to April inclusive, years 2000-2007. Lower panel – scatter plot of 95th percentile of C-HAINES versus the percentage of days for which HI=6 at the gridpoints shown in (a).

The annual cycle of days/month when this 8-month 95th percentile is exceeded is shown in Fig. 6, together with the number of days per month that the HI equalled 6. As might be expected, there is a very strong annual cycle at most stations, being particularly strong at Canberra, and rather weaker in northern Tasmania. There are more subtle variations, too, with the peaks occurring earlier in the season at St George, and to a lesser extent at Mt Lofty, while at Perth the distribution shows significant numbers of both counts extending well into autumn.

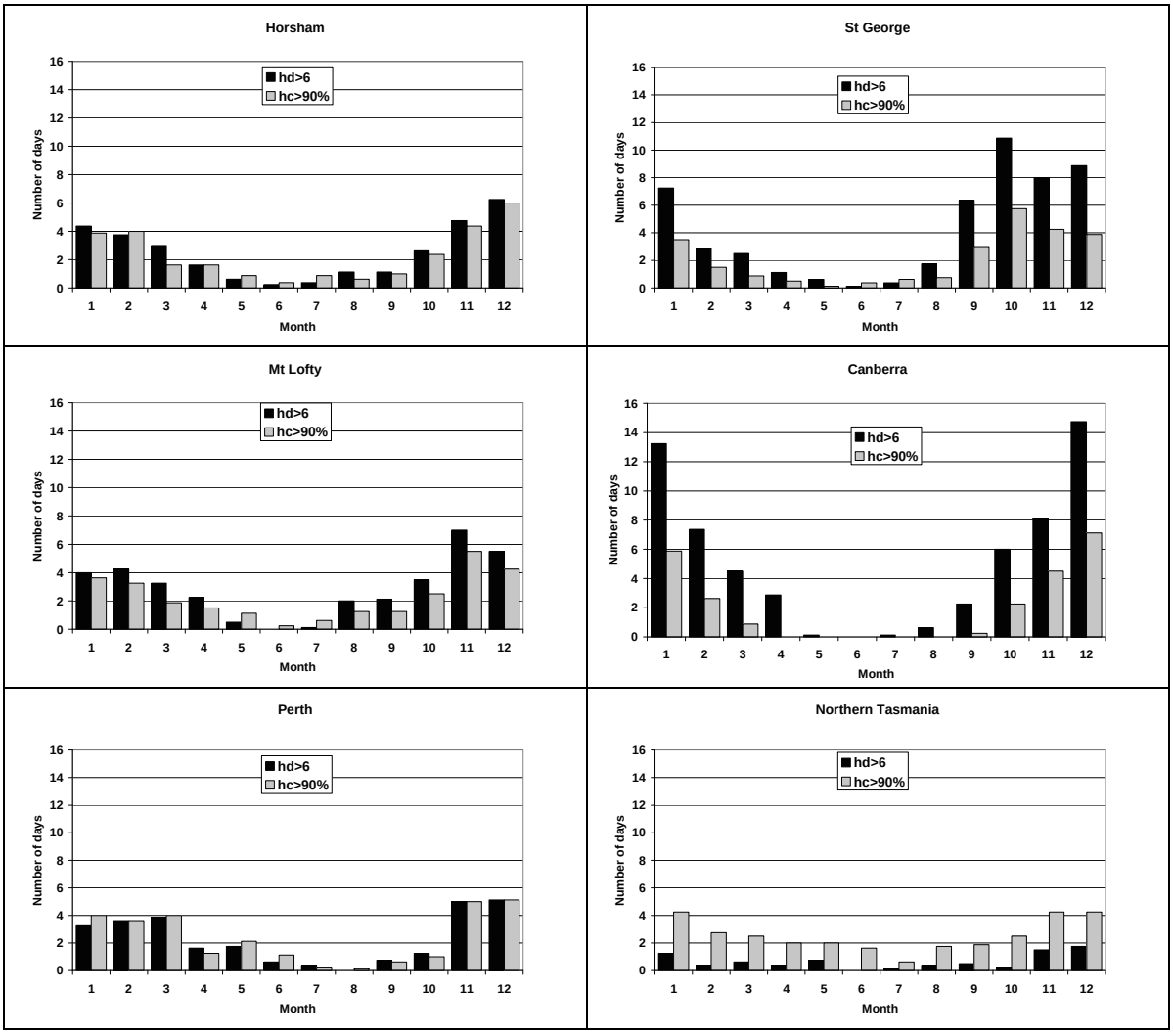

Figure 6. Annual cycle of the number of days per month that exceed the 90th percentile value of C-HAINES (grey bars) and the number of days per month for which HI=6 (black bars) at selected stations.

It is well-known that the FFDI has a pronounced diurnal cycle, as a consequence of the diurnal variations of its input variables. Figure 7 shows the 95th percentile value of C-HAINES at 20 of the stations analysed at the four analysis times (0000, 0600, 1200, and 1800 UTC). The C-HAINES has essentially no diurnal cycle, although there are a few stations where this value is slightly higher at one of the analysis times than the others. This is unsurprising as the ingredients to the HI lie above the levels likely to be affected by surface nocturnal cooling.

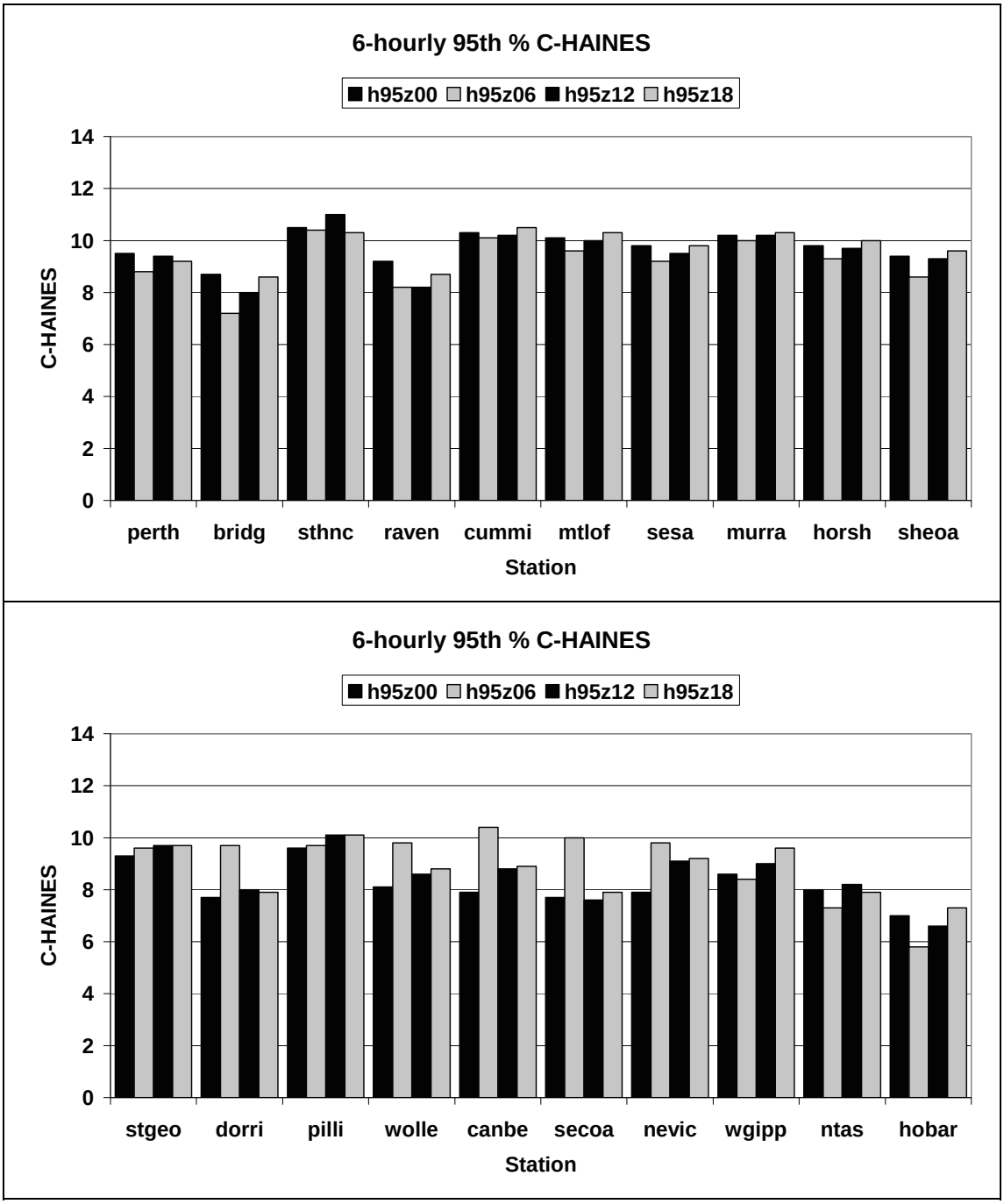

Figure 7. Ninety-fifth percentile of C-HAINES at selected stations at 0000, 0600, 1200, and 1800 UTC (left-to-right). Stations in upper panel, with bracketed numbers referring to the locations in Fig. 1, are perth (#2), bridg (#3), sthnc (#6), raven (#8), cummi (#12), mtlof (#13), sesa (#15), murra (#16), horsh (#18), and sheoa (#19). Stations in lower panel are stgeo (#34), dorri (#33), pilli (#31), wolle (#29), canbe (#28), secoa (#26), nevic (#22), wgipp (#21), ntas (#23), and hobar (#24).

One of the anecdotal limitations of the HI in operational practice in Australia to date has been the very large areas represented at HI=6, which makes discrimination of the locations of the most extreme areas problematic. In Fig. 8 the fields of HI and C-HAINES for two examples from the events listed in Table 1 are shown.

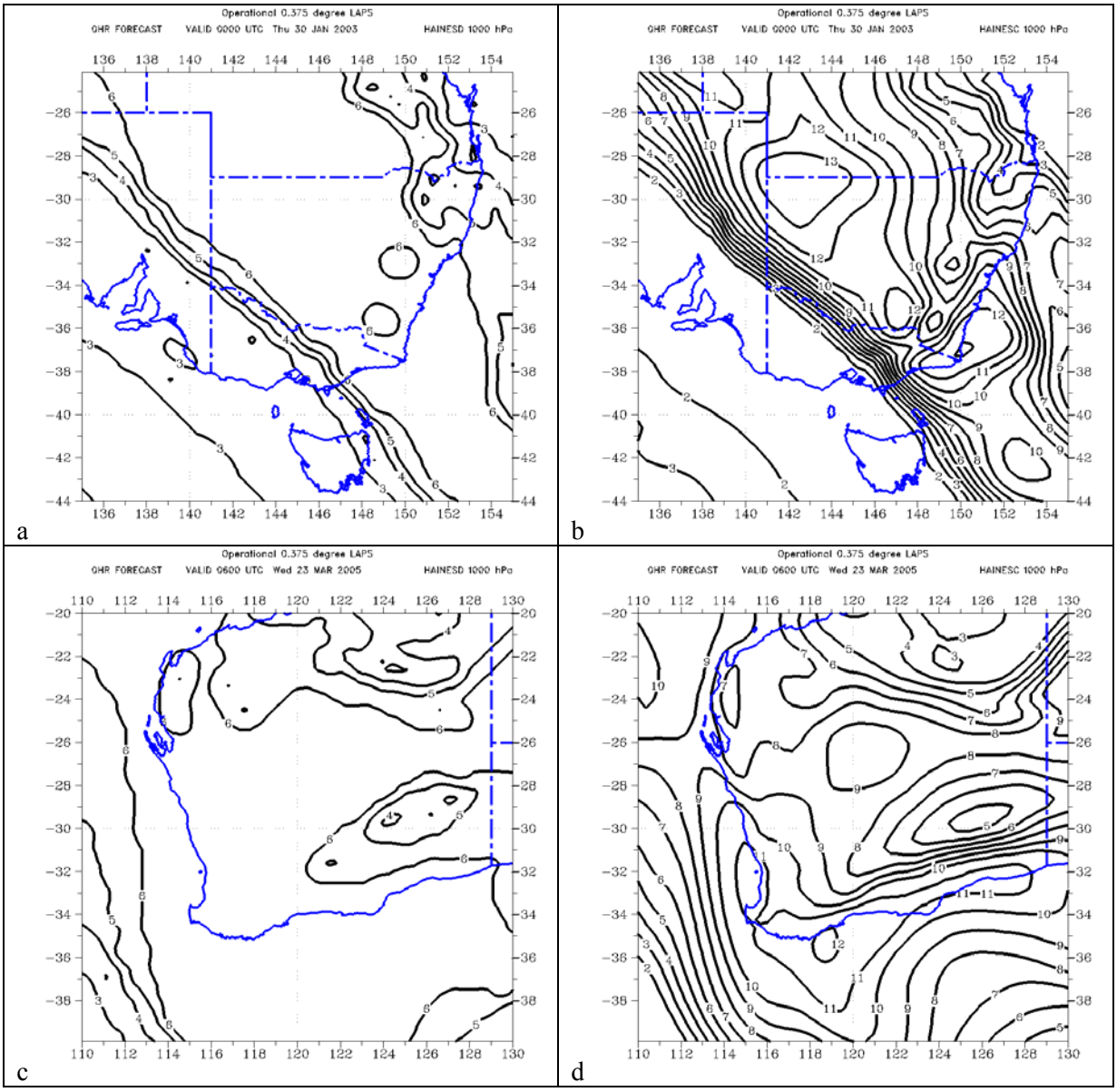

Figure 8. LAPS numerical analyses of mid-level Haines Index (left panels) and C-HAINES (right panels) for the day of the Alpine fires breakout on 30 January 2003 (top panels) and the day of the Bluegum Plantation fire 23 March 2005 (bottom panels).

The first case (upper panels) is the day of the breakout of the Alpine fires in north-east Victoria on 30 January 2003. As well as extreme fire behaviour near Mt Hotham, a pyrocumulus cloud developed on the smoke plume downstream of these fires, and lightning from this convection caused subsequent bushfire ignitions in East Gippsland (Bureau of Meteorology 2003). The second case (lower panels) is that of the plantation fires in the south-west of Western Australia (WA) reported by McCaw and Smith (2008), which exhibited unexpectedly active fire behaviour. In each case vast areas (left panels) show HI=6, while the C-HAINES panels on the right show continuous gradients, with elongated maxima over the regions of fire or pyrocumulus development activity. The majority of the other cases listed in Tables 1 and 2 show similar characteristics, with smaller-scale maxima of considerable amplitude in the C-HAINES patterns, and the evolving patterns reflecting the meteorological drivers of these fields and providing additional insight into the meteorology of the particular event. Further examples are shown in each of the case studies detailed in Appendix 2

4 RELATIONSHIP BETWEEN C-HAINES AND FFDI

For HI or C-HAINES to be useful, it must not only show a relationship to some measure of fire activity, but also must provide information independent of that provided by the FFDI. It might be argued on physical grounds that high temperatures (usual on days of FFDI > 50) also tend to be associated with deep mixed layers, which means that the lapse component of C-HAINES also has large values. In addition, the low surface relative humidities necessary for the highest values of FFDI, combined with a deep mixed layer, should also mean low humidities at 850 hPa, and so the dewpoint depression component of C-HAINES may also tend to be large when the FFDI is large. This reasoning suggests that many of the factors that lead to larger FFDI might also favour larger values of C-HAINES. Dowdy et al. (2009) have developed an 8-year gridded data set of NWP-based FFDI values on a 0.25o grid over Australia. Selecting the highest value in the 3x3 array centred on the C-HAINES points in Fig. 1 allows any relationship between the FFDI and the C-HAINES to be explored.

Scatter-plots of FFDI vs. C-HAINES for six of the target stations are shown in Fig. 9. These are chosen to have a range of climates, with the 95th percentile of C-HAINES ranging from 7.2 at Bridgetown to 10.4 at Canberra (cf Fig. 5a). Allowing for the differing fire weather climates of these stations, the broad patterns of the scatterplots are similar, with a clustering towards the lower values, a generally positive relationship, and an increasingly broad scatter at the higher end of the joint distribution (note the increasing sensitivity of FFDI with increasing magnitude, as described in Dowdy et al. 2009).

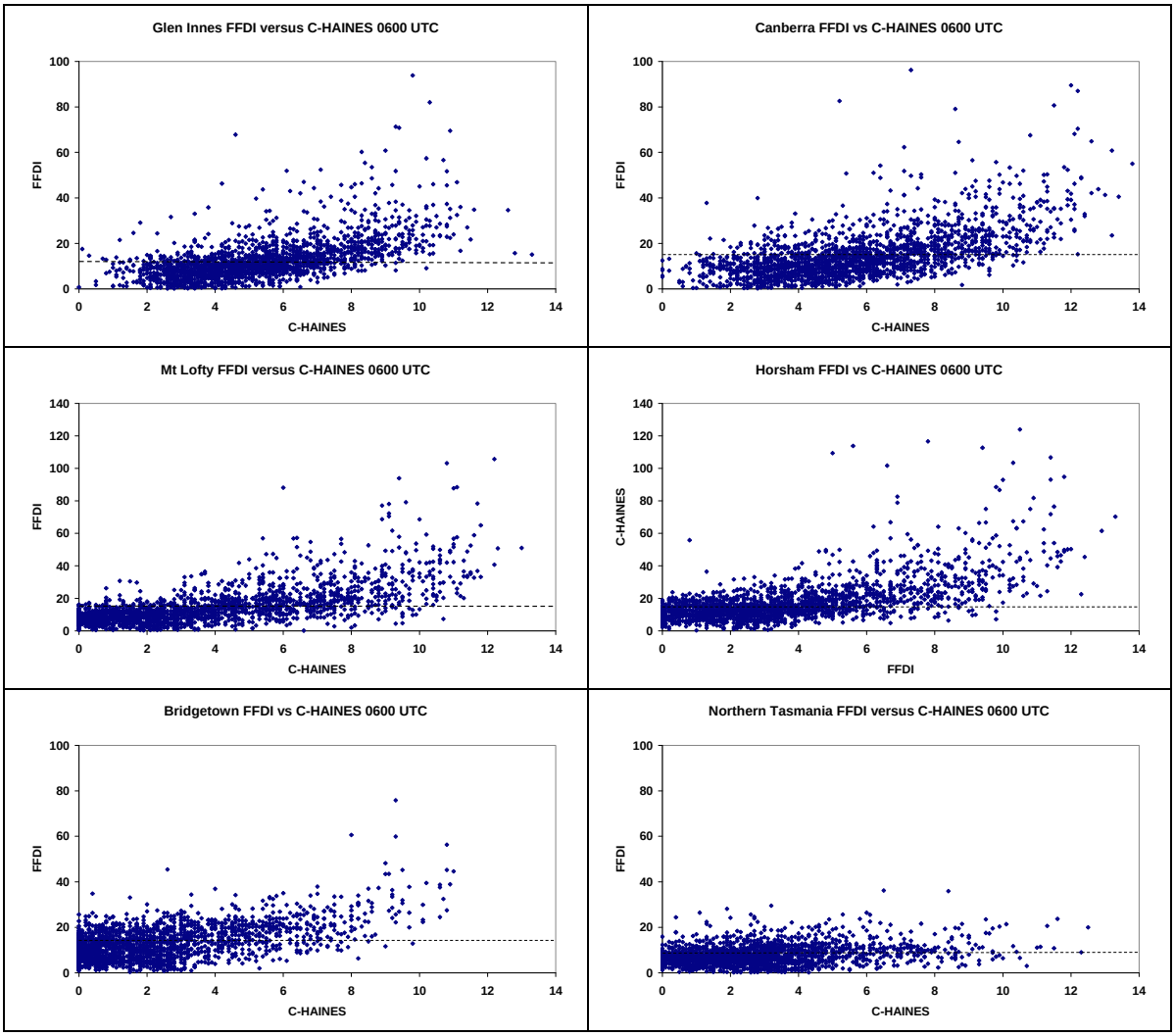

Figure 9. Scatterplot of FFDI versus C-HAINES at selected gridpoints for the 8-year September-April data set at Glen Innes (#32), Canberra (#28), Mt Lofty (#13), Horsham (#18), Bridgetown (#3), and Northern Tasmania (#23). The dashed lines show the 60th percentile values of FFDI.

These scatterplots indicate that while there is some association of higher values of C-HAINES and higher values of FFDI, there are also a number of situations when low values of C-HAINES are associated with high values of FFDI, and vice-versa. Correlations between the two parameters provide support for this premise. Because the distributions are weighted heavily towards lower values of each parameter, points with FFDI in the lower 60% of its distribution (shown by the horizontal dashed lines in Fig. 9) and C-HAINES values less than 4 were excluded from the calculation of correlations between the two sets of data at each station. The resulting correlation coefficients range from as low as 0.15 in northern Tasmania to 0.57 in the Great Southern District of WA (Fig. 10). The median correlation coefficient for all 35 stations is 0.44 (explained variance approximately 20%), suggesting that there is independent information in the two indices.

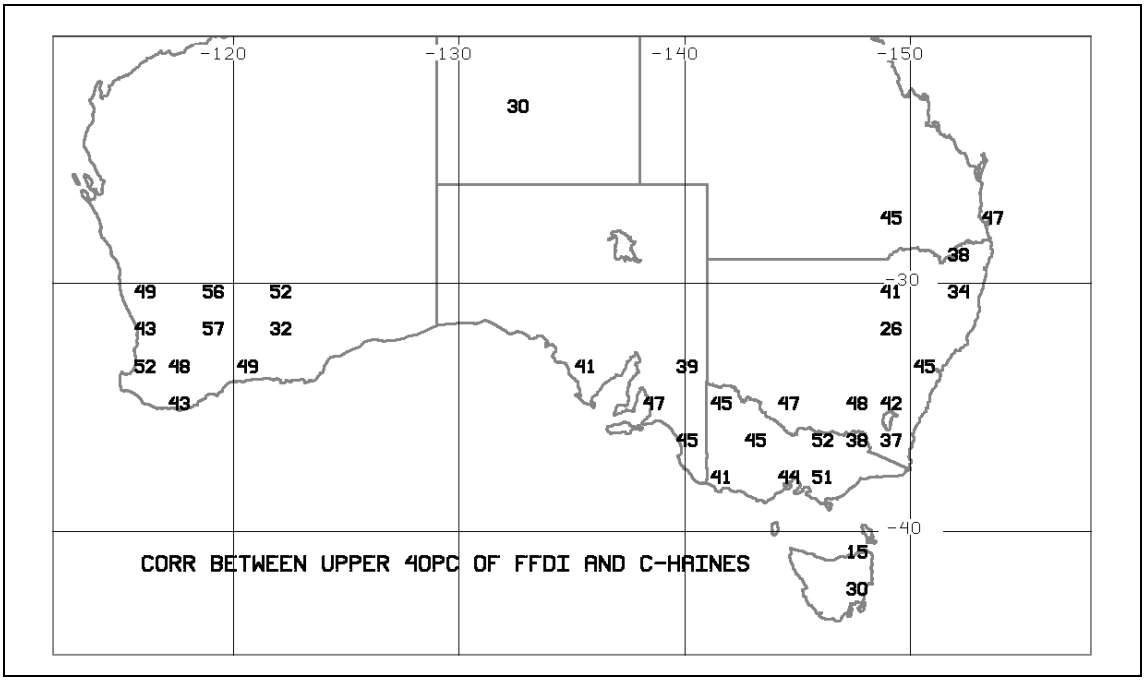

Figure 10. Correlation coefficient (x100) at the selected locations for the relationship between the upper 40% of FFDI values correlated with C-HAINES > 4.

This does not, of course, demonstrate that the C-HAINES has a relationship to fire behaviour. In later sections the association between C-HAINES and the fire and pyrocumulus events listed in Tables 1 and 2 is discussed, and the case study analyses of 13 of these events (presented in Appendix 2) are summarised. Before this is presented, though, several other measures of atmospheric stability that have been shown to be, or proposed to be, associated with more active fire behaviour are described. These measures were also calculated from the LAPS analyses, and are also discussed in relation to the fire events for comparison with the C-HAINES.

5 ALTERNATIVE FIRE WEATHER STABILITY INDICES

5.1 An energy perspective

Potter (2002) used physical arguments to develop measures of how easily an air parcel near the ground can exchange with the air above the mixed layer. He argued that the energy necessary to raise an air parcel from low in the mixed layer to a pressure level above the mixed layer is

$$ASCNT = g \int_0^z [(\theta(0) - \theta(z`))/(\theta(z`)]dz` \quad (6)$$

or the convective available potential energy (CAPE), where g is the acceleration due to gravity, θ is the potential temperature, and z is the height to which the parcel is raised from a reference level zo. An equivalent descent energy, the energy necessary to lower a parcel from an upper level to a level near the ground, is

$$DSCNT = g \int_z^0 [(\theta(z) - \theta(z`))/(\theta(z`)]dz` \quad (7)$$

These areas will be equal if the upper level is within the mixed layer. Both ASCNT and DSCNT are minimised with a deep mixed layer and weak stability above the mixed layer. In this case fire or other processes may lead to a more ready exchange of air from higher levels above the entrainment layer with the surface.

The relative balance of ASCNT and DSCNT energies in any given situation depends on the depth of and the stability above the mixed layer, with, for example, a deep mixed layer with some moderate stability above the entrainment layer giving low ASCNT energy relative to the DSCNT energy for a level a little above the top of the mixed layer, while for a shallow mixed layer the relative balance is reversed.

Potter (2002) then proposed a Parcel Exchange Potential Energy (PEPE) to be the sum of the ascent and descent energies

$$PEPE(z) = ASCNT(z) + DSCNT(z) \quad (8)$$

This was intended to synthesise the two measures, with low magnitudes indicating an easier exchange of air parcels between the levels above the mixed layer and the immediate fire environment. These energies have been calculated from an NWP model sigma level approximately 70m above ground to both the 0.6 and 0.5 sigma levels (prior to May 2006 there were no intervening levels between 0.6 and 0.5 in the numerical analyses).

5.2 Depth of the mixed layer

Potter et al. (2002) showed that there was a strong relationship between the frequency of HI=6 and the depth of the mixed layer, and argued that this was a consequence of the fixed levels used to specify the HI, and that the "Haines layer" should span the inversion layer if the index was to work as intended. There is some evidence that deep mixed layers are present in documented cases of high HI – for example both the cases analysed in Werth and Ochoa (1993) show deep mixed layers in the Boise radiosonde, as do the vertical temperature profiles at Wagga on the morning of 18 January 2003, the day of the Canberra fires (Mills 2005), and at Adelaide Airport on the

morning of 11 January 2005, the day of the disastrous fires on Lower Eyre Peninsula in South Australia (Mills 2008a). There is obviously a relationship between deep mixed layers and high near-surface temperatures, and thus a probable relationship between deep mixed layers and higher than normal FFDI. However, the fact that the mixed layer is neutrally buoyant means that vertical exchanges to a considerable depth (around 600 hPa in the cases cited in this paragraph) are possible in these circumstances suggest that there may be information relevant to fire behaviour in this field.

In this study, using either radiosonde or numerical model data, the depth of the mixed layer is defined as the highest level for which the virtual potential temperature is less than 1C greater than the 10m virtual potential temperature. For deep mixed layers there will be some sampling issues, as particularly for the NWP fields the vertical resolution is relatively coarse (although this has been alleviated to some extent since the increase of LAPS levels in May 2006).

5.3 Stability of the entrainment layer

The stability of the layer above the mixed layer, the "inversion layer" or "the entrainment layer" (Stull 1988) will affect the freedom by which air parcels reaching that level can entrain and mix air from above into the mixed layer, and will also affect how quickly the mixed layer can deepen under diurnal heating – the less stable that layer, the less the potential temperature of the mixed layer must increase in order to deepen the mixed layer by a given amount. Mills (2008b) showed that environments with deep mixed layers and only weakly stable entrainment layers are associated with many of the abrupt surface drying events described in that paper, and argued that these events were associated with the dry convective mixing of mid-tropospheric dry air to the near surface layers (e.g. Mills 2005, Mills 2008a,b). To some extent this effect is measured by the ASCNT and DSCNT energies above, but to focus only on this parameter the lapse rate between the potential temperature at the top of (but still within) the mixed layer and that at a level k above the mixed layer, STAB, is defined as

$$STAB = (\theta k - \theta bl) / (zk - zbl). \qquad (9)$$

For the purposes of this study, the upper level (k) is defined to be the model's sigma = 0.5 level, while the level bl is the highest model level that is still within the diagnosed mixed layer.

5.4 A case-study example

These "stability indicators" were contoured for all the cases listed in Tables 1 and 2, and subjectively assessed for patterns that might focus attention on particular areas. The example in Fig. 11 is for the WA case shown in the lower panels of Fig. 8, where the MSLP field (for reference as a more traditional form of guidance), the boundary-layer depth, the STAB parameter, and Potter's ascent, descent, and exchange energies are shown. In this case the energies are calculated between the near-surface layer and sigma level 0.6 (approximately 600 hPa). The boundary layer depth is substantial near Bridgetown, but does not show any particular geographic focus. The STAB and all three exchange energies, though, do show the region of greatest (dry) instability focussed over the far south-west of WA, and over the area of the fire, suggesting that these parameters might also be used to draw attention to the area of greatest stability-related fire danger.

Many of the other cases also showed apparently instructive patterns in these fields, but the difficulty is in deciding if this provides additional insight or useful fire-weather forecast guidance. To address this issue the values of these various indices, and the value of the FFDI, at each of the fire locations listed in Tables 1 and 2 are presented in the next section, using the climatological distribution of each of these indices at that location as a reference and measure of significance.

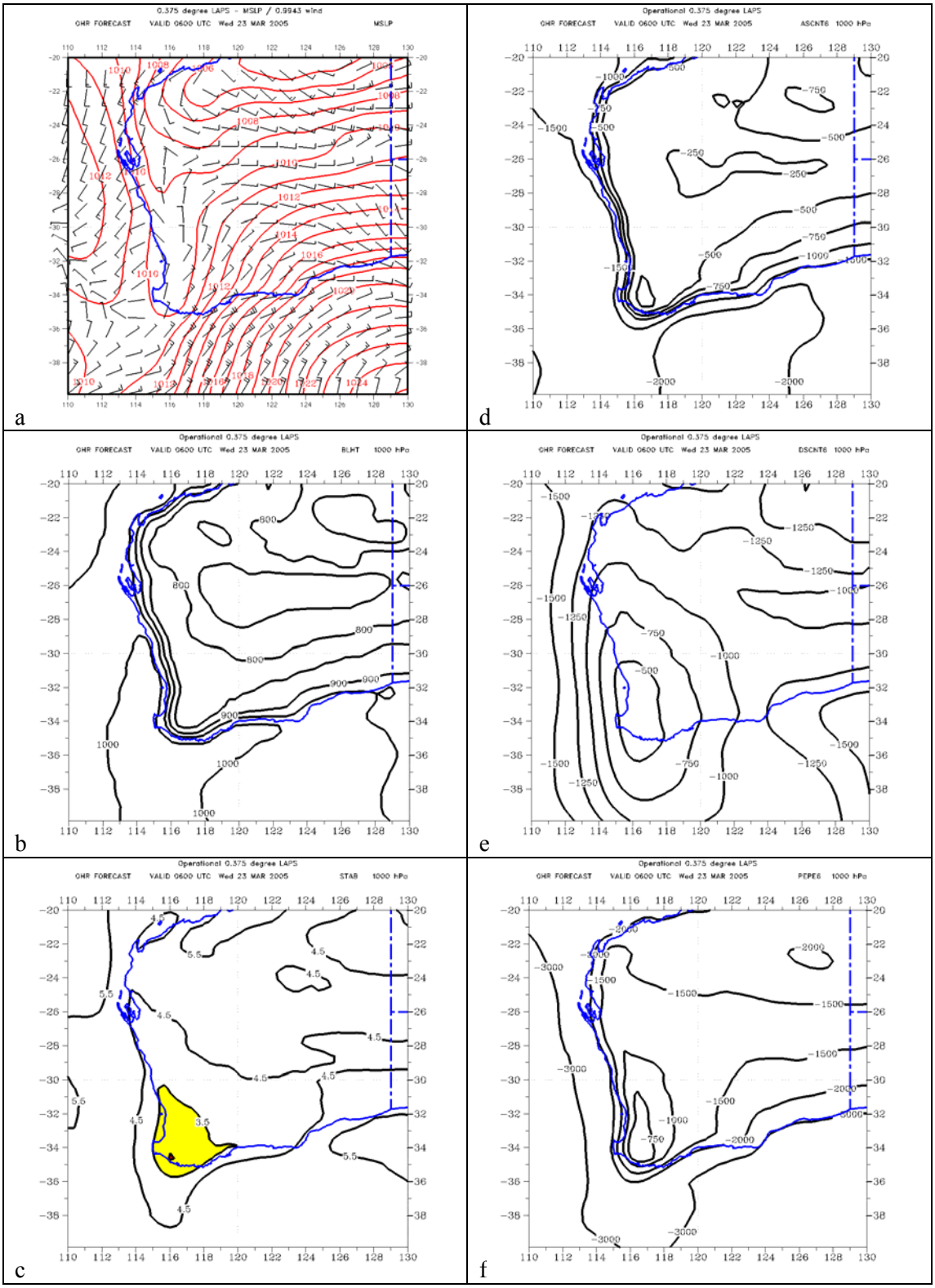

Figure 11 For the Bluegum Plantation fire day of 23 March 2005, (a) MSLP analysis (contour interval 2hPa), overlaid with 10m wind speed and direction, (b) boundary layer depth (hPa), (c) stability of entrainment layer (K km-1) with areas less than 3.5 shaded, (d) ascent energy (J Kg-1), (e) descent energy (J Kg-1), (f) exchange energy (J Kg-1).

6 INSTABILITY INDICES AT FIRE LOCATIONS

While the spatial patterns seen in Figs. 8 and 11, and in many of the other cases, appear to show instructive sub-synoptic scale structures in the C-HAINES field, and in many of the other instability indicators, this does not necessarily relate to variations in fire activity, or necessarily demonstrate that the forecast conditions are unusual. The values of each index at the "fire locations" for the fires listed in Tables 1 and 2, compared with the climatology of the particular index at that location and expressed as a percentile, are listed in Appendix 1, Tables A1 and A2. These tables contain more detail than can comfortably be assimilated in a casual reading, and so to summarise these data, Tables 5 and 6 show the numbers of times, for the fire event set (Table 1) and for the pyrocumulus events set (Table 2), that each stability index exceeds the 90th, 95th, 98th, and 99th percentile of its distribution. For the fire events (Table 5), the largest number of events for which the 90th percentile is exceeded is given by the FFDI, with the C-HAINES a close second, but at the higher percentiles C-HAINES has the highest rank, and its margin increases with increasing percentile threshold. For the pyrocumulus events FFDI has the highest rank for all percentile thresholds, with C-HAINES ranking second. It is also a consistent pattern for the pyrocumulus events that both FFDI and C-HAINES rank very high in their respective statistical distributions. It is perhaps not coincidental that Byram (1959) suggested that "blow-up" fires occur when both the power of the fire, Pf and the power of the wind Pw are both large, but "pulse", or alternate, in their dominance.

Conclusions to be drawn from these results are not definitive, but are intriguing. For the pyrocumulus events, while the various stability indices suggest climatolologically extremely unstable conditions relative to the climate of the particular area, the FFDI is even more climatologically extreme. It thus might be interpreted that the conditions leading to extreme fire danger also include climatologically extreme instability, and that the pyrocumulus is primarily a result of the heat, and perhaps even more importantly, the moisture, released by the very active fire behaviour. There may, however, be other enabling factors contributed by the unstable atmospheric profiles to the development of the pyrocumulus, but these are not immediately apparent from this analysis.

Table 5. Number of fire events for which the listed stability indices exceed the 90th, 95th, 98th and 99th percentiles. Total event days 31. The highest numbers in each column are shaded.

Index	>90th	>95th	>98th	>99th
TLAPSE	26	23	14	8
DPDEP	26	21	16	9
CH	29	27	19	18
BLHT	14	13	9	7
STAB	22	18	12	8
ASCNT5	22	18	11	9
DSCNT5	23	17	15	10
PEPE5	24	20	13	12
ASCNT6	20	14	9	6
DSCNT6	25	20	16	11
PEPE6	25	20	12	9
FFDI	30	26	17	14

Table 6. Number of pyrocumulus events for which the listed stability indices exceed the 90th, 95th, 98th and 99th percentiles. Total event days 25. The highest numbers in each column are shaded.

Index	>90th	>95th	>98th	>99th
TLAPSE	17	13	7	5
DPDEP	16	15	9	8
CH	21	15	12	7
BLHT	15	13	9	6
STAB	10	8	3	2
ASCNT5	17	12	8	6
DSCNT5	13	11	9	7
PEPE5	16	10	7	6
ASCNT6	14	11	9	6
DSCNT6	15	13	7	5
PEPE6	18	14	9	6
FFDI	20	20	14	11

Of the stability indicators tested against the fire events, C-HAINES is clearly that which most often reaches the more extreme values, and so might be the "best" to discriminate active fire behaviour environments. One reason for this may be that it is the only one which incorporates the humidity factor – each of the others is a purely temperature-based index. The data in Tables 5 and 6 also show that the TL and DPD values independently perform less well than does the C-

HAINES (defining performance in terms of the greater extrema of the index in terms of its climatological distribution), and that the numbers of TL above the various percentile thresholds is similar to those of some of the other stability indices. There are some other issues that may affect these conclusions, including the effect of weak stable layers near the surface in the NWP analyses leading to possibly unrepresentative mixed layer depths or exchange energies, and the relatively coarse vertical spacing of the model data above 700 hPa (prior to May 2006) leading to some ambiguity in the calculation of quantities above the mixed layer. These aspects are worthy of future investigation.

There does, thus, appear to be some useful information in the C-HAINES and the energy exchange diagnostics for the active fire cases, with a larger proportion of cases having C-HAINES values at the upper percentile range, , although the FFDI values are still disproportionately high in many of these cases. The fact that the correlations between FFDI and C-HAINES only explain between 25 and 40% of the variance, and the event analysis in this section, support the hypothesis that the C-HAINES does provide information independent of that implicit in the FFDI,.

7 CASE STUDY ASSESSMENT

Of the events listed in Table 1, 25 individual days, indicated by a "Y" in the last column of Table 1, were assessed, comprising eleven separate case studies focussed on particular fire events. These case studies are presented in full in Appendix 2. The case studies were structured to compare C-HAINES and FFDI for each event, looking at the afternoon (0600 UTC) sequence of FFDI and C-HAINES leading up to and through the event, and comparing these values with the climatological distribution at that location. Six-hourly values of C-HAINES are shown in time sequence and compared with time-series of observations from nearby representative observing sites, and the spatial distribution of C-HAINES, its lapse and dewpoint depression components, and more traditional meteorological fields are presented. The individual case studies vary in detail, depending on the degree of documentation of the fire available, and also on the particular features of the meteorology of the events. In this section those aspects of the case studies where C-HAINES might provide a qualitative indication of fire behaviour that was not evident from the FFDI are summarised.

7.1 Fire activity under low or decreasing FFDI

This aspect is difficult to quantify, particularly as both FFDI and C-HAINES are at the outer extrema of their statistical range for a number of the fire and the pyrocumulus events. However, unexpectedly active fire behaviour which included complete crown scorching during prescribed burns was identified in the Hovea and Randall Block case studies, while major fire spread under relatively mild FFDI conditions was observed with the Berringa fire, the Lake Tay fire, and the Randall Block (Perth Hills) fire in October 2005. While it might be difficult to uniquely assign these fire spreads to atmospheric stability effects, as, for example, the Berringa fire was also moving into heavier (forest) fuel types at the same time as the FFDI was declining rapidly under the influence of both cooler south-westerly winds and of diurnal cooling, there does appear to be some positive association with fire activity and C-HAINES in these cases.

7.2 Nocturnal Breakouts

The Billo Road and the Pickering Brook fires both showed significant fire runs overnight, under relatively mild FFDI conditions, but extreme values of C-HAINES. The exact physical process that relates C-HAINES and this overnight fire activity is unclear, but one factor may be the heat of the fire itself "breaking" the nocturnal inversion, or inhibiting its formation, allowing the surface meteorological conditions at the fire to be more representative of those associated with the free atmosphere rather than those of conditions within the surface nocturnal inversion. This association prompted two more case studies – the Mt Cooke fire in WA and the Cobaw State Forest fire in Victoria. These fires also showed unusually active behaviour overnight, and this activity coincided with periods of extremely high C-HAINES.

It is worth noting that all these fires were in hilly country, posing the hypothesis that nocturnal inversions would have been less developed on the ridges, perhaps making the lower tropospheric air represented by the Haines layer more easily exchanged with plumes rising from the fires on the ridgetops.

7.3 Association of high values of C-HAINES and weak overnight relative humidity recovery

For a number of the fire events (the Big Desert fire, the Billo Road fire (day2), the Mt David fire, the Denbarker Block fire, the Scamander fire, the Murray Sunset NP fires, the Little Desert and Casterton complex fires, and the north-east Victorian fires on 10 December 2006) showed very high values of C-HAINES for one to several days prior to the day of the fire ignition, and in general, given the very weak diurnal variation in C-HAINES, these conditions continued through the night before the ignition day. It was demonstrated for several of those cases that the periods of high C-HAINES coincided with very weak overnight relative humidity recovery (eg Mt Cooke, Cobaw Ridge, and Bluegum Plantation fires). These examples prompt the hypothesis that extremely high C-HAINES environments also favour these weak overnight relative humidity recovery events, which in turn lead to very dry fine fuels, favouring ease of ignition or more active fire behaviour. These situations perhaps overlap those discussed in the preceding paragraph, with the difference being the presence or absence of a fire.

The examples of coinciding weak overnight relative humidity recovery and high values of C-HAINES seen in these case studies do not, however, show that high C-HAINES values necessarily provide a prediction of low overnight relative humidity recovery. To test the hypothesis that an unusually high value of C-HAINES may indicate a lower than normal overnight relative humidity recovery, the maximum overnight relative humidity, the average overnight relative humidity between 1400 and 1900 UTC (1600 and 2100 UTC in WA) were computed from a nearby AWS station for a number of the locations shown in Fig. 1 for every day of the 8-year September-April data-set, and matched with the overnight (1800 UTC) values of C-HAINES. The hypothesis was then put that if the value of C-HAINES exceeded its 90th or 95th percentile for that location, what is the likelihood that the overnight average or maximum relative humidity was in its lowest 5th or 10th percentiles? Probabilities of Detection (POD), False Alarm Ratios (FAR), and Equivalent Threat Scores (ETS) (see Ebert and McBride 1997 for definitions) were computed. Using the C-HAINES greater than its 95th percentile value as a predictor that the overnight average relative humidity will be below its 10th percentile value gave the highest POD for the majority (24/26) of stations . The lowest FAR for the majority of stations (25/26) is gained if C-HAINES greater than its 90th percentile value is used to predict that the average overnight

relative humidity will be below its 5th percentile value, and the highest ETS is achieved for 15/26 stations if C-HAINES greater than its 90th percentile value is used as a predictor of average overnight relative humidity being below its 10th percentile value. These results are summarised in Table 7, and indicate that use of C-HAINES as an indicator of weak overnight relative humidity recovery provides a POD ranging up to ~0.8, depending on station, but with quite high FAR, suggesting that this alone is not a sufficient predictor of low overnight relative humidity.

Table 7. Tests of forecast performance of C-HAINES as a predictor of low overnight relative humidity.

C-HAINES Gridpoint (FIG. 1)	AWS AVID	Highest POD C-HAINES > 95th and RHAV < 10th	Lowest FAR C-HAINES > 90th and RHAV < 5th	Highest ETS C-HAINES > 90th and RHAV < 10th
2	YPPH	0.36	0.50	0.16
3	BDGN	0.33	0.64	0.15
4	KTNG	0.47	0.48	0.18
5	RKG	0.33	0.61	0.13
6	YSCR	0.53	0.38	0.27
8	MUNW	0.55	0.25	0.28
9	YPKG	0.57	0.36	0.29
12	YPLC	0.31	0.54	0.12
13	CRAW	0.56	0.33	0.27
14	YREN	0.56	0.32	0.32
15	YMTG	0.34	0.53	0.16
16	WALP	0.59	0.22	0.35
17	YHML	0.37	0.38	0.20
18	YHSM	0.42	0.30	0.24
19	SHEO	0.31	0.38	0.20
20	YWGT	0.33	0.44	0.17
21	YLTV	0.13	0.80	0.06
22	HUHI	0.56	0.58	0.22
24	YMHB	0.11	0.77	0.06
27	YSWG	0.61	0.29	0.33
28	YSCB	0.61	0.77	0.15
29	MTBO	0.90	0.41	0.36
30	YSDU	0.61	0.50	0.25
32	YGLI	0.57	0.76	0.15
33	YKMP	0.06	0.96	0.02

It may be, however, that these results are over-pessimistic, as the AWS data with which the C-HAINES are compared may suffer from errors of representivity, as the exposure of the particular observing site may be more or less subject to nocturnal inversions or other processes that might affect the results (see the difference between the Manjimup and Bridgetown meteograms for the Bluegum Plantation fire, Appendix 2, Fig. A1.3). There may also be other factors that, in combination with the atmospheric environments characterised by high values of C-HAINES, lead to low overnight relative humidity. One such additional factor that might be worth considering is that of warm advection. It is evident in several of the case studies cited in this sub-section that both daytime and night-time temperatures steadily increased for two or three days leading to the period of anomalously low overnight humidity, (the Cobaw Ridge fire, the Billo Road fire, the Big Desert fire, the Murray-Sunset fire in September 2002). Variations in wind speed are also a factor, since mechanical mixing may inhibit the development of a surface radiation inversion.

In spite of the somewhat pessimistic conclusion of the previous paragraph, there is a higher probability of low overnight relative humidity if C-HAINES is very high. Thus understanding of

the relationships between C-HAINES and low overnight relative humidity recovery is a worthwhile research task.

It is not, of course, necessary to use C-HAINES to infer a lack of overnight relative humidity recovery – so long as representative screen-level observations are available, this information can be monitored and input to fuel-moisture models (e.g. Matthews 2006), or indeed fuel moisture might be monitored directly. C-HAINES does, however, provide a relatively simple and robust spatial product with which to assess "danger areas" and in a forecast mode may well be more robust than predictions of some of the surface variables.

7.4 Penetration of frontal inversions

There were several events when active fire spread occurred after the passage of a dry "cool change", and above which active convective activity or pyrocumulus development was noted. These include the Berringa fire, the Denbarker Block fire, and the Pickering Brook fire. In each of these events the C-HAINES was extremely high at the time, although conditions at the surface were cooler and more humid that normally expected for active fire behaviour, albeit perhaps with strong wind-driven component to the fire spread. It may be speculated that the heat from the fire may well have been sufficient in these cases to penetrate the frontal inversion and so mix the drier air from aloft to the fire, enhancing the fire activity.

The results of Kiefer et al. (2009) are intriguing in this context, as their idealised modelling studies suggest regimes of more intense convective response above a heat source under certain conditions of vertical wind shear that they note are similar to those at a frontal inversion.

7.5 Small-scale atmospheric circulation features

While some of the regions of very high C-HAINES may be extensive and very obvious (e.g. Fig. 8), there are other cases where quite small-scale, and definitely sub-synoptic, atmospheric circulation features are identified by high C-HAINES features (e.g. the Hovea fire, the Bluegum Plantation fire, the Pickering Brook fire, the Randall Block fire, and the Scamander fire). These are cases where mesoscale NWP model forecasts show considerable promise for providing alerts to fire managers. An additional factor to consider in this context is the gradient of the atmospheric features – if there is a forecast of strong gradients (e.g. the Randall Block fire), then some allowance must be made for the possibility that the forecast could have a spatial error.

7.6 Ingredients-based assessment

The HI and the modified C-HAINES index each include both a temperature lapse (instability) ingredient, and a dewpoint depression (atmospheric dryness) component. The discussion of the data in Tables 5 and 6 suggested that this may be a strength of the index, and is the reason why it identifies a greater proportion of the case study events than do some of the more physically-based instability indicators such as Potter's (2002) exchange energies, or either of the input ingredients alone. This strength, though, may come at the cost of there not being a single physical process that links fire or pyrocumulus activity with C-HAINES (see also Potter et al. 2002). Amongst the case studies there are examples where C-HAINES is dominated by the instability ingredient (eg Scamander on the afternoon on 11 December 2006 and the Pickering Brook fire), and others

where the humidity component is stronger (e.g. the Hovea fire, the Bluegum Plantation fire, the Randall Block fire, and the Big Desert fire). In the former cases the effects on the fire might be more likely to be due to mixing from aloft of high momentum air (gustiness), while in the latter the effects are more likely to be via the reduction of fine fuel moisture content. The dryness-dominated cases also probably have a large overlap with the abrupt surface drying hypotheses documented in Mills (2008a,b) (e.g. Hovea fire). Of course there are also cases where both ingredients are very high.

It should be noted that the maxima in the lapse and the dewpoint depression fields are usually not completely in phase, and so the field of C-HAINES shows the combination of these two independent fields. Accordingly, in an operational (forecast) environment the optimum practice should be (as with all indices) to use the C-HAINES forecast as an alert to the high C-HAINES environments, and then to assess the ingredients to understand the processes that might be acting to affect fire behaviour on the particular day in question.

7.7 Pyrocumulus events

Most of the pyrocumulus events listed in Table 2 show not only extremely high values of C-HAINES, but also FFDI. Thus while the presence of a pyrocumulus cloud might suggest atmospheric instability, very active (wind driven) fire behaviour was already present, and thus the development of the pyrocumulus may have been driven by the combustion products from a high rate of fuel consumption (Potter 2005), although the instability values are also in general in the upper parts of their ranges as well. Any feedback processes that might then occur is not revealed in this analysis, but the presence of a tornado during the Canberra fire of 18 January 2003 shows that such complex effects do occur, although the precise sequence and interactions of fire activity and atmospheric drivers is exceedingly complex. Studies such as that of Cunningham and Reeder (2009) are a likely path forward here.

8 DISCUSSION

In the first part of this paper, the climatological distribution of the traditional mid-level Haines Index was examined over southern Australia, and by converting the discrete inputs to the traditional HI into linear functions of the temperature lapse and dewpoint depression ingredients a continuous index, C-HAINES, was proposed. This C-HAINES shows a considerable geographic variation in its statistical distribution, with its 95th percentile value ranging from around 7 in Tasmania and the far south-west of WA to more than 10 near Canberra and inland. This formulation allows a particular day to be defined as unusual in terms of its joint (in)stability and dryness by means of the local percentiles, and thus alleviates the lack of discrimination of the traditional mid-level HI in warmer climates (McCaw et al. 2007, Werth and Werth 1998).

The contoured fields of C-HAINES show sub-synoptic maxima that correspond with known fire events, and focus attention on the regions of maxima, rather than on the vast areas of HI=6 commonly seen over southern Australia in summer. Comparing values of C-HAINES with FFDI shows that, excluding the lowest 60% of FFDI values, and C-HAINES values less than 4, the two indices are weakly correlated at best, suggesting that there may be information content independent of the FFDI in the C-HAINES index. However, neither the HI nor the proposed C-HAINES, have any direct physical relationship to fire activity or behaviour. Comparing the percentile values of C-HAINES and FFDI for a number of known pyrocumulus and fire activity days, it was shown that a larger proportion of fire events were associated with a larger proportion of the most extreme values of C-HAINES, while the for the pyrocumulus days there were a larger proportion of the most extreme FFDI values. While these statistics are undoubtedly affected by the sampling of the case selection used, there does seem to be some encouragement to further test the use of C-HAINES in Australia.

While a statistical relationship between HI and area burnt has been demonstrated in Tasmania (Bally 1995) and parts of the US (eg Saltenberger and Barker 1993), this is yet to be demonstrated for the C-HAINES, and is a subject for future research. In order for this relationship to be tested it will be necessary for a systematic data-set of fire activity for a large number of fires from all the southern states of Australia be collected. Further, these measures should be collected with a time resolution of not longer than daily intervals, although given the variations in meteorological fields throughout the day (see Appendix 2) continuous measures of fire activity would be desirable. This is a demanding requirement, and until available the assessment of the utility of the C-HAINES to fire managers will rely on experience gained in daily operations, with the "significance" of a particular value of C-HAINES being its percentile value for its local climatology.

A fire activity data set such as that described above could also be used to statistically tune the C-HAINES by determining the optimum relative weighting of the lapse and humidity ingredients, and also by testing alternative combinations of levels.

Other measures of atmospheric stability that have arguably stronger physical basis, but little demonstrated systematic relationship with fire activity were also assessed in the same way, and while several of these showed geographic patterns that appeared to focus attention on the areas of the fire events studied, their statistical distributions for the case studies examined made a case for adoption less compelling than those of either the FFDI or the C-HAINES. A strength of the HI/C-HAINES may be that they combine both an atmospheric stability component and a dryness component, and so encapsulates a wider range of physical processes that may enhance fire activity. However, further examination of these measures is definitely warranted.

Closer examination of a number of the fire events listed in Table 1 showed interesting aspects. There are a number of examples where unexpectedly active fire behaviour occurred in conditions of relatively lower FFDI but extremely high C-HAINES, and some of these were prescribed burn situations. In another category were examples of overnight increases in fire activity under conditions of C-HAINES well above its 95th percentile for that location. If this result can be found to be more widely applicable, then the use of C-HAINES may avoid some "nasty surprises" in conditions of relatively lower FFDI.

A variety of other interesting features were revealed – some of the case studies had major fire runs following a sea-breeze or dry cool change, but showed "unexpected convective activity" above the fire, and each of these occurred with extreme values of C-HAINES, with the Haines layer being above the frontal inversion. In these cases it was hypothesised that the heat from the fire was sufficient to mix through the frontal inversion and to entrain air from above the cool-change layer into the fire zone. In such cases the FFDI at a nearby AWS would certainly not be representative of the atmospheric conditions being experienced by the fire. The idealised modelling studies of Kiefer et al. (2009) show some broad support for this theory, although much additional research is needed to fully understand these processes.

There were a number of examples where periods of one to several days of very high values of C-HAINES preceded either a fire ignition day or a day of major fire spread during a campaign fire, and several (but not all) of these cases coincided with periods of anomalously low near-surface relative humidity, and in particular nights with very weak relative humidity recovery. It thus seems that the conditions in which high C-HAINES occurs might also favour the conditions that lead to anomalously low fine fuel moisture content. However, testing forecast performance for all days in the data set showed that not all nights of low overnight relative humidity occurred under conditions of extremely high C-HAINES, while using an extreme value of C-HAINES as a predictor of low overnight relative humidity would lead to a large FAR. Thus while a forecast of high C-HAINES might provide an alert to this likelihood of low overnight relative humidity, there are other factors that also affect this likelihood, and further research is needed to understand the physics of this process..

As discussed in the introduction, and also demonstrated in the case studies, there are arguably a number of physical processes that the HI encapsulates, and so the C-HAINES forecast should be used as an alert rather than a simple cause and effect relationship to fire activity. Indeed, the simple separation between wind-driven and plume-driven fires is probably rarely found in nature. Accordingly, examining the components of the C-HAINES to understand the drivers of C-HAINES should be the practice, as this can show the relationships between the free atmosphere aspects of fire weather indices (C-HAINES) and the more traditional indices such as FFDI which represent the wind-driven, or near-surface, fire danger.

9 ACKNOWLEDGEMENTS

Many of the pyrocumulus events have been brought to the author's attention by Dr. Mike Fromm of the Naval Research Laboratory, in conjunction with Rick McRae and Andrew Tupper. Mr. Mark Chladil of the Tasmania Fire Service assisted with details of the Scamander fire. The authors have received useful and constructive feedback from John Bally, of CAWCR, and Kevin Parkyn of the Bureau of Meteorology, and Scott Collis and Gary Weymouth provided constructive reviews of the first draft of this report. Klaus Braun, Gavin Wornes, Mike Wouters, and Kevin Pollock all contributed additional information included in some of the case studies.

10 RERERENCES

Bally, J. 1995. The Haines Index as a predictor of fire activity in Tasmania. *Proceedings of Bushfire '95, Australian Bushfire Conference,* 27-30 September 1995, Hobart, Tasmania.

Bureau of Meteorology. 2003. Meteorological aspects of the eastern Victorian fires January-March 2003. *Bureau of Meteorology, Victoria*. 82pp.

Bureau of Meteorology. 2005. Meteorological Report on the Wangary and Black Tuesday fires Lower Eyre Peninsula, 10-11 January 2005. *Bureau of Meteorology, South Australian Region*, October 2005.

Bureau of Meteorology. 2008a. Fire Weather Directive – Tasmania and Antarctic Regional Office, November 2008. *Bureau of Meteorology, Hobart, Tasmania*. 53pp.

Bureau of Meteorology. 2008b. Meteorological aspects of the Boorabbin Fire 28 December 2007 – 8 January 2008. *Bureau of Meteorology, Perth, WA*. 51pp.

Byram, G.M. 1954. Atmospheric conditions related to blowup fires. *USDA Forest Service Research Paper* SE-35. 34pp.

Byram, G.M. 1959. Forest Fire behaviour. In "Forest fire: control and use". (Ed K.P. Davis) pp 90-123. (McGraw-Hill, New York).

Chandler, R. 2005. Blackwood prescribed burn BB012 Hovea-Greater Preston National Park. *Unpublished report, Department of Environment and Conservation*, WA.

Cheney, P. 2009. Fire behaviour during the Pickering Brook wildfire, January 2005 (Perth Hills Fires 71-81). Submitted to *Conservation Science*, Department of Environment and Conservation WA.

Cruz, M. G. and Plucinski, M. P. 2007. Billo road fire: report on fire behaviour and suppression activity. *Bushfire Cooperative Research Centre*, *Melbourne*, *Victoria*, *Australia*. Report no. A.07.02.

Cunningham, P. and Reeder, M. 2009. *Geophysical Research Letters 36*, L12812, doi:10.1029/2009GL039262.

Deeming, J.E., Burgan, R.E. and Cohen, J.D. 1977. The national fire-danger rating system- 1978. General technical report INT-39. Ogden, UT: US Department of Agriculture, Forest Service, Intermountain Forest and Range Experiment Station. 63pp.

de Groot, W. J., Wardati, B. and Wang, Y. 2005. Calibrating the Fine Fuel Moisture Code for grass ignition potential in Sumatra, Indonesia, *International Journal of Wildland Fire* ***14***, 161-168.

Dowdy, A., Finkele, K., Mills, G.A. and de Groot, W. 2009. Australian fire behaviour as represented by the McArthur Forest Fire Danger Index and the Canadian Forest Fire Weather Index. *CAWCR Technical Report CTR010*, 84pp. (http://www.cawcr.gov.au/publications/technicalreports.php).

Ebert, E.E. and McBride, J.L. 1997. Methods for verifying quantitative precipitation forecasts: application to the BMRC LAPS model 24-hour precipitation forecasts. *BMRC Techniques Development Report No 2*. 87pp.

Ellis, P. 2003. Spotting and firebrand behaviour in dry eucalypt forest and the implications for fuel management in relation to fire suppression and to ember (firebrand) attack on houses. *Proceedings of the 3rd International Wildland Fire Conference and Exhibition*, 3-6 October 2003, Sydney, New South Wales.

Forestry Tasmania. 2007: 2007 Annual Report. *Forestry Tasmania*.

Fromm, M., Tupper, A., Rosenfeld, D., Servranckx, R. and McRae, R. 2006. Violent pyroconvective storm devastates Australia's capital and pollutes the stratosphere, *Geophys. Res. Lett.* ***33***, L05815, doi:10.1029/2005GL025161.

Goodrick, S.L. 2003. Relationship between atmospheric stability and area burned during the 1998 Florida wildfires. *In: Second International Wildland Fire Ecology And Fire Management Congress And Fifth Symposium On Fire And Forest Meteorology*, November 16-20, Orlando, Florida, p. 1-5. American Meteorological Society.

Haines, D.A. 1988. A lower atmospheric severity index for wildland fires. *National Weather Digest* ***13***, 23-27.

Jenkins, M.A. 2002. An examination of the sensitivity of numerically simulated wildfires to low-level atmospheric stability and moisture, and the consequences for the Haines Index. *International Journal of Wildland Fire* ***11***, 213-232.

Jenkins, M.A. 2004. Investigating the Haines Index using parcel model theory. *International Journal of Wildland Fire* ***13***, 297-309.

Kallberg, P., Berrisford, P., Hoskins, B., Simmons, A., Uppala, S., Lamy-Thepaut, S. and Hine, R. 2005. ERA-40 Atlas, ERA-40 *Project Report Series, No 19*. European Centre for Medium Range Weather Forecasts.

Kaplan, M.L., C. Huang, Y-L. Lin, and J.J. Charney. 2008. The development of extremely dry surface air due to vertical exchanges under the exit region of a jet streak. *Meteorol. Atmos. Phys.* ***102,*** 63-85.

Kiefer, M.T., Parker, M.D. and Charney, J.J. 2009. Regimes of dry convection above wildfires: idealised numerical simulations and dimensional analysis. *J. Atmos. Sci.* ***66***, 806-836.

Long, M. 2006. A climatology of extreme fire weather days in Victoria. *Aust. Meteor. Mag.* ***55***, 3-18.

Luke, R.H. and McArthur, A.G. 1978. *Bushfires in Australia*. Australian Government Publishing Service, Canberra, Australia. 359 pp.

Matthews, S. 2006. A process-based model of fine fuel moisture. *International Journal of Wildland Fire* ***15***, 155–168.

McCaw, L., Marchetti, P., Elliott,G. and Reader, G. 2007. Bushfire weather climatology of the Haines Index in south-west WA. *Aust. Meteor. Mag.* ***56***, 75-80.

McCaw, L. and Smith, B. 2008. Fire behaviour in a 6 year old Eucalyptus globulus plantation during conditions of extreme fire danger – a case study from south-west WA. *Bushfire Cooperative Research Centre*, *Melbourne*, *Australia*.

Mills, G.A. 2005. On the sub-synoptic scale meteorology of two extreme fire weather days during the Eastern Australian fires of January 2003. *Aust. Meteor. Mag*. ***54***, 265-290.

Mills, G.A. 2008a. Abrupt surface drying and fire weather Part 1: Overview and case study of the South Australian fires of 11 January 2005. *Aust. Meteor. Mag.* ***54***, 299-309.

Mills, G.A. 2008b. Extreme surface drying and fire weather Part 2: A preliminary synoptic/dynamic climatology in the forested areas of southern Australia. *Aust. Meteor. Mag.* ***57***, 311-328.

Potter, B.E. 2002. A dynamics based view of atmosphere-fire interactions. *International Journal of Wildland Fire* ***11***, 247-255.

Potter, B.E. 2005. The role of moisture in the atmospheric dynamics associated with wildland fires. *International Journal of Wildland Fire* ***14***, 77-84.

Potter, B.E., Borsum, D. and Haines, D. 2002. Keeping Haines Real - Or Really Changing Haines? *Fire Management Today* ***62(3)***,41-46.

Potter, B.E. and Goodrick, S. 2003. Performance of the Haines Index during August 2000 for Montana. *In: Proceedings of the 4th Symposium on Fire and Forest Meteorology; 2001 November 13-15; Reno, NV*. Boston, MA: American Meteorological Society. Pp 233-36.

Puri, K., Dietachmeyer, G.D., Mills, G.A., Davidson, N.E., Bowen, R.A. and Logan, L.W. 1998: The new BMRC Limited Area prediction System, LAPS. *Aust. Meteor. Mag.* ***47***, 203-223.

Rothermel, R.C. 1991. Predicting behaviour and size of crown fires in the Northern Rocky Mountains. Research Paper INT-438. US Department of Agriculture, Forest Service, Intermountain Research Station. 46pp.

Saltenberger, J. and Barker, T. 1993. Weather related unusual fire behavior in the Awbrey Hall Fire. *Natl. Wea. Dig.* ***19***, 20-28.

Smith, R. 2007. Key Issues Identified from Operational Reviews of Major Fires in Victoria 2006/07. Department of Sustainability and Environment, Victoria. 96pp.

Stull, R.B. 1988. An introduction to boundary layer meteorology. Kluwer Academic Publishers. 666pp.

Tolhurst, K.G. and Chatto, K. 1999. Development, behaviour and threat of a plume-driven bushfire in west-central Victoria. *In Research Report No 48, "Development, behaviour, threat and meteorological aspects of a plume-driven bushfire in west-central Victoria*". Department of Natural resources and Environment, Ed. K. Chatto. 66pp.

Werth, P. and Ochoa, R. 1993. The evaluation of Idaho wildfire growth using the Haines Index. *Wea. and Forecasting* ***8***, 223-34.

Werth, J. and Werth, P. 1998. Haines Index climatology for the western United States. *Fire Management Notes* ***58***, 8-17.

Zimet, T., Martin, J.E. and Potter, B.E. 2007. The influence of an upper-level frontal zone on the Mack Lake wildfire environment. *Meteorol. Appl.* ***14***, 131-147.

APPENDIX 1

Tables of parameter values and percentiles of those values for each of the fire activity days and pyrocumulus event days listed in Tables 1 and 2. In these tables the Event Number refers cross-references to tables 1 and 2 in the main body of this report, and the parameters in the first columns are:

TL: temperature lapse from 850-700 hPa (C)

DPD dewpoint depression at 850 hPa (C)

HD mid-level Haines Index

CH C-HAINES

BLHT Depth of mixed layer (hPa)

STAB Stability between top of mixed layer and 500 hPa (K km-1)

A5 Potter's ascent energy to sigma level 0.5 (J kg-1)

D5 Potter's descent energy to sigma level 0.5 (J kg-1)

P5 Potter's exchange energy to sigma level 0.5 (J kg-1)

A6 Potter's ascent energy to sigma level 0.5 (J kg-1)

D6 Potter's descent energy to sigma level 0.5 (J kg-1)

P6 Potter's exchange energy to sigma level 0.5 (J kg-1)

FFDI Forest Fire danger Index

The upper set of these parameters in each table show the actual value of that parameter, while the lower set list the percentile of the value within the September – April climatology.

Table A1. Fire activity event data

.

Event No	25	46	39a	39b	39c	39d	39e	47d	31a
Date	25 Feb 1995	12 Dec 2002	17 Dec 2002	18 Dec 2002	19 Dec 2002	20 Dec 2002	21 Dec 2002	10 Feb 2003	10 Jan 2005
TL	16.2	15.5	15.0	14.2	15.7	14.5	16.1	12.1	14.9
DPD	20.0	24.1	29.4	18.7	16.9	33.0	27.1	32.9	26.3
HD	6	6	6	6	6	6	6	6	6
CH	11.4	11.8	12.4	10.2	10.5	12.7	12.6	11.5	11.8
BLHT	699	683	971	805	703	803	701	940	804
STAB	2.9	2.8	1.2	1.9	3.5	3.3	3.4	3.5	2.2
A5	-245	-380	-626	-422	-559	-7.5	-472	-1778	-553
D5	-1060	-1054	-686	-906	-1311	-1730	-1318	-1583	-1083
P5	-1305	-1434	-1312	-1328	-1871	-2444	-1790	-3362	-1636
A6	-18	-113	-365	-169	-206	-276	-156	-1065	-226
D6	-400	-453	-250	-390	-564	-584	-442	-791	-555
P6	-418	-566	-616	-558	-769	-860	-600	-1856	-781
FFDI	77*	47.6	46.2	43.9	42.4	44.9	48.6	32	51.3
TL	99	99	96	93	98	94	99	91	97
DPD	95	99	99	91	87	99	98	99	98
CH	99	99	99	96	96	99	99	99	99
BLHT	99	98	1	66	97	66	98	04	90
STAB	91	98	99	99	83	88	86	85	93
A5	99	99	90	96	93	86	96	35	97
D5	99	99	99	99	93	72	93	90	98
P5	99	95	99	99	95	87	96	67	99
A6	99	98	73	92	90	83	93	20	95
D6	99	99	99	98	94	93	97	89	94
P6	99	99	96	97	94	91	97	63	95
FFDI	99	99	95	94	93	95	96	95	96
	BERRINGA (Sheoaks)	Denbarker Block (Katannaing)	Big Desert	Big Desert	Big Desert	Big Desert	Big Desert	LakeTay Fire (Ravensthorpe)	Wangary 1

Table A1 (continued)

Event No	31b	12	32	36b	38	15	51b	51c	51d (17)
Date	11 Jan 2005	17 Jan 2005	23 Mar 2005	15 Oct 2005	17 Dec 2005	19 Sep 2006	20 Nov 2006	21 Nov 2006	22 Nov 2006
TL	15.3	12.9	14.1	14.9	9.2	14.7	15.4	16.0	15.4
DPD	29.6	19.5	23.5	16.9	18.5	17.2	24.3	22.9	23.5
HD	6	6	6	6	5	6	6	6	6
CH	12.6	9.7	11.0	10.1	7.4	10.1	11.7	11.8	11.6
BLHT	952	927	842	962	998	675	717	643	642
STAB	1.9	2.3	2.7	2.3	4.4	2.6	2.0	2.8	2.0
A5	-861	-851	-684	-1167	-2419	-258	-375	-265	-208
D5	-1077	-1343	-1579	-1059	-2134	-1012	-926	-1018	-788
P5	-1937	-2194	-2263	-2227	-4554	-1268	-1301	-1283	-997
A6	-488	-406	-295	-649	-1398	-34	-136	-52	-31
D6	-348	-681	-394	-862	-1460	-383	-340	-294	-312
P6	-835	-1087	-689	-1512	-2858	-417	-476	-346	-343
FFDI	105	30.2	44.6	26.9	8.1	117.1	42.5	47.6	81.1
TL	98	95	99	98	80	95	98	99	98
DPD	99	95	99	94	97	87	99	99	99
CH	99	98	99	97	95	95	99	99	99
BLHT	10	23	63	0	1	99	91	99	99
STAB	95	98	98	99	71	96	99	95	99
A5	88	94	97	57	2	99	99	99	99
D5	98	96	92	98	52	98	99	99	99
P5	96	97	97	90	13	99	99	99	99
A6	78	90	95	40	1	98	98	99	99
D6	98	95	99	81	35	98	99	99	99
P6	94	95	99	65	6	99	99	99	99
FFDI	99	95	99	91	30/44	99	96	98	99
	Wangary 2	Perth	Bluegum Plantation	Perth Hills Complex (Hyden 12Z?)	Hovea	Murray-Sunset NP	Grose Valley (Wollemi)	Grose Valley (Wollemi)	Grose Valley (Wollemi)

Table A1 (continued)

Event No	41	42	33	34	35	43	44	44a	45
Date	20 Nov 2006	21 Nov 2006	10 Dec 2006	11 Dec 2006	19 Dec 2006	1 Dec 2006	10 Dec 2006	14 Dec 2006	11 Jan 2007
TL	15.4	14.6	15.6	14.4	14.3	13.8	15.6	14.7	15.3
DPD	22.9	18.2	18.6	18.1	14.5	17.0	23.8	23.7	25.3
HD	6	6	6	6	6	6	6	6	6
CH	11.5	10.3	10.9	10.2	9.0	9.6	11.8	11.3	11.9
BLHT	769	715	681	727	845	743	647	690	734
STAB	1.7	2.4	2.6	3.0	2.7	2.9	2.5	4.1	2.8
A5	-391	351	-484	-673	-838	-837	-398	-615	-520
D5	-840	1078	-1004	-1339	-1549	-1391	-991	-1872	-1435
P5	-1230	1429	-1488	-2012	-2386	-2228	-1389	-2488	-1955
A6	-164	105	-171	-272	-368	-375	-122	-205	-170
D6	-292	356	-596	-667	-749	-799	-492	-629	-498
P6	-456	462	-767	-938	-1117	-1174	-614	-833	-667
FFDI	76.5	103.4	30.6	46.2	39.9	48	47.9	60.6	63.3
TL	99	97	97	88	87	84	98	95	97
DPD	97	93	93	92	83	93	98	98	98
CH	99	97	97	94	88	94	99	99	99
BLHT	88	97	96	85	10	75	99	96	85
STAB	99	98	95	94	95	93	99	55	97
A5	98	99	97	90	80	86	99	95	98
D5	99	98	97	93	81	90	99	44	89
P5	99	99	99	94	83	92	99	80	97
A6	95	97	99	86	73	83	99	94	97
D6	99	99	95	91	87	82	98	95	98
P6	99	98	96	91	83	84	99	96	98
FFDI	99	99	93	98	96	99	98	99	99
	Little Desert (Horsham)	Casterton Complex (Horsham)	Billo Road #1	Billo Road #2	Mount David	Alpine Fires Ignition (SECOAST	Nevic (Tatong)	Nevic (Coopers Crek)	Nevic (Tawonga Gap)

Table A1 (continued)

Event No	61f	61i	61u	50
Date	10 Dec 2006	11 Dec 2006	14 Dec 2006 (00Z)	30 Dec 2007
TL	15.3	12.2	9.8	15.8
DPD	28.9	7.3	18.7	22.5
HD	6	5.0	5.0	6
CH	12.5	5.2	8.0	11.6
BLHT	985	713	938	645
STAB	2.1	5.9	4.0	4.1
A5	-1357	-874	-1906	-379
D5	-955	-2305	-1927	-1541
P5	-2312	-3179	-3884	-1919
A6	-864	-212	-1085	-89
D6	-406	-1287	-1072	-282
P6	-1271	-1499	-2158	-371
FFDI	20.0	29.5	23.9	55.5
TL	100	97	81	99
DPD	98	73	95	98
CH	100	86	97	99
BLHT	2	99	64	99
STAB	99	3	65	33
A5	86	99	39	95
D5	99	24	61	82
P5	98	82	47	91
A6	64	100	34	94
D6	99	96	72	99
P6	97	93	55	99
FFDI	98	99	99	99
	Scamander/St Mary's ignition	Scamander House loss	Four Mile Creek house loss	Boorabbin (Southern Cross)

Table A2. Pyrocumulus event parameters

Event No	25	2	3	4	5	6	7	8a	8
Date	25 Feb 1995	18 Jan 2001	22 Sep 2001	22 Dec 2001	25 Dec 2001	5 Dec 2002	17 Dec 2002	17 Jan 2003	18 Jan 2003
TL	16.2	15.1	11.2	13.8	15.2	14.7	15.0	16.7	15.4
DPD	20.0	11.7	5.9	13.7	15.1	14.5	29.4	33	22.6
HD	6	5	4	6	6	6	6	6	6
CH	11.4	8.4	4.6	8.5	9.6	9.2	12.4	13.8	11.5
BLHT	699	681	819	711	704	706	971	655	654
STAB	2.9	4.5	3.6	3.4	3.8	4.2	1.2	4.1	3.9
A5	-245	-528	-1069	-701	-554	-790	-626	-456	-358
D5	-1060	-1746	-1719	-1374	-1569	-1705	-686	-1639	-1530
P5	-1305	-2274	-2788	-2074	-2122	-2495	-1312	-2095	-1888
A6	-18	-111	-480	-278	-182	-291	-365	-94	-36
D6	-400	-740	-1044	-758	-510	-899	-250	-553	-526
P6	-418	-851	-1524	-1036	-692	-1191	-616	-648	-562
FDI	77*	53.3	8.1	18.9	94.1	44.4	46.2	55.0	80.7
TL	99	99	61	88	97	94	96	99	96
DPD	95	80	41	85	90	88	99	99	97
CH	99	93	69	89	94	93	99	99	98
BLHT	99	99	52	95	97	97	0.5	98	98
STAB	91	57	77	83	69	50	97	57	67
A5	99	96	71	92	96	88	90	98	99
D5	99	74	71	99	83	72	99	98	99
P5	99	90	73	94	93	84	99	92	96
A6	99	97	71	91	96	89	73	98	99
D6	99	86	60	88	97	76	99	96	96
P6	99	93	68	90	98	85	97	98	99
FDI	99	98	40	76	99	97	95	99	99
	BERRINGA (Sheoaks)	Dundas	Wollemi	Wollemi	Wollemi	Wollemi	Murraylands	Canberra	Canberra

Table A2 (continued)

Event No	9	10	11	12	13	14	15	16	17
Date	30 Jan 2003	24 Feb 2003	1 Dec 2004	17 Jan 2005	5 Feb 2005	22 Jan 2006	19 Sep 2006	21 Nov 2006	22 Nov 2006
TL	16.3	11.5	16.4	12.9	11.2	15.2	14.7	16.0	15.4
DPD	24.0	14.5	20.9	19.5	24.2	17.4	17.2	22.9	23.5
HD	6	6	6	6	6	6	6	6	6
CH	12.1	7.6	11.7	9.7	9.6	10.4	10.1	11.8	11.6
BLHT	628	738	667	927	823	918	675	643	642
STAB	4.9	5.2	3.4	2.3	2.9	2.3	2.6	2.8	2.0
A5	-550	-1391	-466	-851	-715	-622	-258	-265	-208
D5	-1867	-2137	-1369	-1343	-1438	-1666	-1012	-1018	-788
P5	-2418	-3528	-1835	-2194	-2152	-2288	-1268	-1283	-997
A6	-118	-622	-105	-406	-321	-225	-34	-52	-31
D6	-721	-1450	-735	-681	-480	-498	-383	-294	-312
P6	-839	-2072	-840	-1087	-801	-722	-417	-346	-343
FDI	94.3	15.8	39.9	30.2	57.5	53.9	117.1	47.6	81.1
TL	97	58	99	95	79	99	95	99	98
DPD	98	85	99	95	99	93	87	99	99
CH	99	81	99	98	97	98	95	99	99
BLHT	99	77	98	23	57	67	99	99	99
STAB	58	10	86	98	94	97	96	95	99
A5	97	29	99	94	90	98	99	99	99
D5	82	18	94	96	91	81	98	99	99
P5	97	20	98	97	92	94	99	99	99
A6	99	37	99	90	83	98	98	99	99
D6	98	7	92	95	96	97	98	99	99
P6	99	15	97	95	94	98	99	99	99
FDI	99	67	98	95	99	99	99	98	99
	SEcoast (lightning on smoke plume)	Nevic	Dorrigo	Perth	Dundas	Sheoaks	Murraylands	Wollemi	Wollemi

Table A2 (continued)

Event No	18	19	20	21	22	23	24
Date	29 Nov 2006	14 Dec 2006	15 Dec 2006	6 Jan 2007	6 Feb 2007	13 Sep 2007	22 May 2007
TL	12.1	14.7	14.7	14.5	12.4	15.0	5.8
DPD	26.1	23.7	13.7	14.9	18.8	15.0	26.7
HD	6	6	6	6	6	6	4
CH	10.4	11.3	8.8	9.2	9.4	9.5	7.4
BLHT	885	690	730	712	823	707	890
STAB	2.4	4.1	3.7	6	1.8	4.9	4.9
A5	-1028	-616	-606	-1310	-681	-721	-1982
D5	-1213	-1872	-1718	-2489	-832	-2239	-2113
P5	-2241	-2488	-2324	-3799	-1513	-2960	-4095
A6	-538	-205	-182	-504	-368	-227	-1093
D6	-762	-629	-616	-1521	-468	-679	-1259
P6	-1300	-883	-798	-2024	-836	-907	-2352
FDI	55.7	60.6	46.0	33.4	38.6	36.5	14.9
TL	65	94	93	93	72	65	18
DPD	99	98	85	87	96	40	99
CH	98	98	90	93	93	53	97
BLHT	11	96	91	91	9	71	86
STAB	97	59	72	2	99	40	20
A5	44	95	89	36	92	65	24
D5	96	44	67	80	99	33	65
P5	84	80	81	12	99	48	47
A6	27	94	88	56	78	63	19
D6	78	94	88	4	99	79	53
P6	58	95	90	18	97	75	33
FDI	99	99	97	95	97	88	82
	Pilliga	Nevic	Pilliga	Nevic	Nevic	Tanami	Bribie island

APPENDIX 2 – CASE STUDIES

These case studies are not complete studies of each event, and some are more comprehensive than others. In each case the primary focus was on the C-HAINES and the FFDI indices both for the day of, and through the lead-in period to, the fire. However, in some of the cases interesting aspects of the synoptic or sub-synoptic meteorology of the event have been presented as well. The selection of the cases was not based on uniform criteria. Some are included because they have some formal, and available, documentation, while others were suggested because of anecdotal or documented unexpected fire activity.

At the end of each case-study summary points are made in italics, and it is these points which were used to develop the "case study summary" section in the main body of this report. In the discussions to follow, a mix of date-time conventions is used. If the discussion is primarily focussed on NWP model data, the UTC is the preferred convention, as that is the time convention used to "tag" the model data. If the primary discussion is focussed on observations, or on fire behaviour, then local time is used.

When referring to ranges of FFDI, capitalised descriptors such as "Very High" and "Extreme" refer to the fire danger ratings used in Australia prior to the 2009-10 summer, while in lower case refer to qualitative measures of their scale in terms of their statistical distribution.

The first 11 cases are included in the statistical analysis presented in the first part of this report, and listed in Tables 1 and 2. Cases 12 and 13 were included later in the process of this study as they included unusual night-time fire activity.

The cases are:

A.1 The Bluegum Plantation fire

A.2 The Billo Road fire

A.3 The Randall Block (Perth Hills) fire – 15 October 2005

A.4 The Hovea fire

A.5 The Pickering Brook (Perth Hills) fire

A.6 The Denbarker Block fire

A.7 The Lake Tay fire

A.8 The Big Desert Fire of December 2002

A.9 Victorian Fires 2006-2007

A.10 The Scamander/St Mary's fire

A.11 The Berringa fire

A.12 The Mt. Cooke fire

A.13 The Cobaw Ridge prescribed fire

A.1 The Bluegum Plantation Fire

This case was a single-day fire event on 23 March 2005, and has been reported by McCaw and Smith (2008), who drew attention to the unusual/unexpected degree of crown-fire activity observed, and to an observed dramatic fall in near-surface humidity during the afternoon which contributed to higher than usual values of fire danger index. McCaw and Smith (2008) noted that the degree of crown-fire activity was greater than that experienced in previous bluegum plantation fires under Extreme FFDI conditions, and attributed this to the increased litter load in this slightly older plantation.

Figure A1.1 shows the scatter plot of FFDI versus C-HAINES for Bridgetown (point 3 in Fig. 1) for the dependent 0600 UTC climatology used in this report, with the afternoon of 23 March 2005 highlighted. While the statistics shown in Table A1 would suggest that there is little discrimination between the FFDI and the C-HAINES in this case, both being beyond the 99th percentile, Fig. A1.1 shows that the value of C-HAINES was the highest at the Bridgetown gridpoint in the eight years of the data set, perhaps indicating that, in addition to the factors proposed by McCaw and Smith (2008) the fire activity may have been exacerbated by the factors highlighted by C-HAINES environment of the day.

Figure A1.2 shows the time-series of 0600 UTC FFDI and C-HAINES for several days before and after the day of the fire, and while the day of the fire activity was the day on which both these parameters were at their greatest, the previous day also showed very large values of C-HAINES and FFDI. Figure A1.3 shows that the diurnal cycle of relative humidity was relatively normal at Bridgetown in the days leading up to the fire, and indeed reached over 90% overnight before the fire. The very abrupt decrease in dewpoint around 2300 UTC 22 March (0800 WST 23 March) is, however, very like the “abrupt surface drying” behaviour described by Mills (2008b), and several of the ingredients described in that paper were present on this day. However, as pointed out by McCaw and Smith (2008), at Manjimup there is an abrupt decrease in dewpoint and relative humidity beginning at about around 1500 UTC (2300 WST) 22 March (also Fig. A1.3), against the normal diurnal trend. Figure A1.4 shows the 6-hourly time series of C-HAINES, and it is seen that this increases very rapidly from 1200 UTC 21 March, and from 1800 UTC 21 March until 24 March remains far above the 95th percentile value. While there is no lower than normal relative humidity at Manjimup in association with the high values of C-HAINES on the night of 21-22 March, there is a dramatic association on the night of 22-23 March.

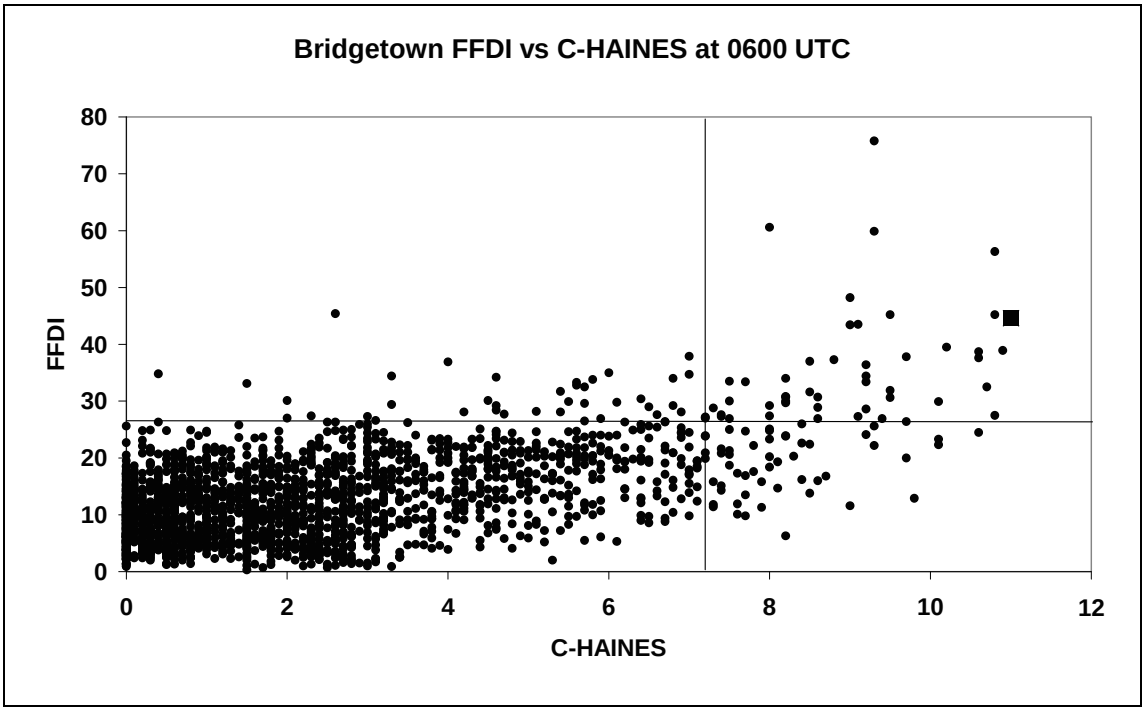

Figure A1.1. Scatterplot of FFDI vs C-HAINES for the “Bridgetown” gridpoint at 0600 UTC for the 8-year climatology in this report. The lines show the 95th percentile values of C-HAINES and FFDI respectively, and the highlighted point is that of 23 March 2005.

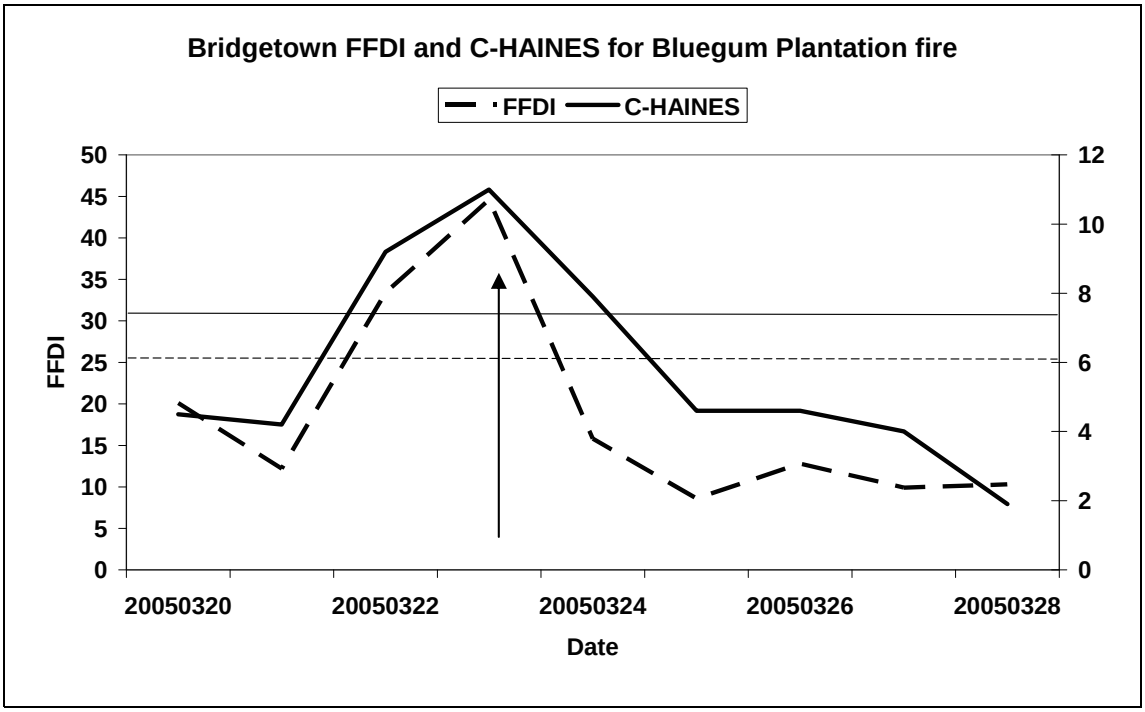

Figure A1.2. Time series of daily FFDI (dashed) and 0600 UTC C-HAINES (solid) from 20 to 28 March 2005 at the “Bridgetown” gridpoint. The horizontal lines indicate the 95th percentile values for the two parameters, and the arrow indicates the fire activity day.

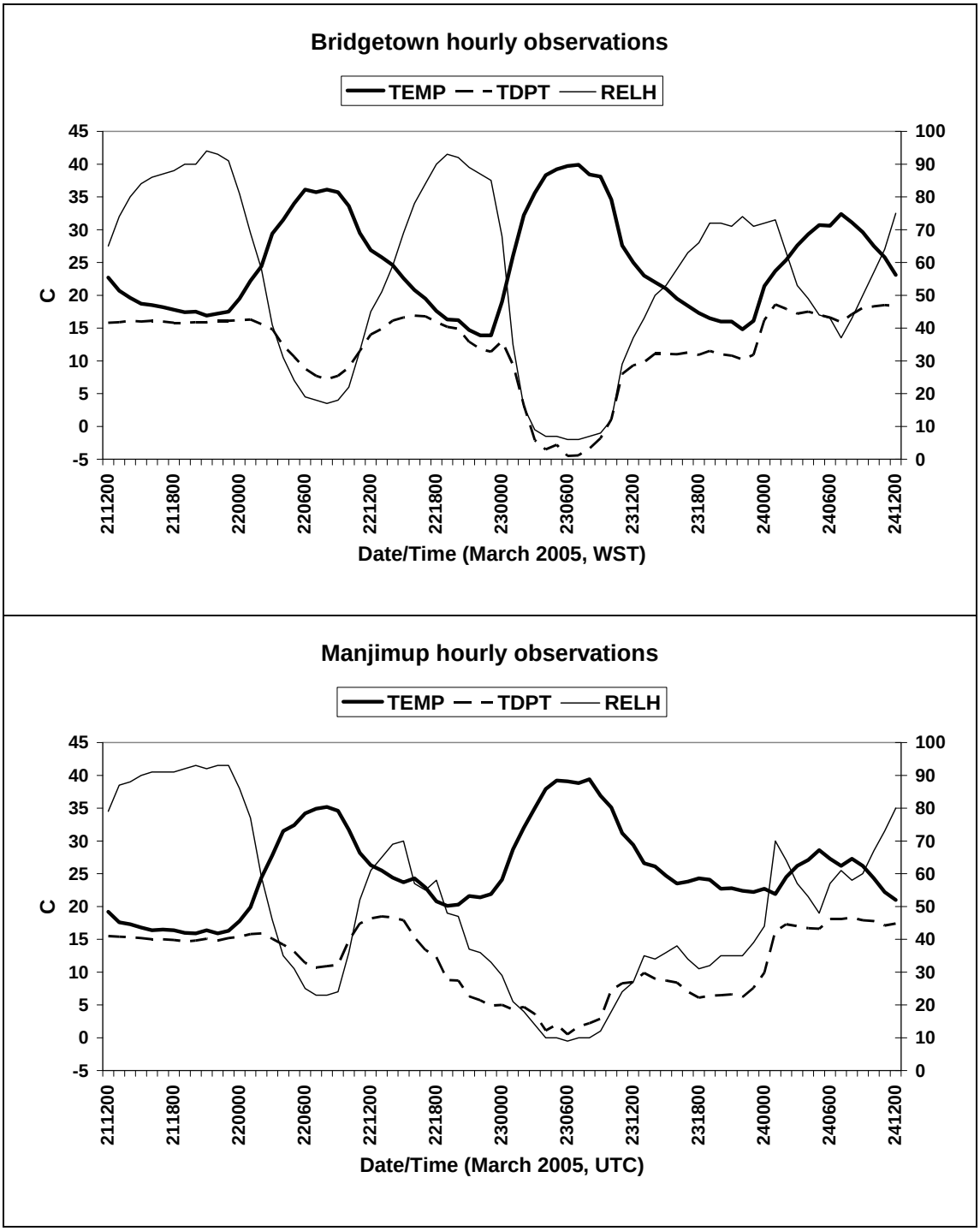

Figure. A1.3. Hourly AWS observations from the Bridgetown and Manjimup AWS from 1200 UTC 21 March to 1200 UTC 24 March 2005.

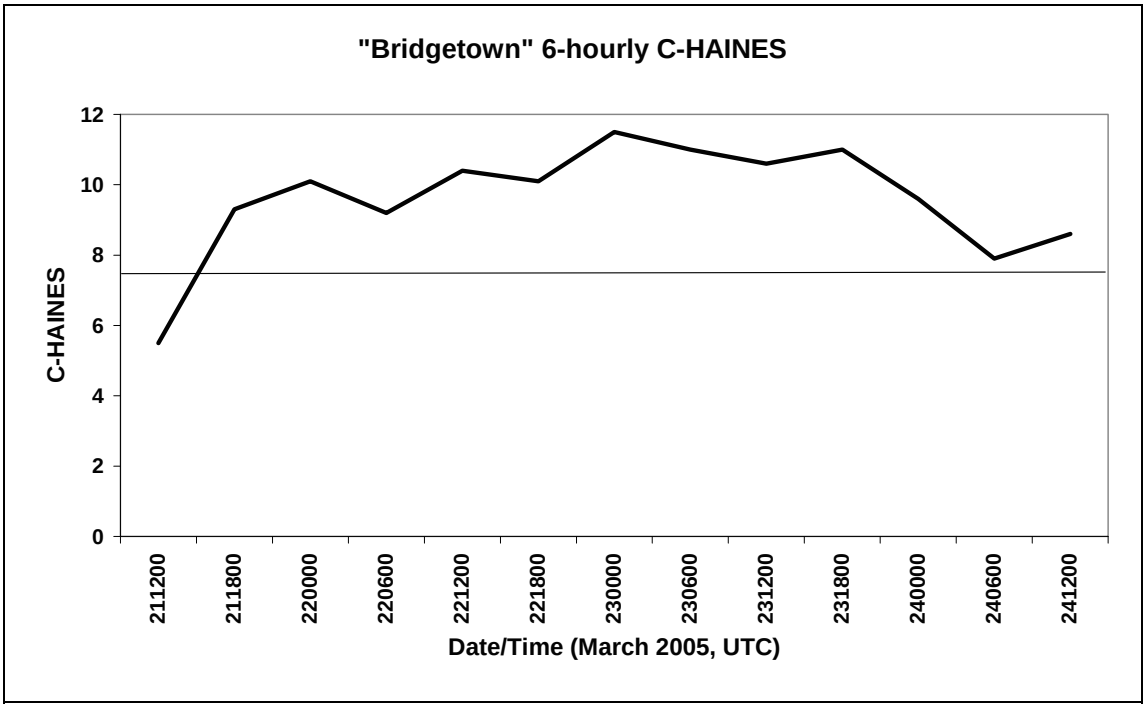

Figure A1.4. Time-series of 6-hourly C-HAINES from 1200 UTC 21 March 2005 to 1200 UTC 24 March 2005. The horizontal line indicates the 95th percentile value for the C-HAINES at 0600 UTC.

The broad synoptic patterns of the indices seen in Figs. 8 and 11 suggest useful spatial discrimination of the instability indices, Figs A1.5 and A1.6 show higher time and spatial resolution forecast patterns. Figure A1.5 shows the screen-level potential temperature and low-level wind forecasts at 0000, 0500, and 0800 UTC, and the GFDI (GFDI is used for the Bureau's fire weather warnings in WA) forecasts (assuming 100% curing) at the same times. At 0000 UTC (1200 WST) north-north-easterly winds cover the South-west Land Division of WA, with a trough-line paralleling the western coast some 0.5o to 1o longitude offshore. The highest GFDI values at this time are in the areas of strongest north-easterly winds north of Perth and near Mt Barker. By 0500 UTC (1700 WST) the coastal convergence zone had focussed along the coast, responding to the diurnal heating of the land-mass, and apart from the far south-west, where winds from the north-north-west were producing slightly lower temperatures and higher humidities, GFDI values were well into the Very High (>32 in WA) range. By 0800 UTC (2000 WST) the higher GFDI values had extended into the southern parts of the South-west District, while the west-coast trough was beginning to move inland. The wind change reached Manjimup at 1800 WST.

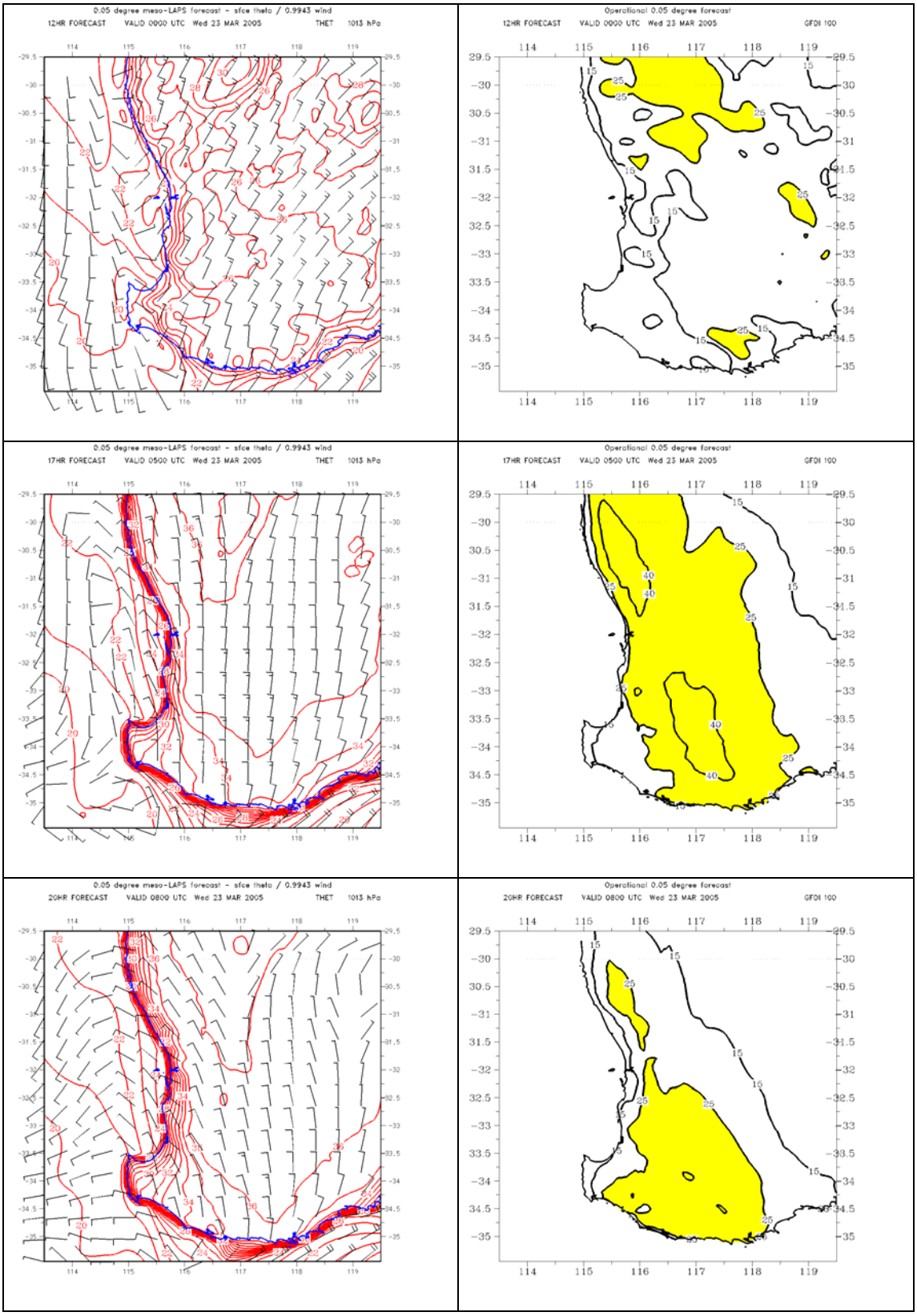

Figure A1.5. Left panels: forecast screen-level potential temperature and 70m wind barbs at 0000, 0500, and 0800 UTC 23 March 2005 from the 0.05^{o} grid-spacing meso-LAPS forecast. Right panels: forecast GFDI (assuming 100% curing) at same times.

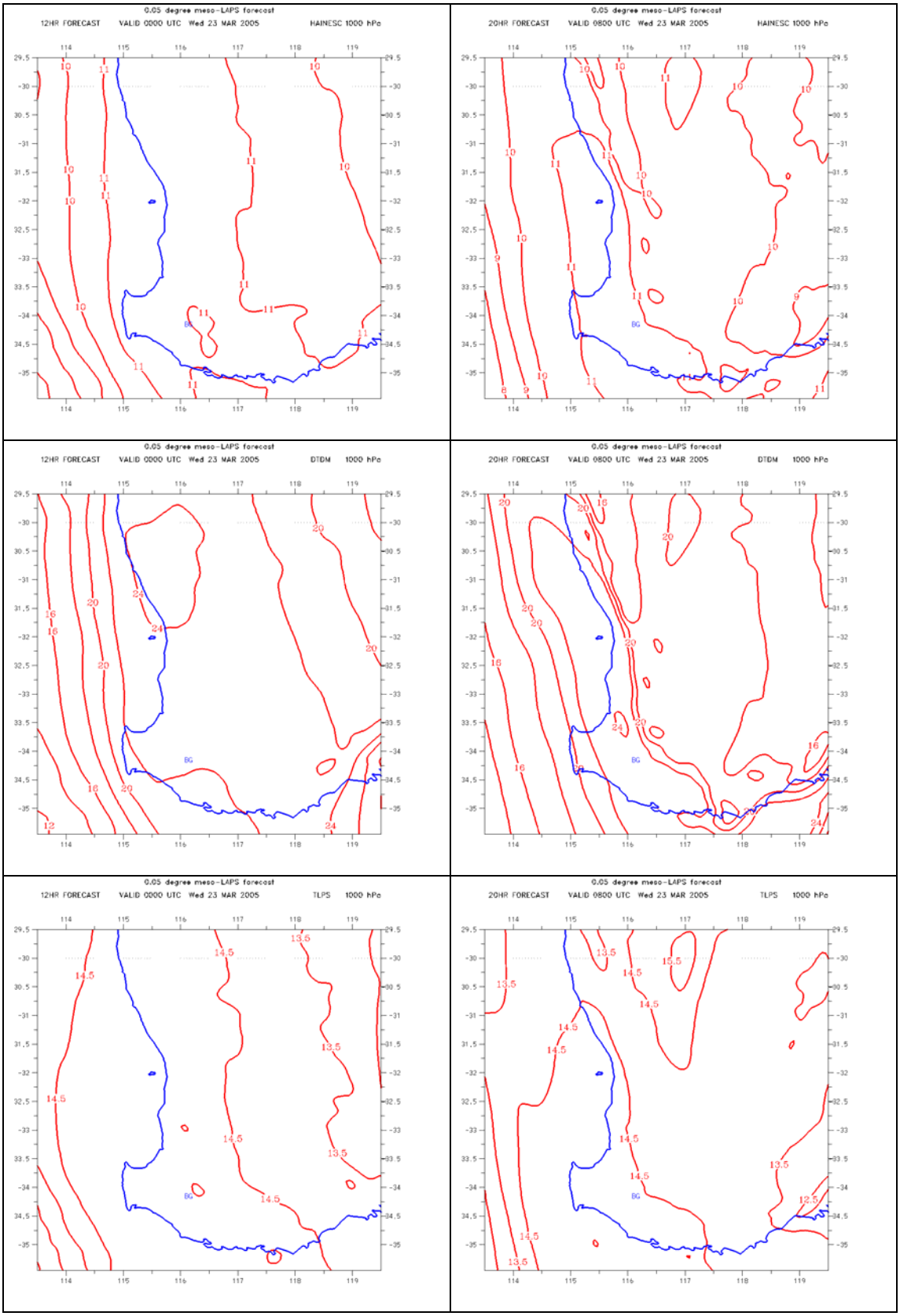

Figure A1.6. Top row: C-HAINES forecasts from the 0.05^{o} grid spacing mesoLAPS forecast for 0000 and 0800 UTC 23 March 2005. Middle and bottom rows show the corresponding 850 hPa dewpoint depression and 850-700 hPa lapse rate forecasts.

Figure A1.6 shows the forecast C-HAINES distribution at 0000 and 0800 UTC, together with the dewpoint depression and temperature lapse ingredients at the same times. A broad, north-south oriented zone of C-HAINES>11 is seen at both times, although it narrows and contracts slightly south-westwards with time. The dewpoint depression field is perhaps the most instructive here, with a tongue of very dry air extending southwards to be almost directly over the fire location at 0800 UTC. Note that, while the climatology above was based on LAPS analyses, and these fields are much higher resolution forecasts, C-HAINES values greater than 11 are essentially unknown near Bridgetown in the 8-year data set used for the climatological analysis.

C-HAINES values on the day of fire were extra-ordinarily high, providing perhaps some alert of unusual behaviour, although FFDI/GFDI may well have indicated fire activity sufficient to cause crown fires.

C-HAINES was extra-ordinarily high for 2 days prior to the fire, and showed essentially no diurnal variation. While there was no association between the high C-HAINES and low overnight relative humidity at the Bridgetown AWS, there was an association with the Manjimup observations. Which of these sets of observations was more representative of the conditions at the fire cannot be determined, but the evidence is sufficient to suggest that there may have been a pre-conditioning of the fuels due to low overnight relative humidity before the day of the fire.

Using C-HAINES as a forecast alert, but then "drilling down" to the ingredients would have indicated the narrow very dry band of air that was perhaps the crucial factor in this event. This is an example of the overlaps between "Haines" concepts and other physical processes, such as the abrupt surface drying concepts described in Mills (2008a,b).

The narrow dry band extending north-north-west/south-south-east along the coastline is interesting, and investigations of the dynamics and structure of west-coast trough changes should consider this feature, particularly as it is also evident in other case studies in this Appendix.

A.2 The Billo Road and the Mount David Fire

The Billo Road Fire

Over 10000 ha of pine forest near Tumut, NSW was burnt between 10 and 14 December 2006, and aspects of the behaviour of this fire were reported by Cruz and Plucinski (2007), hereafter CP. Following an arson ignition overnight on 9-10 December, CP state that 3 major fire runs on the first two days contributed the majority of the area burnt. Two of these runs were on the afternoons of 10 and 11 December, and a separate run occurred between 2100 and 2400 hours (local time) on 10 December. CP note that the fire behaviour was not well predicted by the McArthur FFDI, but that improved behaviour predictions for the daytime fire-runs were obtained using the Canadian fire behaviour models. CP attributed this to the latter being developed for vegetation types that are more typical of the dominant fuel type in this forest (radiata pine). However, CP also showed that none of the fire danger indices tested predicted the rates of spread during the second (overnight) fire run particularly well, and drew attention to the antecedent extreme and sustained drought that had led to dead fuels being extremely dry.

The 0600 UTC FFDI/C-HAINES scatter plot for the Canberra gridpoint (point 28 in Fig. 1) of the 8-year climatology prepared in this paper (Fig. A2.1), and the time-series of 0600 UTC FFDI and C-HAINES through the lead-up period to the fire ignition and extending beyond the day of the Mt David fire (Fig. A2.2) show that for both of the afternoon fire runs, C-HAINES values were around or slightly above the 95th percentile value. On the 10th the FFDI was below its 95th percentile, but well above that value on the 11th. It is also interesting to note the sustained period of high afternoon values of C-HAINES (Fig. A2.2) prior to the ignition day. However, in contrast to some other case studies in this series, Fig. A2.3 shows that there is a definite diurnal cycle in C-HAINES until the night of the 10-11 December (the night of the second major fire run) when C-HAINES remained above its 95th (0600 UTC) percentile value overnight. The Canberra Airport AWS data (Fig. A2.4) show a regular diurnal cycle in relative humidity until the night of 10-11 December when unusually low relative humidity was observed. This was driven partly by higher overnight temperatures, but more strongly by lower than usual dewpoints. (It must be remembered that there is considerable topographic relief between Canberra Airport and Billo Road (near Tumut), so the possibility that the Canberra AWS data may not be representative of conditions at the fire site must be recognised.)

There are two interesting, if perhaps tangential, points to make here:

Canberra and its surrounding stations do show a climatological tendency for the highest C-HAINES values to occur at 0600 UTC (Fig. 7), in contrast to many other areas that showed very little systematic variation. Reasons for this type of behaviour are worth further investigation.

Figure A2.4 shows interesting abrupt reductions in relative humidity on the afternoons of 5, 7, 8, and 9 December, akin to those discussed in Mills (2005, 2007, 2008a, 2008b).

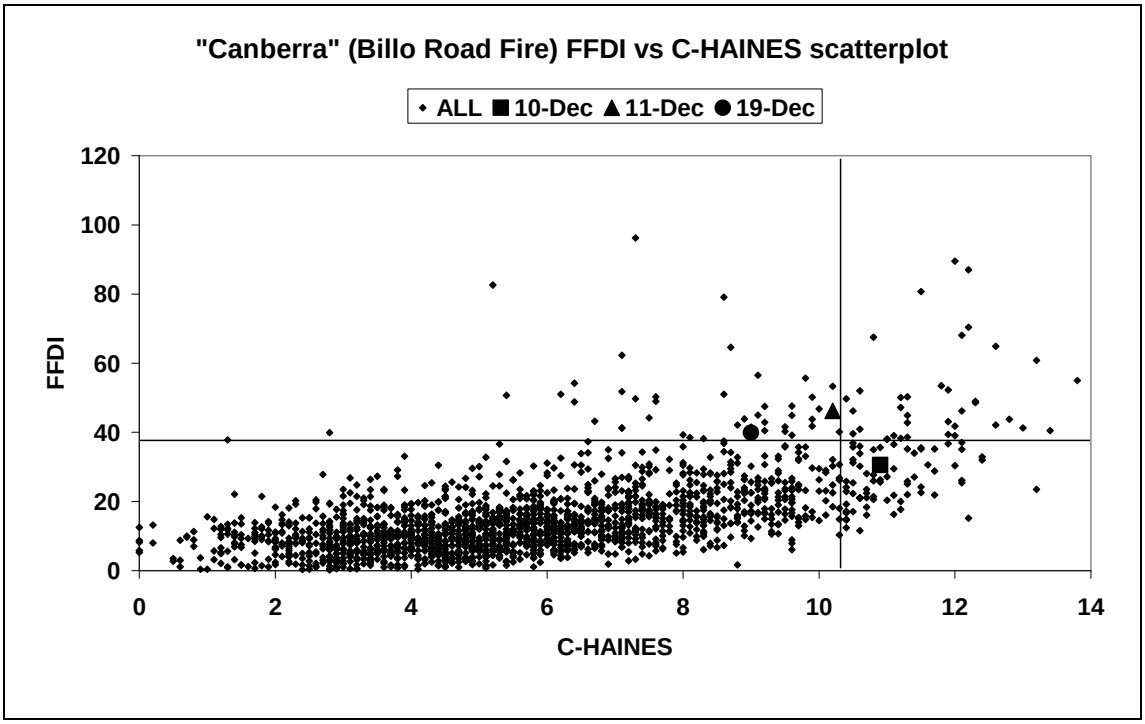

Figure A2.1. Scatterplot of FFDI vs C-HAINES for the “Canberra” gridpoint at 0600 UTC for the 8-year climatology in this report. The lines show the 95th percentile values of C-HAINES and FFDI respectively, and the highlighted points are for the days of major fire activity at Billo Road and Mt. David.

.

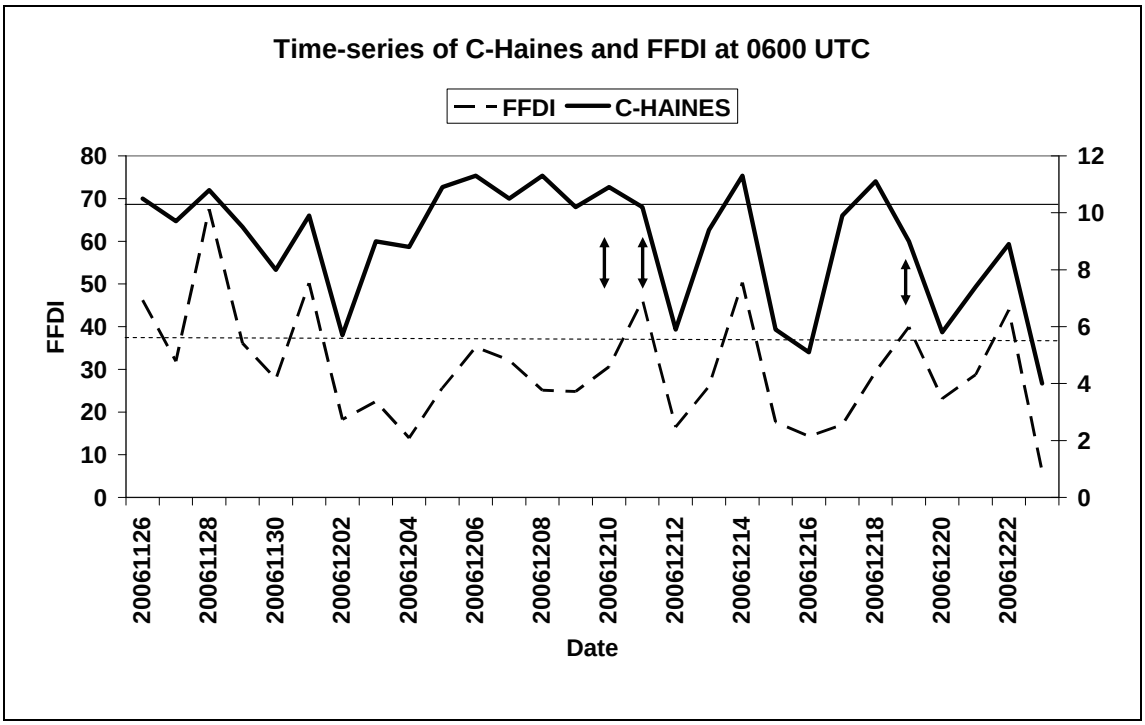

Figure A2.2. Time series of daily FFDI (dashed) and 0600 UTC C-HAINES (solid) from 26 November to 23 December 2006 at the “Canberra” gridpoint. The horizontal lines indicate the 95th percentile values for the two parameters, and the arrows indicate the fire activity days.

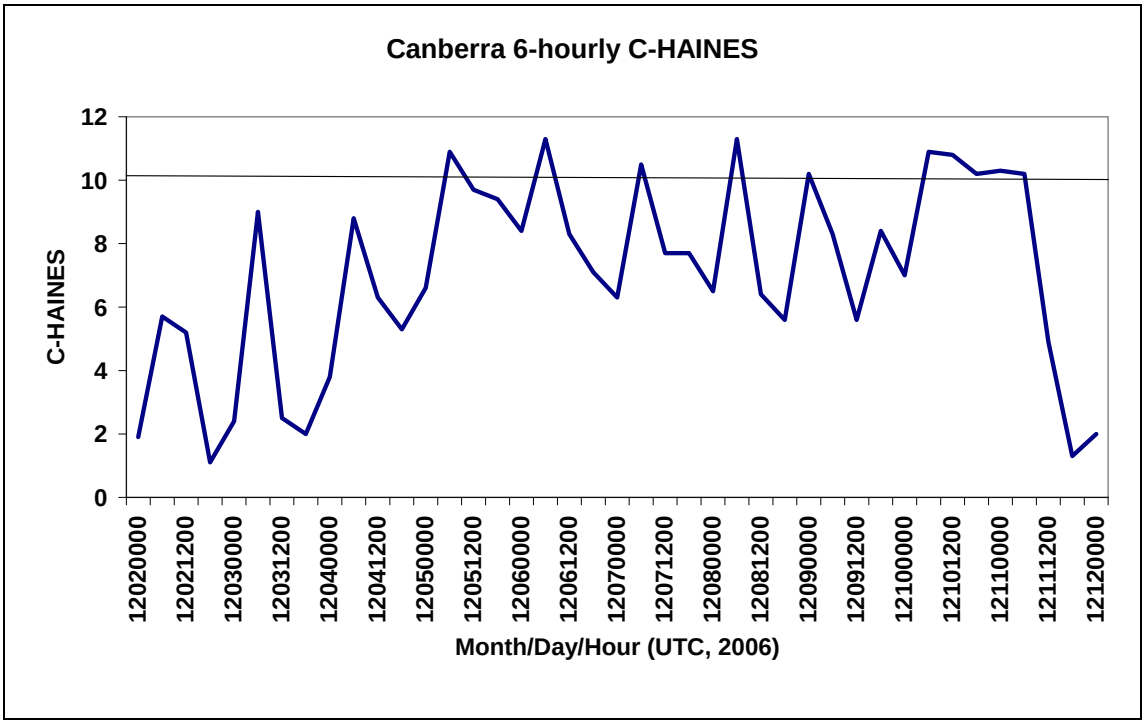

Figure A2.3. Time-series of 6-hourly C-HAINES from 0000 UTC 2 December to 0000 UTC 12 December 2006 at the "Canberra" gridpoint. The horizontal line shows the 95th percentile value of the 0600 UTC C-HAINES.

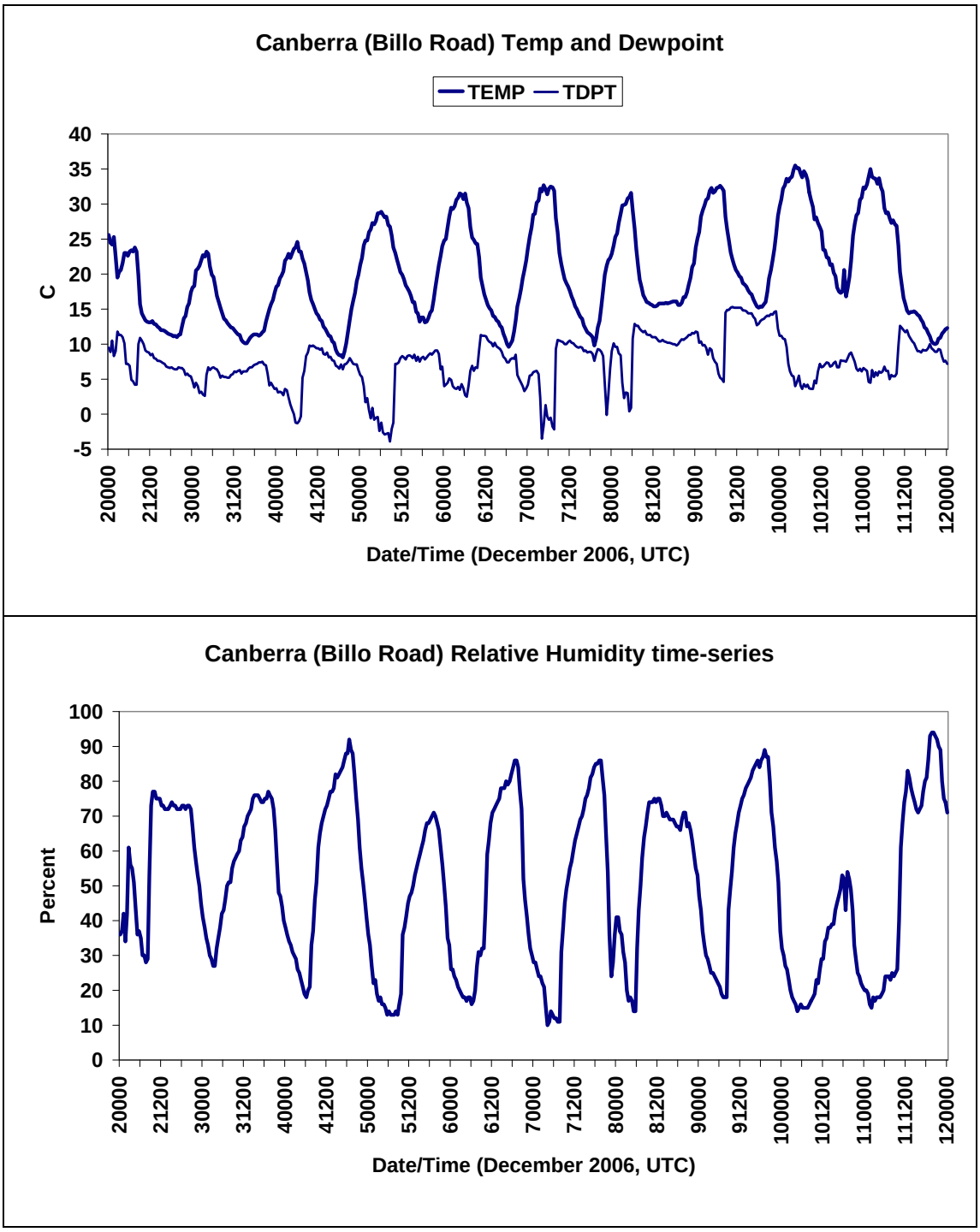

Figure A2.4. Time series of Canberra Airport AWS data from 0000 UTC 2 December to 0000 UTC 12 December 2006. Upper panel temperature (thick lines) and dewpoint (thin lines) in C, lower panel relative humidity (percent).

Figure A2.5 shows the MSLP/low level wind and the FFDI forecasts from the meso-LAPS125 operational forecast for 0300, 0900, and 1500 UTC 10 December 2006. A pressure trough with associated wind change ahead of a deeper cold-frontal wind change was moving north-eastwards through Victoria and into southern NSW during this period, with evidence of blocking of the change by the Victorian topography. Extreme FFDI was forecast during the daytime hours, with the gradient to lower values on the south-west side a result of the major cold front, rather than the pressure trough change that preceded it. The band of highest FFDI can be seen moving north-eastwards, but moderating during the night.

Figure A2.6 shows the C-HAINES forecasts for the same time, and the progression of a band of high C-HAINES north-eastwards matches the progression of the band of maximum FFDI. There are two notable things here, though. First, the band of highest C-HAINES lies south of Canberra at 0600 UTC, so the climatological extremity of the data point for that afternoon in Fig. A2.1 probably under-represents the extreme that affected the fireground, and, second, the band of highest C-HAINES moves over the fire-ground in the hours up to 1500 UTC, roughly when the overnight fire run occurred, and, as shown in Fig. A2.3, the C-HAINES field does not weaken overnight as does the FFDI.

Figure A2.7 shows the TL and DPD ingredient fields for C-HAINES at 0900 UTC. While there is a very large area of essentially dry-adiabatic lapse rate over all of northern and eastern Victoria, and over most of NSW, the band of driest air is rather narrower and overlaps the southern portion of the area of steep lapse rates. This causes the focus of the highest C-HAINES values to be in this region. This band of very dry air moved across the fire ground in the hours to midnight.

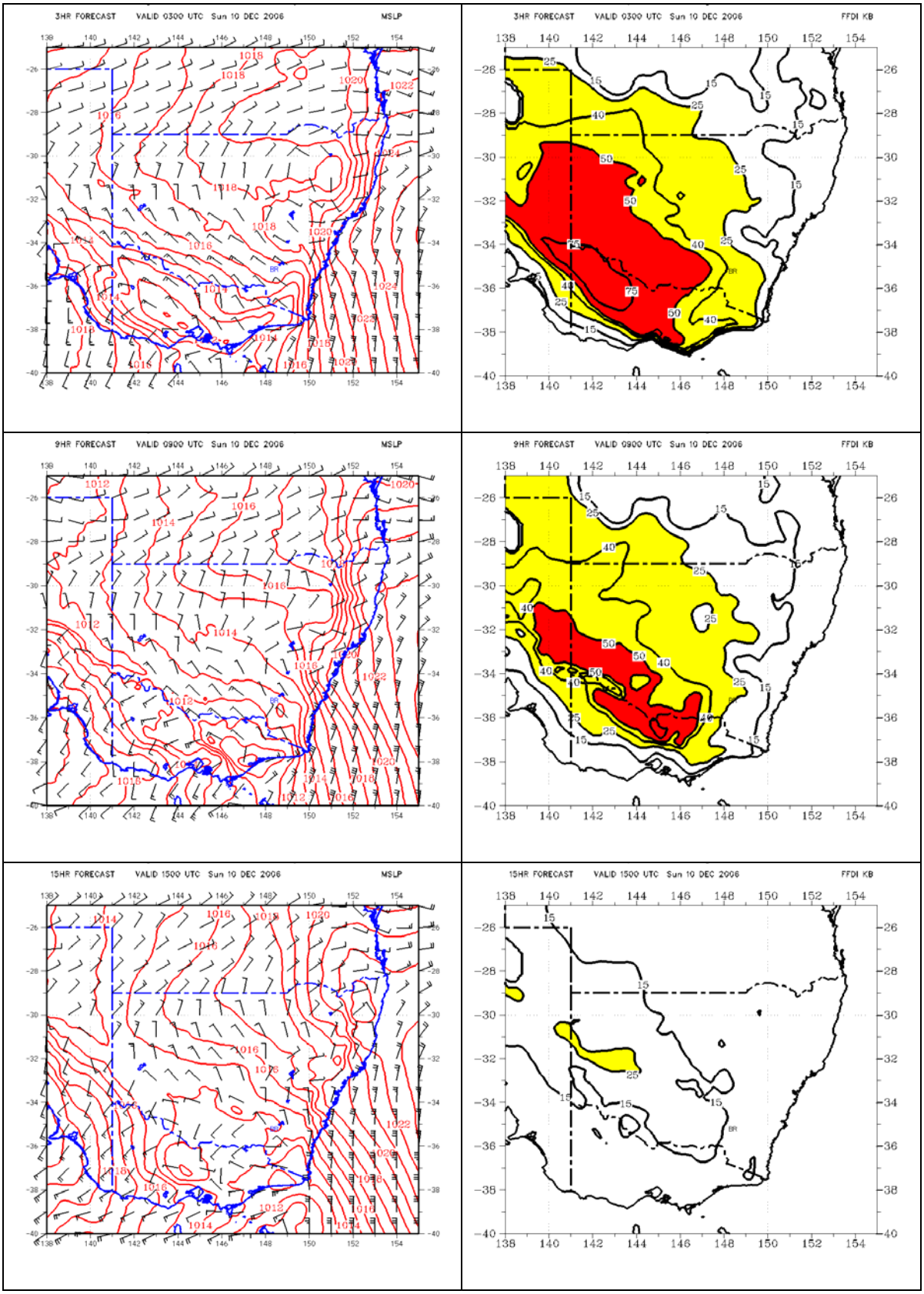

Figure A2.5. MSLP and 70m wind field forecasts (left panels) and FFDI forecasts (right panels) from the operational meso-LAPS125 NWP model forecast for 0300, 0900, and 1500 UTC 10 December 2006.

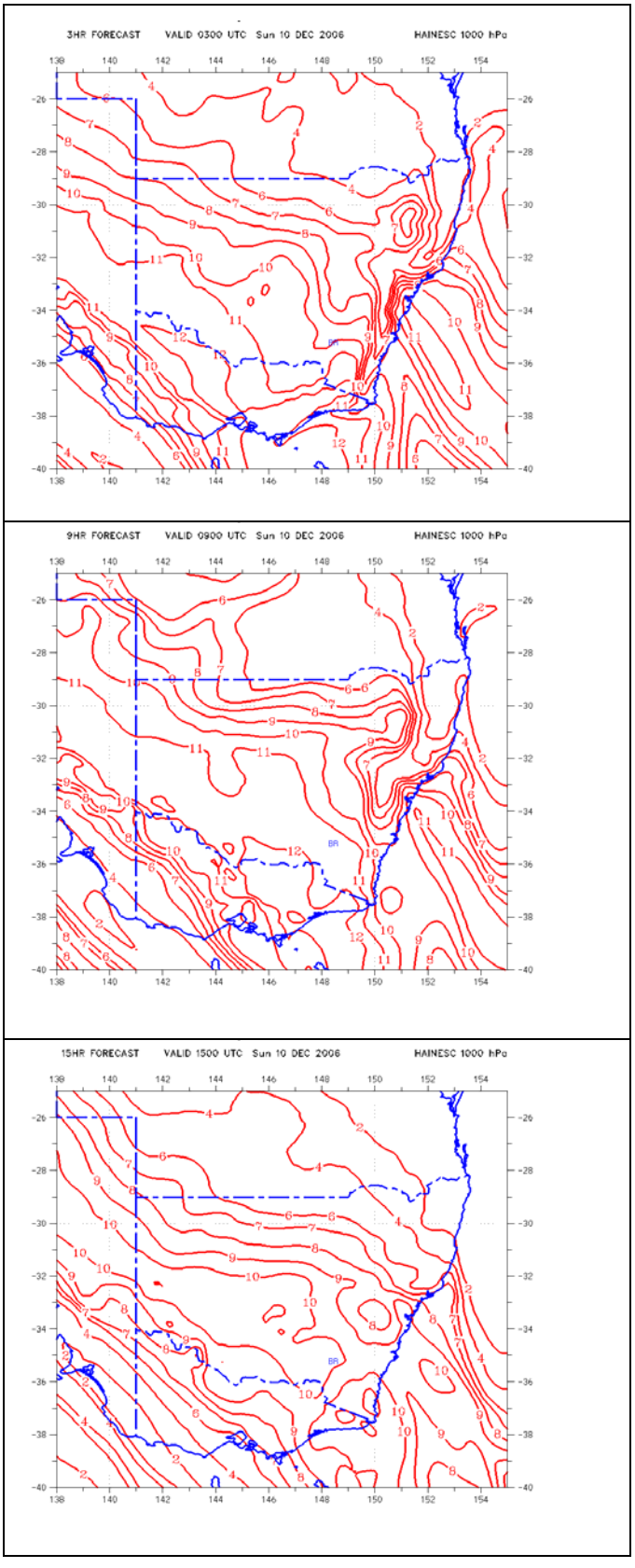

Figure A2.6. Forecasts of C-HAINES from the operational meso-LAPS125 NWP model forecast valid at 0300, 0900, and 1500 UTC 10 December 2006.

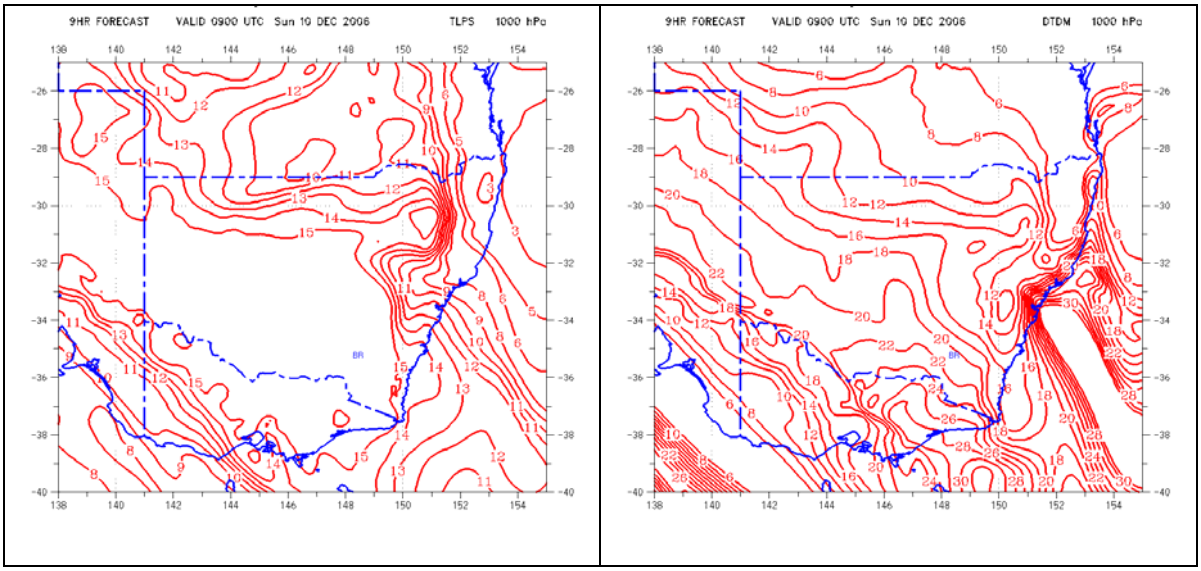

Figure A2.7. Forecasts of the 850-700 hPa lapse rate (C, left) and 850 hPa dewpoint depression (right, C) valid at 0900 UTC 10 December 2006.

On the day of 11 December, when, driven by a sustained increase in wind speed following a shift to westerly winds (CP, Page55), a major fire run occurred between 1400 and 1900 EDST, the screen-level temperature and wind fields from meso-LAPS125 fields show the cool change moving strongly into NSW (Fig. A2.8). A sustained area of strong winds following the change maintained large areas of forecast FFDI>40. The distortion of the change due to the effects of the south-eastern Australian topography is evident, meaning that in the area of Billo Road higher temperatures were maintained for much of the day. The C-HAINES fields show the maximum C-HAINES zone moving north-eastwards across NSW, and being very high over Billo Road early in the day, but decreasing with time.

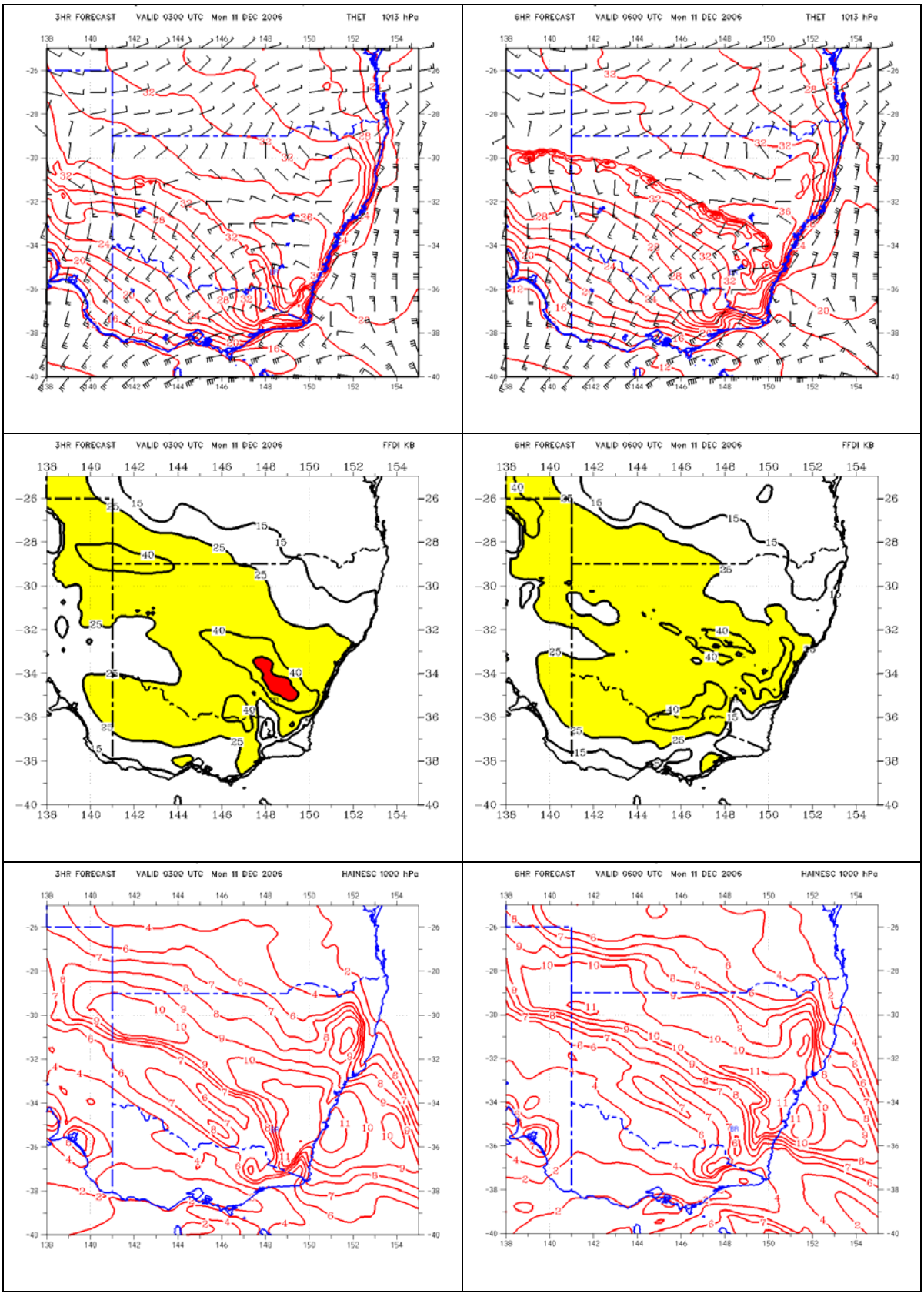

Figure A2.8. MSLP and 70m wind field forecasts (top panels), FFDI forecasts (middle panels), and C-HAINES forecasts (bottom panels) valid at 0300 and 0600 UTC 11 December 2006 from the operational meso-LAPS125 NWP model forecast.

The high values of C-HAINES during the daytime fire runs are unusual, but given that very high values of FFDI were also experienced at these times, it is not necessarily evident that the C-HAINES would be an aid to discriminating the enhanced fire activity during these phases of the event. However, the very high C-HAINES band (with very dry air) moving over the fireground overnight may be a potential forecast aid.

It should perhaps be noted that the high overnight C-HAINES values may not have only indicated increased overnight fire activity, but may have also indicated a weaker overnight recovery of fuel moisture than would otherwise have been the case, leading to enhanced fire activity on the 11 December.

It is of interest for future research to understand those particular features of the C-HAINES that associate with weak overnight relative humidity recovery, so that the physical processes can be understood in the context of the underlying meteorology.

The Mount David Fire

CP also discuss the behaviour of a fire in a pine plantation at Mt David, some 50 km south of Bathurst on 19 December 2006. The fire burnt actively during the day under Very High FFDI conditions, and continued to spread after an easterly change that arrived on the fire-ground around 1500 EDST. CP emphasised two particular aspects of this case – the lack of a preceding overnight recovery in the relative humidity, predisposing the fuels to be extra-ordinarily dry, and the afternoon spread of the fire under westerly winds.

First, referring to Figs. A2.1 and A2.2, the FFDI was above its 95th percentile on the 19 December, while the C-HAINES was a little below its 90th percentile (Table A1). Figure A2.2 shows, though, that there was a period of very high C-HAINES for two days before the fire, including the previous night.

Figure A2.9 shows the overnight (1800 UTC) forecast fields of MSLP overlaid with low level wind barbs, the C-HAINES field, and the temperature lapse and dewpoint depression ingredient fields. A cool change was moving northward along the southern NSW coastline, and also moving inland into southern NSW, but the Australian Alps were blocking the change from affecting the Southern and Central Tablelands. A maximum in the C-HAINES field, oriented just ahead of the advancing change, stretched across NSW, and was approaching the Mt David area. The C-HAINES ingredients show tongues of high temperature lapse, and also high dewpoint depression contributing to the C-HAINES maximum, with the band of high dewpoint depression being just slightly south of the band of high temperature lapse.

Figure A2.10 demonstrates the situation on the afternoon of 19 December. By 0300 UTC westerly winds had penetrated to the fire area, and an easterly change was developing on the eastern side of the NSW divide, in an almost classic example of the process described by Mills (2007). Very High values of FFDI, reaching above 40 across central NSW by 0600 UTC are seen, as well as a band of extremely high C-HAINES. It is also seen in CP that there were very low relative humidities observed at their AWS station prior to the arrival of the easterly change (which they refer to as a "sea-breeze"). The abrupt reduction in relative humidity immediately before the easterly change is a regular feature in these situations, as described by Mills (2005, 2007). Figure A2.11 demonstrates this in a different way, with the Bathurst Airport AWS data showing the relative humidity responding almost solely to the temperature during the 18 December (very little variation in dewpoint), but responding strongly on the 19th to an abrupt reduction in dewpoint in the two hours after 2200 UTC 18 December (0900 EDST 19 December), before abruptly increasing with the arrival of the easterly change between 0530 and 0600 UTC 19 December.

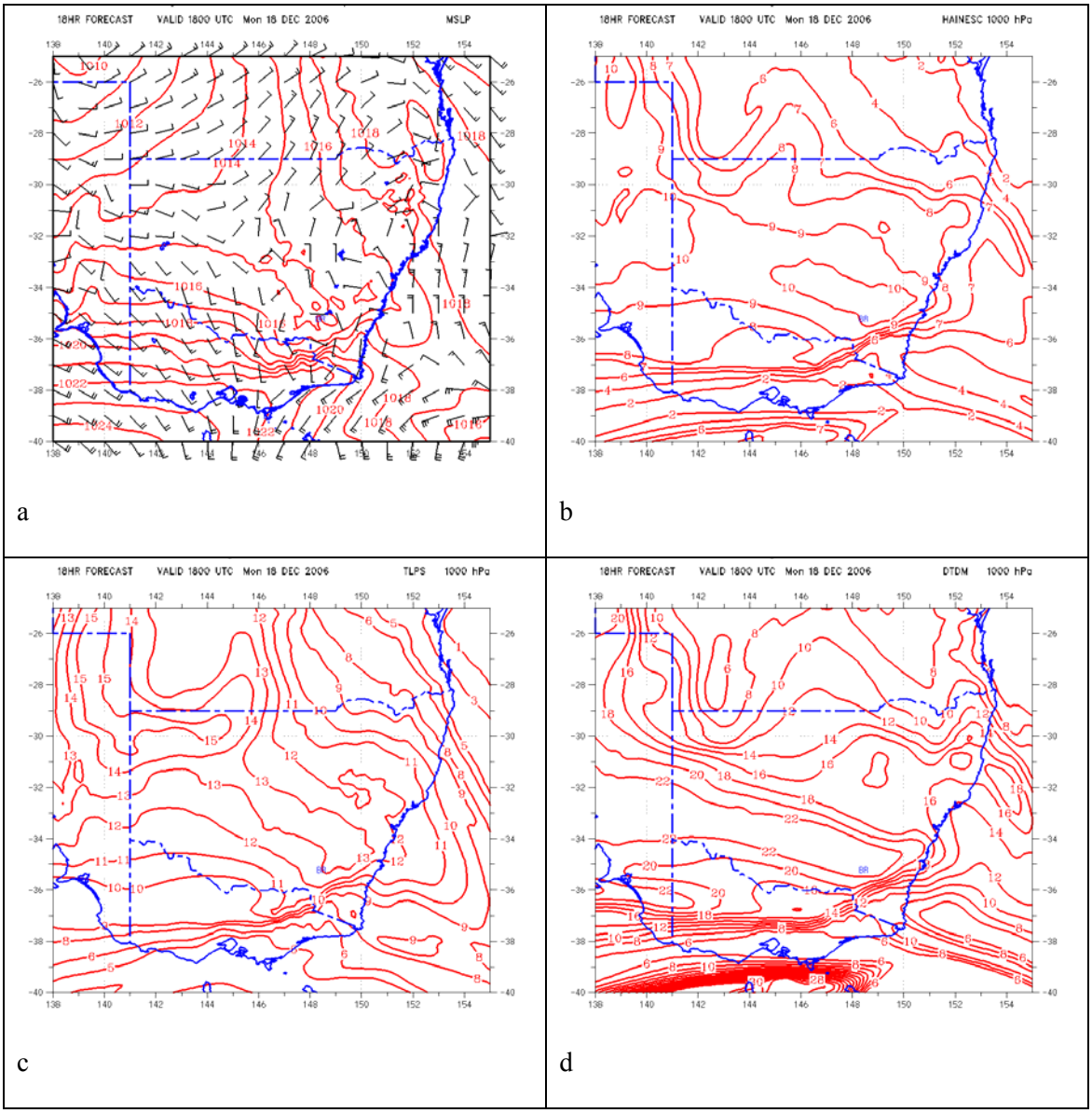

Figure A2.9. Forecast fields valid at 1800 UTC 18 December 2006 from the operational meso-LAPS125 model. (a) MSLP and 70m wind fields, (b) C-HAINES, (c) 850-700 hPa temperature lapse (K), and (d) 850 hPa dewpoint depression (K).

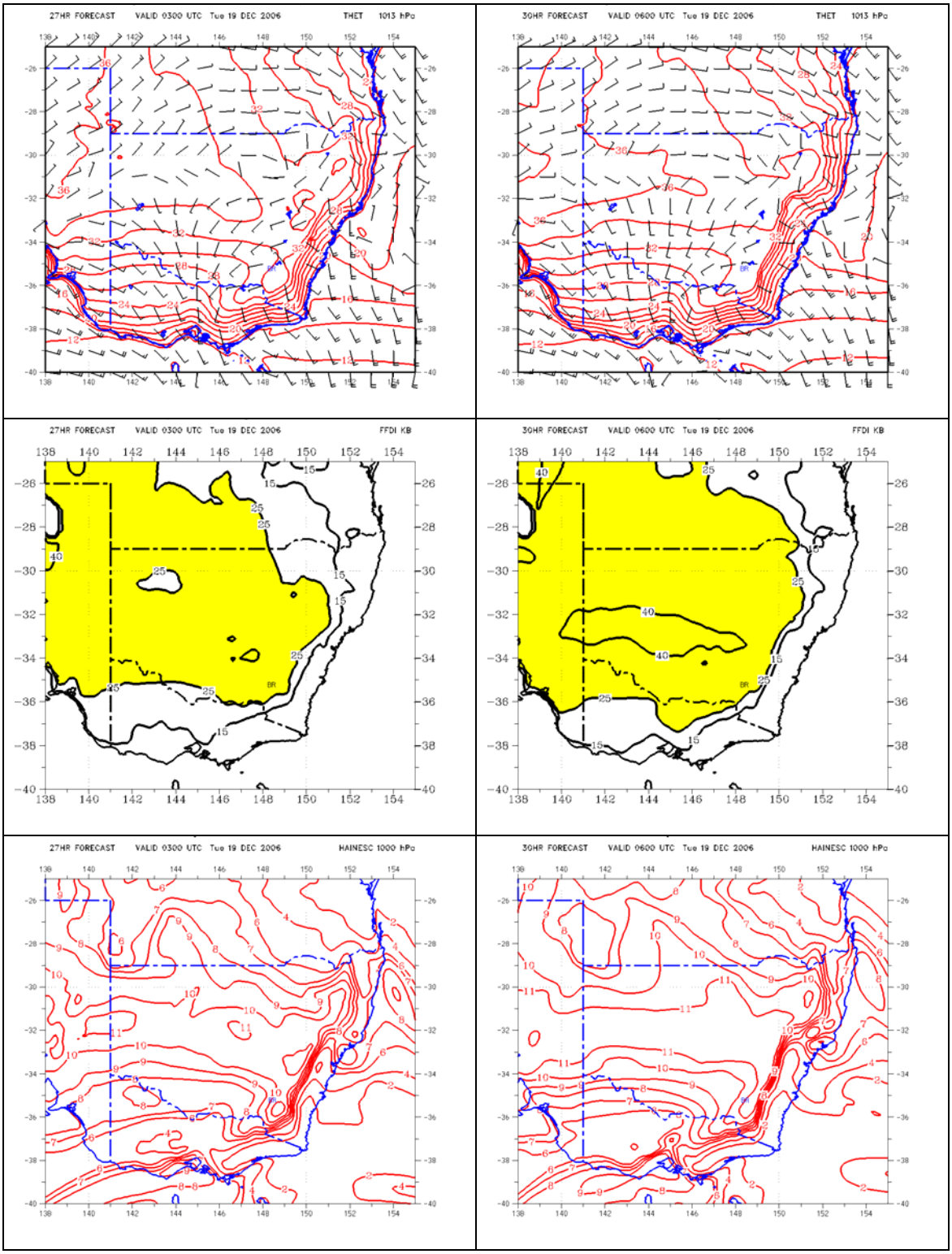

Figure A2.10. Upper panels –MSLP and 70m wind forecasts from the operational meso-LAPS125 model. Middle panels – FFDI forecasts. Lower panels – C-HAINES forecasts. Forecasts are valid at 0300 (left column) and 0600 (right column) UTC 19 December 2006.

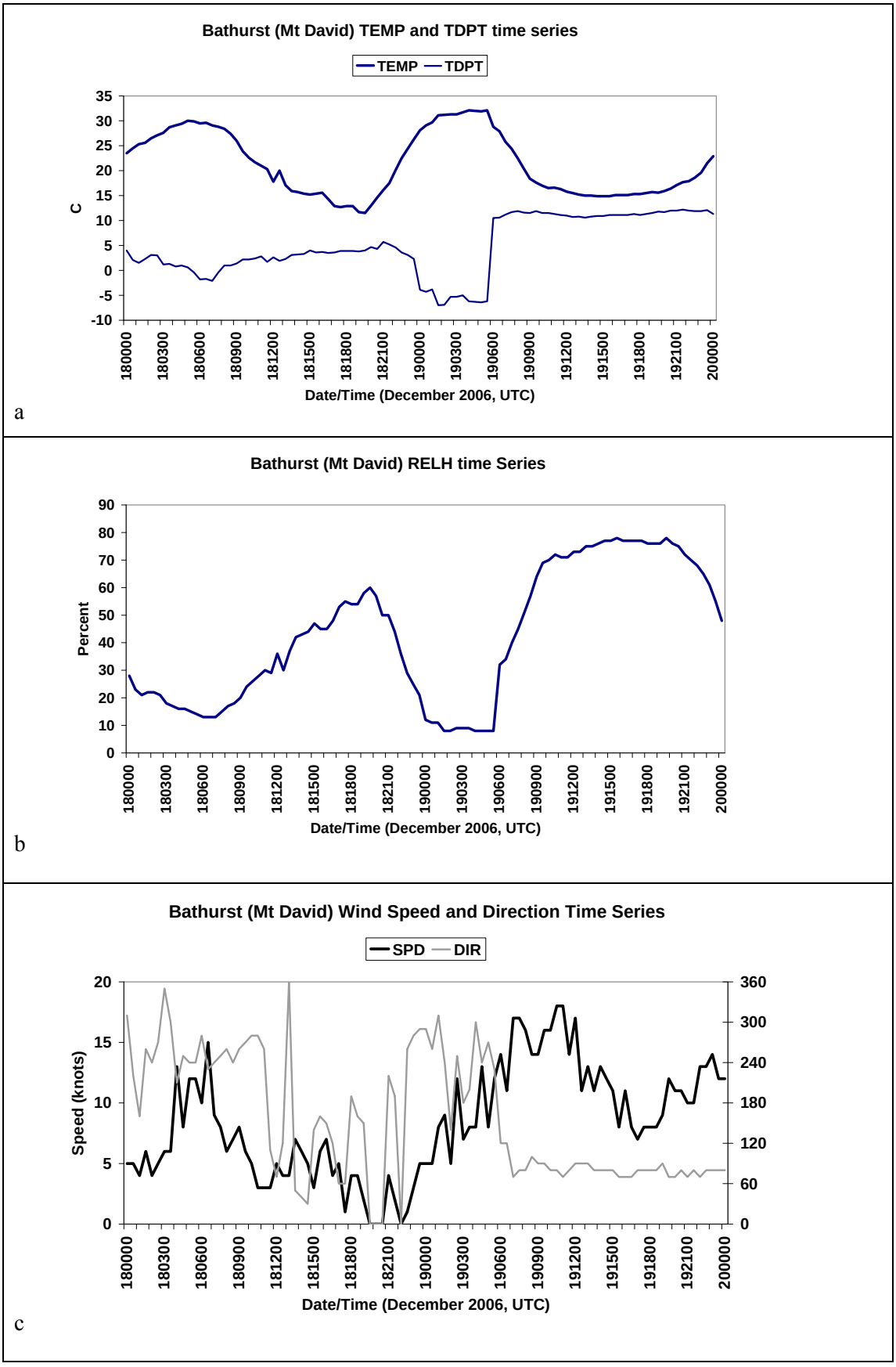

Figure A2.11. Bathurst Airport half-hourly AWS observations. (a) Temperature (bold) and dewpoint, (b) relative humidity (percent), and (c) wind speed (black) and direction (grey).

The C-HAINES values are very high for the two days preceding the fire, and overnight before the fire (Figs. A2.1 and A2.9), and CP note the lack of overnight relative humidity recovery may have enhanced the dryness of the dead fuels prior to the fire, providing an example of high overnight C-HAINES in the lead-in period to a day of active fire spread.

C-HAINES was very high prior to the arrival of the cool change, but FFDI was also very high (and statistically was perhaps more extreme), so any support for the premise that C-HAINES provides additional warning of extreme fire danger is weak for this afternoon.

This case provides an example of the overlap between environments highlighted by large values of C-HAINES and those conducive to abrupt surface drying events as described by Mills (2008a, b). Such joint environments are characteristic of conditions that occur when an easterly change is advancing over the elevated areas of southern NSW (Mills 2007).

A.3 Randall Block (Perth Hills) Fire – 15 October 2005

This case study relates to unexpectedly active fire behaviour during a prescribed burn in jarrah forest at Randall Block, 60 km south-east of Perth. The extent of canopy scorch was much greater than expected for mild burning conditions in spring.

The climatological analysis of C-HAINES and FFDI at the Perth gridpoint (point 2 in Fig. 1) showed that neither were at all extreme (6.8 and 10.2 respectively, Table A1), although examination of the patterns in the plots such as those of Figs. 8 and 9 suggest that the sampled "Perth" gridpoint might be in an area of strong gradient of the C-HAINES field, and thus may not have been representative of the actual conditions over the fire. Accordingly a brief synoptic assessment has been undertaken, together with the presentation of C-HAINES and STAB forecasts from the higher resolution meso-LAPS05 operational forecast model.

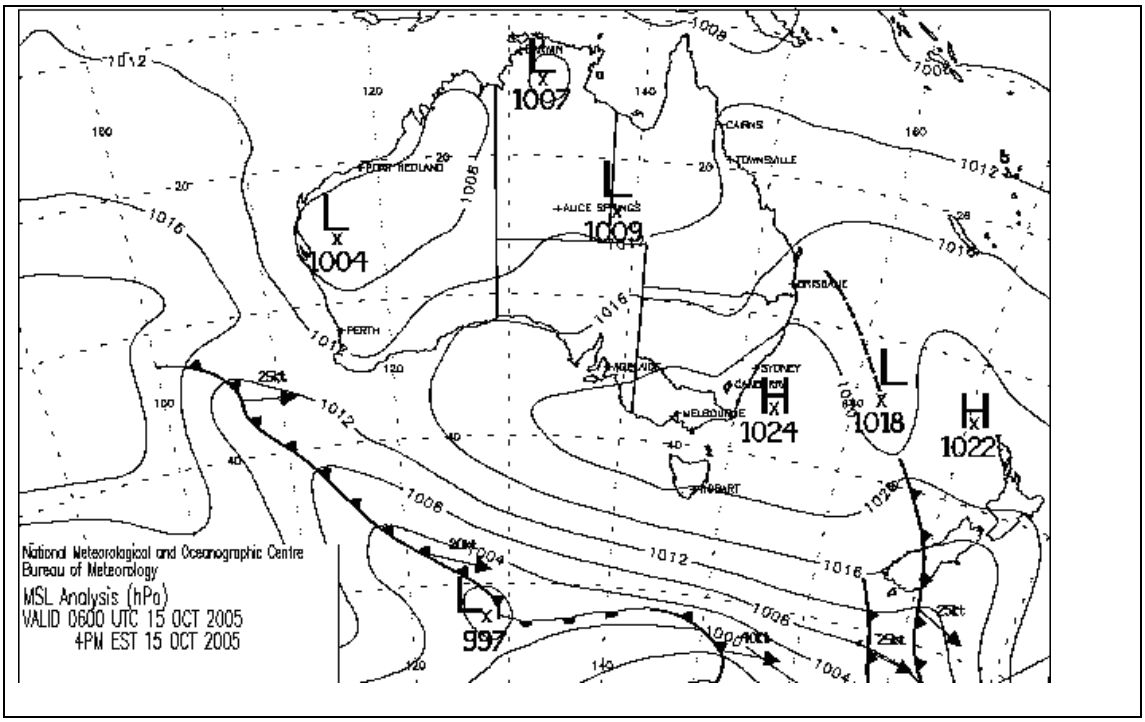

Figure A3.1. Mean-sea-level pressure analysis for 0600 UTC 15 October 2005.

The MSLP analysis for the afternoon of 15 October 2005 (Fig. A3.1) shows a developing trough over inland WA, and a front moving towards the south-west of WA. The axis of the developing trough remained east of Perth in the subsequent 12 hours, and the front to the south weakened. Observations at Perth Airport (Fig. A3.2) show a sea-breeze change/coastal trough passage at 1430 WST (0630 UTC), but prior to this dewpoints had dropped below 0C (relative humidity less than 20%) with temperatures around 25C. Wind speeds were less than 10 knots. It was also noted in Department of Environment and Conservation (WA) correspondence from the day that low relative humidity was also observed at Bickley and at Wandering, both in the Darling Ranges a little south-east of Perth Airport.

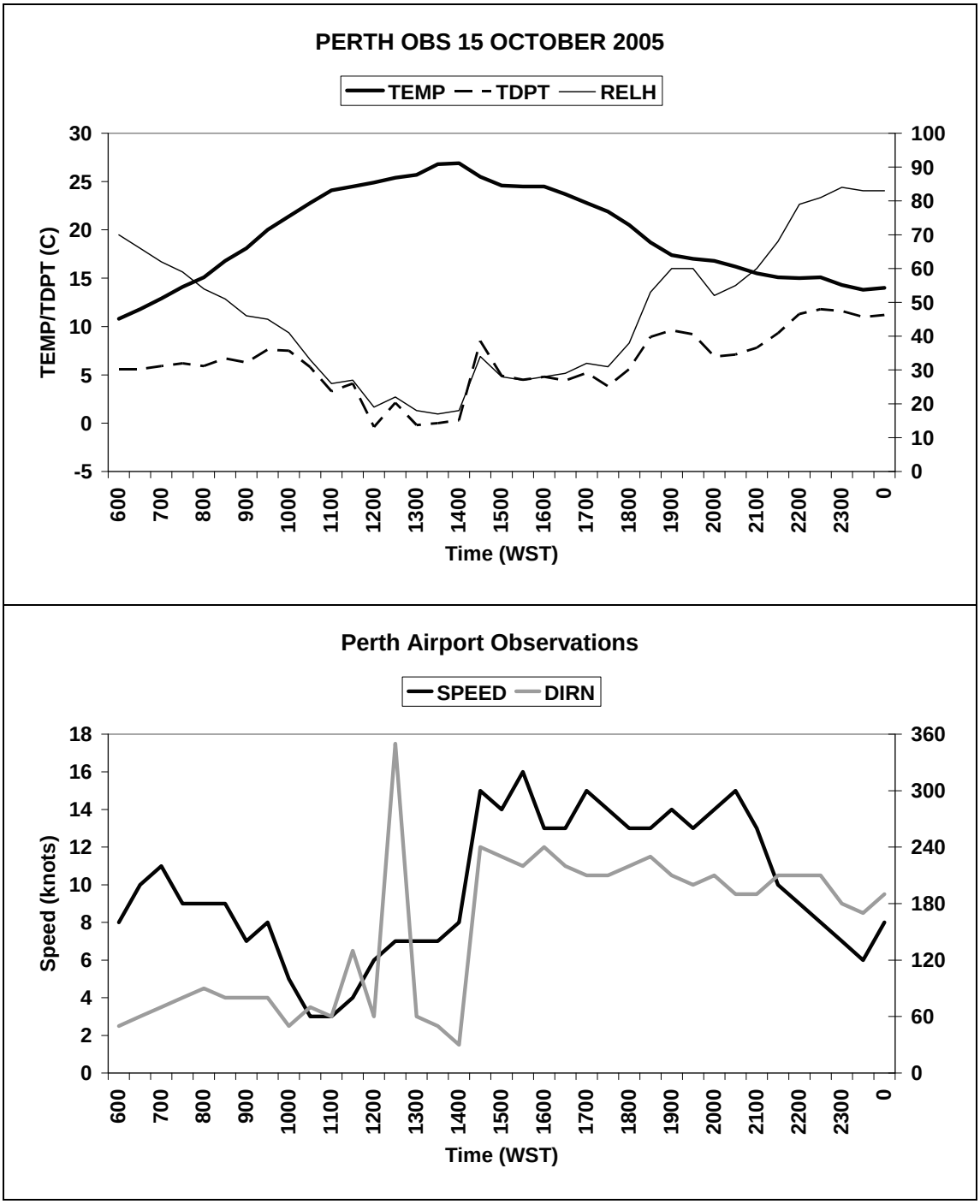

Figure A3.2. Time series of observations from the Perth Airport AWS from 0600 WST to midnight WST on 15 October 2005. Upper panel shows temperature (bold), dewpoint (dashed), and relative humidity (light). Lower panel shows wind speed (black, and direction (grey).

As the relative humidity dropped from 41% at 1000 WST to 17% at 1400 WST, being driven by both diurnal temperature increases and decreasing dewpoint between 1000 and 1200 WST, it is worth considering whether the upper-level "dry slot" phenomenon (Mills 2008a,b) was a contributor to this humidity reduction. The Water Vapour channel geostationary satellite image at 1230 UTC 15 November is shown in Fig. A3.3, and a clear "dry slot" is seen immediately north-west of Perth. The upper flow patterns (Fig. A3.4) show that the south-north dry oriented dry (dark) area over the ocean west of Perth (marked A in Fig. A3.3) is associated with the cyclonic flank of a southerly (polar front) jet streak on the western flank of the upper trough approaching WA, while the north-west-south-east oriented dry area "pointing" at Perth (B) is associated with

the cyclonic shear on the poleward flank of the north-westerly subtropical jet crossing the WA coastline between 28 and 24S.

Perth Airport radiosonde soundings (Fig. A3.5) show that at 0000 UTC (blue trace) the air is particularly dry above about 850 hPa, and while a surface inversion is present at this time, the observed rise in temperature to around 25C by early afternoon would, in the absence of any other changes, have allowed mixing of this air to the surface (cf Fig. A3.2). By 1200 UTC the coastal change had moved through Perth, and extended from the surface to ~870 hPa (~1200m), and while very dry air was still present some 50 hPa above the surface, there is also a very clear dry zone above 640 hPa corresponding to the dark (dry) band seen in the WV imagery. Moistening in the 840-640 hPa layer suggest that other more complex processes were also in play.

The forecasts of C-HAINES from the meso-LAPS05 NWP model for 0600 and 1200 UTC are shown in Fig. A3.6, and during this time a high C-HAINES band moved slowly towards the south-east, crossing the coast and moving slightly inland near Perth. Not shown are the dewpoint depression fields, but the increase in C-HAINES is largely driven by this ingredient. While the "Perth" climatological gridpoint shows a C-HAINES of 6.8 at 0600 UTC, and the fine-mesh forecast is in agreement with this value, the strong gradient to the west of this point, and close to the location of the fire in the Perth Hills, and the increase to 9.5 by 1200 UTC (around the 95th percentile) suggests that unusual stability/humidity conditions were developing over the fire ground. Ebert (2008) argues the benefits of taking a probabilistic approach to the interpretation of mesoscale NWP forecast guidance in cases of strong gradients near a forecast location.

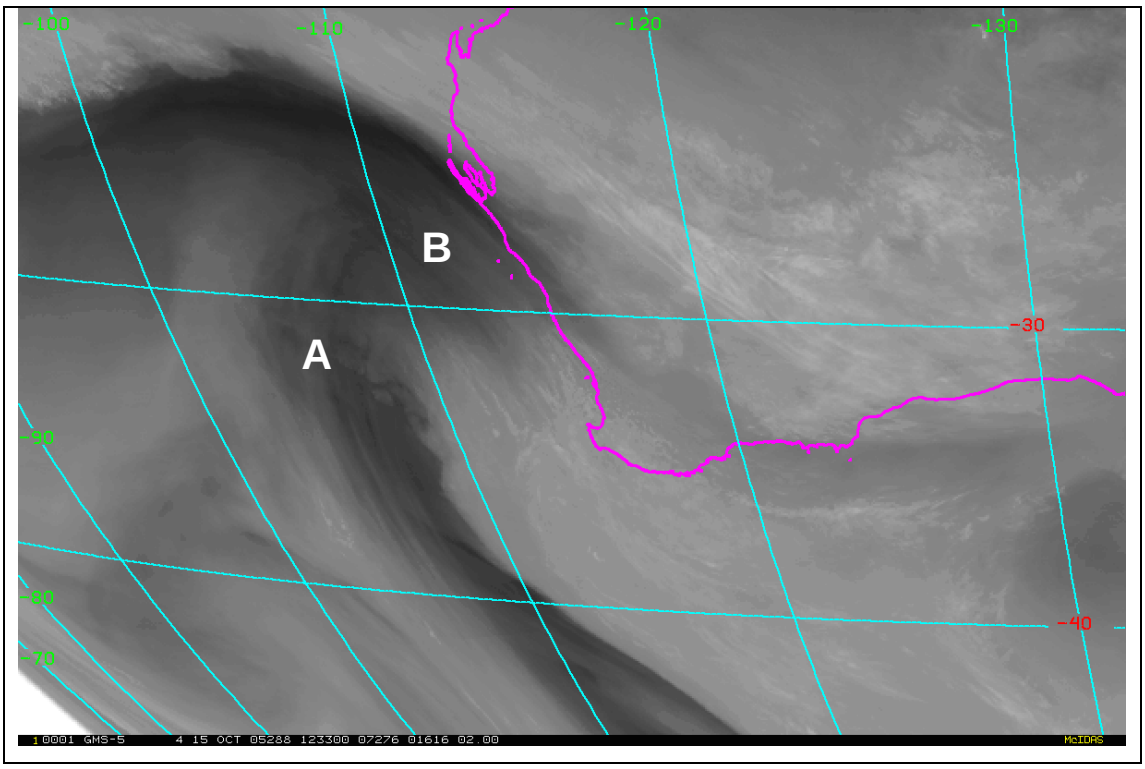

Figure A3.3. Geostationary satellite Water Vapour Channel image for 1230 UTC 15 October 2005. The letters refer to features described in the text.

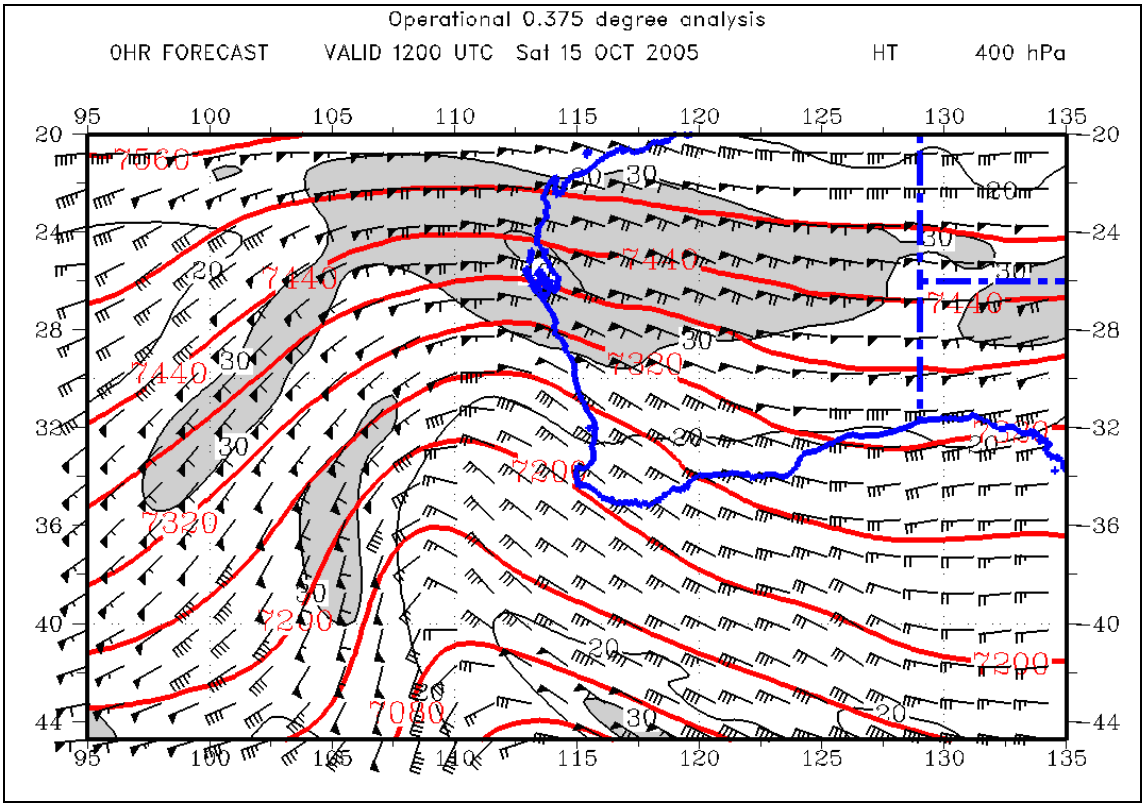

Figure A3.4. LAPS 400 hPa height/wind analysis at 1200 UTC 15 October 2005. Red contours show geopotential heights in gpm, grey shading shows wind speeds greater than 30m s-1, and the wind barbs have their usual meteorological meaning.

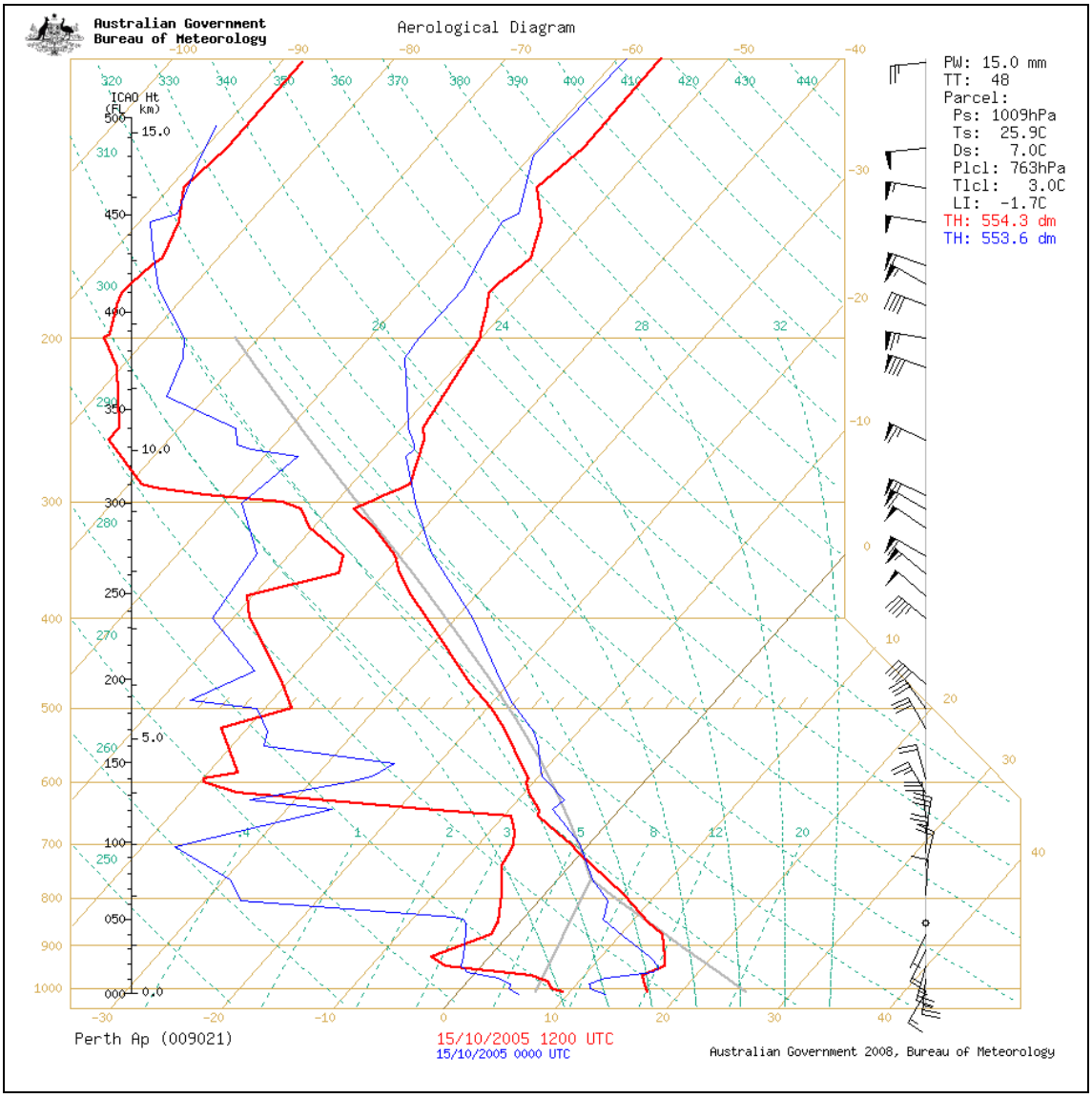

Figure A3.5. Perth Airport radiosonde data for 0000 UTC (blue) and 1200 UTC (red) 15 October 2005.

While not definitive, this study, which is for a somewhat unusual west-coast trough change pattern, combined with a report of enhanced fire activity under what should have been relatively benign fire weather conditions, indicates that perhaps the dry-slot phenomenon, or, alternatively, the Haines Index factors, may have contributed to the enhanced fire activity on that day. The forecasts of C-HAINES from mesoscale NWP models may have provided an alert to this possibility.

The case also suggests the benefits of not only considering exact coincidence of forecast risk factors and fire location, but also to consider a more probabilistic interpretation in conditions of high gradients in these forecast fields.

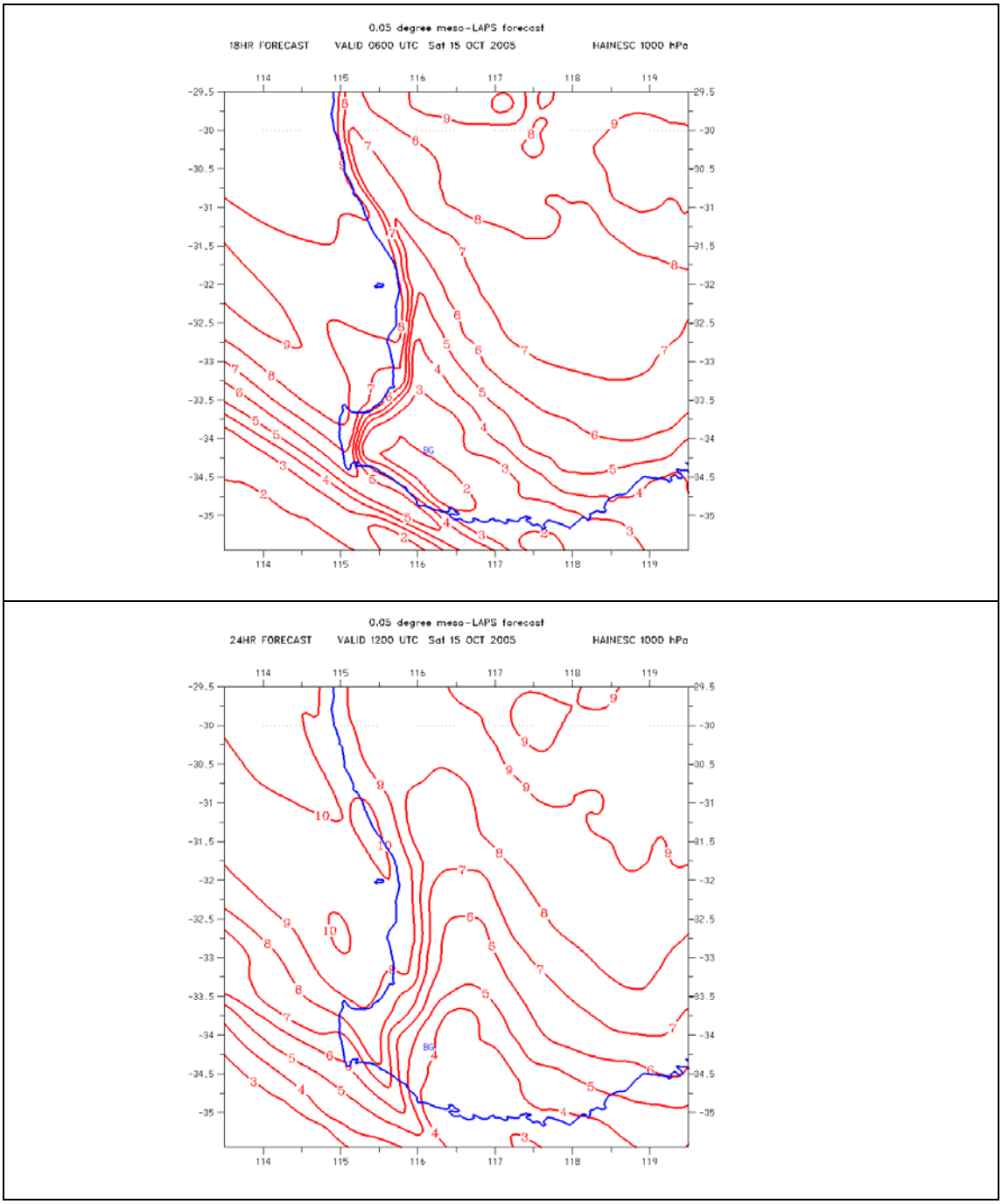

Figure A3.6. C-HAINES forecasts for 0600 and 1200 UTC 15 October 2005 from the operational 0.05° mesoLAPS NWP model output.

A.4 The Hovea Fire

This was a prescribed burn on 17-18 December 2005 in the Greater Preston National Park, about 15km east of Donnybrook, WA (~25-30 km south-west of the nearest AWS at Collie East, and about 50 km north of Bridgetown). FFDI values were at best in the lower part of the Very High range, but extensive areas of crown scorch were noted in the mature jarrah forest, a result of the fire being more active than anticipated (Chandler 2005, unpublished CALM report).

Figure A4.1 shows that, based on the 0600 UTC Bridgetown (point 3 in Fig. 1) climatology, both FFDI and C-HAINES were at quite benign levels on 17 and 18 December, and no large values of either were observed in the days preceding the event (not shown).

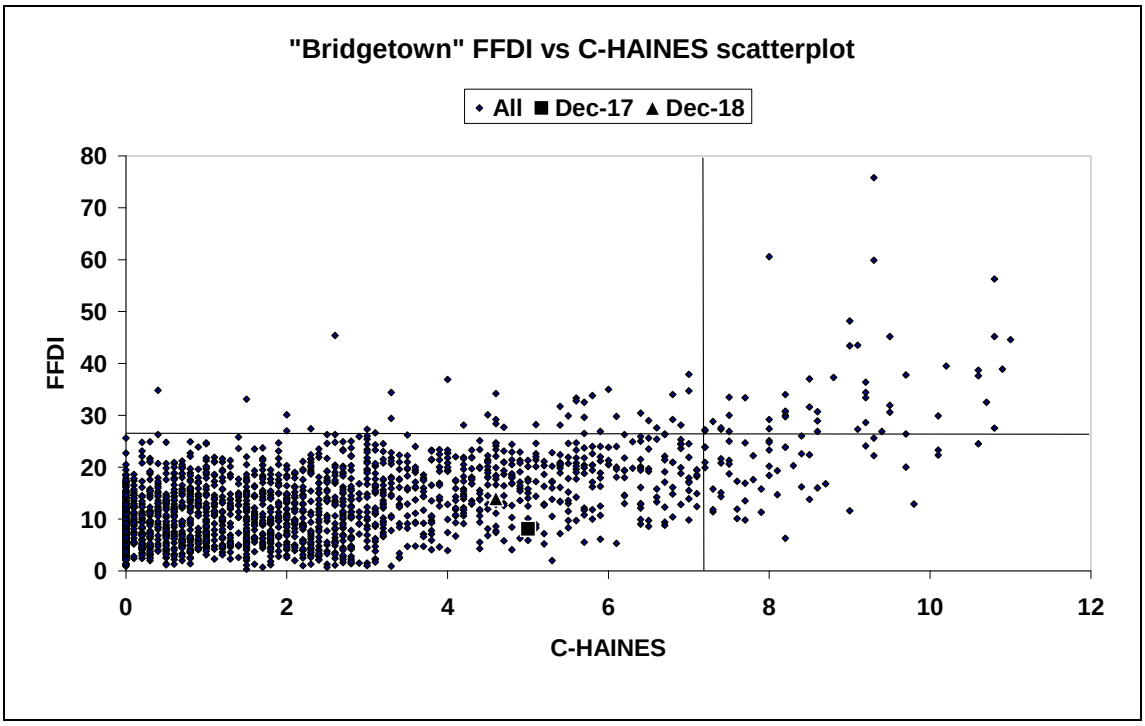

Figure A4.1. Scatterplot of FFDI vs C-HAINES for the "Bridgetown" gridpoint at 0600 UTC for the 8-year climatology in this report. The lines show the 95th percentile values of C-HAINES and FFDI respectively, and the highlighted points are for the 17 and 18 December 2005.

The MSLP analysis (Fig. A4.2) shows no strong circulation features in the area, with a ridge extending east-west through south-west WA and a small high cell just off Cape Leeuwin. This suggests perhaps that there would have been a weak change moving through the south-west during that day. The 18-hour 0.05o meso-LAPS forecast screen level potential temperature and 70m wind forecast (Fig. A4.3) shows westerly winds across the south-west, a sea-breeze change beginning to move inland from Perth northwards, and a sea-breeze convergence focused along the coastline east of Albany. None of these patterns would suggest unusual fire weather conditions in the area of the prescribed burn. Accordingly meso-scale model forecasts were examined to see if any small-scale (space or time) features could be discerned during the period of the fire.

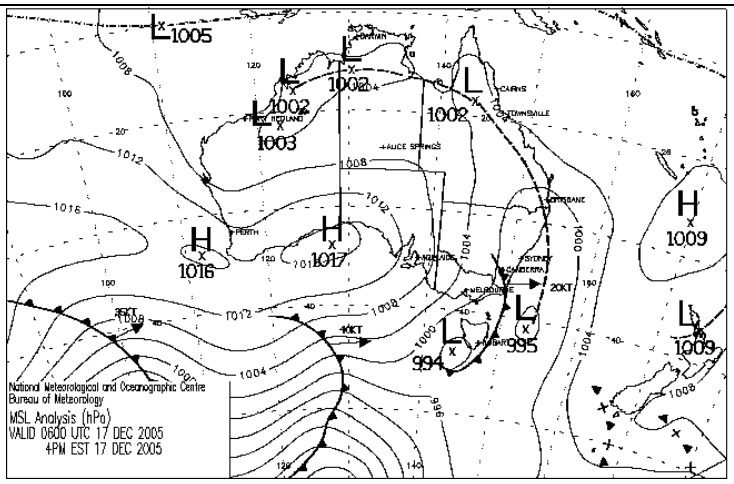

Figure A4.2. Mean-sea-level pressure analysis for 0600 UTC 17 December 2005.

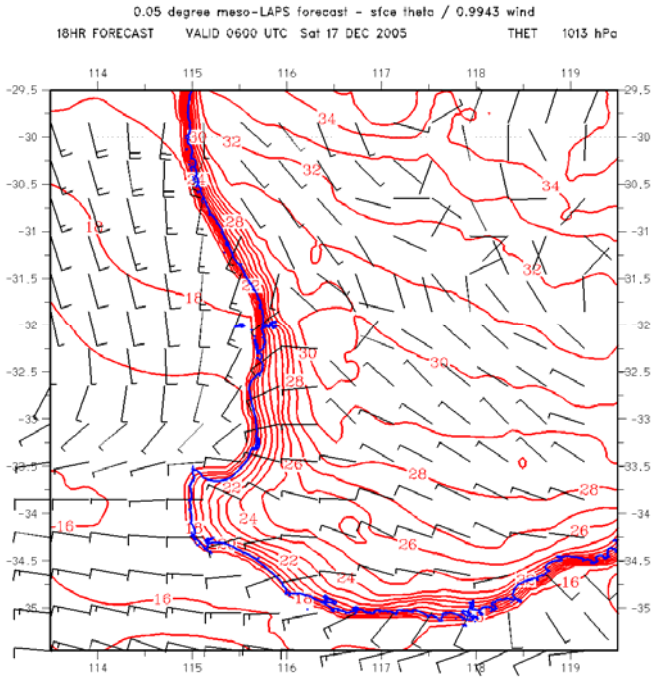

Figure A4.3 : Forecast screen-level potential temperature and overlaid 70m wind barbs for 0600 UTC 17 December 2005 from the 0.05° meso-LAPS NWP model.

The C-HAINES forecast for 0600 UTC 17 December (Fig. A4.4) shows a band of moderately high (around 90th percentile) C-HAINES extending north-west/south-east a little north of Bridgetown, but the strong gradient to its south, and the fact that it is largely driven by the dewpoint-depression ingredient (Fig. A4.4, lower), indicates support for the hypothesis (Chandler 2005) that the lower humidity observed north of the Hovea Block at Collie East may have been more representative of conditions at the fire site than were the forecast (or the observed) conditions at Bridgetown.

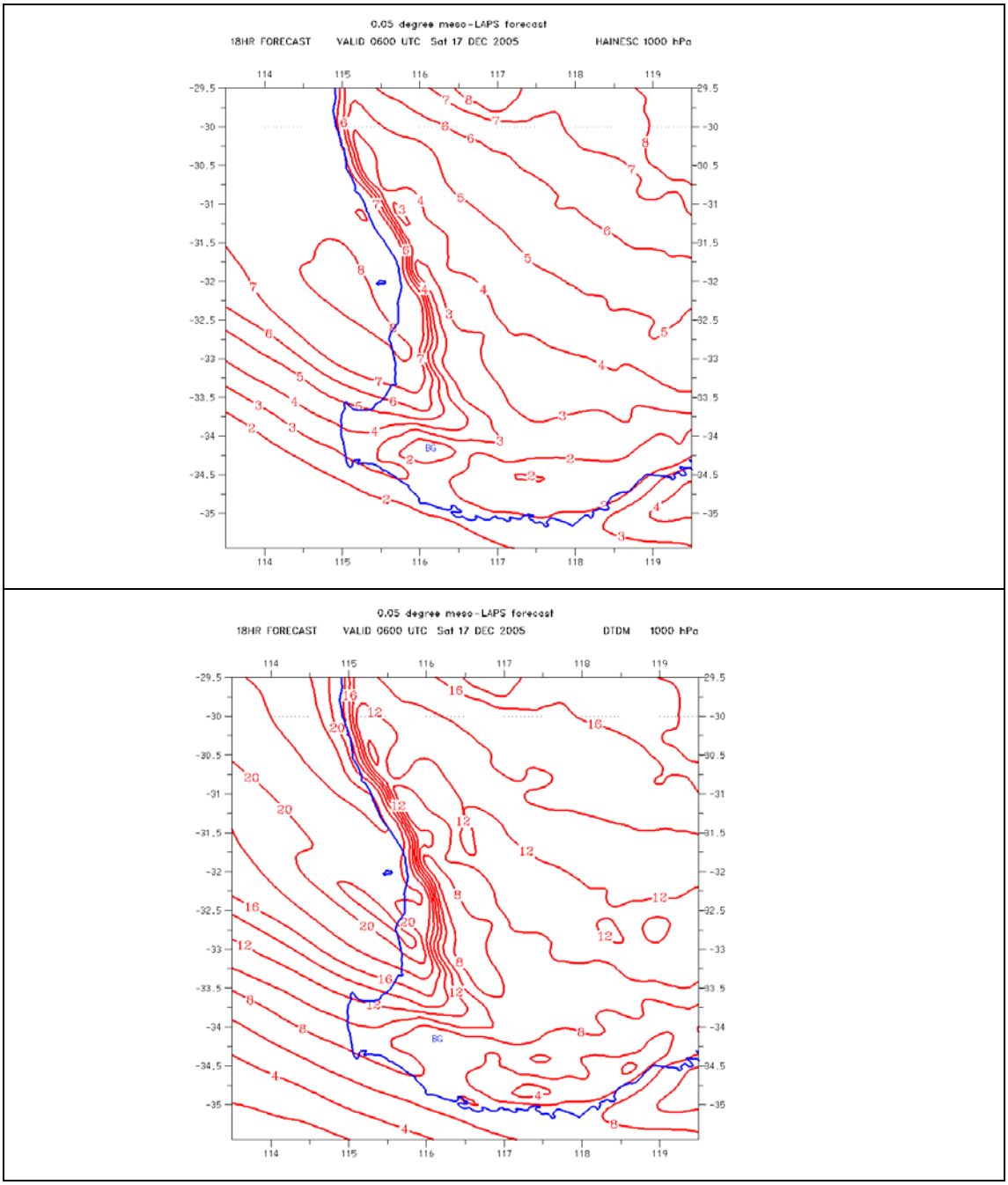

Figure A4.4. Forecasts of C-HAINES (upper panel) and 850 hPa dewpoint depression (lower panel) valid at 0600 UTC 17 December 2005.

The 850 hPa dry air zone draws parallels with some of the effects described in association with abrupt surface dryings described in Mills (2008,b). However, geostationary satellite 6.7 µm channel "Water Vapour" imagery (Fig. A4.5) does not show a band of dry air aligned with that shown in the 0.05o grid NWP forecast of 850 hPa dewpoint depression (Fig. A4.4), though it should not necessarily be expected to do so, with its peak weighting in the middle troposphere, well above 850 hPa. However, it does show a vast area of dry air associated with an upper ridge immediately north of the fire area, so in this regard does fit one of the upper tropospheric patterns associated with abrupt surface dryings at Bridgetown (Mills 2008b). However the lack of one of the low-level ingredients described in Mills (2008b), together with the forecast narrow 850 hPa dry air zone, suggests that this latter type of circulation feature may be worthy of further investigation.

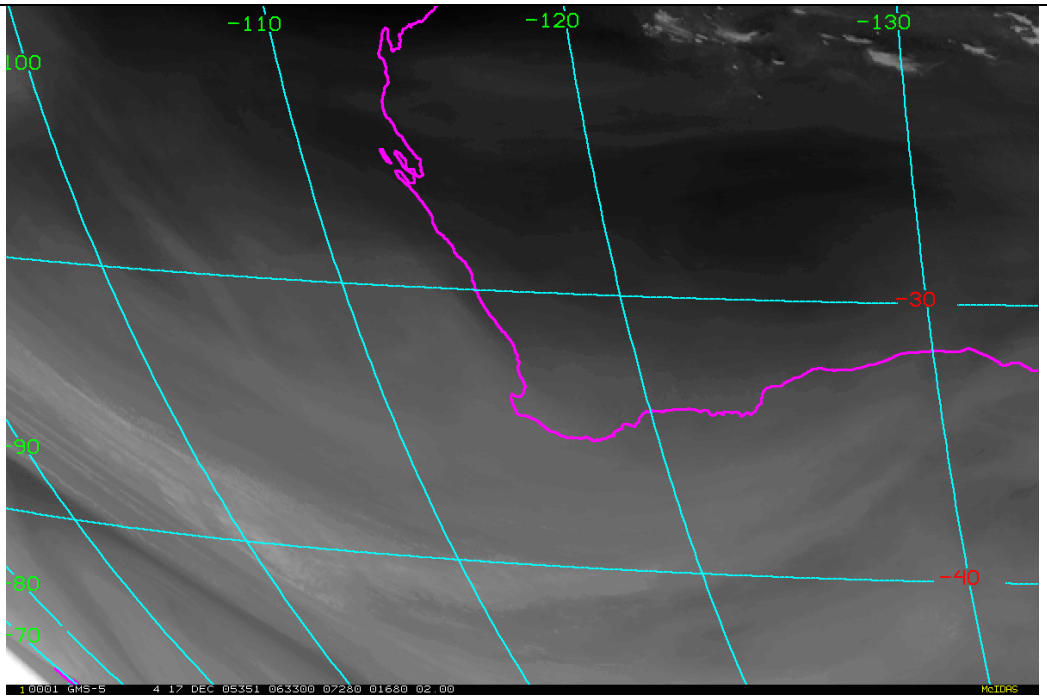

Figure A4.5. Geostationary satellite enhanced water vapour image at 0630 UTC 17 December 2005.

C-HAINES does show a small-scale maximum in an area where subsequent fire activity was greater than anticipated.

Use of the ingredients as well would have shown the role of the narrow tongue of low dewpoint air moving in from the north-west. It is unlikely that this would be identified using satellite observations, demonstrating the benefits of mesoscale NWP.

A.5 The Pickering Brook Fire (Perth Hills 15-25 January 2005)

Cheney (2009) has described the spread of this fire until 1000 WST on 17 January 2005 in detail, and also provides some discussion of its subsequent evolution. Three deliberately lit fires on 15 January burnt, spread, and merged over the next 10 days. Major fire runs occurred during the afternoon of 16 January under easterly winds, and to the south-west overnight on 17 January after the winds shifted north-easterly. On that night there was only small overnight relative humidity recovery. The majority of fire spread was halted around 1000 WST on 17 January when winds abated, but during that afternoon a massive convection column was seen above the fire. The spectacular photos of this pyrocumulus cloud attracted much media attention, and featured in the Bureau's weather calendar of 2006. It is also interesting that a new lightning-ignited fire was detected on 18 January (Cheney 2009), apparently as a result of this pyrocumulonimbus development. The fire continued until 25 January, but most areas affected during this later period were on the eastern and northern flank of the fire.

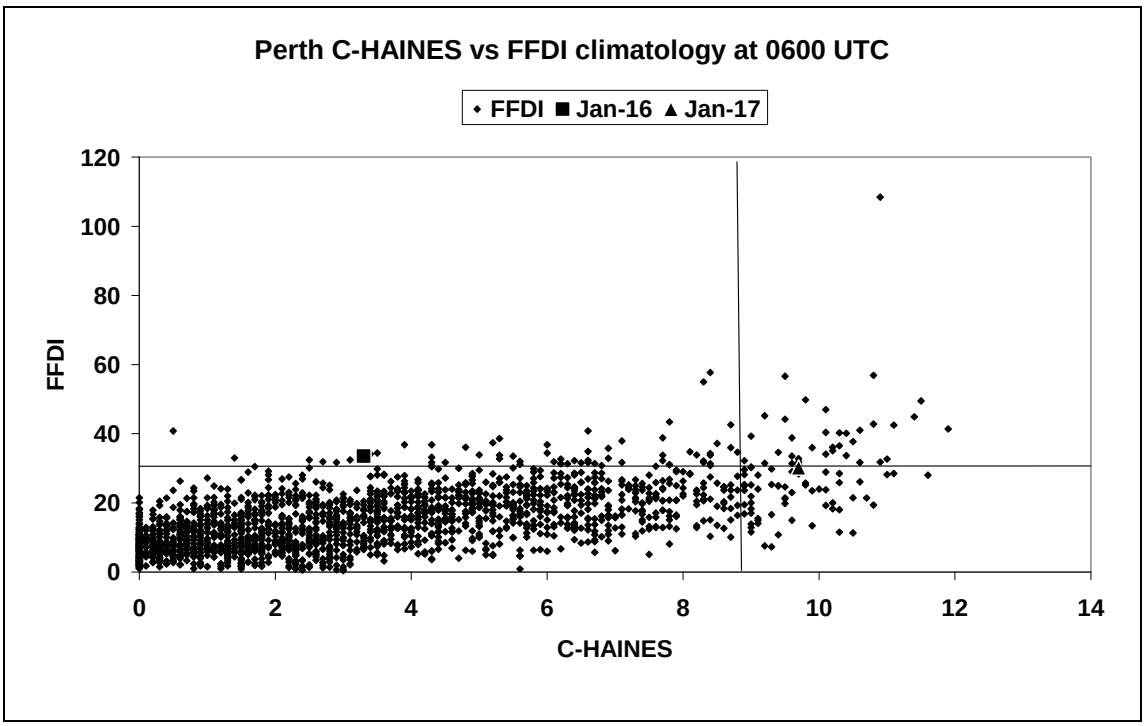

Figure A5.1 Scatterplot of FFDI vs C-HAINES for the "Perth" gridpoint at 0600 UTC for the 8-year climatology in this report. The lines show the 95th percentile values of C-HAINES and FFDI respectively, and the highlighted points are those of 16 and 17 January 2005.

Figure A5.1 shows that on 16 January FFDI values at the Perth gridpoint (point 2 in Fig. 1) were in the Very High range, and just above the 95th percentile, while C-HAINES values were very low. On the afternoon of the 17th, though, while FFDI was a little lower, extra-ordinarily high values of C-HAINES are seen. The daily 0600 UTC time-series of C-HAINES and FFDI (Fig. A5.2) shows a single very large spike in the C-HAINES time-series on 17 January, the day on which the pyrocumulus cloud attracted so much attention. There is another maximum in both C-HAINES and FFDI on 23 January, but in the absence of fire spread data for this day it will not be discussed further in this analysis.

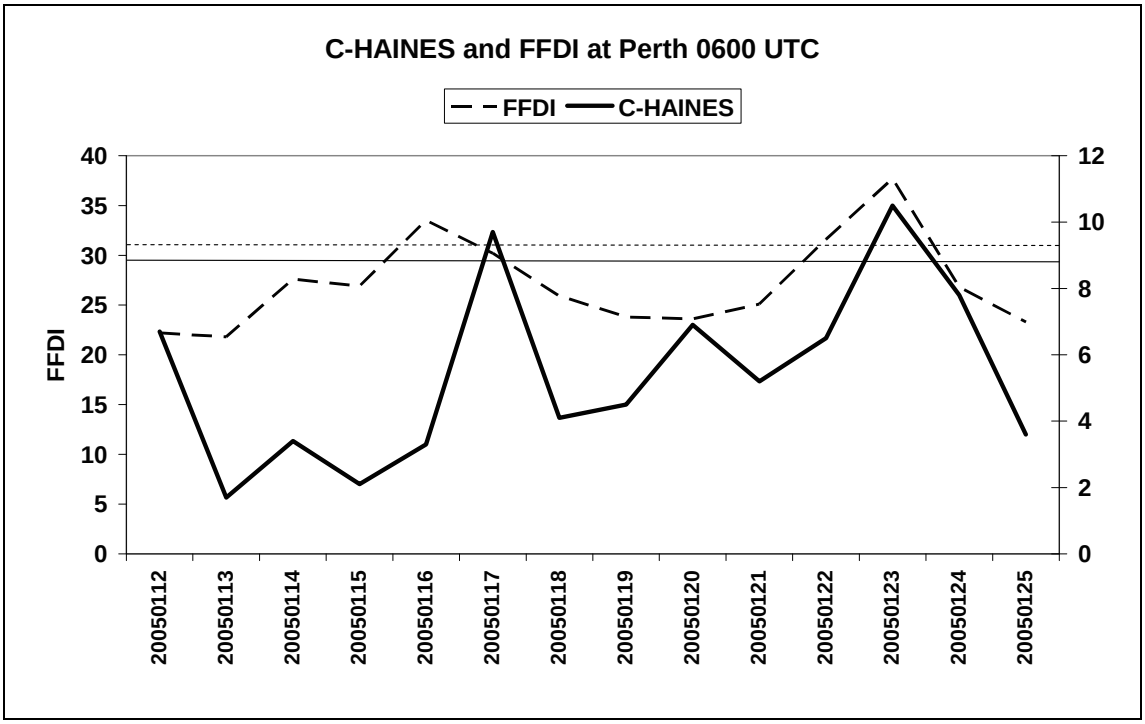

Figure A5.2. Time series of daily FFDI (dashed) and 0600 UTC C-HAINES (solid) from 12-25 January 2005 at the "Perth" gridpoint. The horizontal lines indicate the 95th percentile values for the two parameters

Figure A5.3 shows meteograms of wind speed, gust, direction, and relative humidity at Perth Airport. These show easterly winds through the afternoon of 16 January, gradually easing with time, and relative humidities decreasing steadily until about 1800 WST. This was the period of the first run of the fire to the west. A little before midnight the wind speeds increased significantly, with the direction backing slightly to the east-north-east, and, against the expected diurnal trend, the relative humidity dropped to below 20%, although it did recover somewhat after 0300 WST. This was the period when the fire spread rapidly to the south-west, the previous southern flank of the fire becoming its head. Mills (2008b) notes that overnight abrupt surface drying events at Perth Airport can be associated with gusty easterly wind events.

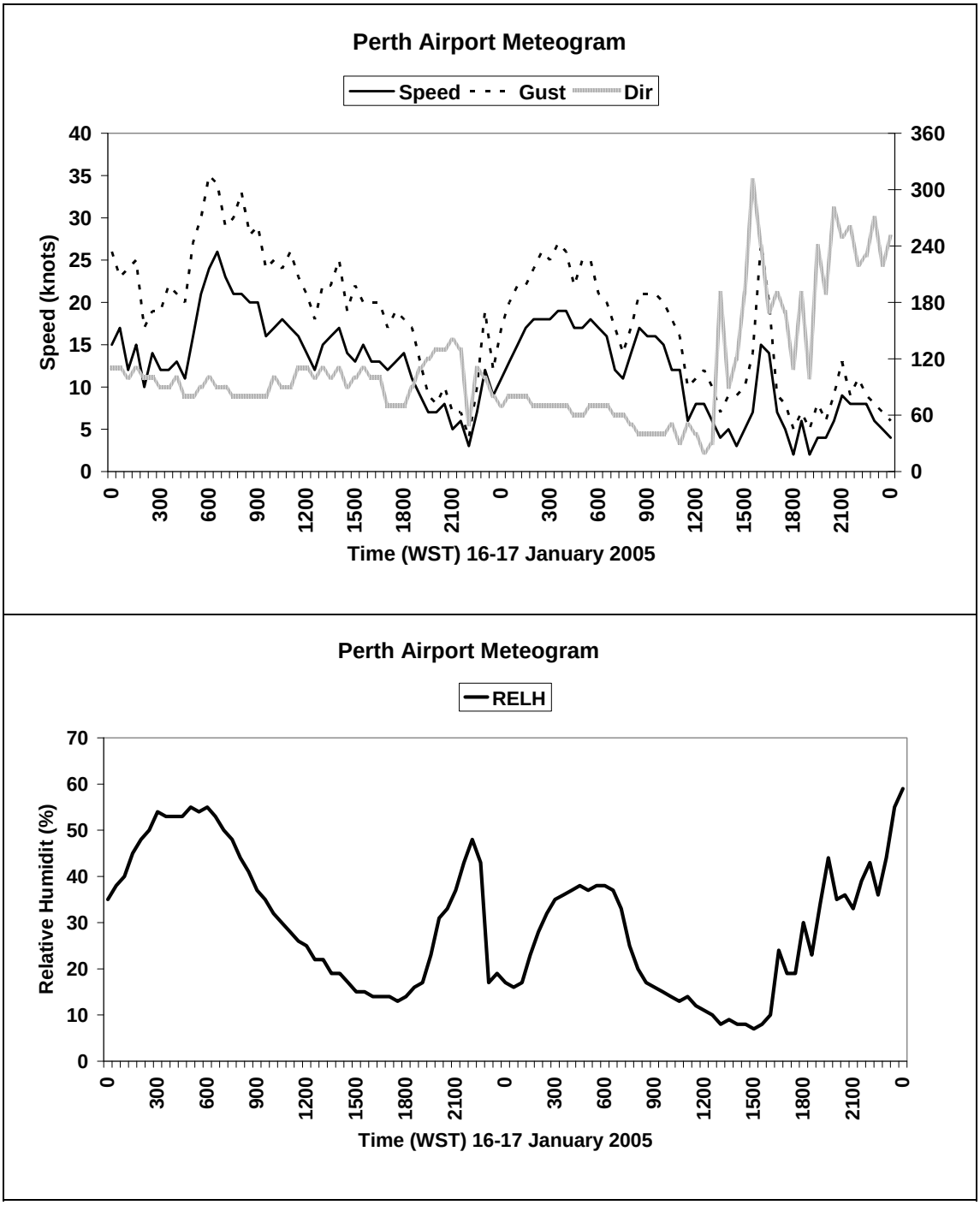

Figure A5.3. Perth Airport observation times series from 0000 WST 16 January to 0000 WST 18 January 2005. Upper panel direction (grey), speed (black, solid), and gust speed (dashed). Lower panel relative humidity.

At around 1000-1100 WST 17 January wind speeds eased, and the fire spread essentially stopped. Around 1600 WST, after some oscillation, a south-westerly wind change moved through Perth Airport (see the relative humidity increase) and wind speeds increased a little, but remained below 10 knots. The pyrocumulus cloud was photographed at around 1500 WST, and convergence at the head of the sea-breeze change may have contributed to this development. The shallowness of this change, though, is seen in the Perth Airport radiosonde trace at 1200 UTC (Fig. A5.4) that shows the sea-breeze to be only a few hundred metres deep at best.

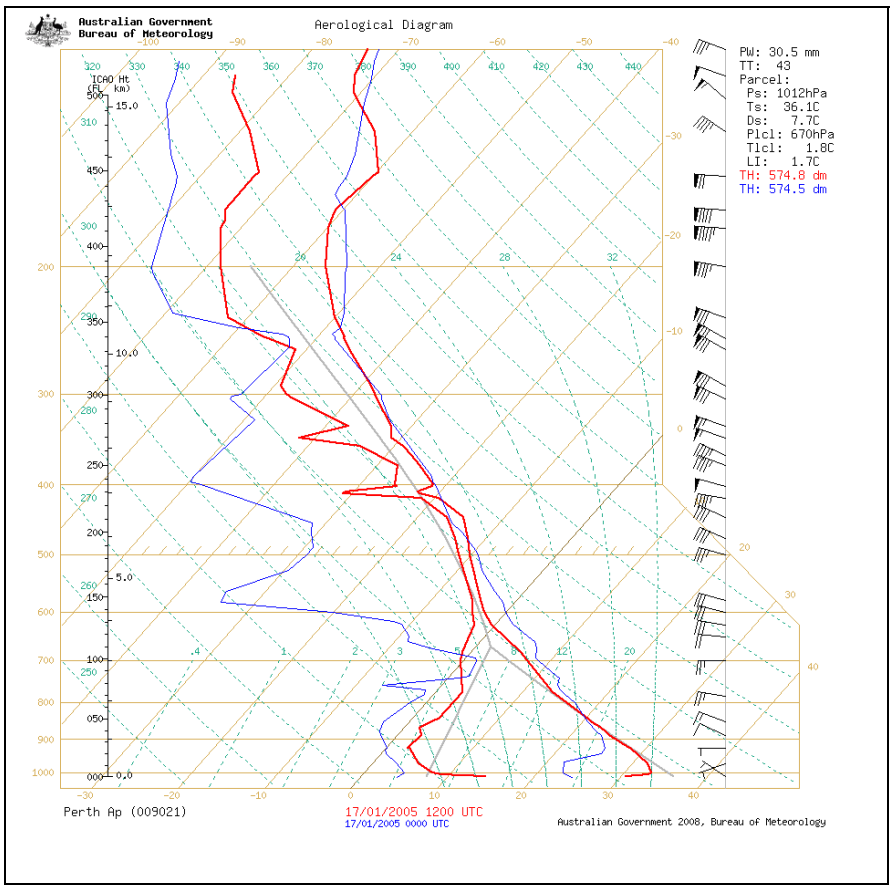

Figure A5.4. Perth Airport radiosonde data. Blue line 0000 UTC 17 January 2005, red line 1200 UTC 17 January 2005.

The space-time evolution of the meteorology of this event is discussed using mesoscale NWP forecasts. At time of this fire the Perth area meso-LAPS05 NWP model was not operational, and so the meso-LAPS125 model output, available 3-hourly, is used. Figure A5.5 shows the low-level potential temperature and wind forecasts and the C-HAINES forecasts for 0600, 1200, and 1800 UTC 16 January, to cover the period of the afternoon and overnight fire runs on 16-17 January, while Fig. A5.6 shows the same forecasts of GFDI. The left-hand panels of Fig. A5.5 show the backing of the wind to the east-north-east, and the strengthening overnight, while the GFDI forecasts (Fig. A5.6) show that values of GFDI above 25 are maintained well into the night, and even increase slightly between 1200 and 1800 UTC. It is also of interest, and perhaps note, that the C-HAINES increases from quite modest values in the afternoon to values around 7 by 1800 UTC, suggesting an increase in emphasis of those physical factors encapsulated in the Haines Index that might have affected the overnight fire behaviour, and associated with the weaker than normal overnight relative humidity recovery.

On 17 January a wind change developed on the coast by 0600 UTC, and had moved inland by 0900 UTC (Fig. A5.7, left panels). However, the fact that the temperature gradient remains focussed on the coast and coastal plains indicates that this is only a weak sea-breeze/west-coast trough change. The forecast wind field evolution is very consistent with the time-series of surface observations, and the radiosonde observations, at Perth Airport. The forecast C-HAINES values (Fig. A5.7, right panels) had continued to increase throughout the day, and extremely high values of C-HAINES are evident by 0900 UTC. This is driven largely by the lapse ingredient of the C-HAINES, evidenced in this example by the time sequence of the STAB forecasts, seen in Fig. A5.8, where stability ahead of and over the leading part of the low-level cool change decreases through the day.

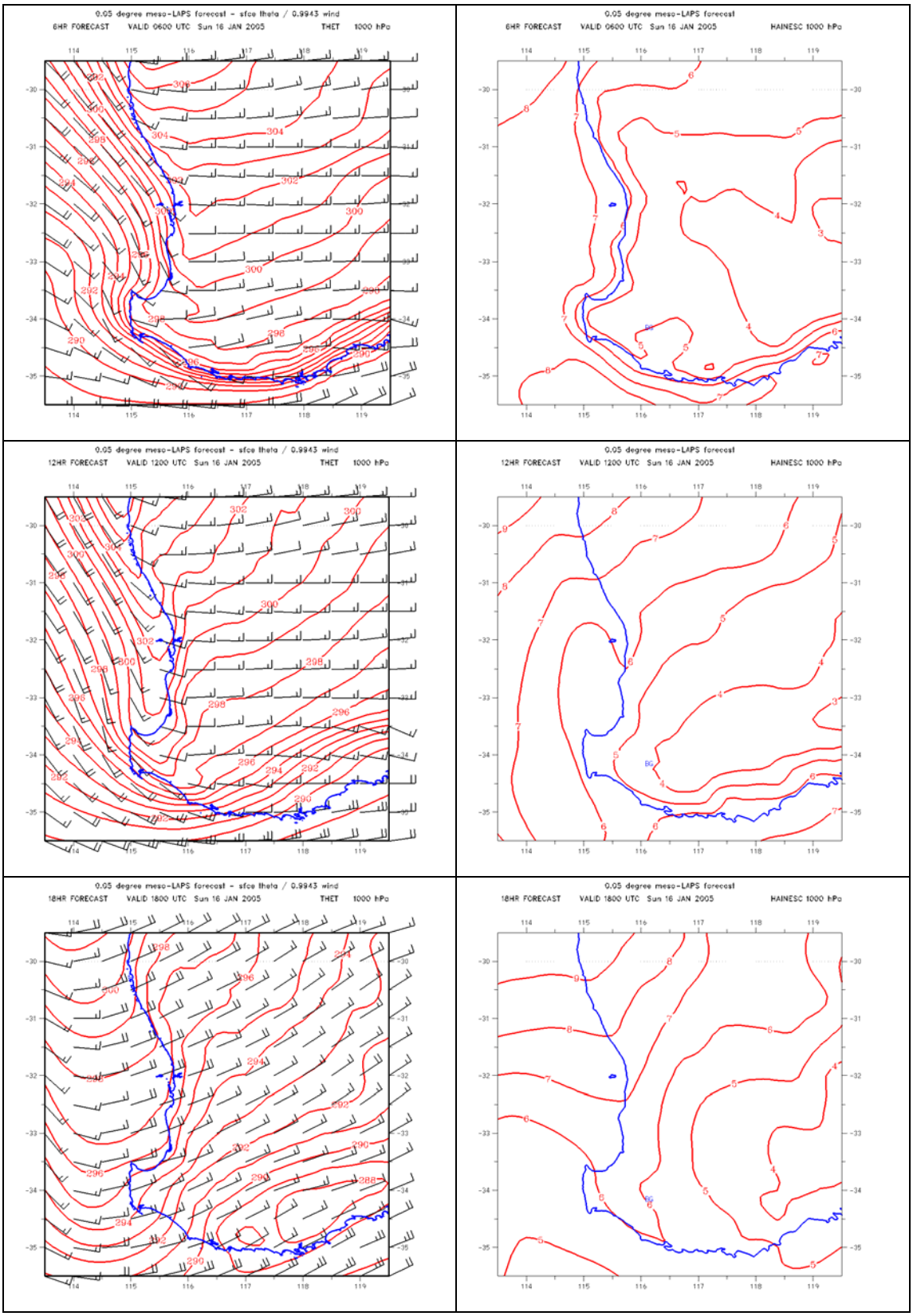

Figure A5.5. Forecasts of screen-level potential temperature and overlaid 70m wind barbs (left panels) and C-HAINES (right panels). Forecasts are valid at 0600 UTC (top), 1200 UTC (middle) and 1800 UTC (bottom) 16 January 2005.

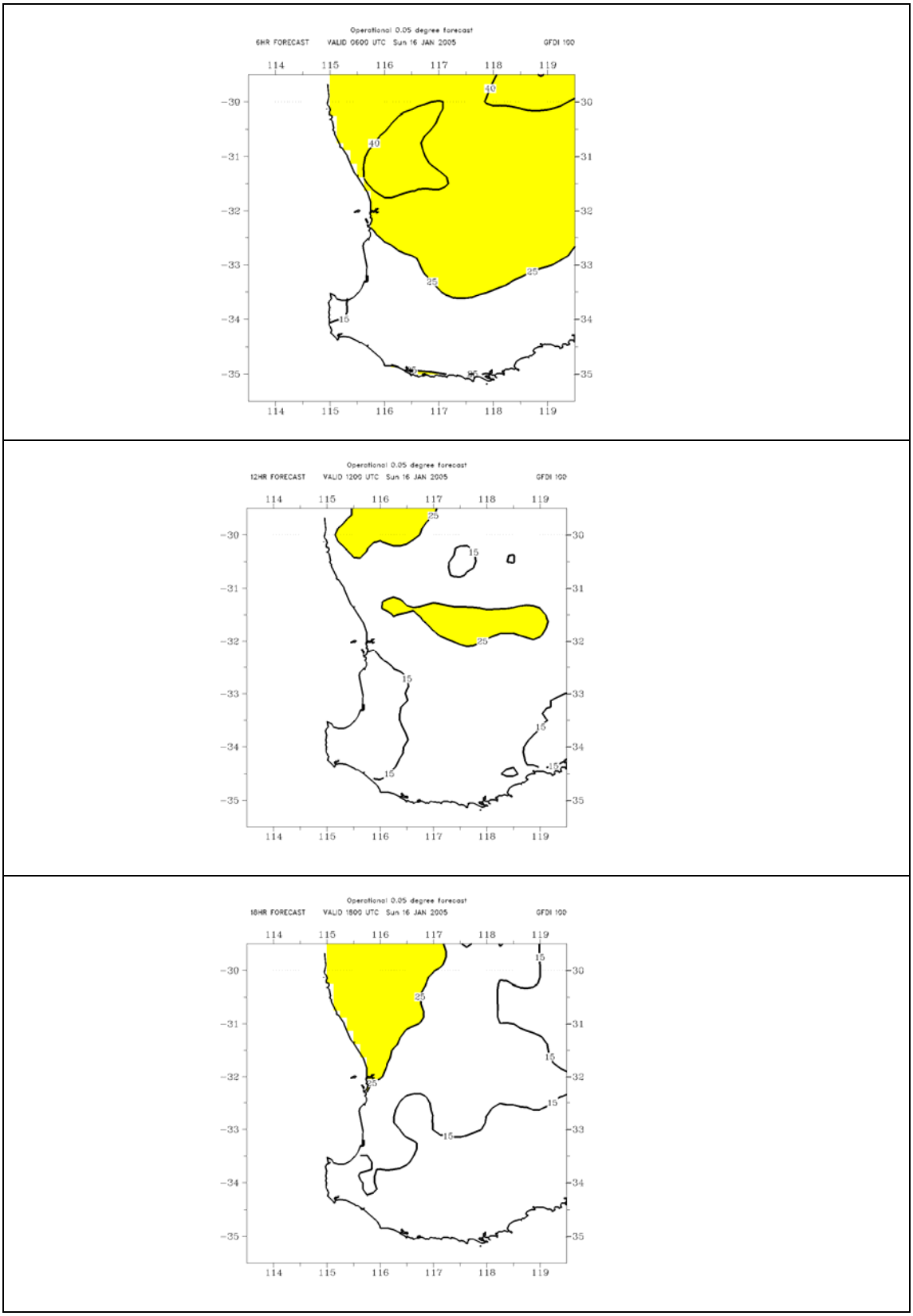

Figure A5.6. Forecasts of Grassland Fire Danger Index (100% curing assumed) valid at 0600 UTC (top), 1200 UTC (middle) and 1800 UTC (bottom) 16 January 2005.

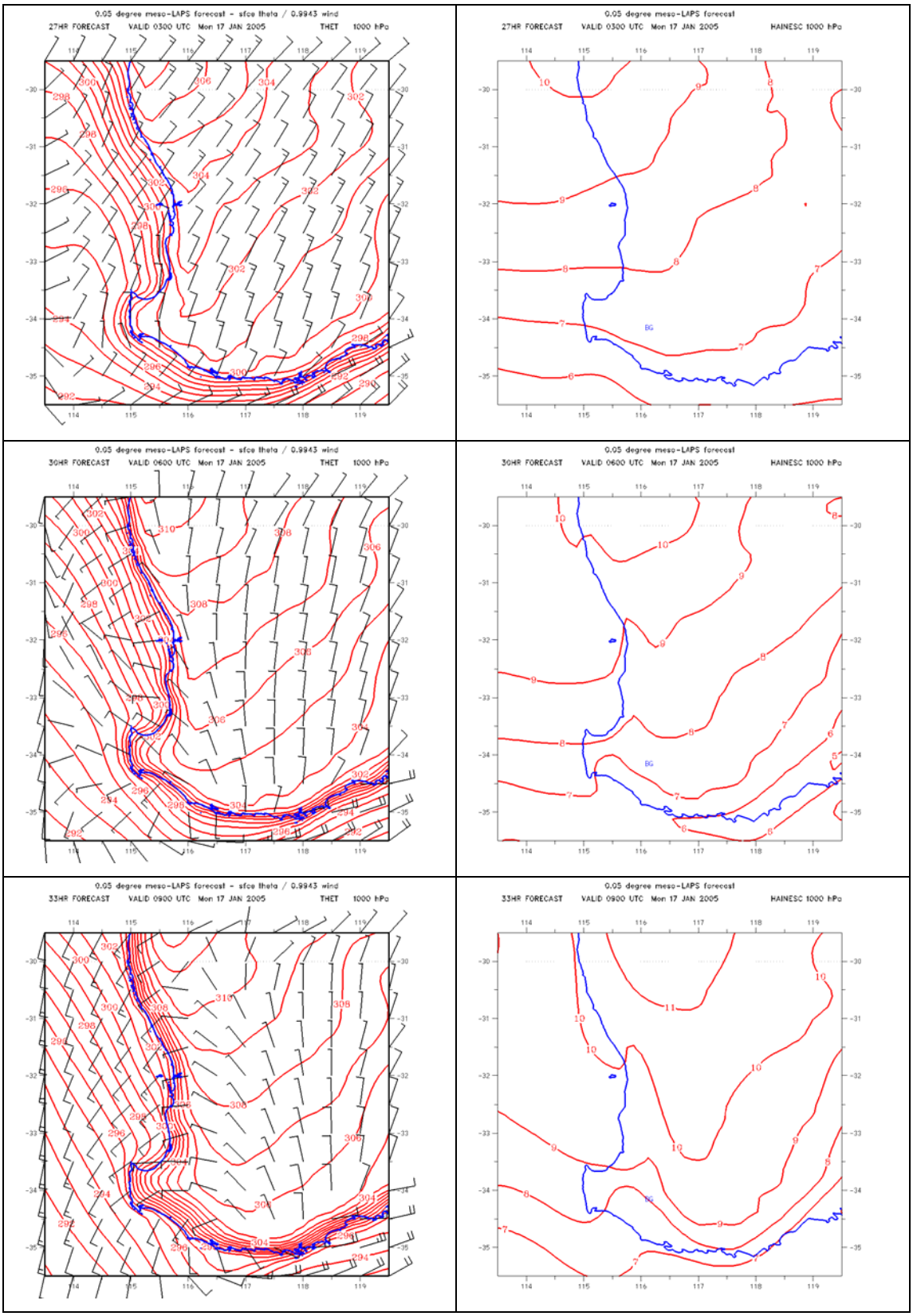

Figure A5.7. Forecasts of screen-level potential temperature and overlaid 70m wind barbs (left panels) and C-HAINES (right panels). Forecasts are valid at 0300 UTC (top), 0600 UTC (middle) and 0900 UTC (bottom) 17 January 2005.

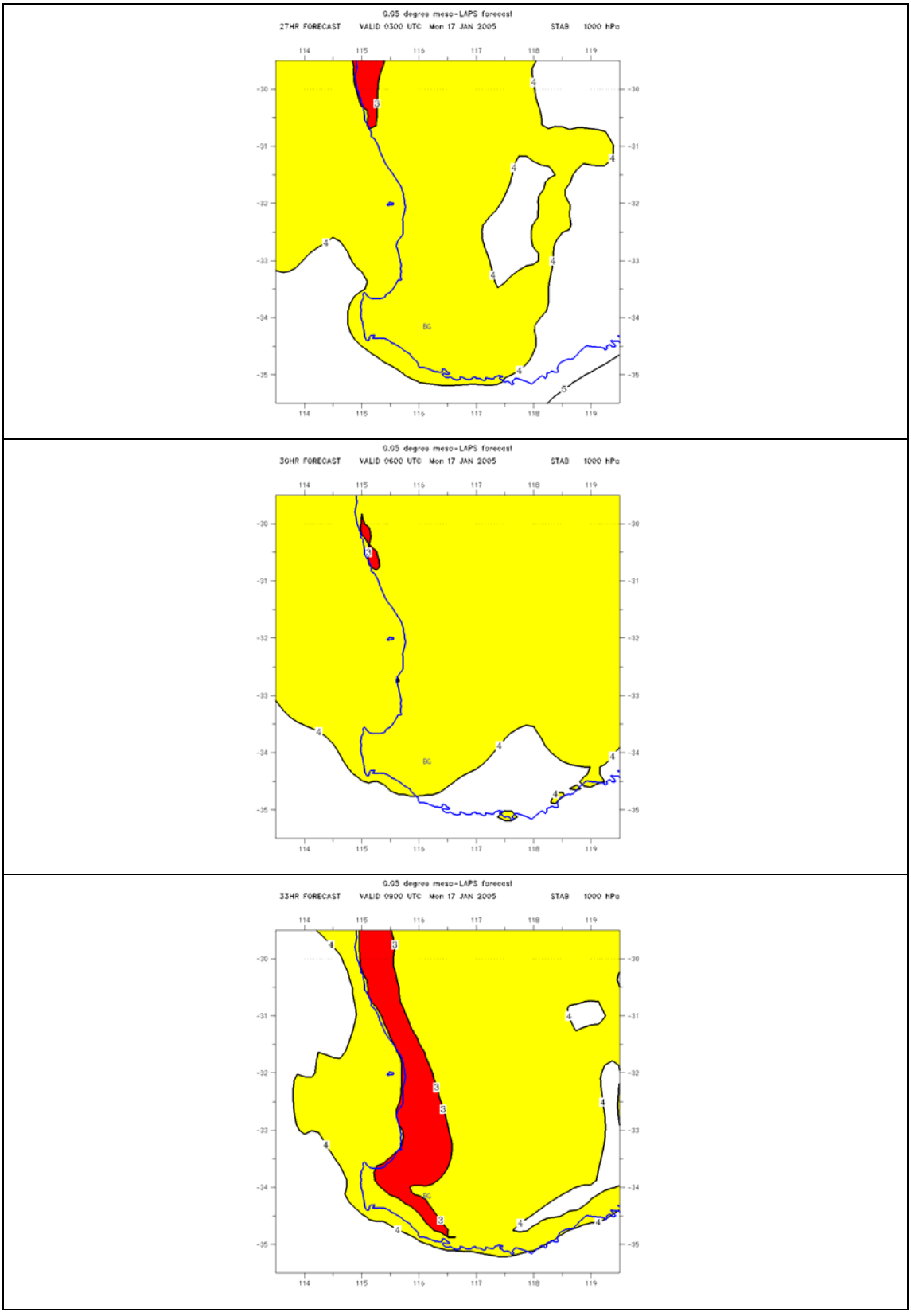

Figure A5.8. Forecasts of the stability of the entrainment layer, STAB (K km^{-1}), valid at 0300 UTC (top), 0600 UTC (middle) and 0900 UTC (bottom) 17 January 2005. Yellow and red shading indicate decreasing levels of stability

C-HAINES shows an increase throughout the period from 0600 UTC 16 December through to 0600 UTC 17 December, with extremely high values on the afternoon of 17th December when the huge pyrocumulus cloud was observed.

It is not clear that the sea-breeze change penetrated the fire area, as it was extremely shallow at Perth Airport. However, it is possible that convergence at the head of the change may have enhanced the development of the pyrocumulus cloud, or alternatively that the heat release from the fire was sufficient to penetrate a weak, shallow frontal inversion.

Notable is the steady overnight (16-17 January) increase in C-HAINES in the region of the fire. The decreasing stability might well have contributed to the gustiness of the winds and to the lower than normally expected overnight relative humidities that aided the spread the fire to the south-west in the early morning hours of the 17th.

The precise physical processes that occur to keep overnight relative humidities low under conditions in which C-HAINES is also high should be investigated.

A.6 The Denbarker Block Fire

This fire started by arson at around 1200 WST on 11 December 2002, grew to some 500 ha on Thursday 12 December, and remained alight overnight, but without significant runs. On the morning of 13 December the fire undertook a major run to the north-east, burning around 3000 ha in 8 hours as a fresh south-westerly change moved through. While the rate of spread was not unexpected given the strong south-westerly winds forecast, several observers remarked on the strong convective activity of the fire on 13 December during its main run, and the low dewpoints forecast for the daytime hours for the days prior to the fire run were also noted (Braun 2003). The fire was contained "when conditions eased after dark" (Klaus Braun, personal communication). A photograph of the fire on the afternoon of 13 December (courtesy Klaus Braun) is shown in Fig. A6.1, and appears to show smoke trapped below an inversion, but with convective activity extending above the inversion.

Figure A6.1. Photograph of the Denbarker Block fire, taken by Klaus Braun at 1643 WST 13 December 2002, from a high point along Spencer Road.

Figure A6.2 shows the scatterplot of 0600 UTC FFDI and C-HAINES for the 8-year climatology at the Mt Barker gridpoint (point 5 in Fig. 1), some 40 km north-east of the fire location, while Fig. A6.3 shows the times series of 0600 UTC FFDI and C-HAINES at Mt Barker from 6-16 December 2002.

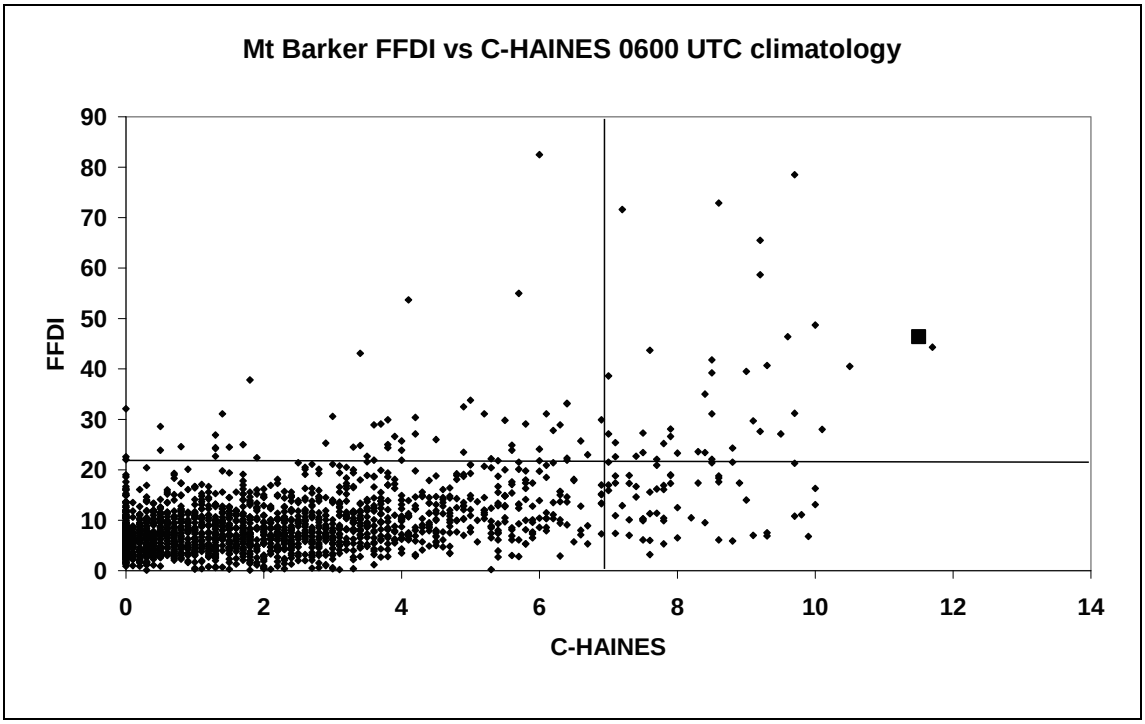

Figure A6.2. Scatterplot of FFDI vs C-HAINES for the "Mt Barker" gridpoint at 0600 UTC for the 8-year climatology in this report. The lines show the 95th percentile values of C-HAINES and FFDI respectively, and the highlighted point is that of 12 December 2002.

Both indices were above their 95th percentile on the 11th and far above their respective 95th percentiles on 12th, even though there was not significant fire spread on that day. On the day of the significant fire spread, though, the values of both indices were low at 0600 UTC, although this time is close to the end of the fire run on that day.

The MSLP analysis for 0600 UTC 13 December (Fig. A6.4) suggests that a west-coast trough change passed through the fire ground overnight, while the front just south of WA suggests that a deeper surge of south-westerly winds was likely during the afternoon. This conjecture is supported by the time-series of Rocky Gully observations (Fig. A6.5), which shows the wind direction backing only slowly throughout the 24-hours from 2000 WST 12 December, with a an initial fluctuation in wind direction at around 11-1200 WST (first vertical line) that was followed by an increase in gustiness and decrease in humidity, until a more significant change between 1600 and 1700 WST 13 December (second vertical line), after which the temperature fell and the humidity increased. From the early morning through the afternoon of 13 December there were relatively fresh and gusty winds – the period of the major fire spread.

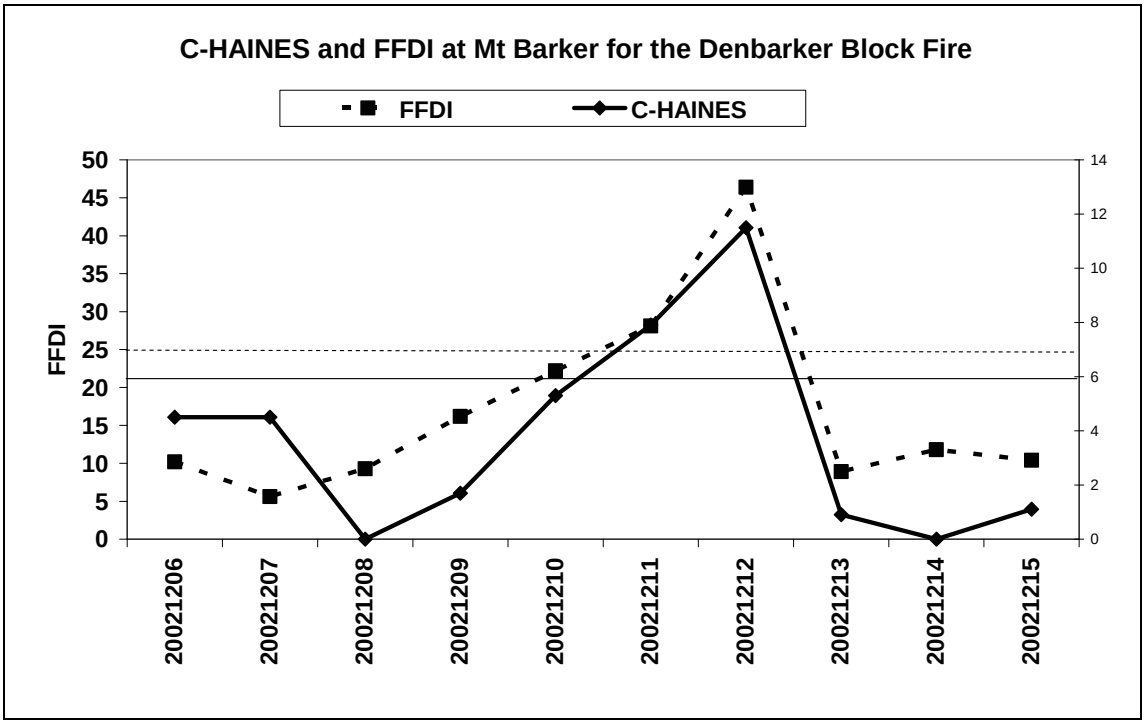

Figure A6.3. Time series of daily FFDI (dashed) and 0600 UTC C-HAINES (solid) from 6 to 25 December 2002 at the "Mt Barker" gridpoint. The horizontal lines indicate the 95th percentile values for the two parameters.

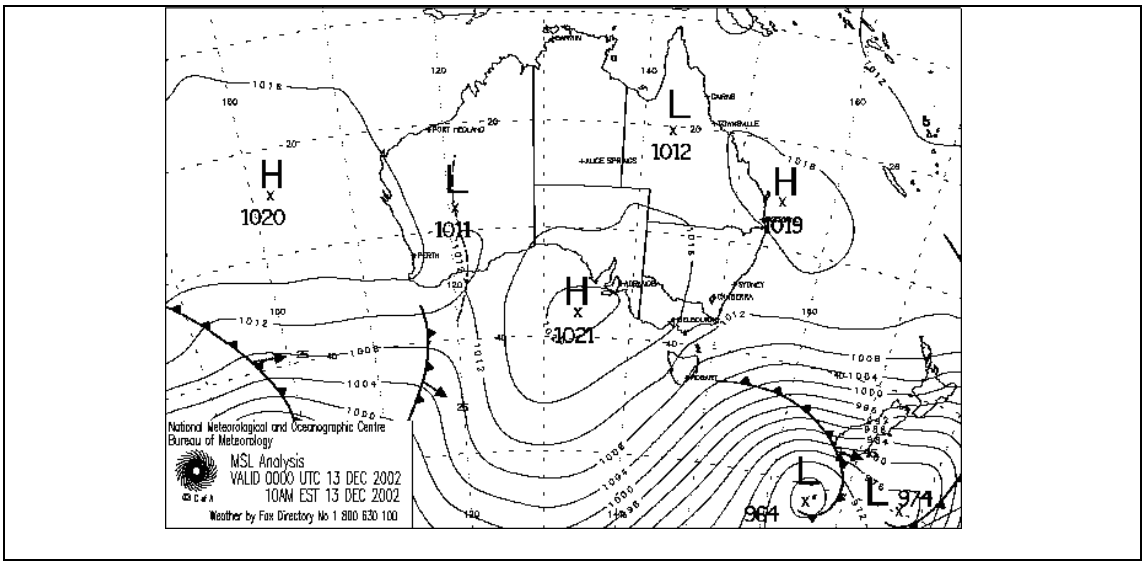

Figure A6.4. Mean-sea-level pressure analysis valid 0000 UTC 13 December 2002 (0800 WST 12 December 2002).

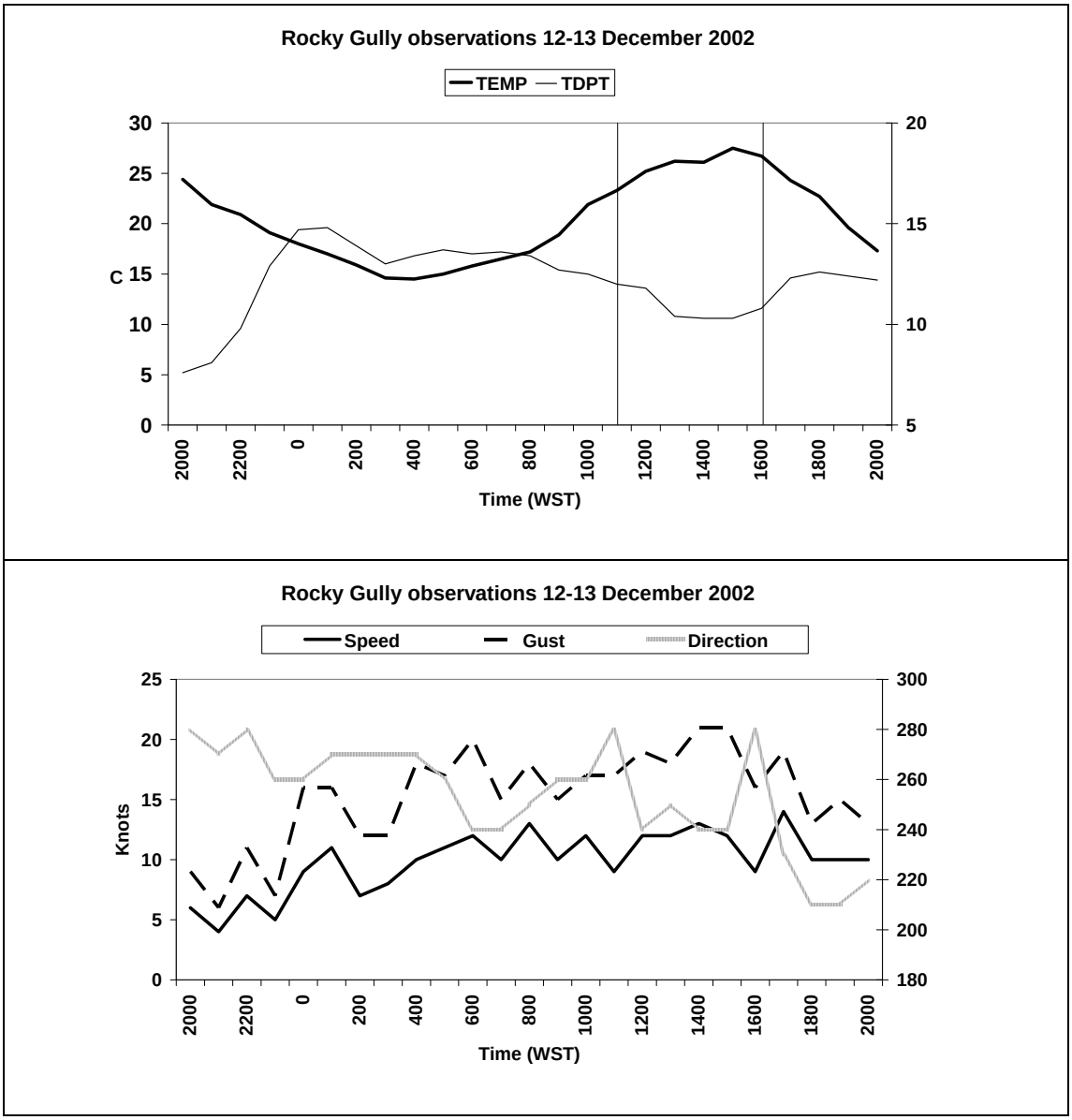

Figure A6.5. Observation time series from the Rocky Gully AWS from 2000 WST 12 December to 2000 WST 13 December 2002. Upper panel shows temperature (bold, left ordinate) and dewpoint (thin line, right ordinate). Lower panel shows wind direction (grey, right ordinate) and speed and gust (solid and dashed black, left ordinate).

Figure A6.6 shows the LAPS375 analysis fields of MSLP and low-level wind, and of C-HAINES at 0600 UTC on 11, 12, and 13 December 2002. Through this two-day period a trough deepened just inland of the WA coastline, and a small low formed over the south-west by the afternoon of the 12th. At the same time a band of very high C-HAINES extended southwards, and exceeded 12 just north of Mt Barker – beyond the 99th percentile at that location – on 12 December. In the final 24-hours both the trough and the band of higher C-HAINES moved eastwards.

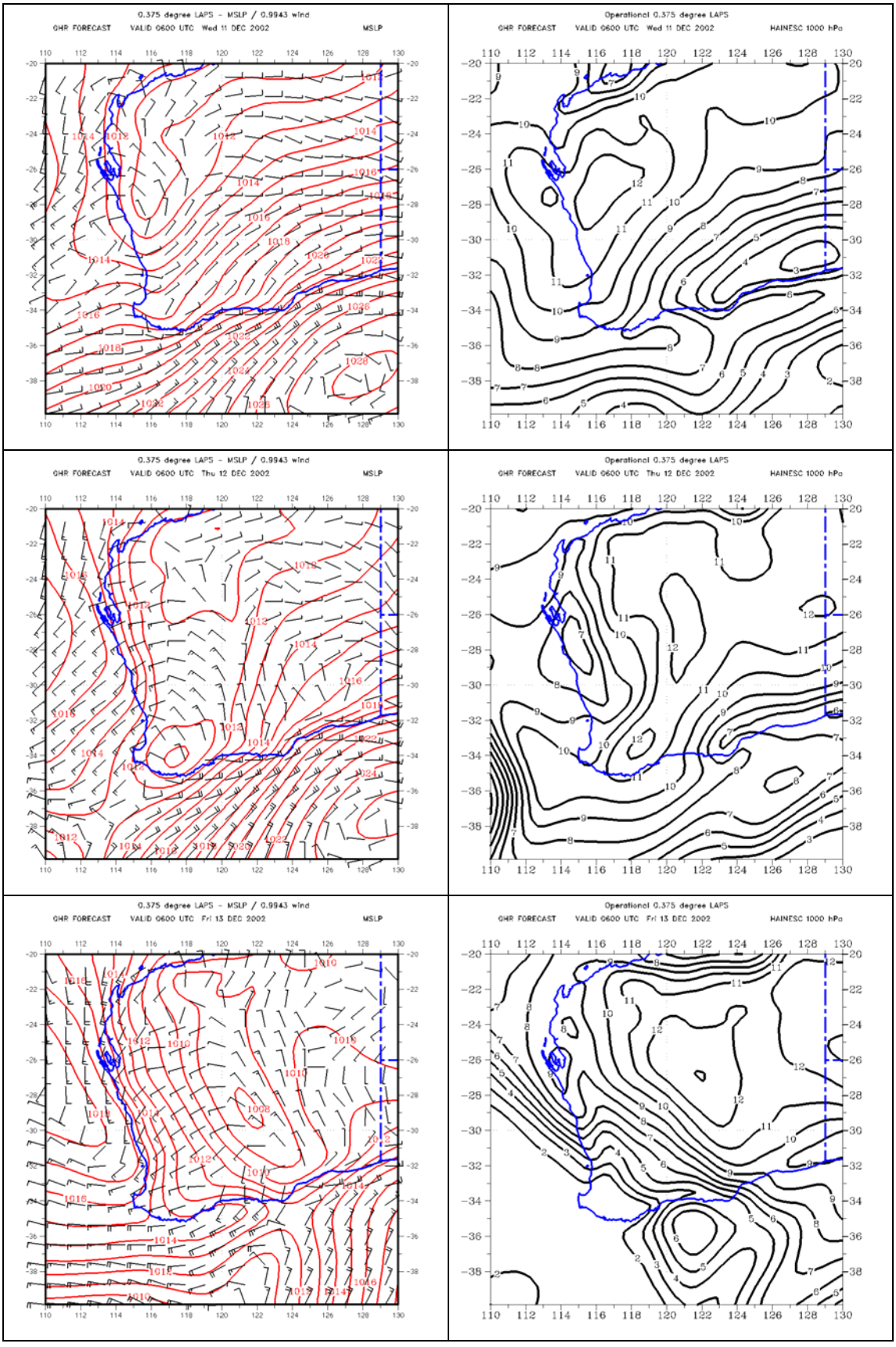

Figure A6.6 Left panels show LAPS MSLP and 70m wind analyses at 0600 UTC 11, 12 and 13 December 2002, with the corresponding C-HAINES analyses in the right column.

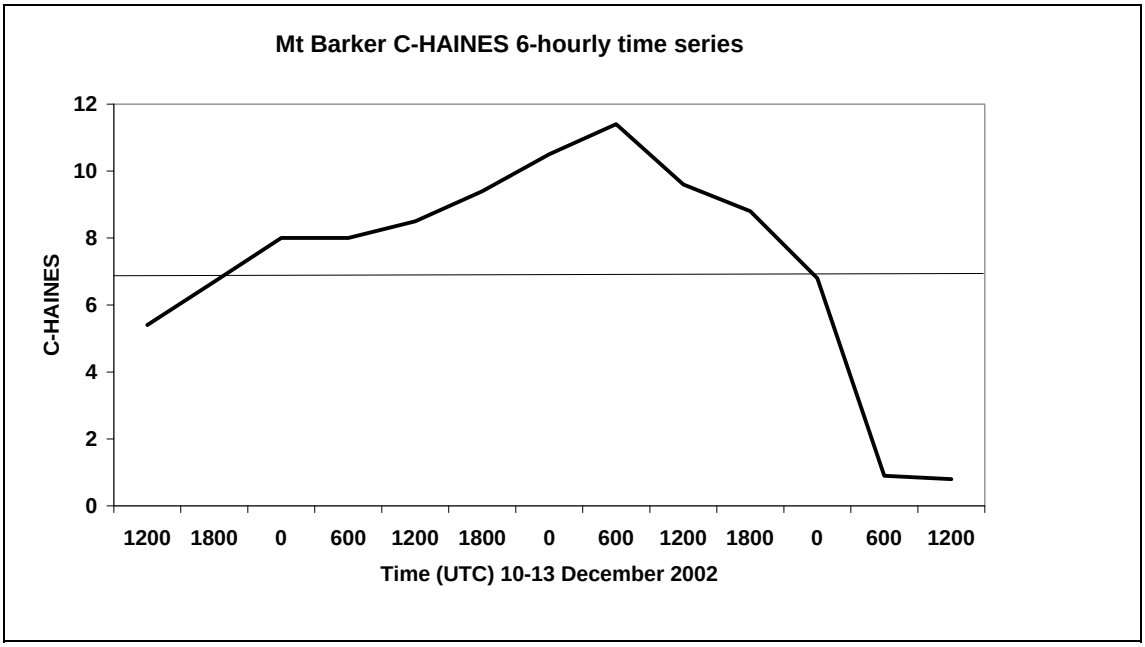

Figure A6.7 Time-series of 6-hourly C-HAINES values interpolated from the LAPS analyses to the "Mt Barker" gridpoint. The horizontal line shows the 95th percentile of the 0600 UTC C-HAINES distribution.

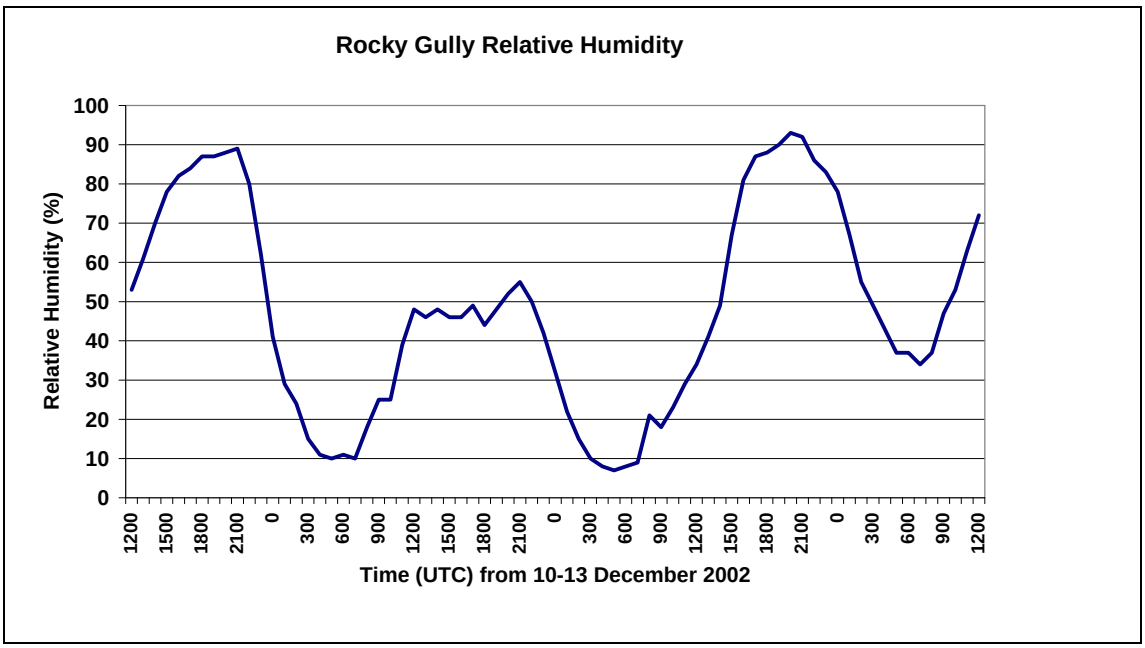

Figure A6.8. Rocky Gully AWS relative humidity from 1200 UTC (2000 WST) 10 December to 1200 UTC 13 December 2002.

The LAPS 6-hourly analysis values of C-HAINES for the period covered by Fig. 6.6 (Fig. A6.7) shows in slightly more detail the passage of this band of high C-HAINES over Mt Barker. There is a sustained period with C-HAINES values well above the 95th percentile (of 0600 UTC values) from early on 11 December (local time). The observed relative humidity at Rocky Gully from 1200 UTC 10 December to 1200 UTC 13 December (Fig. A6.8) shows very low relative humidity during the daytimes of both 11 (ignition) and 12 December, and perhaps also significant, only a weak overnight relative humidity recovery on the night of 11-12 December, coinciding with the sustained period of very high C-HAINES values.

Finally turning to the observed convective activity during the fire run on 13 December, Fig. A6.9 shows the meso-LAPS125 forecast screen level potential temperature and 70m wind forecast and

the C-HAINES forecast for 0000 UTC 13 December 2002. The temperature/wind forecast shows west-south-westerly winds extending right across the plotted domain, but the slow strengthening of the winds and the slightly stronger thermal gradient over the south-west can be interpreted as being the effect of the passage of the front analysed to the south in Fig. A6.4. The C-HAINES values, though, are high as far west as 117E, where values are still around the 95th percentile, although decreasing. Thus the surface westerly change is moving eastwards and slowly deepening beneath a deep layer of dry, unstable air.

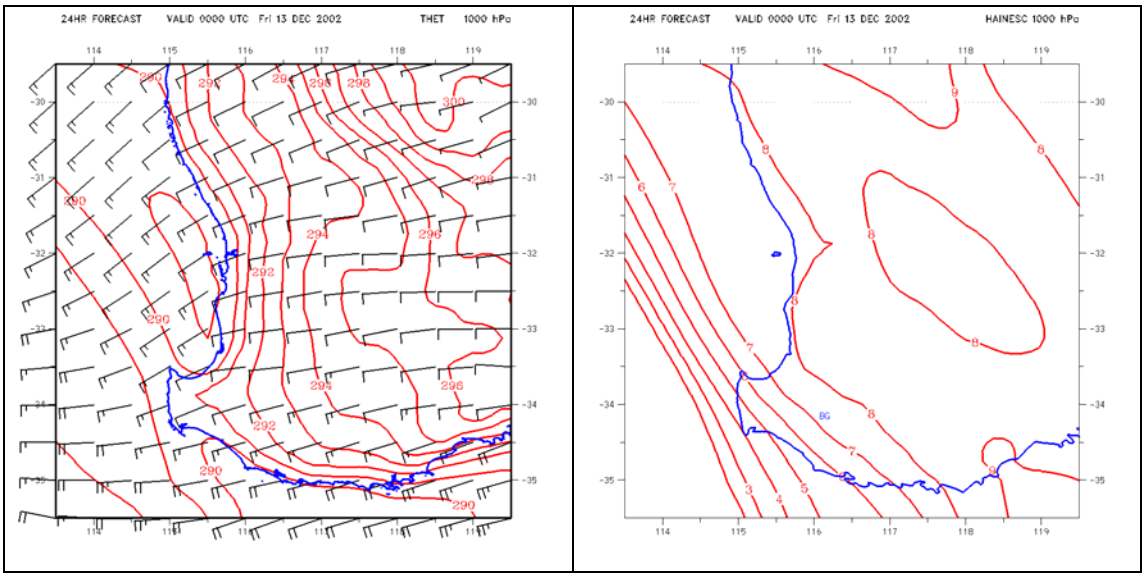

Figure A6.9 Forecasts from the 0.125o mesoLAPS NWP model valid at 0000 UTC 13 December 2002. Left panel: screen-level potential temperature (K) with 70m wind barbs overlaid. Right panel: C-HAINES index.

This is very evident in the 0000 UTC radiosonde sounding at Albany Airport (Fig. A6.10), where a shallow mixed layer is separated from a deep, very dry layer by a strong frontal inversion between 900 and 850 hPa. While this sounding would not suggest the possibility of deep convection, if one modifies the sounding to represent the 1500 WST temperature of 27.5oC at Rocky Gully, and then adds ~3oC (Taylor et al. 1971, Jenkins 2002, Potter 2005, Potter 2007, Clements et al. 2007) to account for the typical effect of a fire at an elevation of ~500 m, then dry mixing to 800 hPa is achieved. This is within the dry “Haines” layer. If one further adds some moisture (3-4 g kg-1) to the low levels, also a combustion product, then moist convection to a considerable altitude is entirely possible, with such a lifted parcel roughly following the moist adiabat from the temperature at the first sharp inversion point (arrowed).

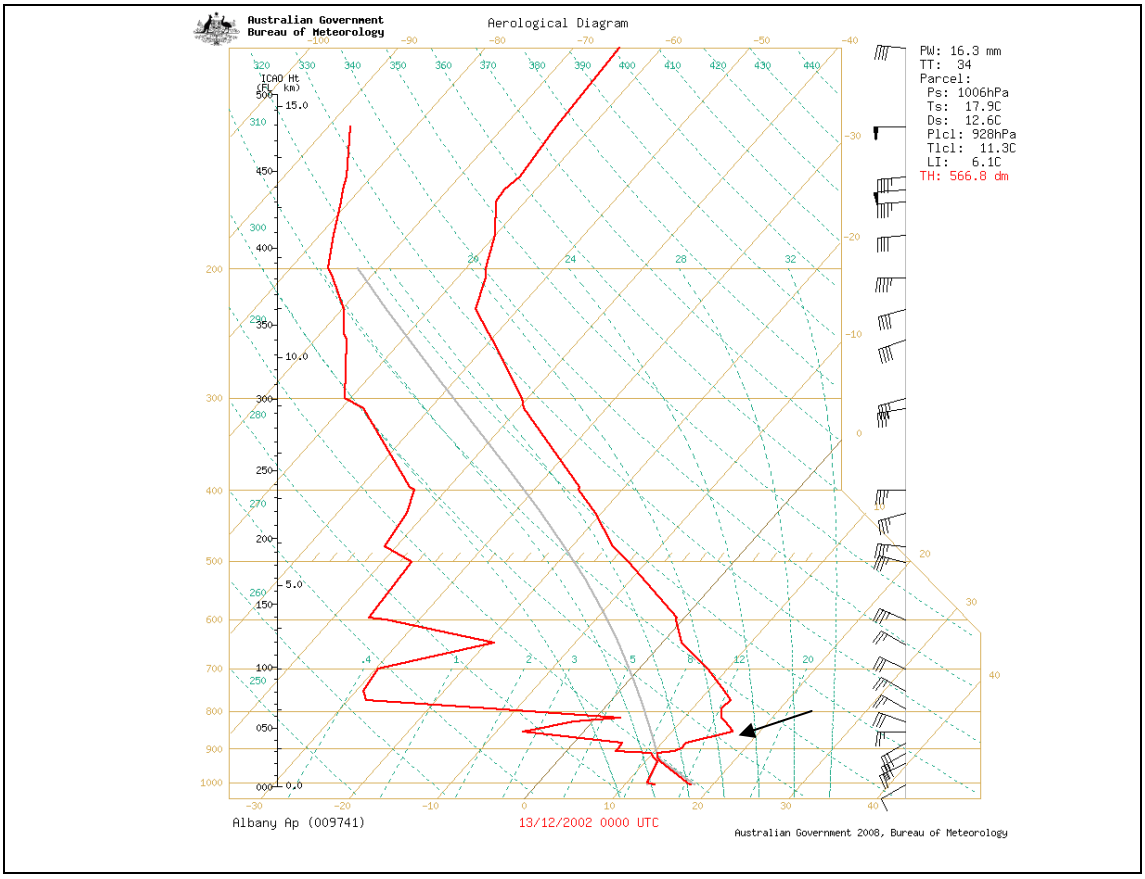

Figure A6.10. Radiosonde ascent from Albany Airport at 0000 UTC 13 December 2002.

Taking the meso-LAPS forecast fields shown in Fig. A6.9, adding a hypothetical 3C and 3 g kg-1 to the temperature and moisture at 500 m elevation, to represent the combustion contribution to these fields, and computing CAPE to the equilibrium level (Fig. A6.11) shows that the evolution of this "FIRE-CAPE" through the day to be complex. Values of FIRE-CAPE in the region of Denbarker were zero at 2100 UTC, but then slowly increased during the day to peak at around 1000 J Kg-1 at around 0900 UTC – quite close to the time of the photo in Fig. A6.1. It must be noted that unmodified model fields generated no CAPE at all throughout the day. In interpreting these fields it is important to remember that this "FIRE-CAPE" can only be realised if a fire is present and releasing enough heat and moisture into the environment above the fire, and so the time evolution at the fire location is perhaps the critical parameter to watch, with the spatial patterns providing some insight into how this potential might evolve.

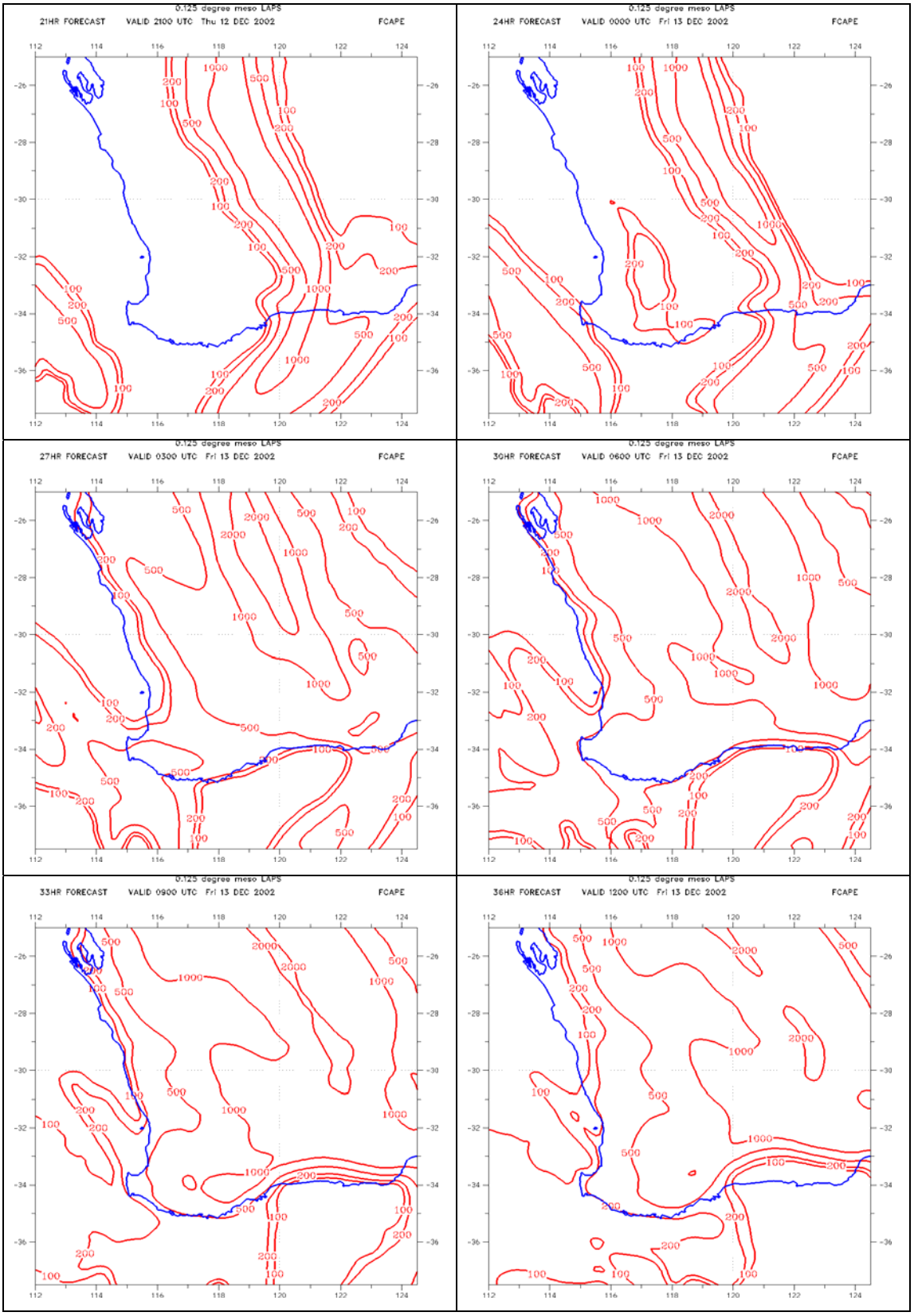

Figure A6.11. Meso-LAPS125 forecast fields of "FIRE-CAPE" (J Kg^{-1}) at 3-hourly intervals from 2100 UTC 12 December to 1200 UTC 13 December 2002.

It is a not unreasonable hypothesis that the heat and moisture from the fire was sufficient to penetrate the frontal inversion, and thus generate convective activity above the inversion. Whether this penetration of the frontal inversion, and convective activity above, provided a

mechanism for the dry air aloft to mix back to the surface is not evident. Afternoon relative humidity was, though, extremely low, as pointed out by Klaus Braun (personal communication), and also evident in the Rocky Gully observations. The analysis by Kiefer et al. (2009) of their idealised modelling experiments indicate a degree of support for this premise, and the need for further research in this area is indicated.

There were very high C-HAINES values for the two days prior to the fire, and also overnight before the major fire run. This provides another example of the association between high C-HAINES environments and low surface relative humidities, and in particular weak overnight relative humidity recovery.

Separation of low levels and the Haines layer by a (stable) frontal inversion in early stages of frontal transition, leads to possibility of heat/moisture contributions from fire "breaking through" the shallow frontal inversion allowing the higher temperature, lower humidity air above the frontal inversion to mix down to the fire, enhancing fire activity.

The "FIRE-CAPE" calculations provide a potential source of guidance to those parts of the forecast area where heat and moisture released from the fire might be sufficient to generate convective instability.

A.7 The Lake Tay Fire

According to notes provided to the authors (Gavin Wornes, personal communication), the Lake Tay fire burnt in an area about 100 km north of Ravensthorpe between 3 and 12 February 2003. The fire was ignited by lightning on 3 February 2003. It began a run to the west on 7-9 February, and from late 9 to late 10 February ran strongly to the south-west, increasing in area from some 30000 ha to some 186000 ha. By the evening of the 11th nearly 275000 ha had been burnt, with a final area burnt of some 300000 ha.

Figure A7.1 shows that the day of the initial big run to the south-west the C-HAINES was essentially the highest in the 8-year climatology for the Ravensthorpe gridpoint (point 8 in Fig. 1), while the FFDI was in the Very High range, approaching its 95th percentile. The time series of 0600 UTC FFDI and C-HAINES (Fig. A7.2) shows that this C-HAINES value on the 10th was the highest for the period of the fire event, while the FFDI was not notably higher than its value on the preceding days. Indeed, the FFDI showed a broadly decreasing trend through the period, while the C-HAINES showed a broadly increasing trend to its peak on 10 February.

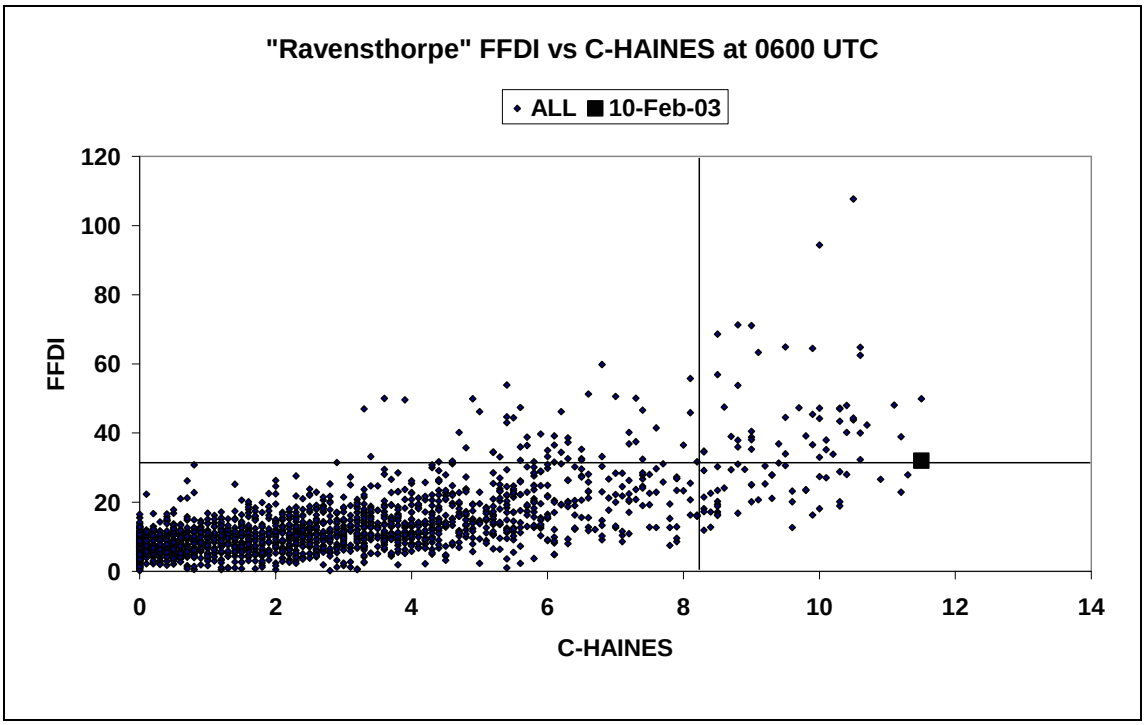

Figure A7.1. Scatterplot of FFDI vs C-HAINES for the “Ravensthorpe” gridpoint at 0600 UTC for the 8-year climatology in this report. The lines show the 95th percentile values of C-HAINES and FFDI respectively, and the highlighted point is that of 10 February 2003.

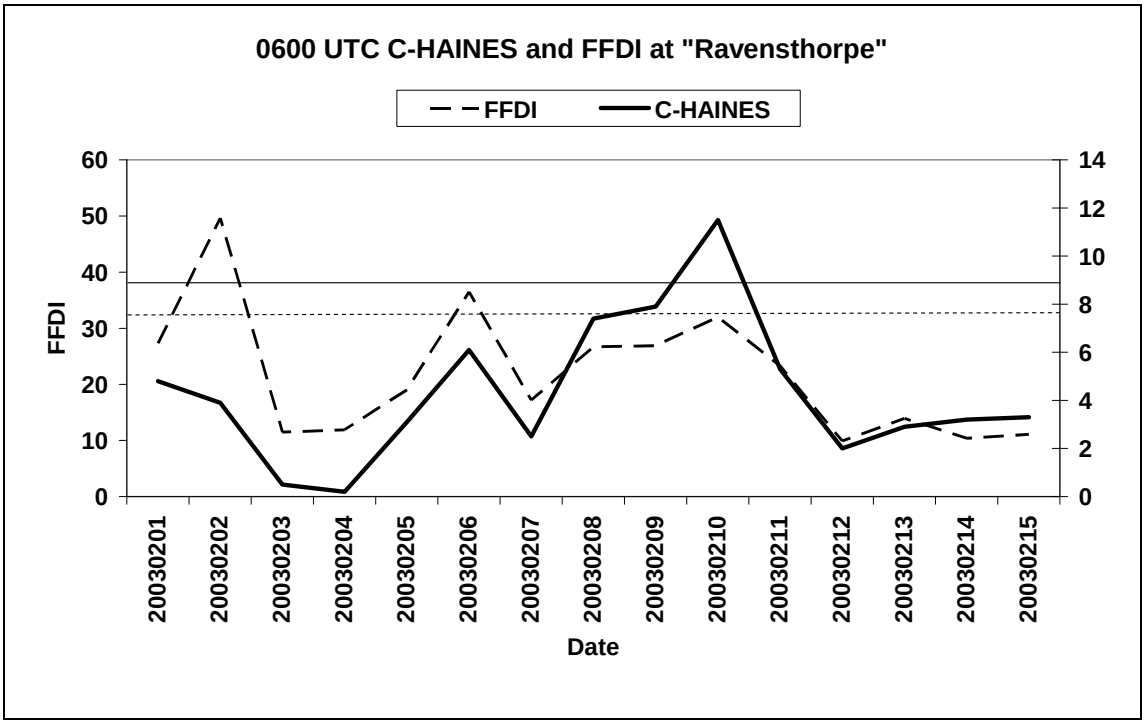

Figure A7.2. Time series of daily FFDI (dashed) and 0600 UTC C-HAINES (solid) from 1 to 15 February 2003 at the "Ravensthorpe" gridpoint. The horizontal lines indicate the 95th percentile values for the two parameters.

The MSLP/low-level wind analyses from LAPS375 for 0600 UTC 9, 10 and 11 February 2002 (Fig. A7.3) show a deep west-coast trough forming on 9 February, with a circulation centre just south of Perth. At this time the winds near the fire site were tending northerly and freshening. A day later, on 10 February, the west-coast trough had begun to move eastwards, and the winds over the fire site were northerly. By the following day the change had passed through the fire site. It was in the period between 0600 UTC 9 February and the passage of the cool change that the major fire spread occurred.

The Munglinup West AWS, selected because of its similar distance from the coast to the fire location, observation time series is shown in Fig. A7.4. Wind speeds are high, particularly through the daytime hours of 9-10 February, with winds slowly backing from north-east to north, until the arrival of a strong south-westerly change between 0800 and 0900 WST on the 11th. The passage of the cold front is also particularly marked in the temperature and relative humidity time series (lower panel), but it is also notable that the relative humidity remained very low throughout the period prior to the change, with only very slight overnight recovery on both the nights shown.

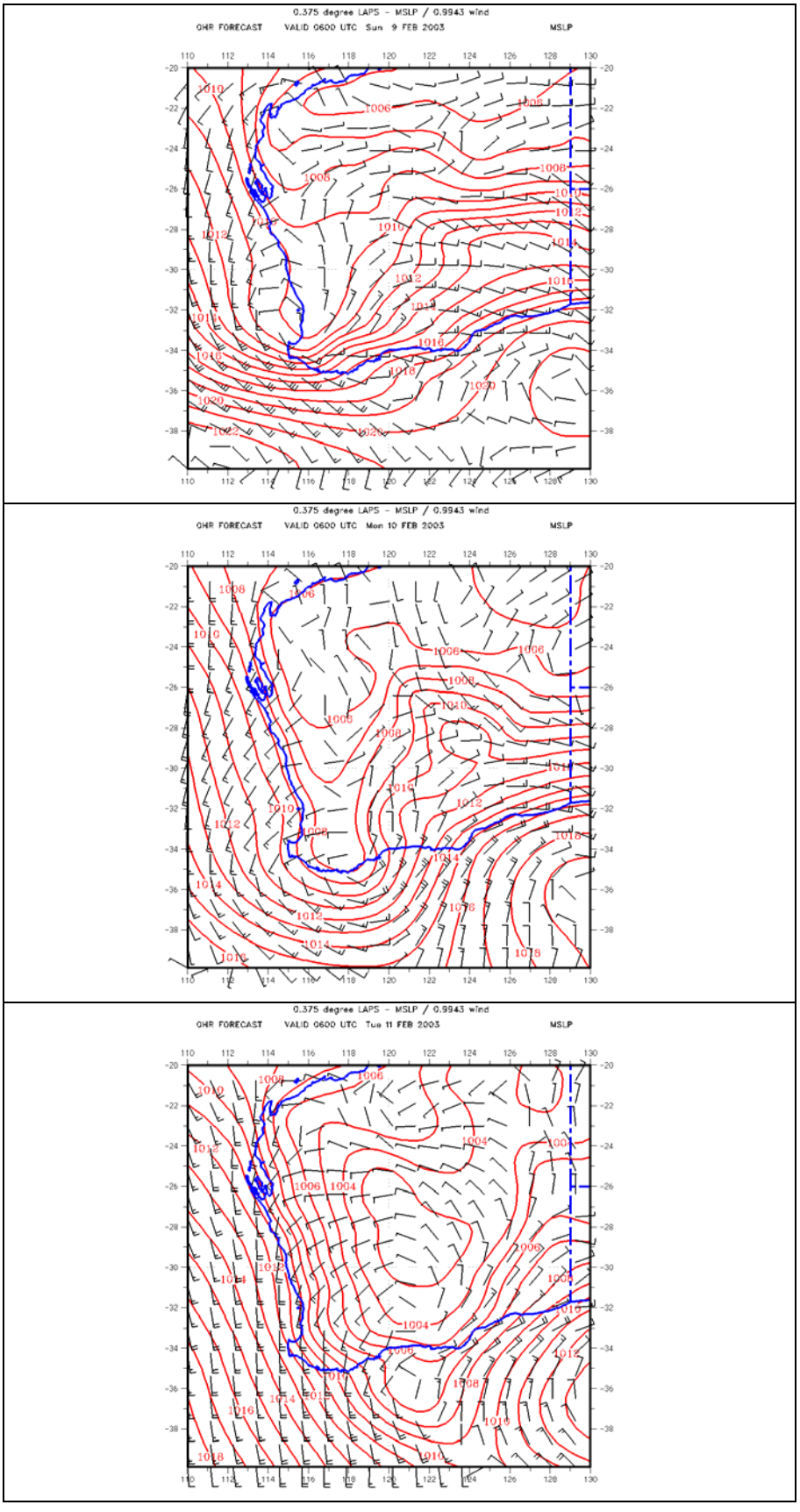

Figure A7.3. MSLP overlaid with 70m wind barbs from the LAPS analyses at 0600 UTC on 9 (top), 10 (middle) and 11 (bottom) February 2003.

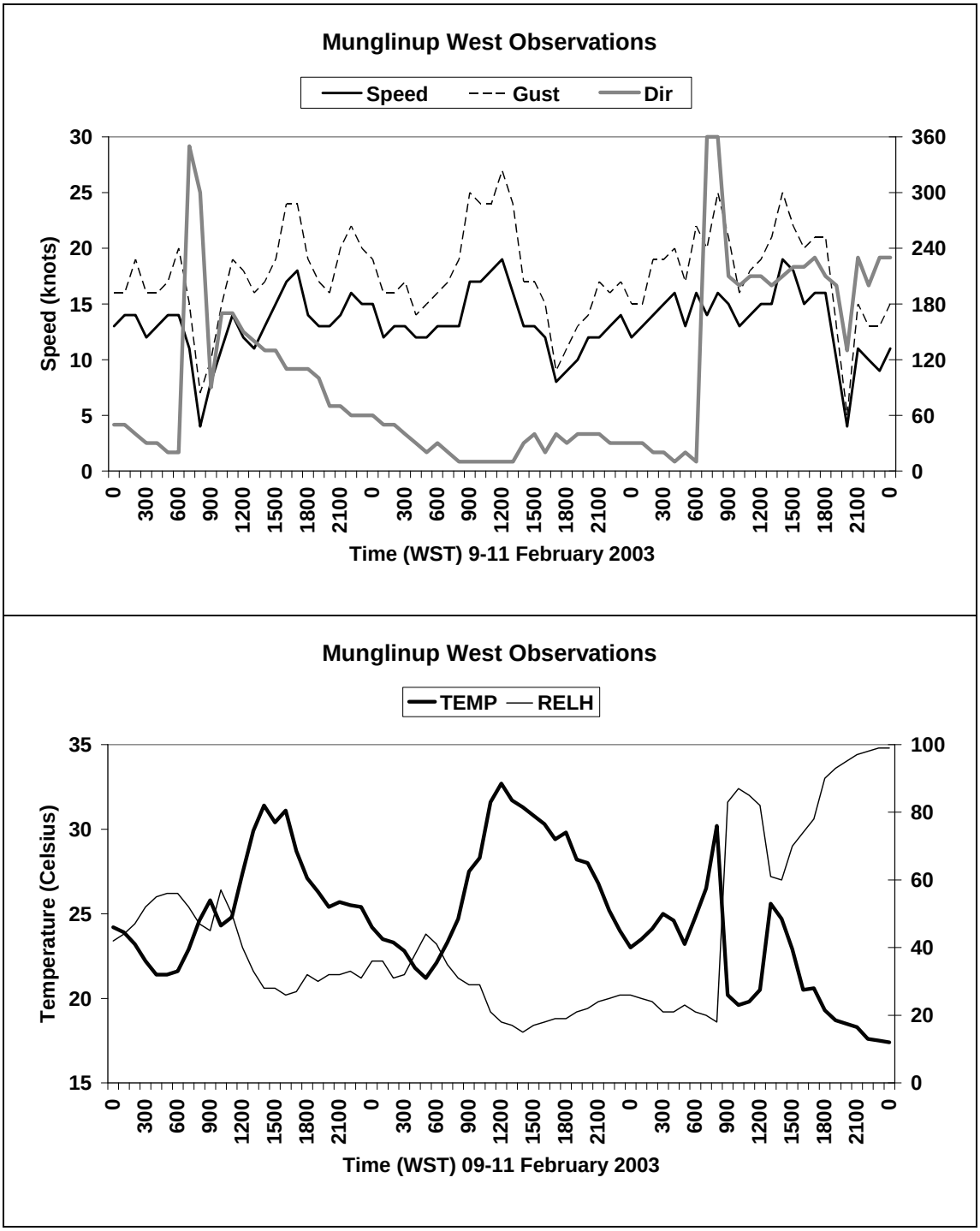

Figure A7.4. Time series of AWS observations from the Munglinup West site. Top panel show wind direction (solid, grey), wind speed (solid, black), and wind gust (dashed). Lower panel shows temperature (heavy line) and relative humidity (thin line). Times are from 0000 hours local time on 9 February to 0000 hours 12 February 2003.

The C-HAINES analysis for the afternoon of 10 February 2003 is shown in Fig. A7.5. An extended band of very high values of C-HAINES aligned just east of the trough axis (cf Fig. A7.3) is seen, with a maximum above 11 in the vicinity of Ravensthorpe. The extreme values in this case are driven largely by the dewpoint depression component (>99th percentile) rather than the temperature lapse component. This band of very high C-HAINES had moved only slowly towards the east over the preceding 24 hours, and so was high overnight, providing another

example of the association between events with both high values of C-HAINES and weak overnight relative humidity recovery.

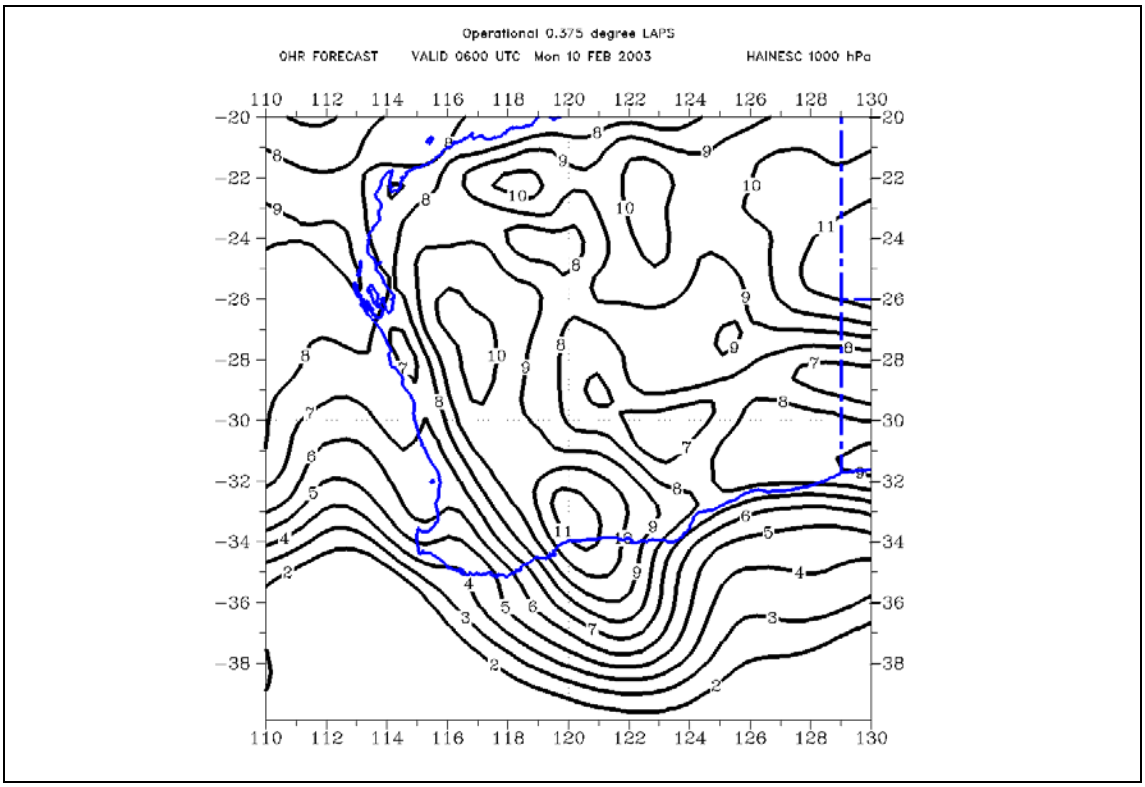

Figure A7.5. Analysed field of C-HAINES from the LAPS analysis for 0600 UTC 10 February 2003.

In this case there seems to be a strong association between the statistically extreme values of C-HAINES and the period of major fire activity. Its use may have assisted anticipation of fire spread.

The sustained period of extremely low humidity during the 24-hours leading to the major fire run may have led to lower than normal fine fuel moisture content and more active wind-driven fire behaviour.

Low overnight relative humidity recovery occurred at the same time as very high overnight values of C-HAINES.

A.8 The Big Desert Fire of December 2002

This fire was ignited by lightning on 17 December 2002, and was estimated to have burnt

65000 ha by 18 December

~100000 ha by 19 December

120000 ha by 20th December

133000 ha by 21 December

179000 ha by 22 December

Conditions then ameliorated, and the fire was declared safe on 31 December, with total area burnt of 181400 ha, and perimeter of 350 km (http://www.dse.vic.gov.au/DSE/nrenfoe.nsf/FID/-0221C9CAD59258EDCA256C96000D82AF?OpenDocument) .

The scatterplot of C-HAINES and FFDI from the 0600 UTC climatology at the Murraylands gridpoint (point 16 in Fig. 1) is shown in Fig. A8.1, with the points for the period 15-22 December 2002 highlighted. Until the 22nd, after conditions began to ameliorate (see below) all days were close to the 95th percentile of FFDI, and above to well-above the 95th percentile of C-HAINES.

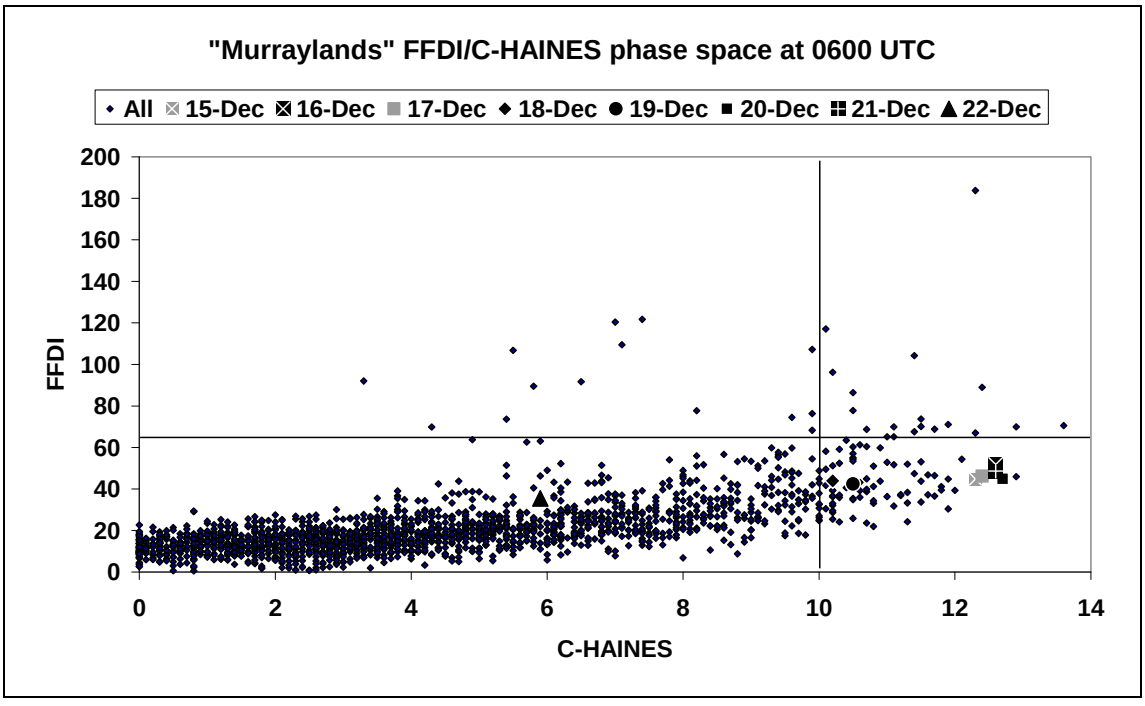

Figure A8.1. Scatterplot of FFDI vs C-HAINES for the “Murraylands” gridpoint at 0600 UTC for the 8-year climatology in this report. The lines show the 95th percentile values of C-HAINES and FFDI respectively, and the highlighted points are for the dates listed in the legend.

The time series of these data at 0600 UTC, from 10-25 December, are shown in Fig. A8.2, together with lines showing the 95th percentiles of each variable, and the arrow showing the ignition day.

Obvious points are:

There were two days of extremely high C-HAINES and FFDI prior to the lightning ignition.

It is statistically a remarkably long period with near-Extreme FFDI and statistically extreme C-HAINES.

The C-HAINES values are statistically more extreme than the FFDI values. Thus while the two time-series in Fig. A8.2 roughly track each other, the very extreme nature of the C-HAINES might contain additional forecast information.

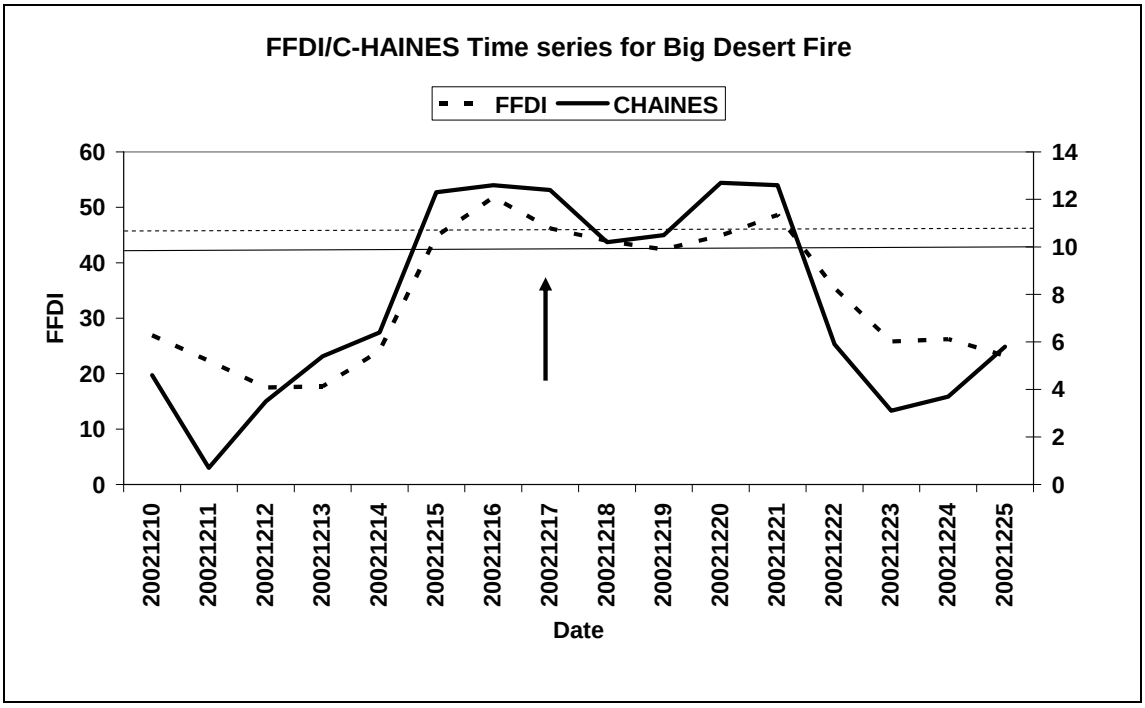

Figure A8.2. Time series of daily FFDI (dashed) and 0600 UTC C-HAINES (solid) from 10-25 December 2002 at the "Murraylands" gridpoint. The horizontal lines indicate the 95th percentile values for the two parameters, and the arrow indicates the ignition day.

To look at the pre-ignition period in a little more detail, the 6-hourly C-HAINES time series is plotted in Fig. A8.3a, with the temperature/dewpoint and the relative humidity time series from the Walpeup AWS in Figs. A8.3b,c.

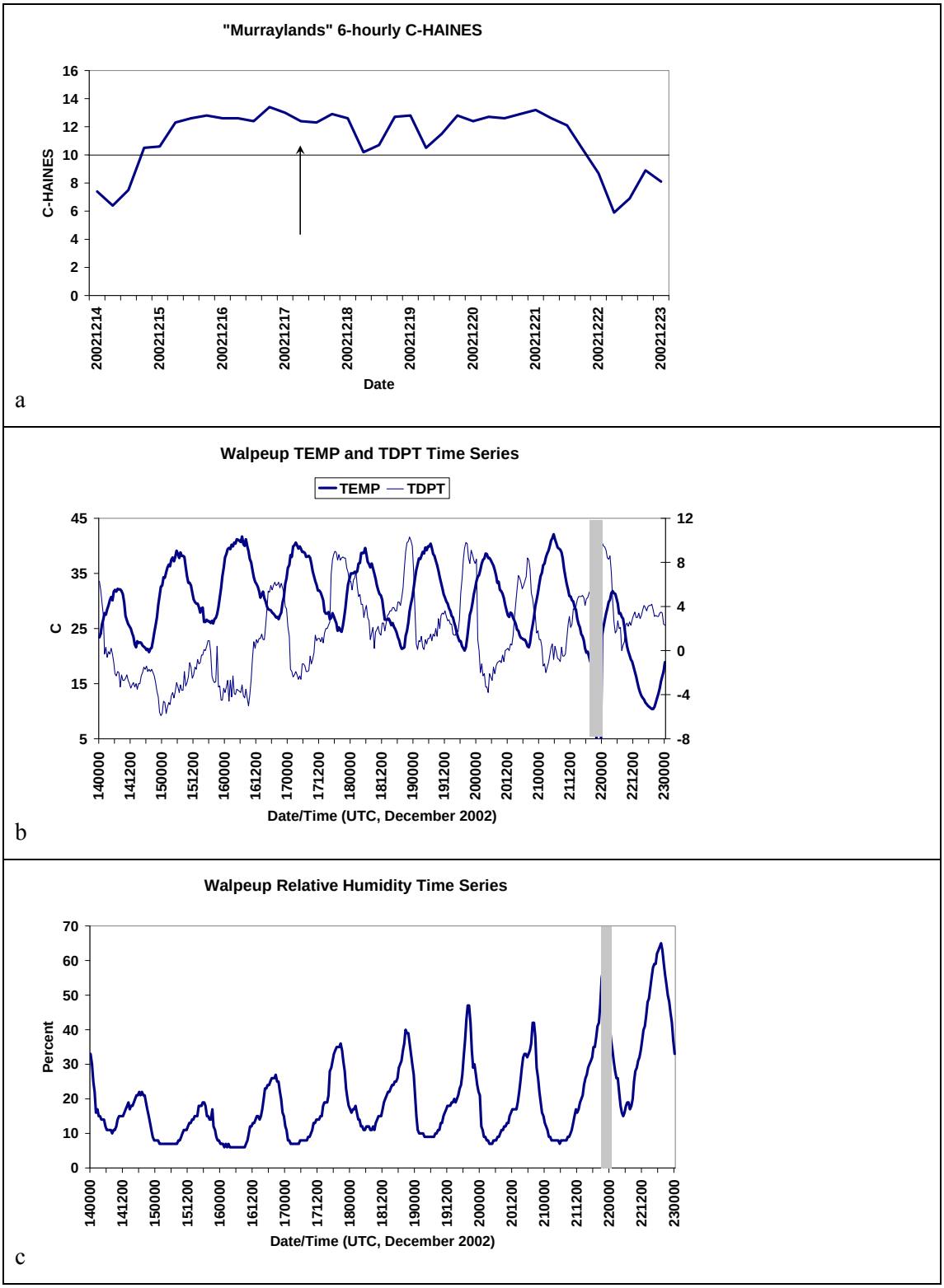

Figure A8.3. Top panel – time-series of 6-hourly C-HAINES from the “Murraylands” gridpoint , with the 95th percentile values at 0600 UTC indicated by the horizontal line, and the ignition day arrowed. Middle panel – time series of temperature (left ordinate) and dewpoint (right ordinate) from the Walpeup AWS. Bottom panel – time series of relative humidity (%) from the Walpeup AWS. All panels cover the same period, from 0000 UTC 14 December to 0000 UTC 23 December 2002, with the grey-shaded areas in the lower two panels representing missing data.

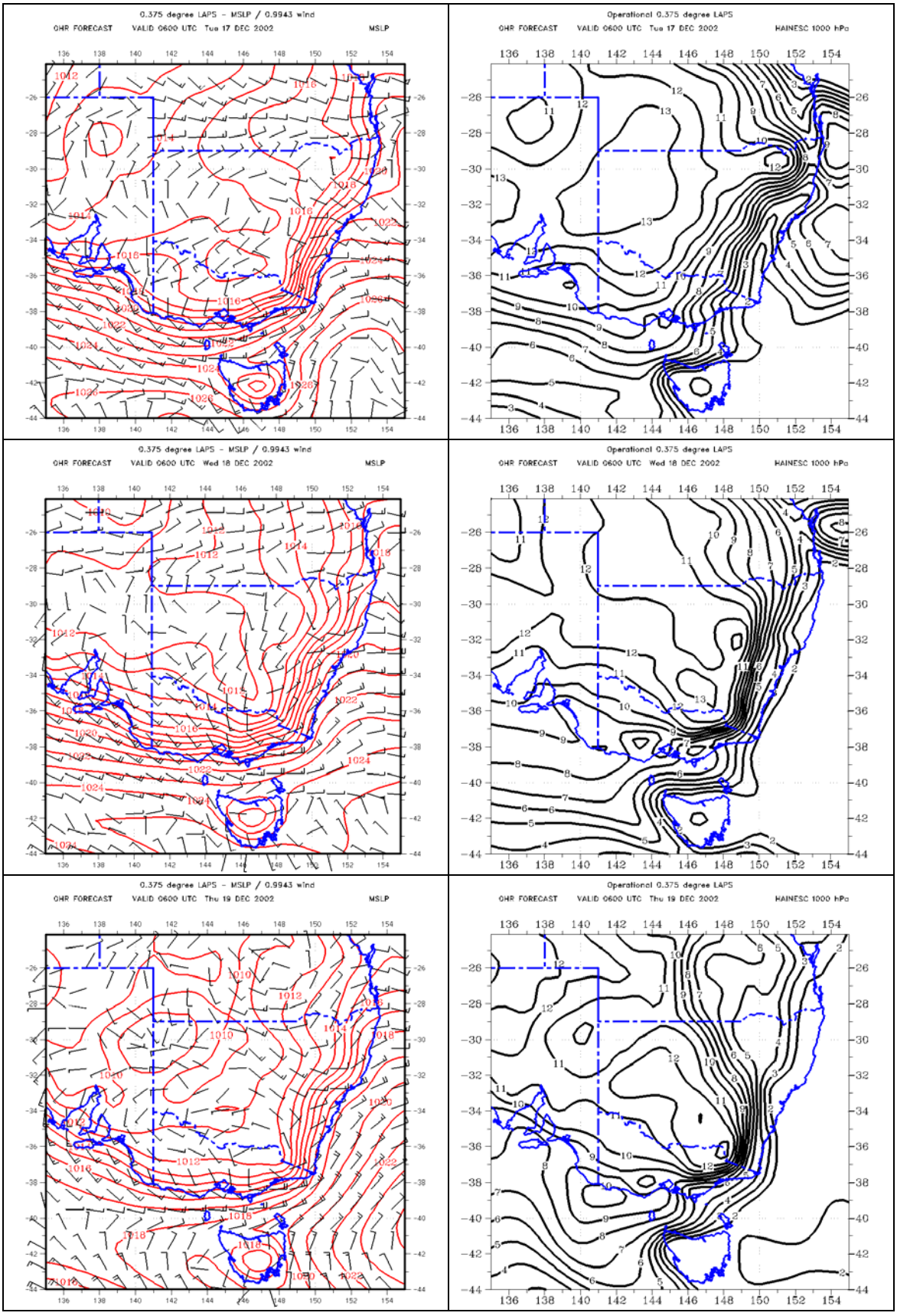

Figure A8.4. Left panels: MSLP and 70m wind barbs over south-eastern Australia from the LAPS numerical objective analyses for 0600 UTC 17, 18, and 19 December 2002. Right panels – C-HAINES fields for the same times.

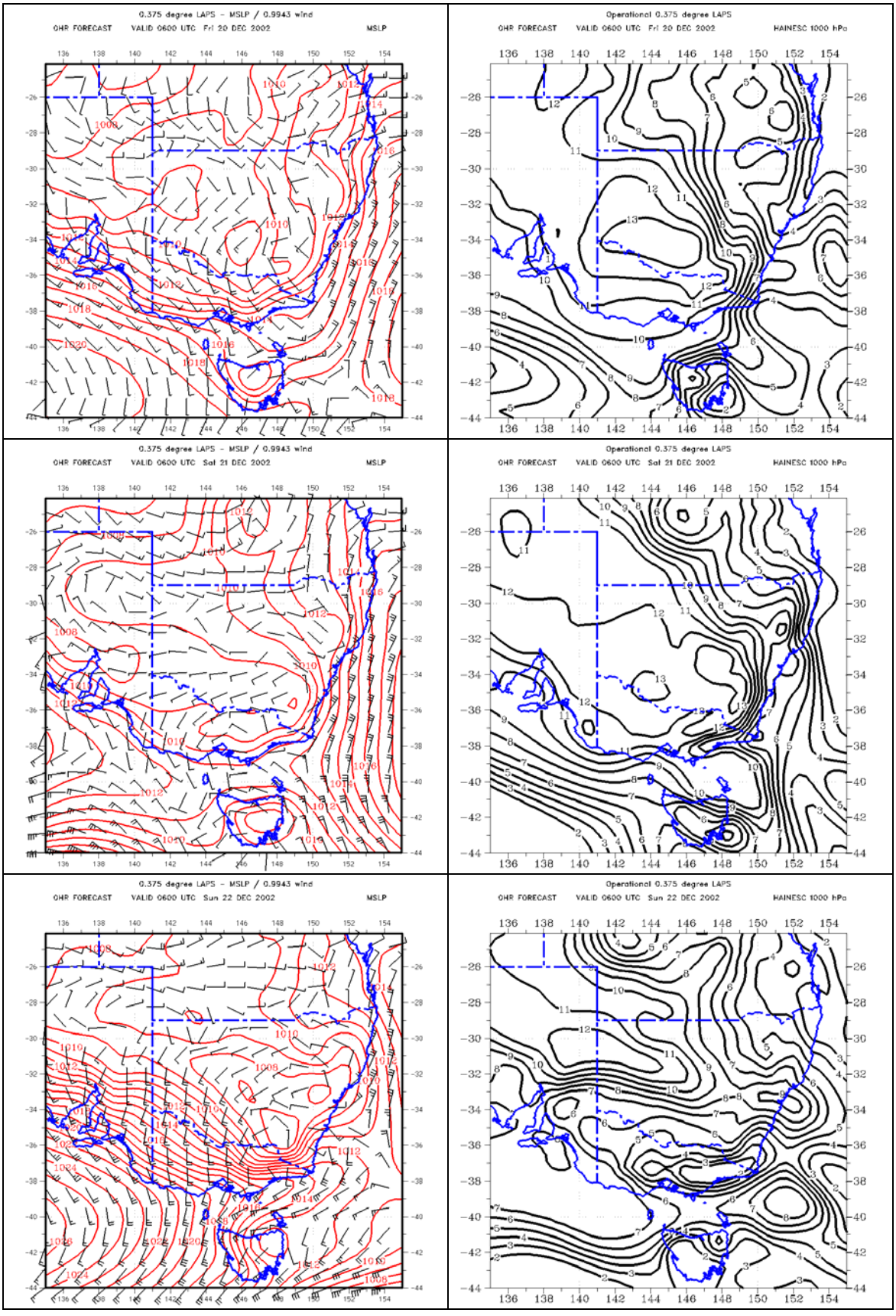

Figure A8.5. Left panels: MSLP and 70m wind barbs over south-eastern Australia from the LAPS numerical objective analyses for 0600 UTC 20, 21, and 22 December 2002. Right panels – C-HAINES fields for the same times.

First, there is very little diurnal variation in C-HAINES, indicating that once the values of this index rose, they remained very high throughout the event. Second, the relative humidity showed very little overnight recovery during, in particular, the days prior to the lightning ignition, and even during the fire period the overnight relative humidity recovery only reaches ~40%. It is particularly noticeable in the early part of this time series that the low relative humidities are being driven by low values of the absolute humidity in the atmosphere. From the night of 16-17 December there is a more-normal (negatively correlated) diurnal cycle of temperature and dewpoint, although the relative humidities are still low. It must also be remembered here that the region was suffering from extreme long-term rainfall, and thus soil-moisture, deficits at this time (Bureau of Meteorology, 2003).

Figures A8.4 and A8.5 show the LAPS375 analysis MSLP/70 m wind and C-HAINES fields at 0600 UTC 17, 18, 19 and 20, 21, 22 December 2002 respectively. The lightning ignitions on the 17th occurred in conjunction with the movement of a weak trough northward across northern Victoria. Thereafter a trough over the interior of SA moved slowly southwards to be over the Mallee on 20-21 December. Associated with this trough were extremely high values of C-HAINES, driven by both extreme values of lapse rate (boundary layer heights were above 650 hPa), and low 850 hPa dewpoints. The C-HAINES values above 13 are approaching the maximum possible. By the afternoon of the 22nd, development of a high pressure system south of SA was bringing cooler southerly winds across the Mallee, and in addition increased the humidity and stabilised the lapse rates, reducing the C-HAINES values as seen in Figs. A8.2 and A8.5.

While FFDI values were quite high throughout this period, the C-HAINES values were also extra-ordinarily high on the day of the lightning ignition, and again on 20 and 21 December.

The C-HAINES values were extra-ordinarily high for the two days prior to the ignition, and correspond to a period of extremely low relative humidity, including a very weak overnight recovery in this quantity, showing an association between high C-HAINES and low overnight relative humidity recovery, and also low relative humidity on the days prior to fire ignition.

A.9 Victorian Fires 2006-7

The 2006-7 summer was one of the worst fire seasons recorded in Victoria, with fire outbreaks in the Mallee in September, south-western Victoria in November, and, following a widespread lightning ignition on 1 December, fires that burnt a huge area of the alpine regions over a 7 week period. The basic information describing major fire outbreaks and activity used in this section is based on Smith (2007) and McCarthy et al. (2008), and focuses on the days of major fire spread listed in those sources. These descriptions are in three sections below, discussing the fire event in the Murray-Sunset National Park on 19 September, then the fires in south-western Victoria on 20 and 21 November 2006, and thirdly a discussion focussing on three major activity days during the fires in eastern Victoria during December 2006 and January 2007.

Murray-Sunset National Park – 19 September 2006

On this day 273 fires were ignited by lightning in the Murray-Sunset NP in north-western Victoria, burning 23000 ha. The scatter-plot in Fig. A9.1 shows that at the Murraylands gridpoint (point 16 in Fig. 1) the FFDI was in the top few in the data (and this in September – very early in the season), while the C-HAINES was around the 95th percentile. The daily time-series of FFDI and C-HAINES (Fig. A9.2) shows that there was a huge spike in the FFDI time-series on 19 September, and also shows high, but not extraordinary, values the day before. The C-HAINES was very high from 17 September, and while not above the 95th percentile, was perhaps more significant given that this was very early in the season. Synoptic considerations (Fig. A9.3) suggest that these high values would have persisted through the night of 18-19 September. This provides another example of C-HAINES being very high for some days prior to an ignition day. It is worth noting that the FFDI was above 80 on 22 September, although the C-HAINES was below 6, showing that not all Extreme fire weather days also have anomalously high values of C-HAINES.

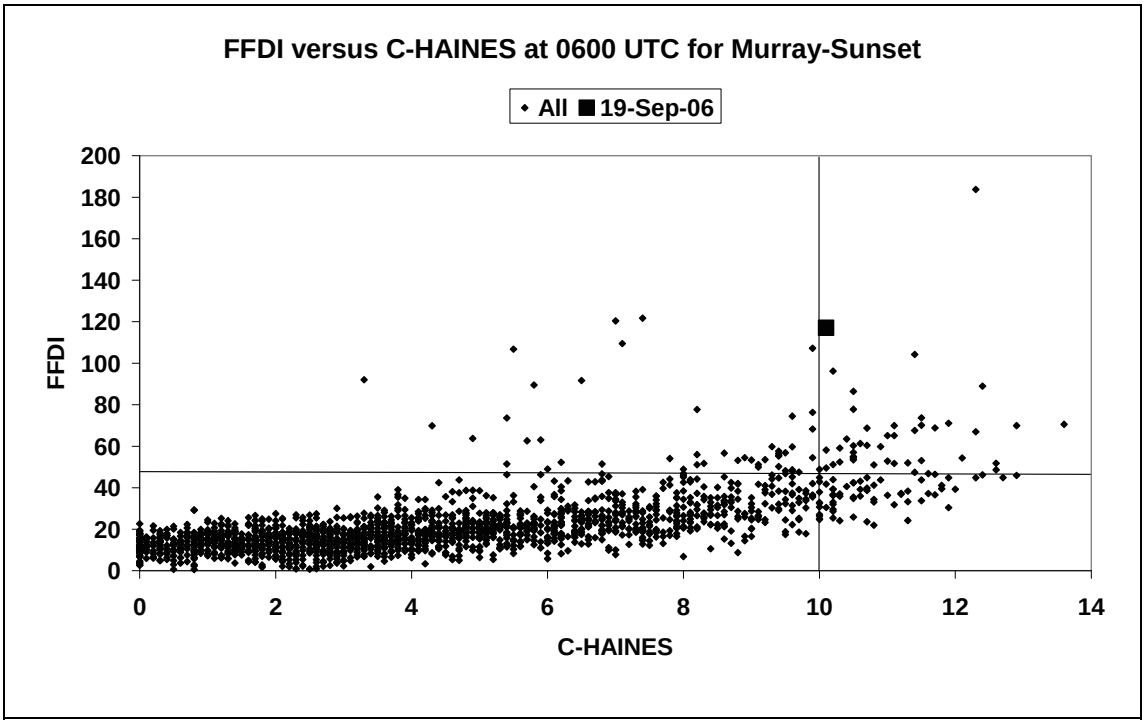

Figure A9.1. Scatterplot of FFDI vs C-HAINES for the "Murraylands" gridpoint at 0600 UTC for the 8-year climatology in this report. The lines show the 95th percentile values of C-HAINES and FFDI respectively, and the highlighted point is that of 19 September 2006.

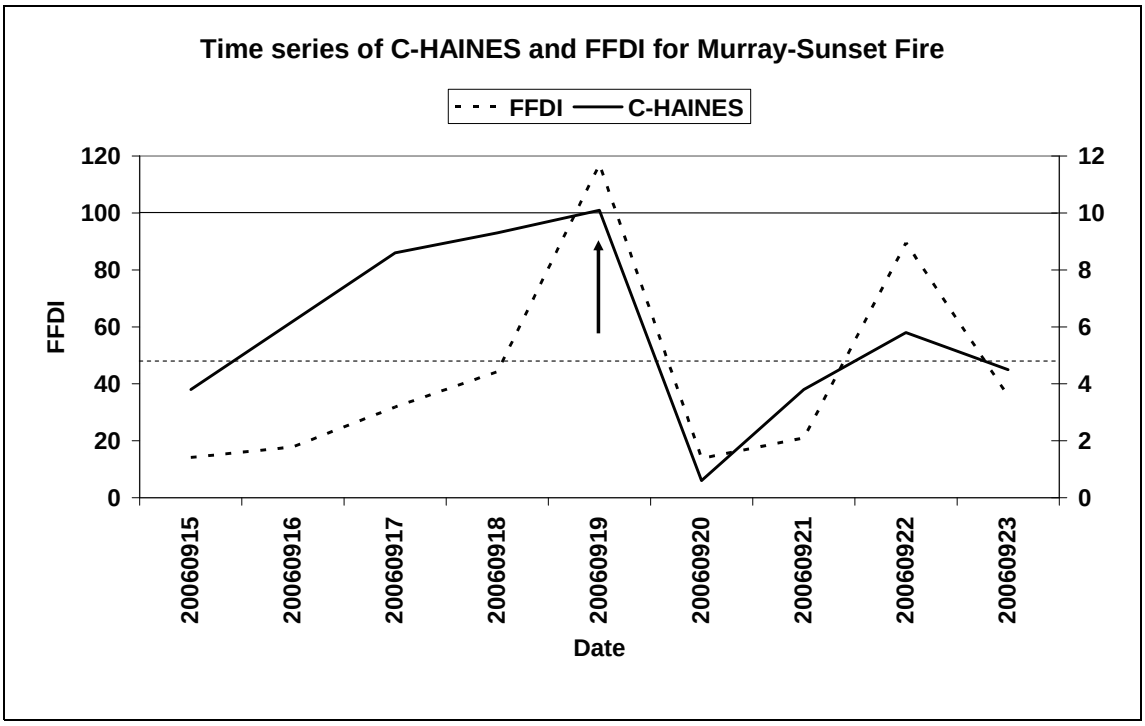

Figure A9.2. Time series of daily FFDI (dashed) and 0600 UTC C-HAINES (solid) from 15-23 September 2006 at the "Murraylands" gridpoint. The horizontal lines indicate the 95th percentile values for the two parameters, and the arrow indicates the fire activity day.

A huge pyrocumulus cloud was reported on this day (see pyrocumulus event 15 in Table 2), and the synoptic situation was characterised by a very strong cold front moving into the area at 0600 UTC (see Fig. A9.3), with an elongated band of high C-HAINES ahead of the front. As the strong gradient on the cool, or encroaching, side of the C-HAINES maximum is just over the sample gridpoint used for this climatology, the representative value for the event may well be a little higher than that plotted. Note that the data tabulated in Table A2 show that extremely high values of both FFDI and of C-HAINES are frequently observed when large pyrocumulus clouds are reported.

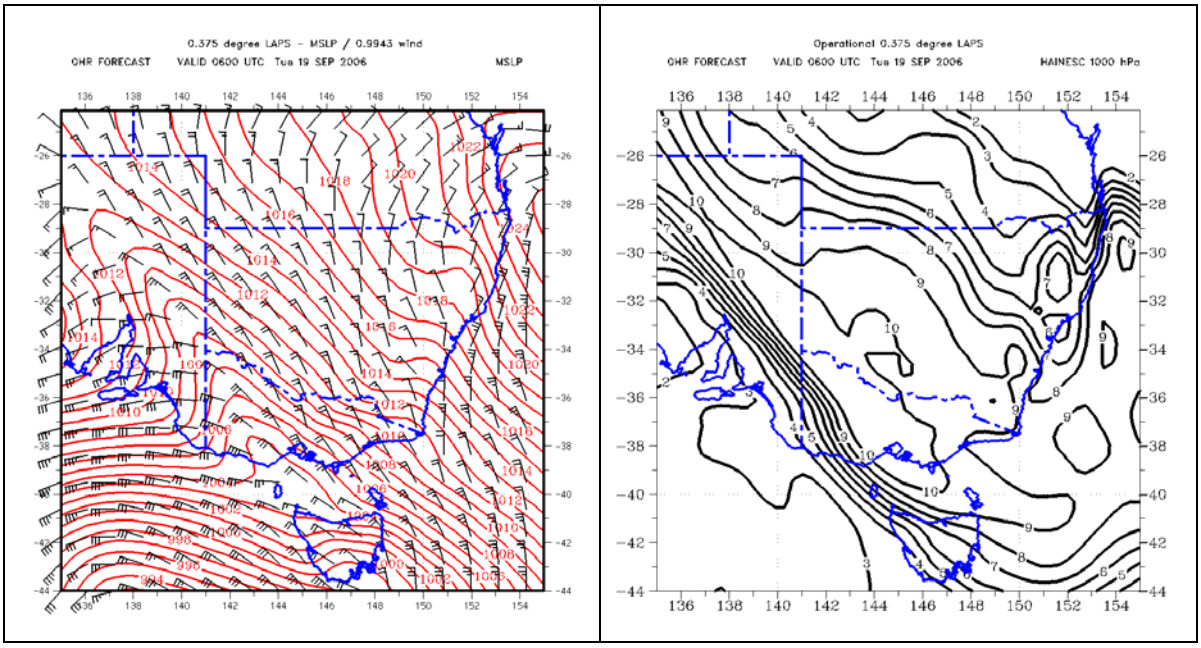

Figure A9.3. Left panel : forecast mean sea level pressure and 70m wind barbs at 0600 UTC 19 September 2006 from the 0.05^{o} grid-spacing meso-LAPS forecast. Right panel: forecast C-HAINES at same time.

There is a period of high C-HAINES for two days prior to the ignition day.

There is the conjunction of extra-ordinarily high values of FFDI and of C-HAINES on the day of major fire activity when a huge pyrocumulus cloud was also generated.

The Little Desert and Casterton Complex Fires

These fires occurred on two successive days, burning an area of 10800 ha in the Little Desert National Park on 20 November 2006 and, and 12500 ha near Casterton 21 November 2006. Both areas are in western Victoria, and so for these events the "Horsham" gridpoint (point 18 in Fig. 1) is chosen to demonstrate the climatological respresentivity (Fig. A9.4) and time sequence (Fig. A9.5) of FFDI and C-HAINES. On both days the FFDI and the C-HAINES values were in the extreme upper range of their distributions. Figure A9.5 shows that C-HAINES reached very high values on 19 November, and that these persisted until a major change moved into Victoria on the afternoon and evening of the 21 November 2006, while the FFDI was relatively lower until 20 November, and was extra-ordinarily high on 21 November 2006.

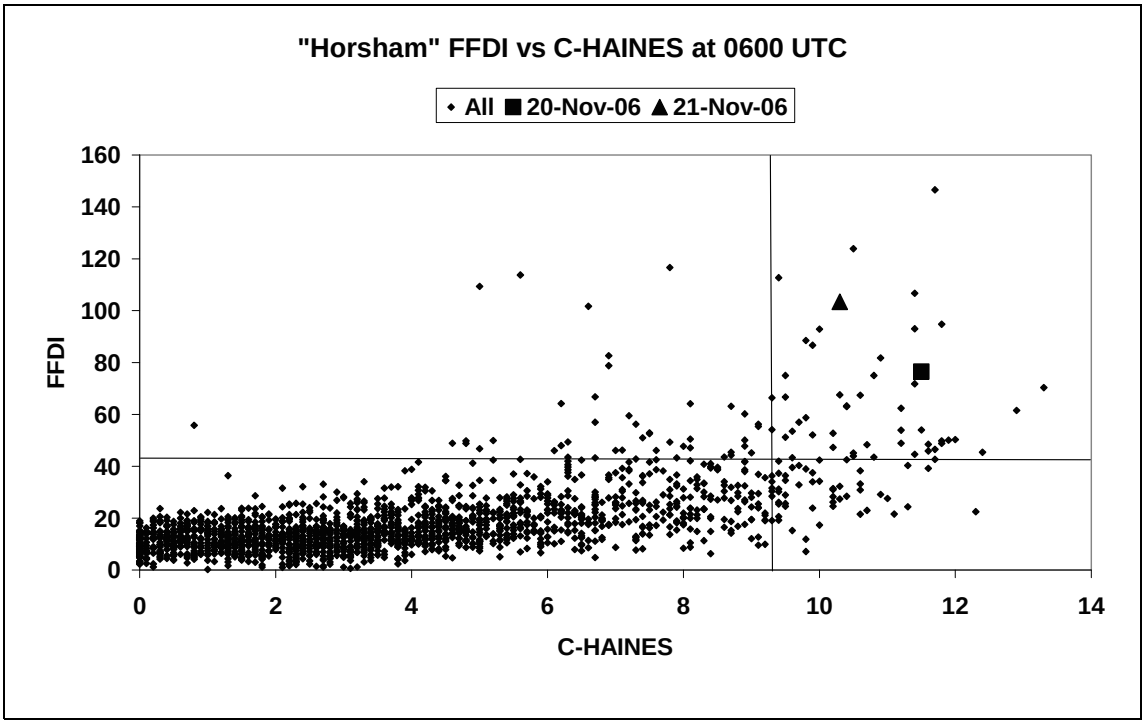

Figure A9.4. Scatterplot of FFDI vs C-HAINES for the "Horsham" gridpoint at 0600 UTC for the 8-year climatology in this report. The lines show the 95th percentile values of C-HAINES and FFDI respectively, and the highlighted points are those of 20 and 21 November 2006.

The time series of temperature and humidity at Horsham Airport AWS (Fig. A9.6) shows only weak overnight relative humidity recovery on 18, 19, and 20 November. With the Little Desert and Casterton fires occurring on 20 and 21 November respectively, fine fuels had 2 and 3 nights respectively of weak overnight relative humidity recovery prior to the days of the fires.

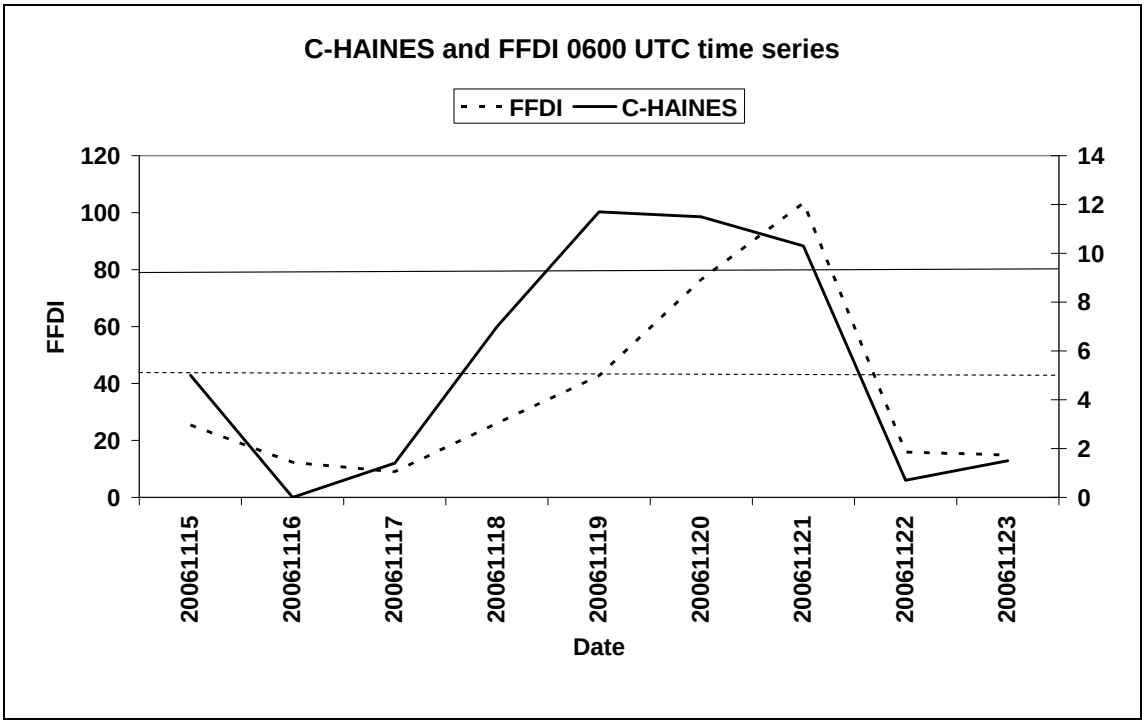

Figure A9.5. Time series of daily FFDI (dashed) and 0600 UTC C-HAINES (solid) from 15-23 November 2006 at the "Horsham" gridpoint. The horizontal lines indicate the 95th percentile values for the two parameters.

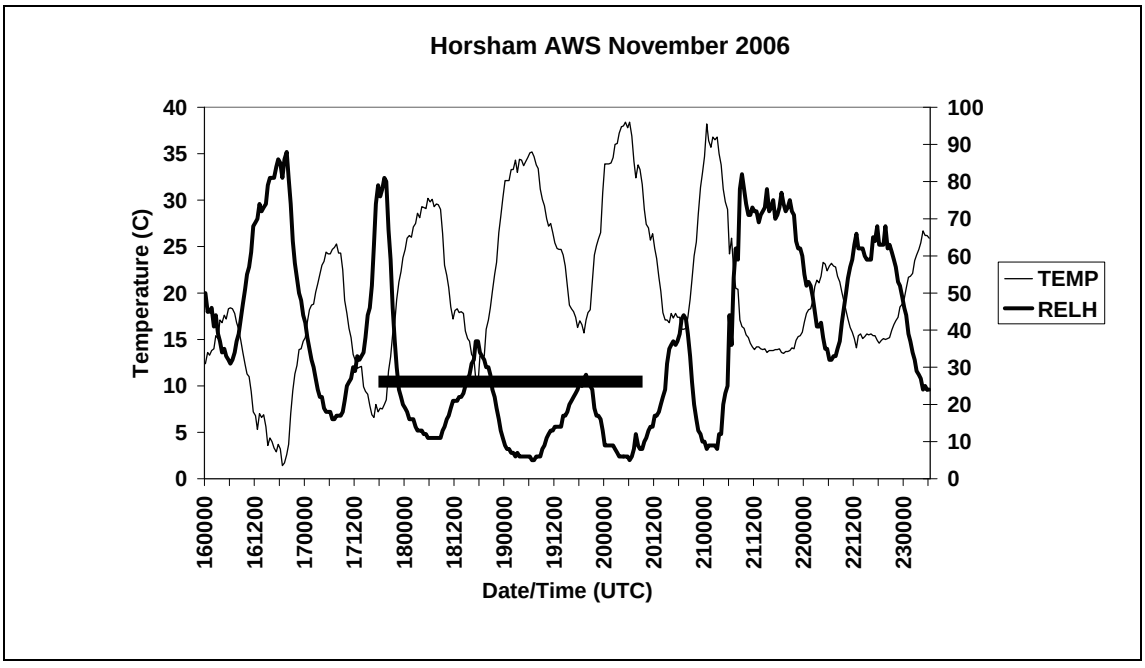

Figure A9.6. Time series of temperature (thin) and relative humidity (thick) from the Horsham airport AWS from 0000 UTC 16 November to 0000 UTC 23 November 2006. The thick horizontal bar runs from 0600 UTC on the 18 November (2 days before the Little Desert fire) to 0600 UTC 21 November 2006 (the afternoon of the Casterton fire).

There is little to no diurnal signal in the C-HAINES time series (Fig. A9.7), with values remaining above 10 from 0000 UTC 19 November to 0600 UTC 21 December. Thus there is again a close association between low overnight relative humidity recovery and high values of C-HAINES.

The MSLP/wind and the C-HAINES fields from the LAPS analyses for 0600 UTC on 20 and 21 November 2006 are shown in Fig. A9.8. On the first day a weak change was moving into south-western Victoria, as part of a trough extending north-westwards into SA. Very high C-HAINES values extend over all Victoria. On the next day, a more substantial change moved into western Victoria and SA, again with very high values of C-HAINES in a broad area east of the change. On each day the stability is very weak, with deep mixed layers ahead of the respective changes.

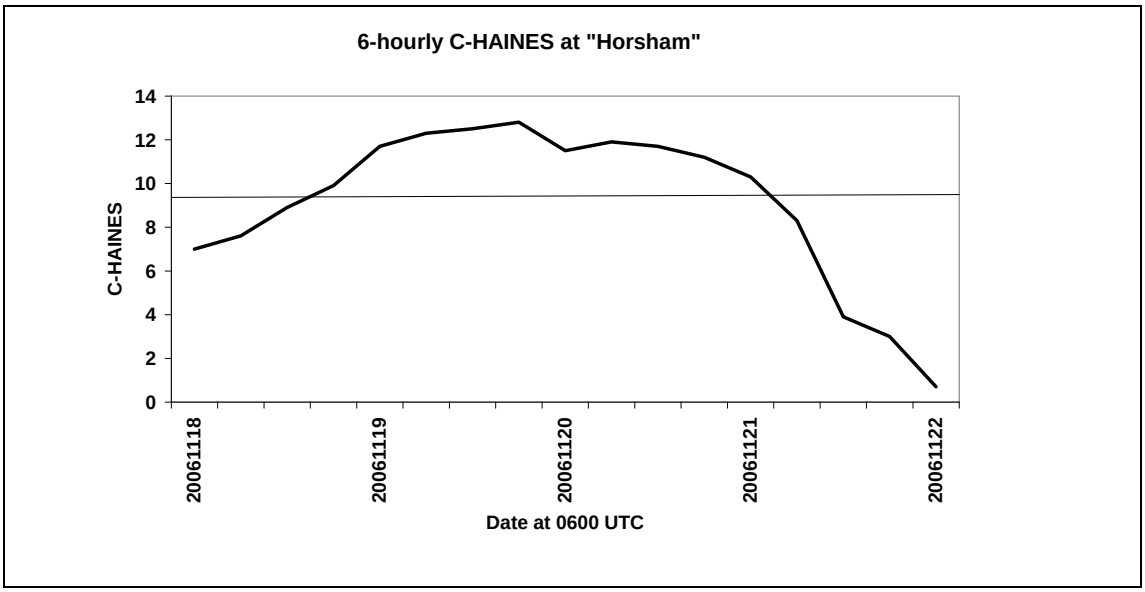

Figure A9.7 Time series of 6-hourly C-HAINES from the LAPS analyses at the "Horsham" gridpoint from 0600 UTC 18 to 0600 UTC 22 November 2006.. The horizontal line shows the 95th percentile of 0600 UTC C-HAINES.

This is another example of the C-HAINES reaching very high values on the days before a fire ignition, perhaps leading to exceptionally dry fine fuels.

Overnight C-HAINES values stayed high, and AWS data indicate relative humidity recovery was very weak on the nights prior to major fire activity.

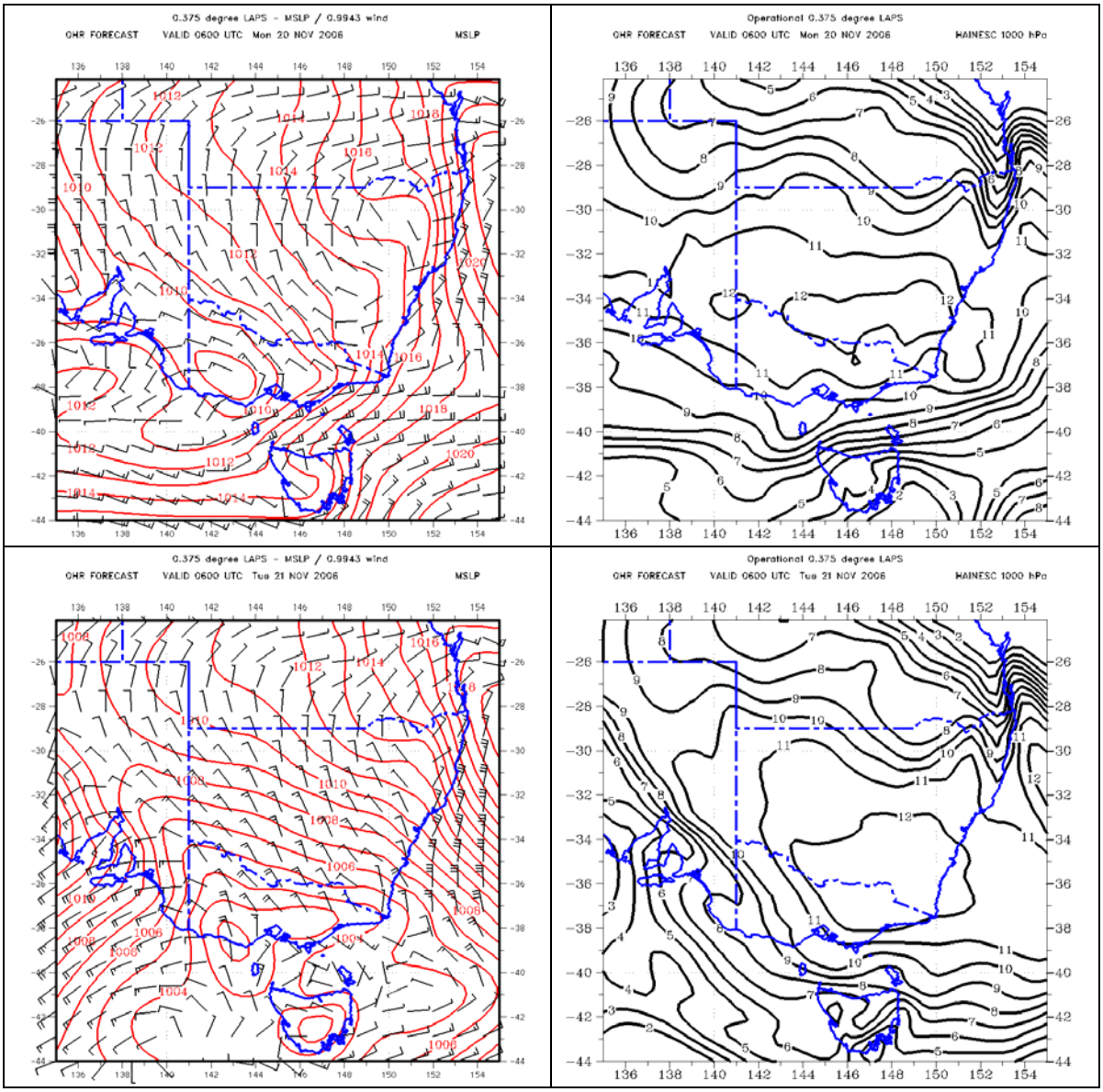

Figure A9.8. Left panels: mean sea level pressure overlaid with 70m wind barbs at 0600 UTC 20 and 21 November 2006 from the LAPS analyses. Right panels: C-HAINES fields at the same times.

December 2006 - January 2007 fires in north-east Victoria

Smith (2007) describes the days of largest areas burnt during the December 2006 - January 2007 fires in north-east Victoria as being on the 10 December 2006 (33500 ha at Tawonga Gap), on 14 December 2006 (deliberately lit fire near Coopers Creek) and 11 January 2007 (33000 ha near Tatong). McCarthy et al. (2008) also mentioned unusually active fire behaviour on 14 December 2006. Spectacular MODIS images of the 10 December, 14 December, and 11 January fire days are seen in Figs. A9.9, A9.10 and A9.11, with huge smoke plumes and well-developed pyrocumulus clouds evident.

Figure A9.9. MODIS image on the afternoon of 10 December 2006 (Tawonga Gap fire).

The scatterplot of FFDI versus C-HAINES for the "NEVIC" gridpoint (point 22 in Fig. 1) is shown in Fig. A9.12, with the three targeted fire days highlighted. These days are in the most extreme range for both FFDI and C-HAINES. The time series of these two parameters from 1 December 2006 to 31 January 2007 are shown in Fig A9.13.

For the 10 December event the C-HAINES reaches very high values for several days before, and on the day of, the event, while the FFDI peaks just on that day. On 14 December both C-HAINES and FFDI peak just on that single day, while on 11 January the C-HAINES increases the day before, but the FFDI shows just a single sharp maximum on that day.

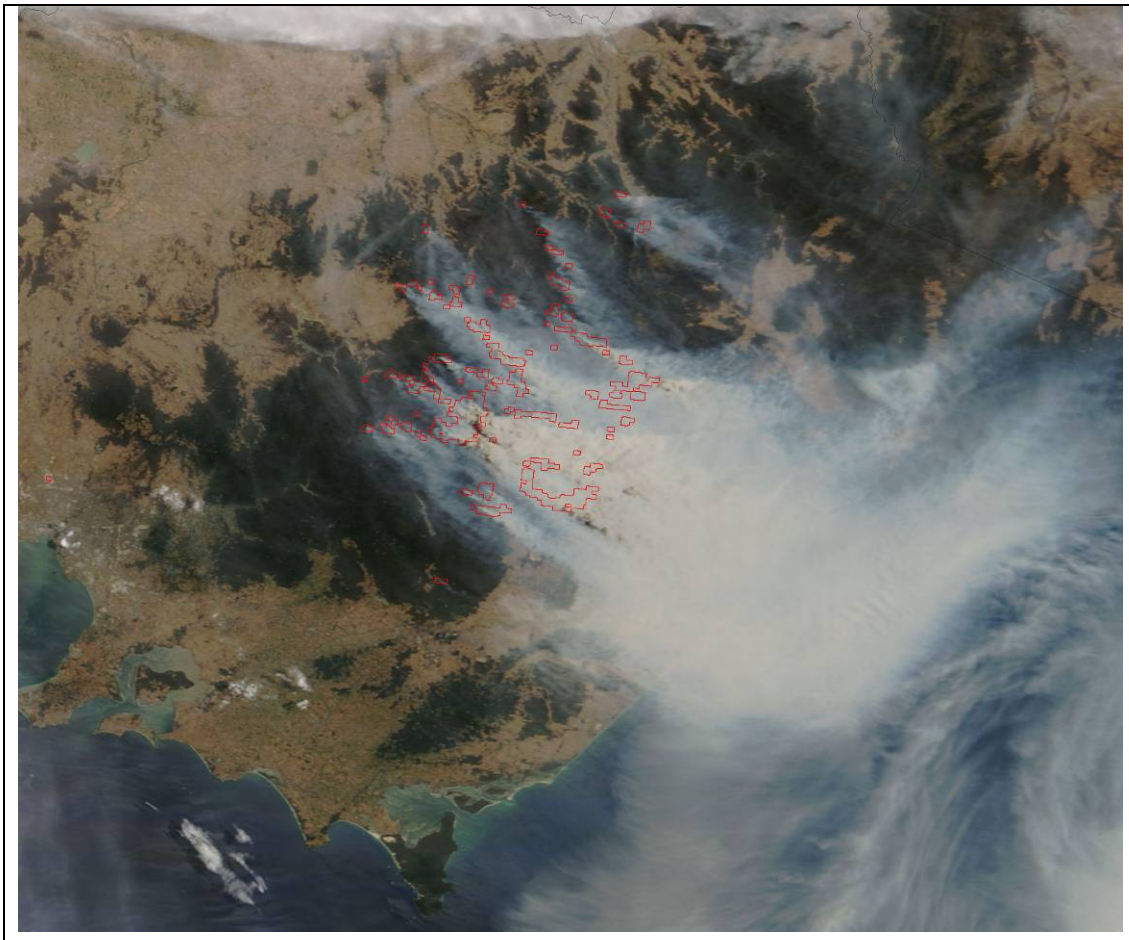

Figure A9.10. MODIS image on the afternoon of 14 December 2006 (Coopers Creek fire).

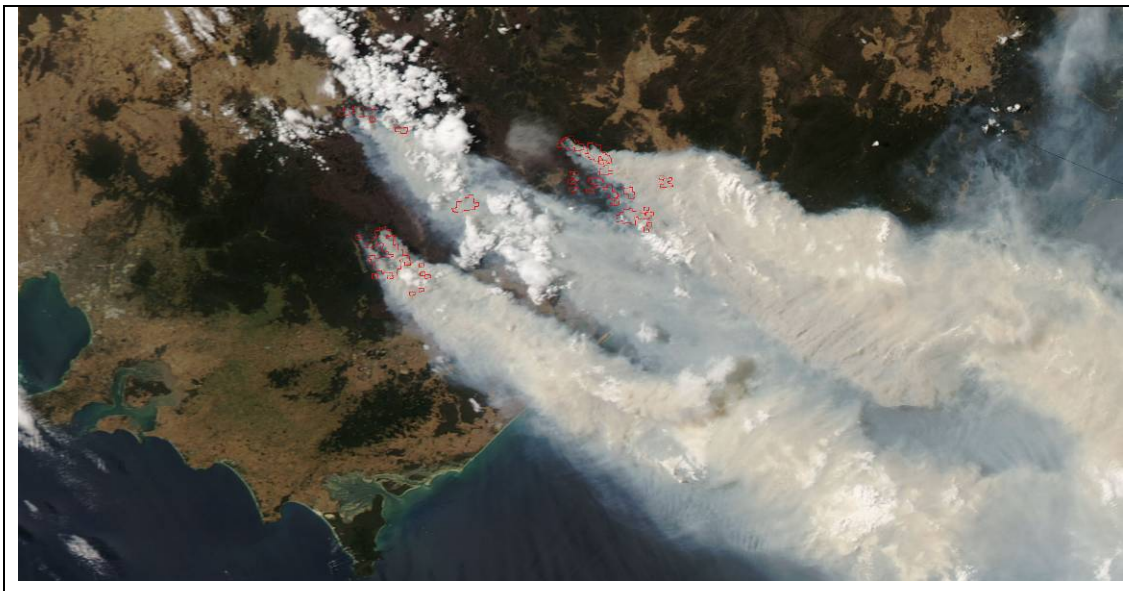

Figure A9.11. MODIS image on the afternoon of 11 January 2007 (Tatong fire).

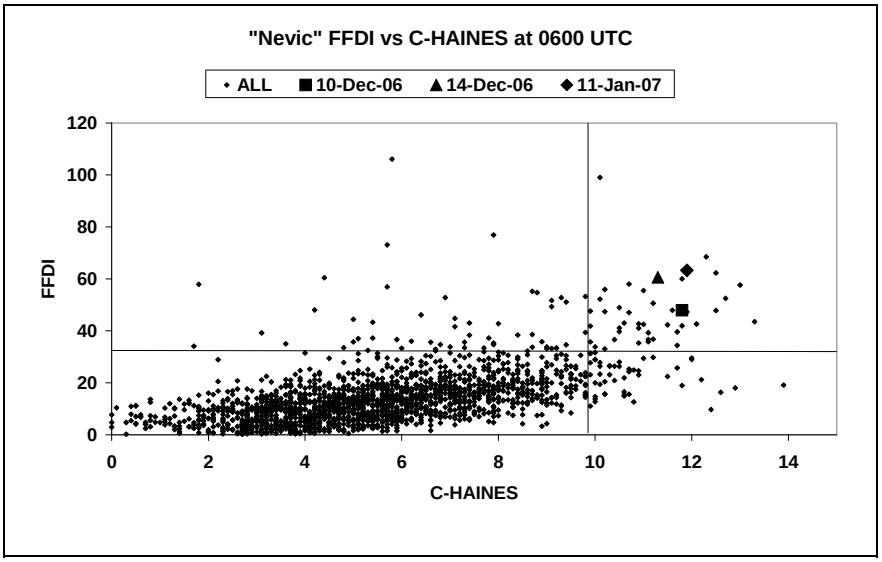

Figure A9.12. Scatterplot of FFDI vs C-HAINES for the "Nevic" gridpoint at 0600 UTC for the 8-year climatology in this report. The lines show the 95th percentile values of C-HAINES and FFDI respectively, and the highlighted points are for the three major fire activity days discussed in this section.

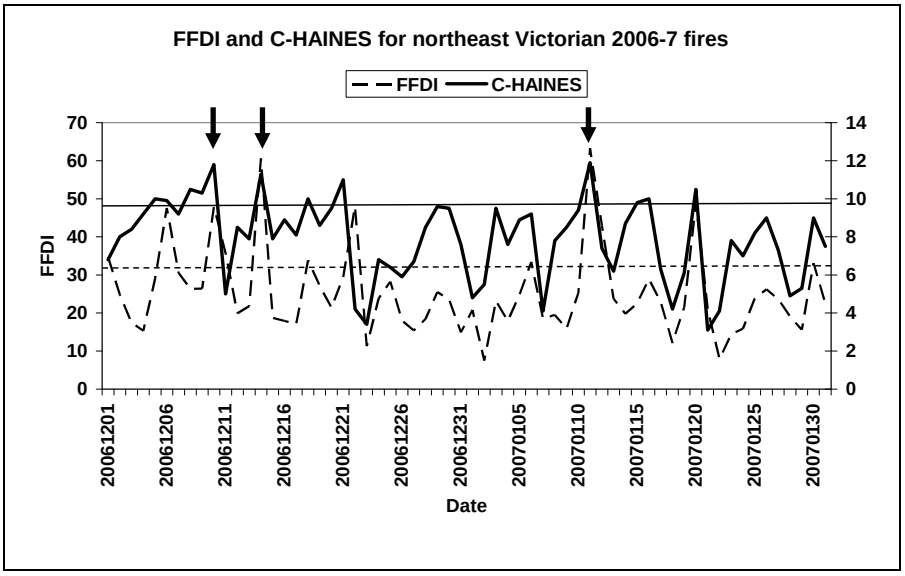

Figure A9.13. Time series of daily FFDI (dashed) and 0600 UTC C-HAINES (solid) from 1 December 2006 to 30 January 2007 at the "Nevic" gridpoint. The horizontal lines indicate the 95th percentile values for the two parameters, and the arrows indicate the three fire activity days discussed in this section.

Particularly for the 10 December fire run, there had been a period of very high C-HAINES for some days before, consistent with some of the other cases in this report.

All three days of extreme fire behaviour also exhibited large pyrocumulus development. Separating out the respective roles of wind-driven (ie FFDI) versus instability effects on the fire behaviour given that the lower stability may have enhanced gustiness and decreased relative humidity, thus enhancing FFDI, let alone the possible interactions with the fire itself, is rather difficult.

All three days of massive fire spread and pyrocumulus development showed values of both FFDI and C-HAINES that were in the outer extrema of their distribution.

A.10 The Scamander / St Mary's Fire of 10-14 December 2006

"The fire started as an escape from a campfire (probably lit the night before) and was reported on December 10 2006 on Lohreys Rd near St Marys. That afternoon houses were threatened near German Town around 1530 local time. On the 11th the fire ran into Dublintown as well as down to Scamander again during the mid afternoon. 17 homes as well as sheds, orchards and businesses were destroyed. The fire made another run on December 14 from about 1300 local time which resulted in the loss of another 9 homes and a business premise with a manager's flat as well as more outbuildings and a footbridge and a childrens playground. The fire also ignited exposed coal seams at Cornwall. Extensive backburning was used to provide secure boundaries for fire and it was contained on December 27 2006, The fire was then patrolled until all above surface fire activity ceased. Tragically a Forestry Tasmania firefighter was killed by a falling tree on January 13 2007, The fire was declared out after 152 days on May 11 2007. The coal seams are likely still burning underground and responsibility for the coal seams was handed over to the Cornwall mine managers. Forest losses were estimated at $M 50 (p.39 FT Annual Report 2006/07)" (M.Chaldil, personal communication).

The fire runs on both 10 and 14 December 2006 were driven by strong westerly winds associated with topographically-modified cold-frontal passages across Tasmania, which resulted in wind changes moving northwards along the eastern Tasmanian coastline. Relationships between C-HAINES and fire behaviour based on the 0600 UTC climatology are complex in this event as the two major fire runs were associated with forcing by strong winds (see Dowdy et al. 2009 for discussion of the day of 11 December 2006). However, the scatterplot of FFDI and C-HAINES in Fig. A10.1 for the North-east Tasmania gridpoint (point 23 in Fig. 1) suggests several points worthy of further investigation. First, the most extreme FFDI values are relatively low in terms of mainland climatologies (cf Dowdy et al. 2009). Second, while the 95th percentile of C-HAINES is also relatively low, being only a little higher than the "6" of the traditional mid-level Haines Index (see earlier), the spread at higher values is still very large, with a few values approaching the C-HAINES upper limit. Third, the pairing of points representing the ignition day (10 December) and first major fire spread day (11 December), and the day before and the day of the Four Mile Creek house losses (13 and 14 December respectively) shows that the C-HAINES was high on the days before the fire activity, while the FFDI was high on the days of the major fire runs. This is perhaps more evident in Fig. A10.2 in which the time series of daily 0600 UTC C-HAINES and FFDI values shows that C-HAINES peaks one day earlier than does the FFDI for each of the fire spread days.

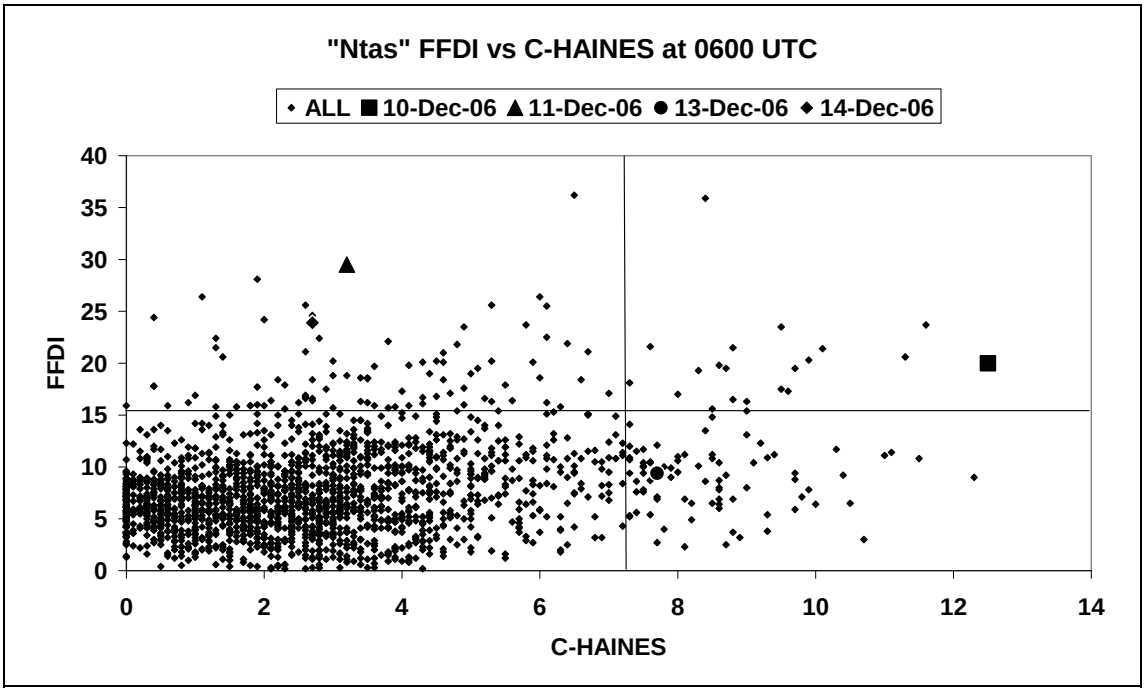

Figure A10.1. Scatterplot of FFDI vs C-HAINES for the “Ntas” gridpoint at 0600 UTC for the 8-year climatology in this report. The lines show the 95th percentile values of C-HAINES and FFDI respectively. The highlighted points show the values for 10 and 11 December 2006 and 13 and 14 December 2006.

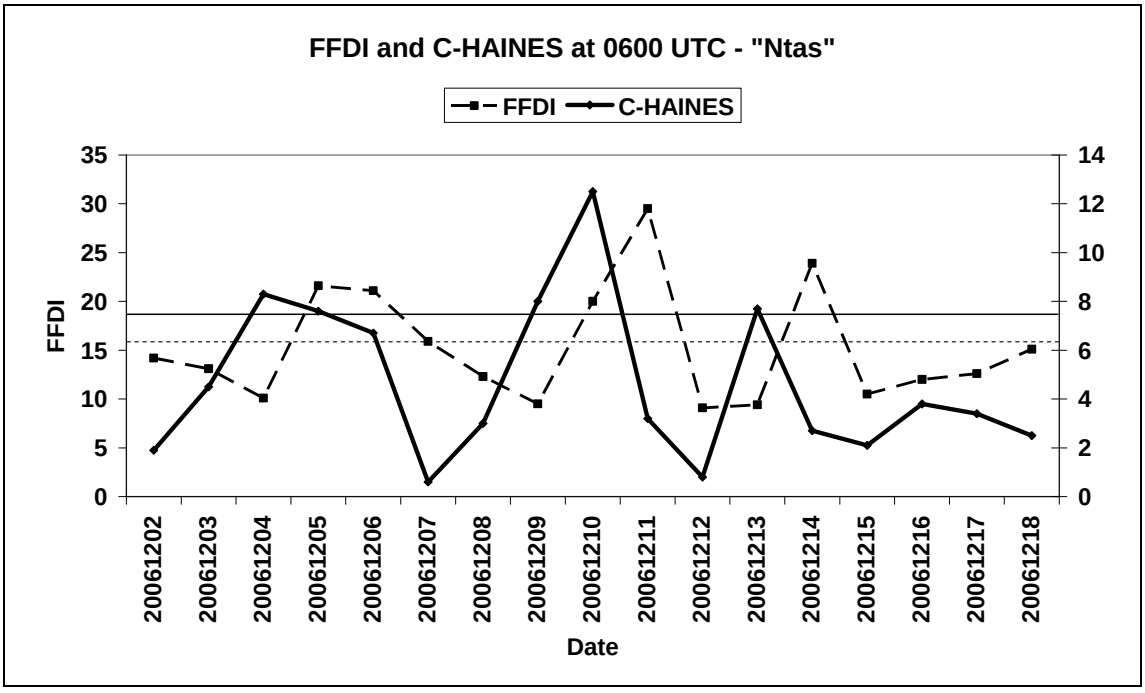

Figure A10.2 Time series of daily FFDI (dashed) and 0600 UTC C-HAINES (solid) from 2 -18 December 2006 at the “Ntas” gridpoint. The horizontal lines indicate the 95th percentile values for the two parameters.

Figure A10.3 shows the 6-hourly time series of C-HAINES, and its temperature lapse and dewpoint depression components, through this period. The C-HAINES reached very high values for more than 24 hours before the day of the ignition, and declined during the early hours of the 11th – before the major fire run that day. It was also very high overnight before the fire run on 14 December. Interestingly, the dewpoint depression component leads the lapse component in each case. The effect of this phase difference is that the C-HAINES peaks on 9-10 and 13-14 December are broader than the peaks in either of the ingredients. This suggests that the balance of physical processes operating in the fire-atmosphere interactions during the periods of high C-HAINES may also have differed at different stages during the high C-HAINES period.

An additional interesting feature is the secondary peak in C-HAINES that occurs at 0600 UTC on 10 December. Inspection of the temperature lapse and dewpoint depression ingredients shows that this is driven almost entirely by the lapse component of the C-HAINES, and a forecast from the meso-LAPS05 NWP model (Fig. A10.4) shows this to be a small-scale region of lower stability that moves northwards during the day, and which is separate from the more northern (pre-frontal) bands of dry air and steep lapse rate that contributed to the overnight maximum in C-HAINES. What effect this may have had on fire behaviour during that afternoon is unclear, but there are anecdotal reports of pyrocumulus activity over the fire on that afternoon.

The C-HAINES reached high values for the 24 hours, including the overnight periods, prior to the two days of major fire runs.

The phase difference between the timing of the temperature lapse and the dewpoint depression maxima suggests that examining the ingredients that lead to large values of C-HAINES may provide additional insight into the fire weather on a given day.

The secondary maximum in C-HAINES, driven entirely by the lapse component, shows the complexity of meteorological processes that can occur, and which may have influenced the interactions of the fire and the atmosphere on that afternoon.

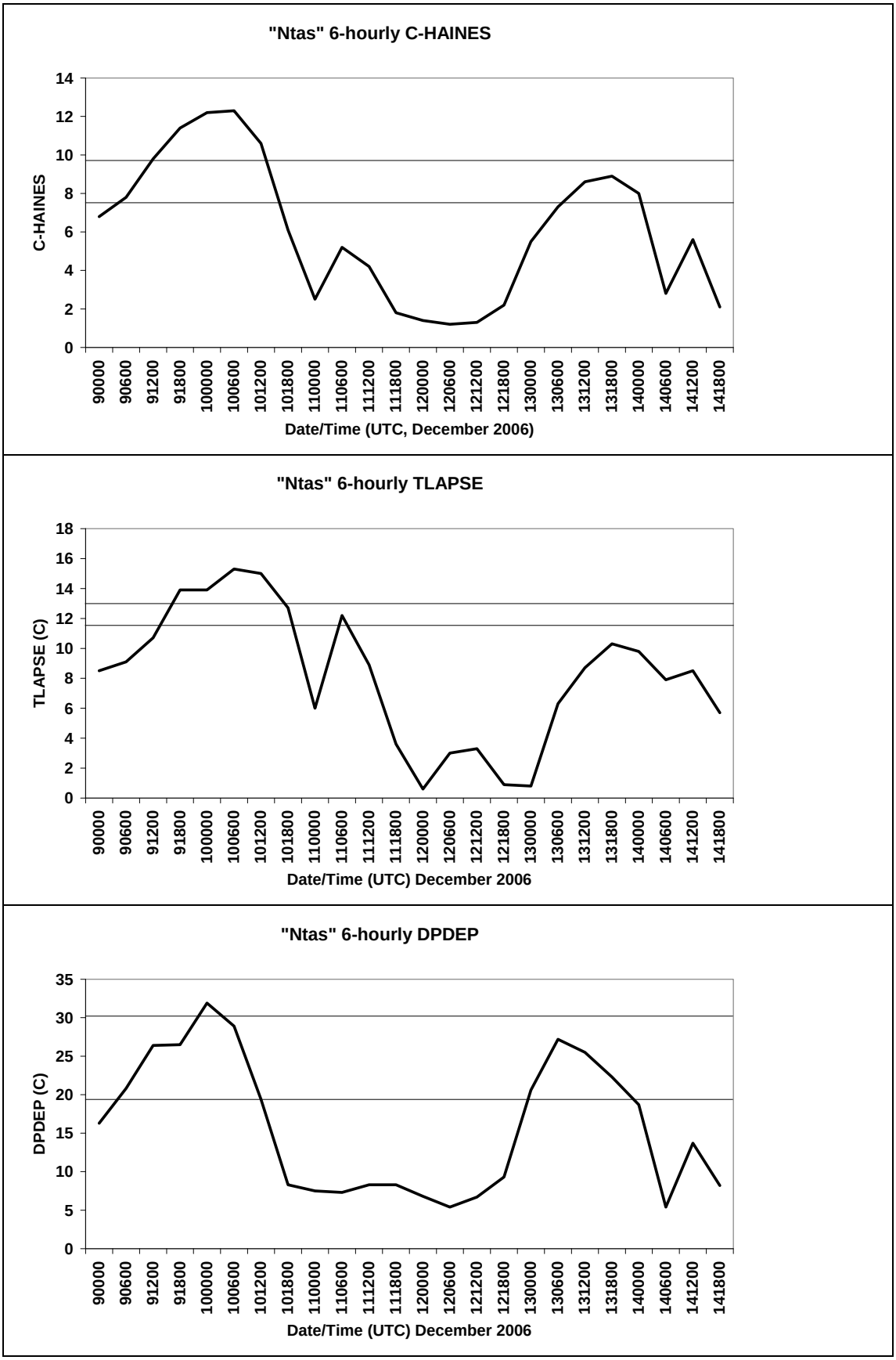

Figure A10.3. Time-series of 6-hourly values of C-HAINES and its temperature lapse and dewpoint depression ingredients for the “Ntas” gridpoint, from 0000 UTC 9 December 2006 to 1800 UTC 14 December 2006.

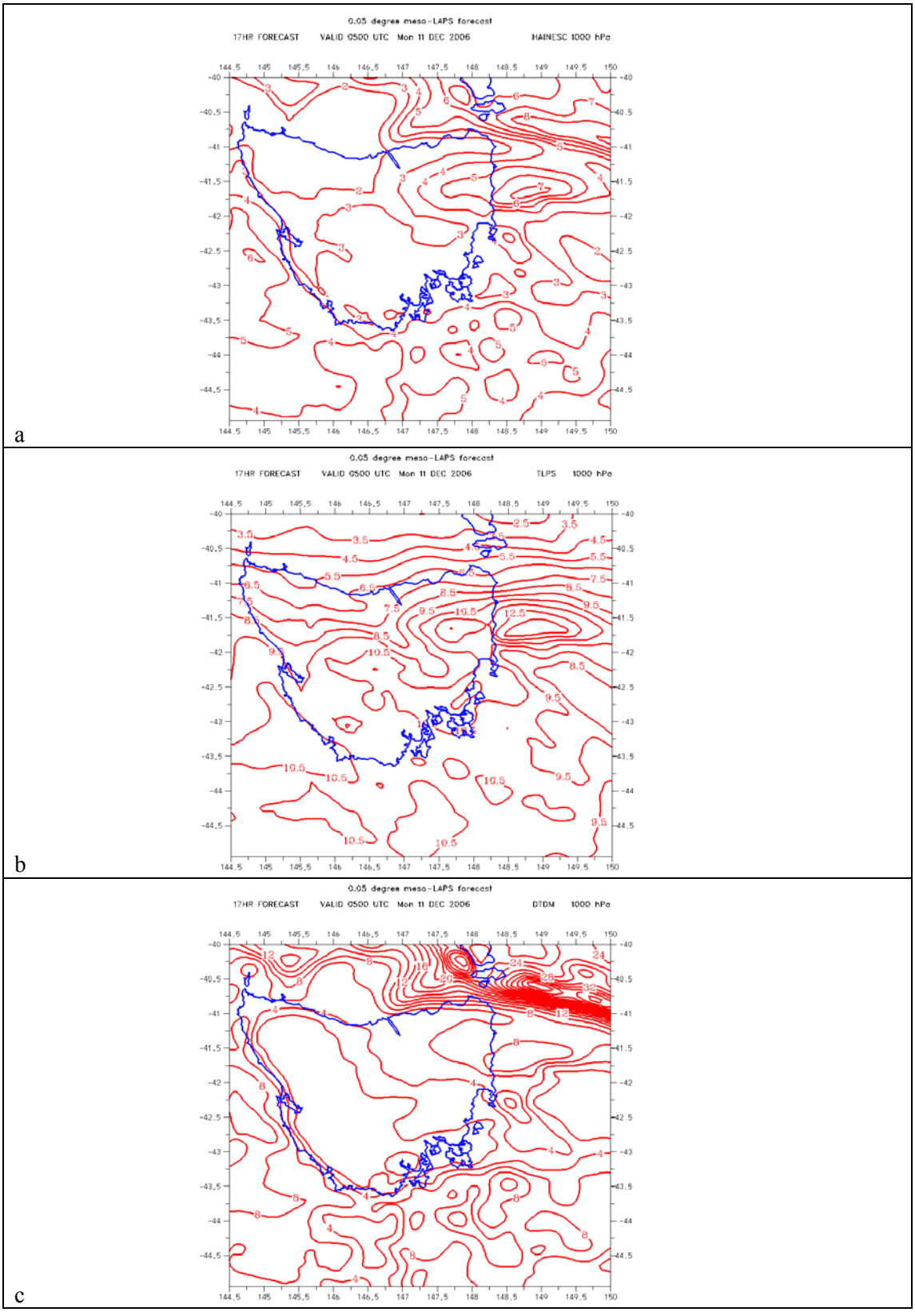

Figure A10.4. Forecast C-HAINES field from the 0.05° meso-LAPS NWP model for 0500 UTC 11 December 2006 (a), and corresponding fields of the temperature lapse (b) and dewpoint depression (c) forecasts.

A.11 The Berringa Fire of 25 February 1995

This fire event is not represented in the dependent database used in the stability climatology studied in this paper, but is included in this report because of the considerable interest generated by the huge pyrocumulus cloud above the fire that could be seen from as far as the eastern suburbs of Melbourne. In addition, it is one of the few fires with associated pyrocumulus which have been documented in Australia (Leggett 1996, Tolhurst and Chatto 1999).

The fire started in grassland around the middle of the day on 25 February 1995, and spread south-eastwards with an elliptical shape until a south-westerly wind change at about 1830 EDST spread the fire into the Enfield State Forest, with about 90% of the 10000 ha burnt occurring in the 6 hours after the wind change (Leggett 1996, his Fig. 12). While this wind change was abrupt in terms of directional change, wind speeds were only moderate before and after the change. The pyrocumulus cloud over the fire developed extremely rapidly immediately after the wind change, with cloud tops reaching 11500m.

Because the LAPS data assimilation system was not operational at the time of this event, NWP data have been generated by taking the ERA40 reanalysis data (Kallberg et al. 2005), and running 0.2o, and then internally-nested 0.05o, grid meso-LAPS forecasts with the initial state and lateral boundary conditions provided by the 6-hourly ERA40 reanalyses from 1200 UTC 24 February 1995.

Figure A11.1 shows the climatological distribution of C-HAINES and FFDI for the 8-year 0600 UTC LAPS data set at the Sheoaks gridpoint (point 19 in Fig. 1), while the circle is centred on the values from the 18-hour forecast from the 0.2o ("coarse") mesh hindcast. (A single point is not shown because this forecast is not statistically homogeneous with the climatology). The C-HAINES in particular is well towards the outer extreme of the distribution, and while the FFDI was also well into the Extreme (>50) range, this was at 0600 UTC, before the combination of diurnal effects and the cool-change reduced the FFDI to more modest levels.

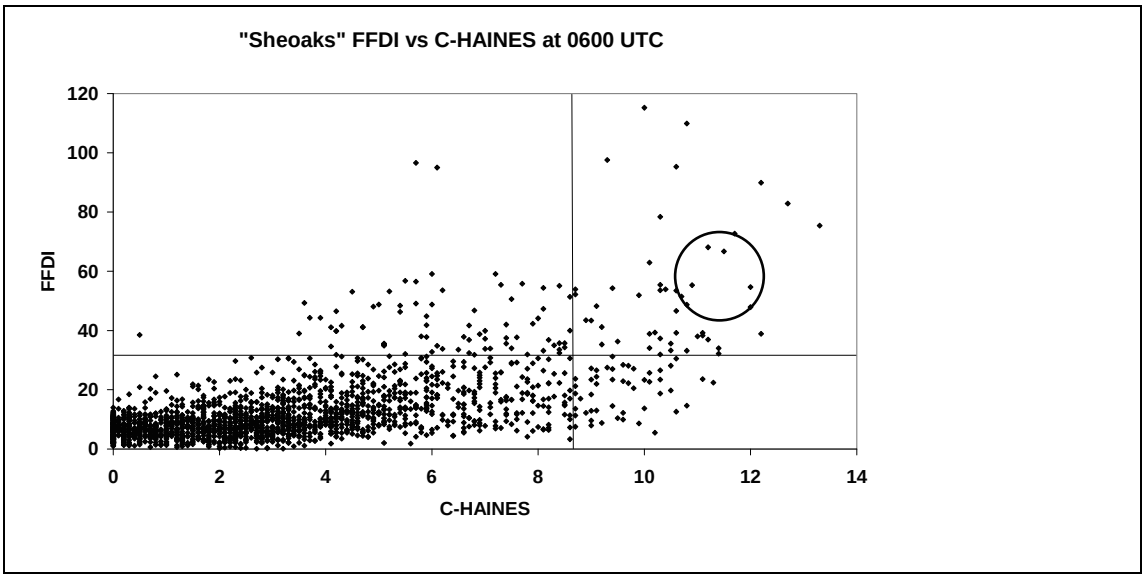

Figure A11.1. Scatterplot of FFDI vs C-HAINES for the "Sheoaks" gridpoint at 0600 UTC for the 8-year climatology in this report. The lines show the 95th percentile values of C-HAINES and FFDI respectively. The circle is centred on the C-HAINES/FFDI point forecast by the ERA40-based NWP hindcast.

Leggett (1996) shows that the FFDI peaked at Sheoaks at 1330 EDST, with a value of 77, had dropped to around 40 by the time the wind change reached the area, and continued to decrease thereafter to be around 10 by 2300 EDST. Thus the majority of the area burnt occurred with FFDI values dropping from around 40, at the time of the wind change, to 10 by 2300 EDST. The FFDI and C-HAINES hourly forecast time-series at the Sheoaks gridpoint from the 0.05^{o} grid NWP hindcast (Fig. A11.2) shows a more-or-less typical diurnal cycle of FFDI, with values rising rapidly during the early daylight hours to reach a little over 40 by 1200 EDST, and then dropping steadily from 1900 EDST when the wind change arrived. The forecast does not replicate the amplitude seen in Leggett's figure (Fig. A11.3), but, making allowance for the spatial and temporal resolution of the model data, is not inconsistent with the observed time series. What is instructive is the difference between the time-evolution of the FFDI and C-HAINES. The C-HAINES increases from values around 8 to over 11 between 1200 and 1600 EDST, and does not begin to decline (and then only slowly) until after 2100 EDST. Thus, during the period of greatest fire spread, and of the greatest development of the pyrocumulus cloud, the C-HAINES remained extra-ordinarily high, while the FFDI was decreasing.

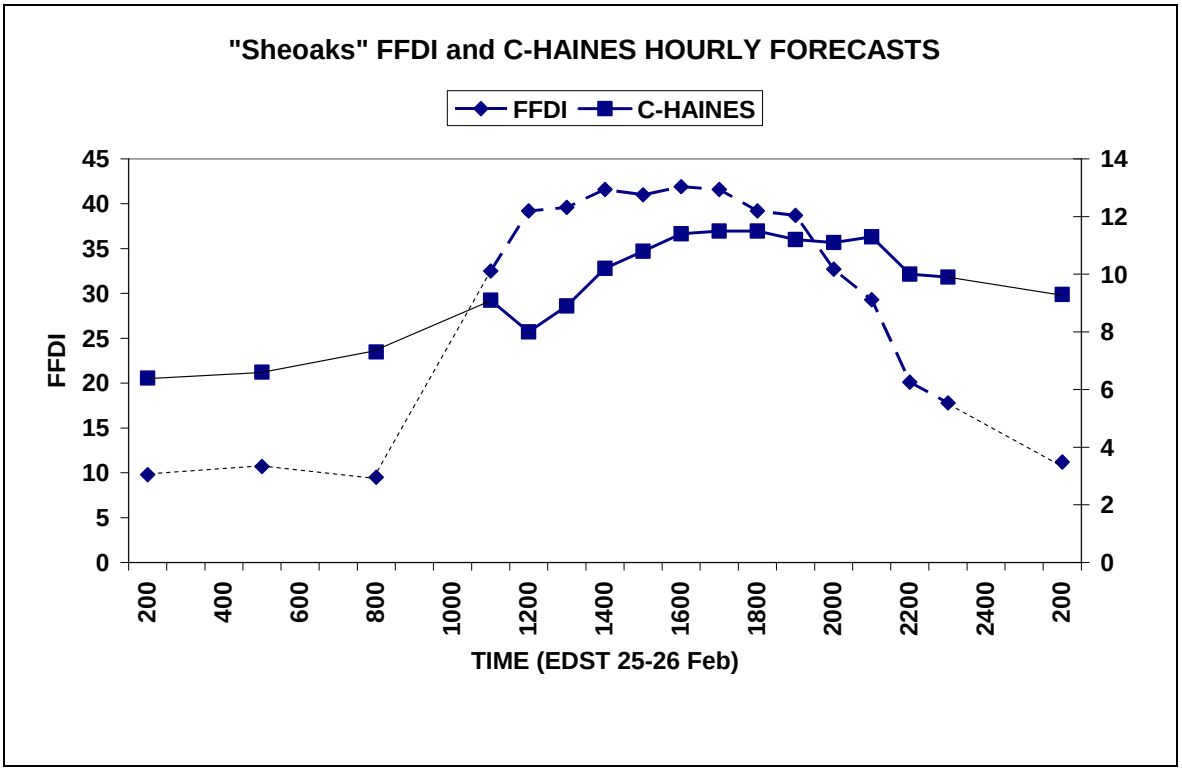

Figure A11.2. Forecast values of FFDI (left ordinate, diamonds) and C-HAINES (right ordinate, squares) at the “Sheoaks” climate point from the 0.05o mesoscale NWP hindcast for the day of 25 February 1995. Forecasts were output hourly between 1100 and 2300 EDST, otherwise 3-hourly.

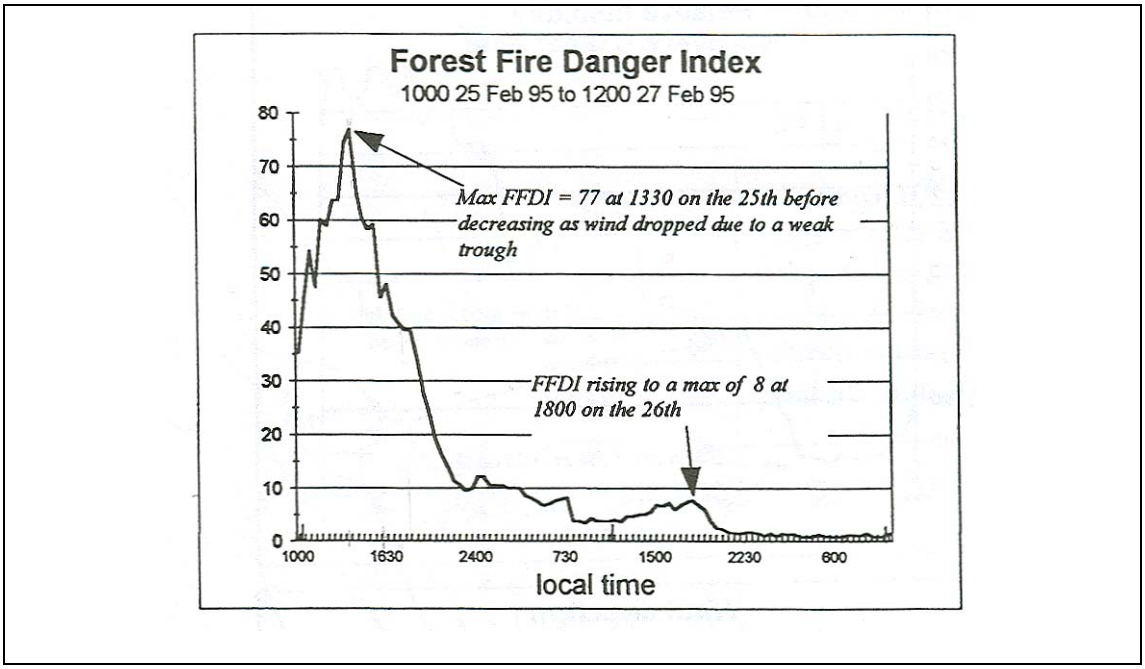

Figure A11.3 Time sequence of FFDI calculated from the Sheoaks AWS data (after Leggett 1996, his Fig. 3).

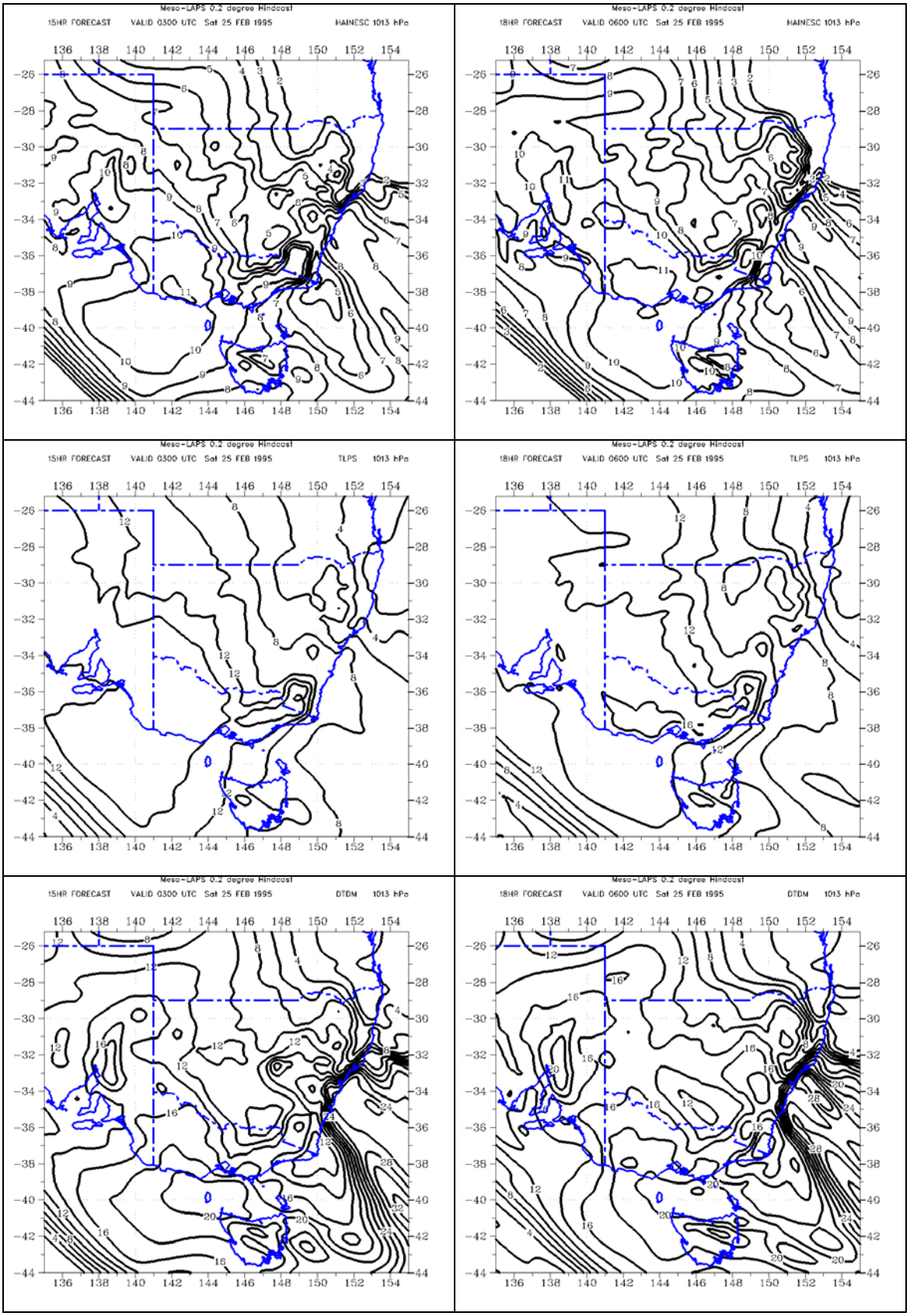

Figure A11.4. Upper panels; C-HAINES forecasts valid 0300 and 0600 UTC 25 February 1995. Middle panels, forecasts of 850-700 hPa lapse-rate (K) for the same times, and, lower panels, forecasts of 850 hPa dewpoint depression for the same times.

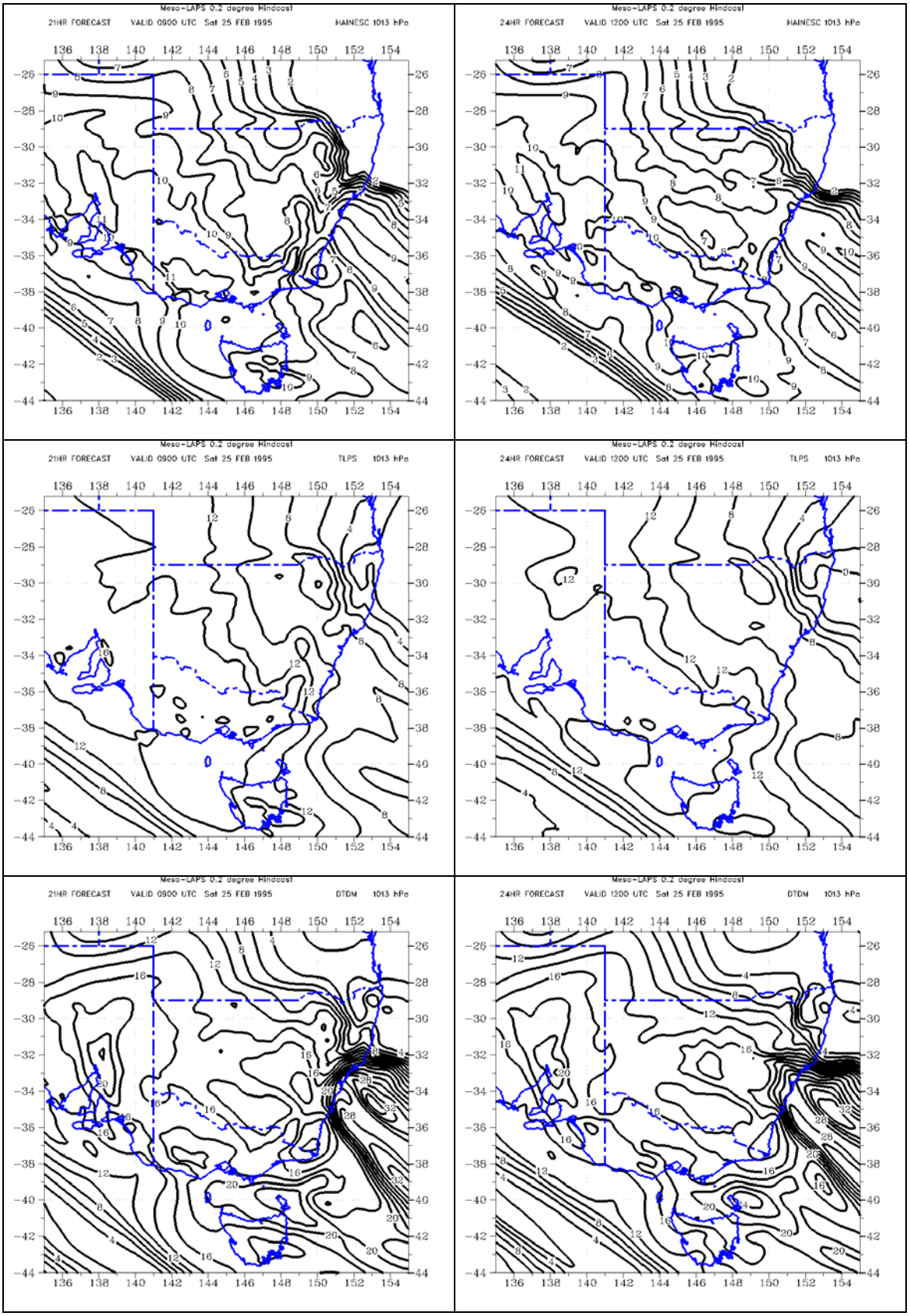

Figure A11.5. Upper panels; C-HAINES forecasts valid 0900 and 1200 UTC 25 February 1995. Middle panels, forecasts of 850-700 hPa lapse-rate (K) for the same times, and, lower panels, forecasts of 850 hPa dewpoint depression for the same times.

A sequence of C-HAINES, DPD, and TL charts at 0300, 0600, 0900, and 1200 UTC (1400, 1700, 1900, and 2300 EDST) are shown in Figs A11.4 and A11.5. At 0300 UTC C-HAINES values over western Victoria and offshore over western Bass Strait are very high - well above the 95th percentile - driven by both very low stability values over most of that area and by very dry conditions at 850 hPa. The highest values of C-HAINES at this time are off the south-west Victorian coastline. At subsequent 3-hourly intervals the stability over land remains essentially dry adiabatic, but the driest air moves north-eastwards and overlies the fire site between 0900 and 1200 UTC. The narrowing north-south dimension of the region of the highest C-HAINES values is driven largely by the focussing of the band of driest air as it moves north-eastwards.

In order to supplement previously-published discussion of this event, some other aspects of the meteorology of 25 February 1995 are presented. The low-level wind change that reached the fire site at 1830 EDST developed on the western Victorian coastline during the day, with the synoptic-scale environment supporting strong coastal frontogenesis. The screen-level potential temperature and low-level wind hindcasts from the 0.05o NWP model simulation are shown in Fig. A11.6 at 0300, 0600, and 0900 UTC 25 February 1995. The generation of wind changes along the south-east SA coastline (0300 UTC), the Victorian coastline west of Cape Otway (0600 UTC), and the Victorian coastline east of Cape Otway (0900 UTC) can all be seen. Discussion of similar coastal frontogenesis events can be found in Mills (2002) and Mills and Morgan (2007). Interestingly, the C-HAINES and other instability indices such as the Surface Lifted Index (not shown) at this time show large (unstable) values both before and after the change line. This is a consequence of the shallowness of the change, demonstrated by the cross-section in Fig. A11.7, and consistent with Treloar's (1999) discussion of the 1100 UTC Laverton radiosonde observations (Fig. A11.8). The cross-section shows a very deep mixed layer to about 650 hPa ahead of the change (the TL contribution to C-HAINES is essentially the maximum possible) and the shallowness of the cool change (defined by the 306-308K isentropes). There is also a typical narrow zone of strong ascent shown above the nose of the surface cool change: this zone of enhanced low-level convergence/ascent may have assisted in the lifting of air parcels from just above the fire to their level of free convection.

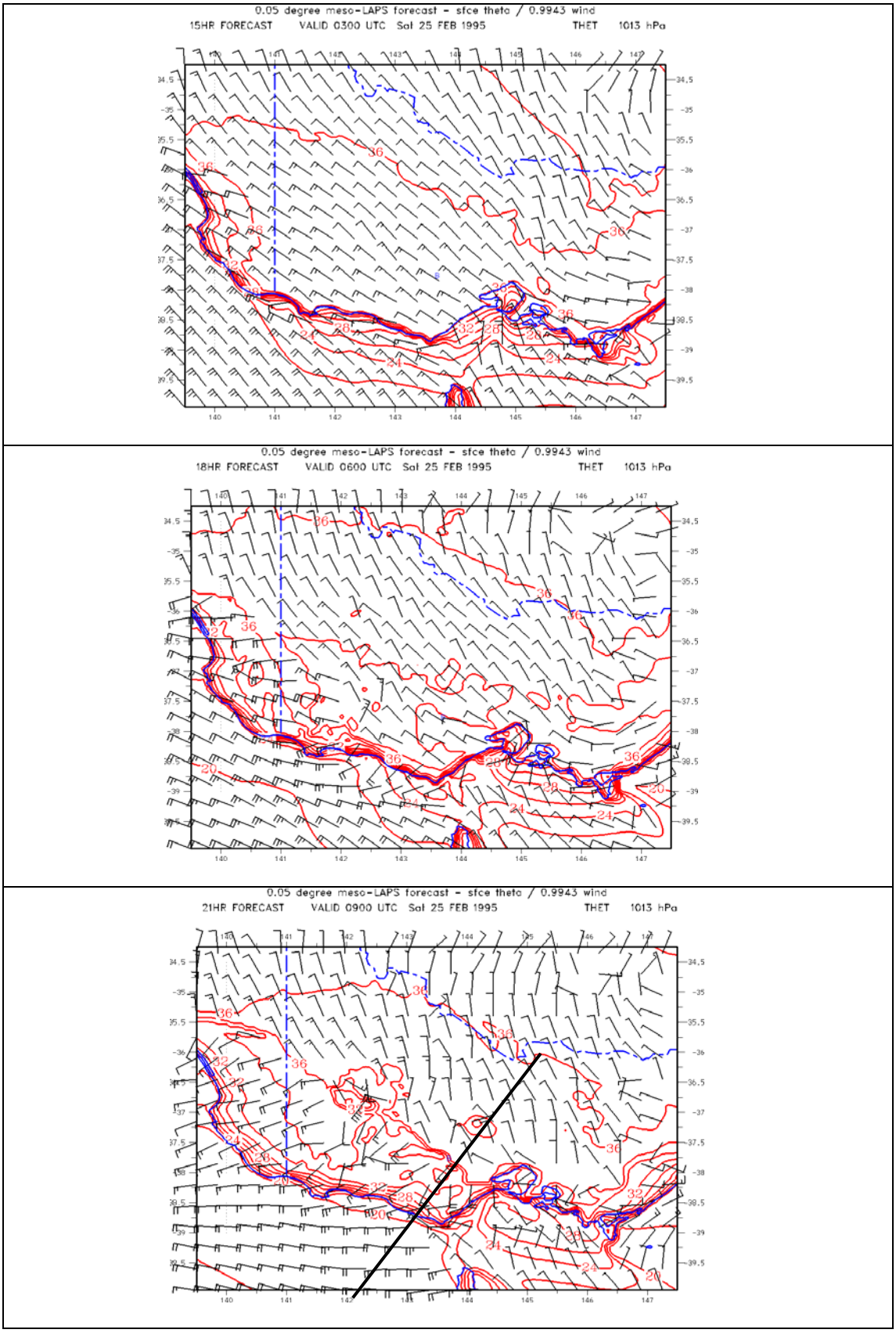

Figure A11.6. Surface potential temperature (C) and 70m wind barb forecasts from the 0.05^{o} mesoscale NWP forecast valid at 0300, 0600, and 0900 UTC 25 February 1995. The line in the lower panel shows the location of the cross-section in Fig. A11.7.

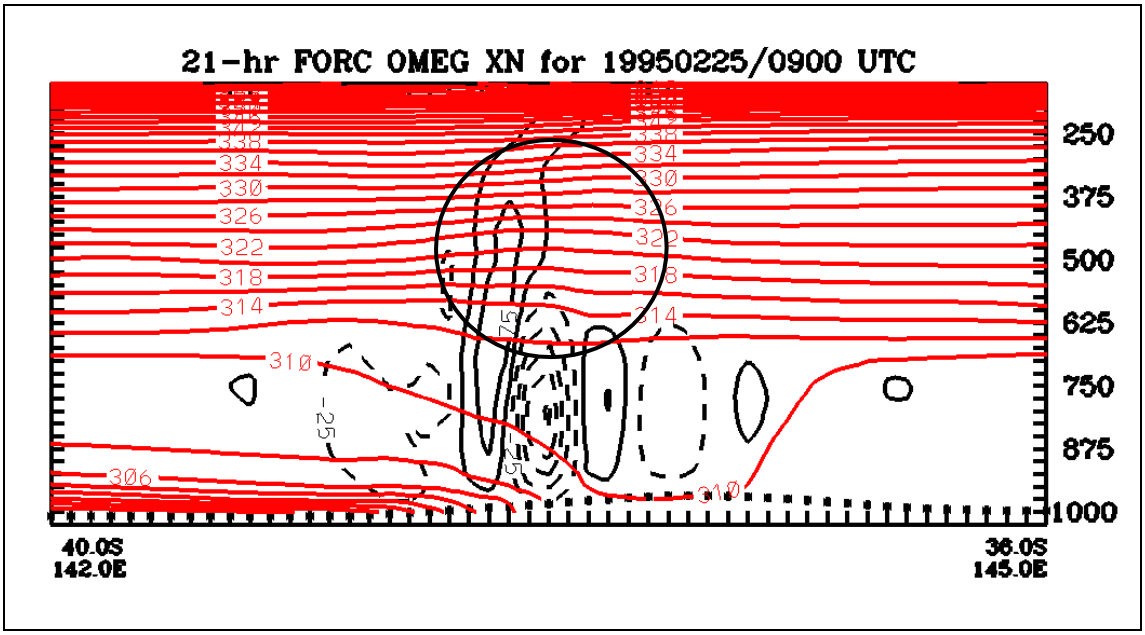

Figure A11.7. Cross-section of potential temperature (red contours, contour interval 2K) and vertical motion (black contours, negative values show ascent and are dashed, contour interval 50 hPa hr-1) from the forecast valid at 0900 UTC 25 February 1995. The line of the cross-section is shown in Fig. A11.6.

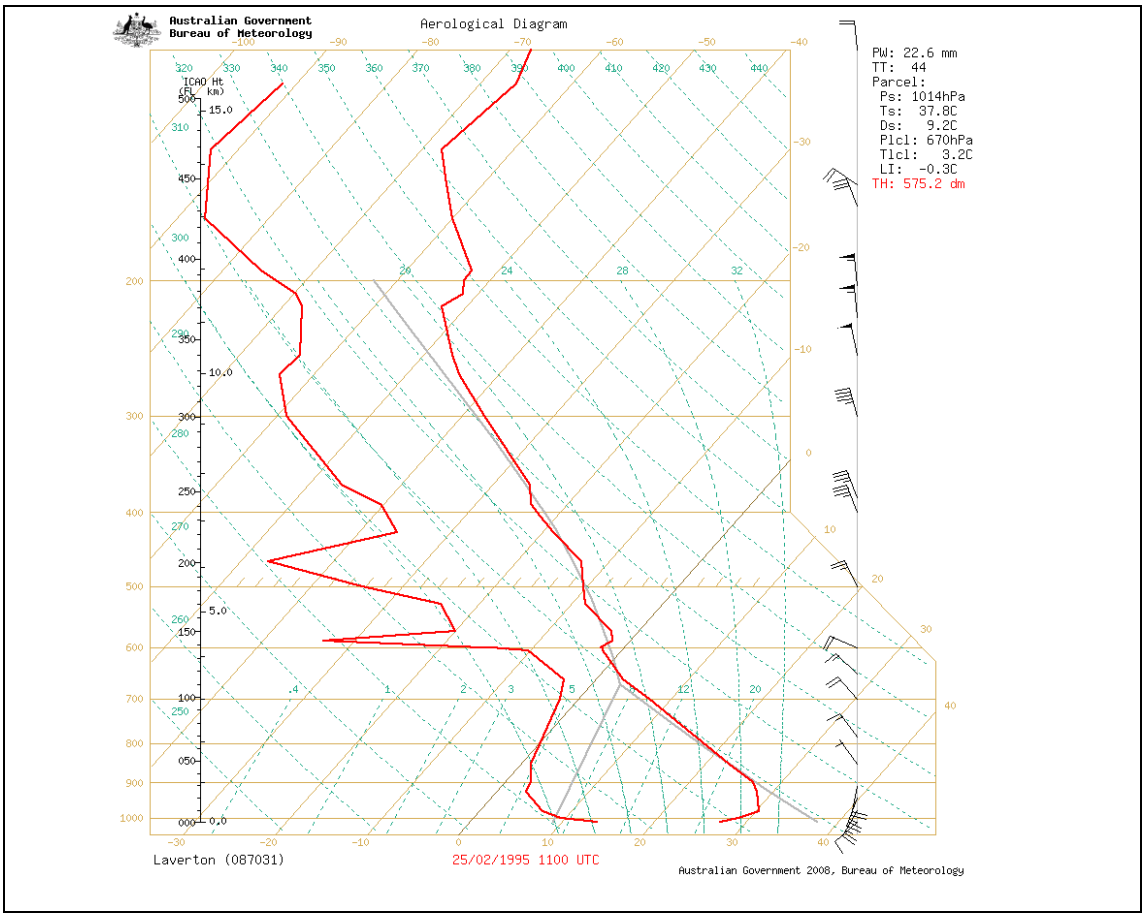

Figure A11.8. Radiosonde ascent from Laverton at 1100 UTC 25 February 1995.

Following the arguments in the Denbarker fire case study (A6), "FIRE-CAPE" was computed from the numerical model fields through the afternoon and evening of 25 February, and while a few small patches of very low CAPE are diagnosed, and all of these being less than 100 J Kg-1, FIRE-CAPE values over much of Victoria during the evening of 25 February (Fig. A11.9) are over 1000 J Kg-1, with values around 1250 J Kg-1 near the fire site, showing the potential for deep convection given an increment in low level moisture and temperature as a result of combustion.

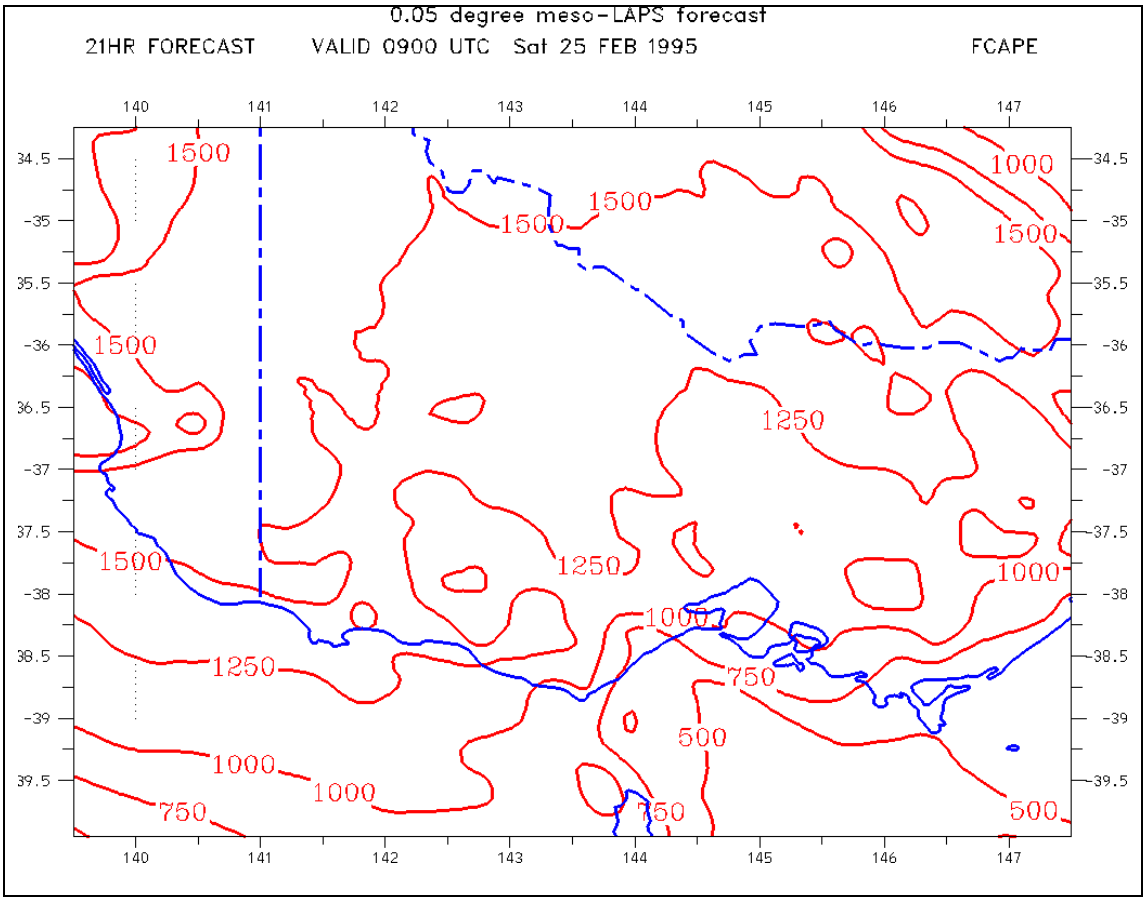

Figure A11.9. Field of "FIRE-CAPE" (J Kg^{-1}) valid at 0900 UTC 25 February 2009, calculated from the 22-hour 0.05° NWP hindcast.

The cross-section in Fig. A11.7 also shows a zone of raised isentropes (cooler air) in the mid-troposphere above the nose of the change (circled). This latter feature indicates a lowering of the mid-level stability in this region, which may also have further facilitated the development of the pyrocumulus cloud. Leggett (1996) described the involuted upper-tropospheric flow pattern that was present during this event, and Fig. A11.10 shows the 250 hPa height/wind field at 0000 and 0900 UTC from the coarse-mesh (0.2o) hindcast. At 0000 UTC there is an anticyclonic circulation in the western Tasman Sea, and a cut-off low over north-eastern SA. Between the two is an anticyclonically-curved northerly jet streak extending from western NSW southwards along the SA/Vic border. By 0900 UTC this jet had moved eastwards and was located over Berringa. Furthermore, the winds are decelerating to the north of that location (barbs directed to higher heights), and accelerating south of that latitude (barbs directed towards lower heights) leading to a focussed mesoscale divergence area almost exactly over the fire location, leading to deeper ascent and a reduction in the stability of the middle troposphere there.

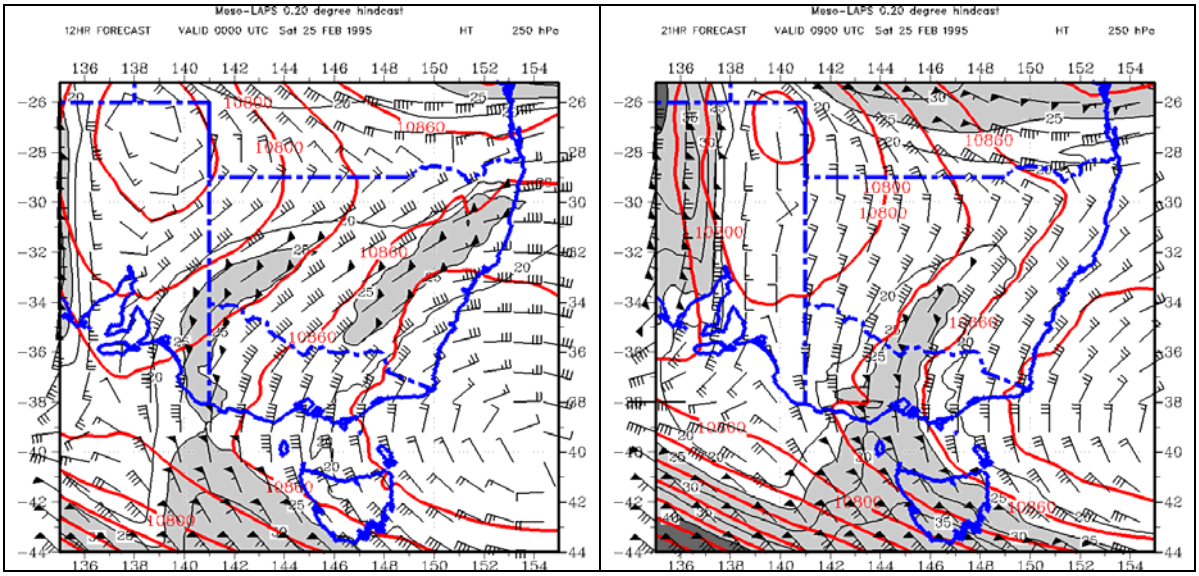

Figure A11.10. Fields of 300 hPa geopotential height (red contours) and wind barbs from the 0.20° forecast at 0000 and 0900 UTC 25 February 1995. Shaded areas show wind speeds greater than 25 m s^{-1}.

In conclusion, there are a number of factors that all contributed to a favourable environment for a pyrocumulus development on the evening of 25 February 1995. First, following the wind change at Berringa the fire moved into a heavier fuel area, providing a supply of heat and moisture to the atmosphere. Second, associated with the cool change was a zone of low-level convergence and vertical motion that may have provided a lifting mechanism to trigger convective development, the lower troposphere was extremely unstable, and the upper-level jet dynamics were such that a local enhancement of the atmospheric instability in the mid to upper-troposphere moved over the fire area at the same time. Thus many of the meteorological ingredients for deep convective development were present, with the extreme dryness of the lower levels being the missing meteorological ingredient, and the examples in Fig. A11.9 show that the fire may well have provided this moisture. It is an intriguing thought that the very dryness of the lower atmosphere enhanced the fire activity, which provided the moisture that fed the pyrocumulus cloud. The more complex modulation of convective mode under conditions of varying vertical wind shear profiles described by Kiefer et al. (2009) may also be relevant in this case.

C-HAINES was extraordinarily high during the initial fire spread, but also remained very high after the FFDI decreased following the arrival of the cool change. This was the period during which the majority of the area was burnt.

It still remains to be demonstrated that pyrocumulus-induced circulations drove the major fire spread into the Enfield State Forest. The effects of the fire in penetrating the frontal inversion may well mean that local atmospheric conditions were different to those observed at the AWS documented in Leggett (1996) and Tolhurst and Chatto (1999).

C-HAINES forecasts may well have provided an alert of fire weather conditions not represented by the FFDI.

A.12 The Mt Cooke Fire of 9-10 January 2003

Mt Cooke (560 m above sea level) is in the Darling Ranges, some 40 km south-east of Perth**.** This fire was ignited by a lightning strike on the evening of 9 January 2003 and developed overnight in steep and inaccessible terrain, attaining a size of about 30 ha by 0800 WST on 10 January. After that time fire behaviour increased markedly and the fire ran in a south-easterly direction throughout 10 January with minimal effect of suppression. The run of the fire was finally halted around 0500 WST on 11 January when it encountered an area burnt 5 years previously where surface fuels and bark were considerably reduced. A photo of a pyrocumulus cloud over the fire, from some 30 km to the north-west of the point of origin (courtesy Klaus Braun, ICS Group) is shown in Fig. A12.1.

Figure A12.1. Photo of the pyrocumulus over the Mt Cooke fire, taken from some 33km north-west at about 1400 WST 10 January 2003 (courtesy Klaus Braun).

The scatter plot of 0600 UTC FFDI and C-HAINES at the Perth gridpoint (point 3 in Fig. 1) is shown in Figure A12.2, with the points for 9 and 10 January 2003 highlighted, while Fig. A12.3 shows the time-series of these values from 0600 UTC 6 to 0600 UTC 12 January 2003. On the ignition day (9 January) both C-HAINES and FFDI were very high, though statistically C-HAINES was more extreme, but on the 10th the C-HAINES was below its 95th percentile, but the FFDI was one of the highest in the record.

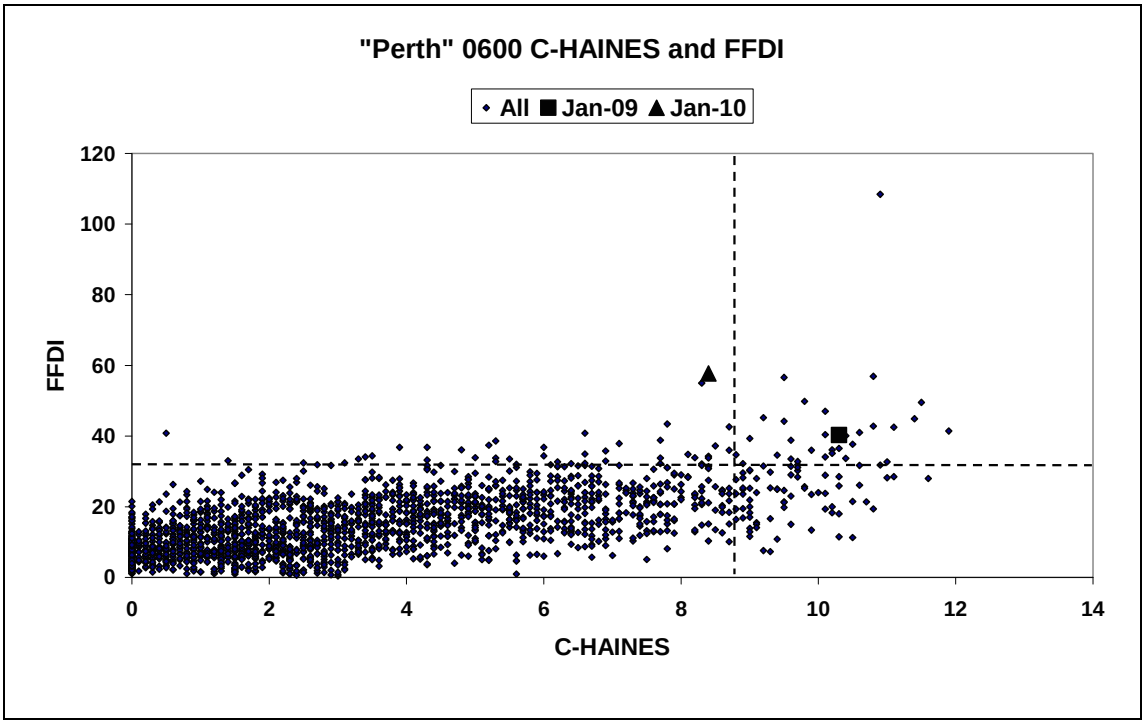

Figure A12.2. Scatterplot of FFDI vs C-HAINES for the "Perth" gridpoint at 0600 UTC for the 8-year climatology in this report. The lines show the 95th percentile values of C-HAINES and FFDI respectively. The highlighted points show the values for 9 and 10 January 2003

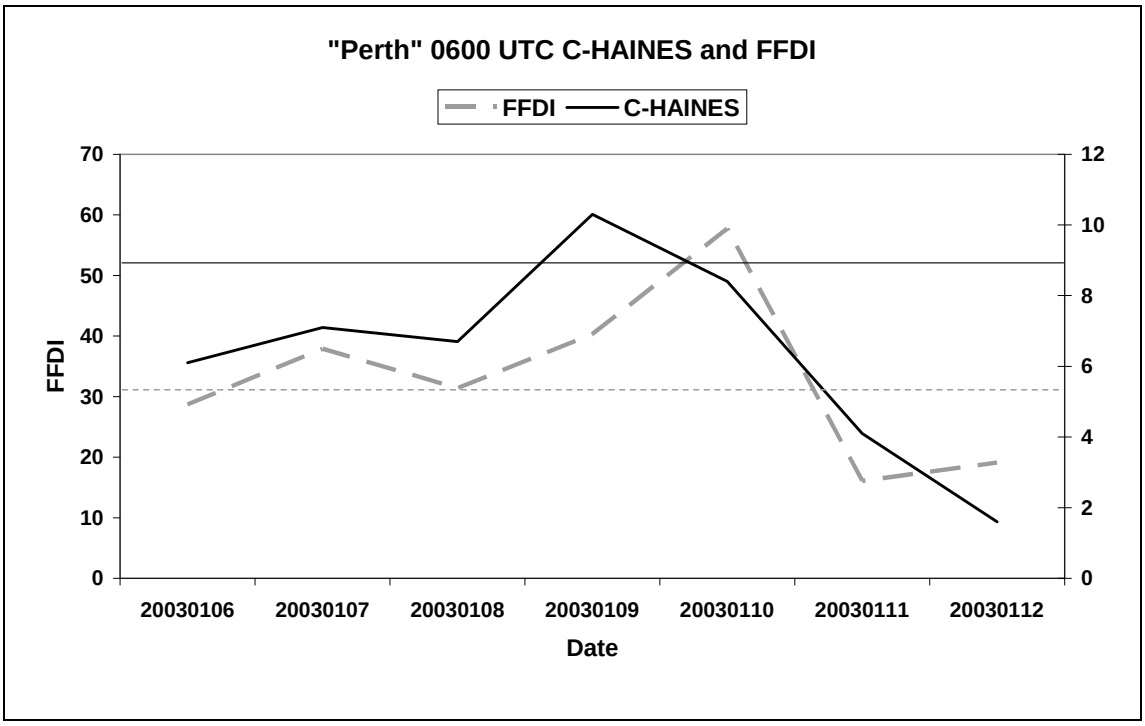

Figure A12.3 Time series of daily FFDI (dashed) and 0600 UTC C-HAINES (solid) from 6 to 12 January 2003 at the "Perth" gridpoint. The horizontal lines indicate the 95th percentile values for the two parameters.

Looking in more detail at the period leading into the fire, Fig. A12.4 shows the 6-hourly time-series of C-HAINES from 1200 UTC 6 January to 1200 UTC 11 January. Values are quite high

until 1200 UTC 8 January, but then increase rapidly and essentially remain above 10.0 (98th percentile value is 9.9) until 0000 UTC 10 January, after which values decline.

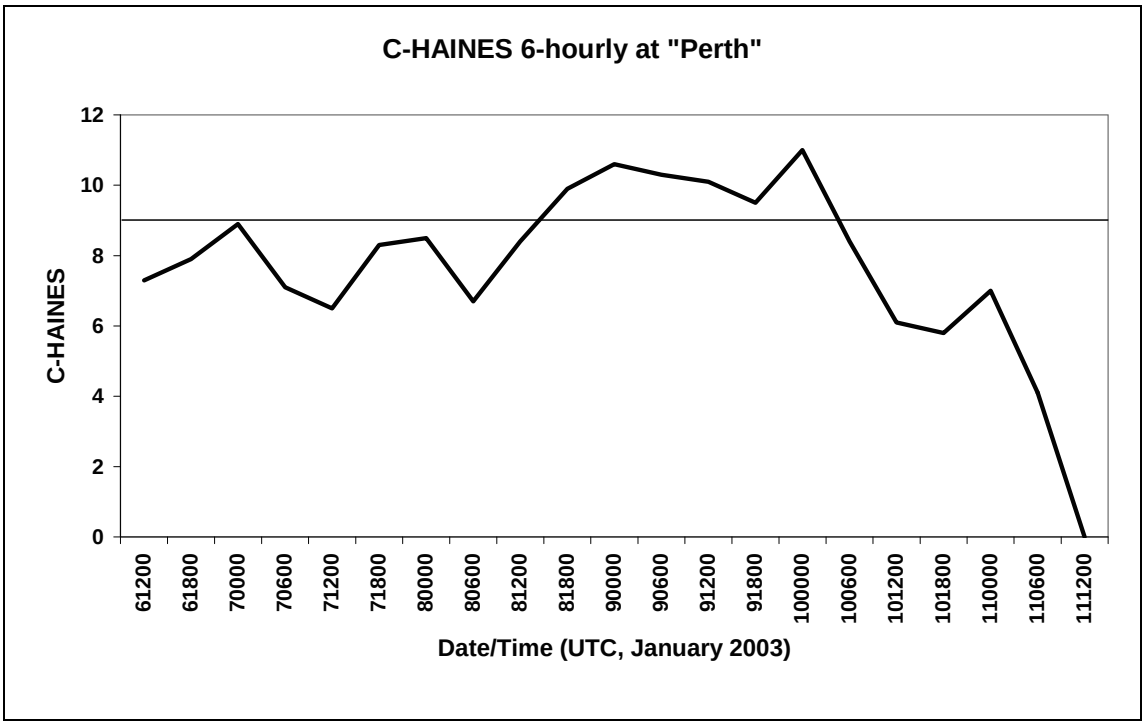

Figure A12.4 Time series from 0600 UTC 6 January to 1200 UTC 11 January 2003 of 6-hourly C-HAINES from the LAPS analyses at the "Perth" gridpoint. The horizontal line shows the 0600 UTC 95th percentile value.

Figures A12.5 and A12.6 show meteograms of AWS observations from Bickley (in the Darling Ranges) and Perth Airport (on the Swan coastal plain a few kilometres west of the escarpment), for the same period as the C-HAINES time series in Fig. A12.4. At both locations there is a sustained period of low humidity coinciding with the period of highest C-HAINES, and in particular both overnight on the 8th and overnight on the 9th there was only weak relative humidity recovery, suggesting that fine fuel moisture would have been very low (<5% o.d.w) on both the ignition day and the second day, when there was major fire activity. These lower than usual overnight relative humidities were partly due to the higher overnight temperatures experienced. In addition, on both these nights wind speeds of above 10 knots at both stations persisted through the night, so after ignition on the 9th, the overnight period was characterised by moderate winds and extremely low relative humidity.

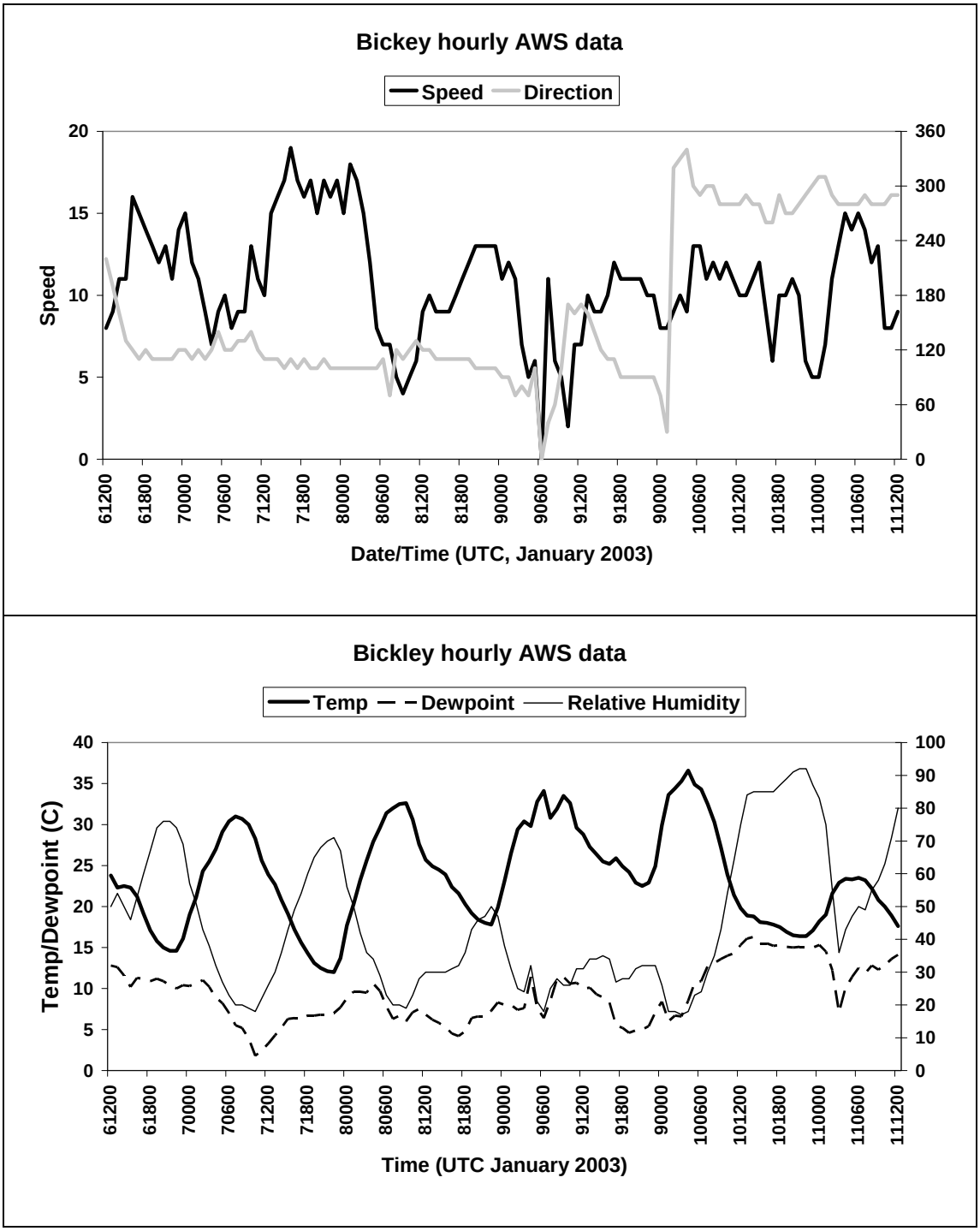

Figure A12.5. Time-series of AWS observations from the Bickley AWS for the period 1200 UTC 6 January to 1200 UTC 11 January 2003. Upper panel shows wind speed (knots, black) and wind direction (grey, degrees). Lower panel shows temperature and dewpoint (C), and relative humidity (%).

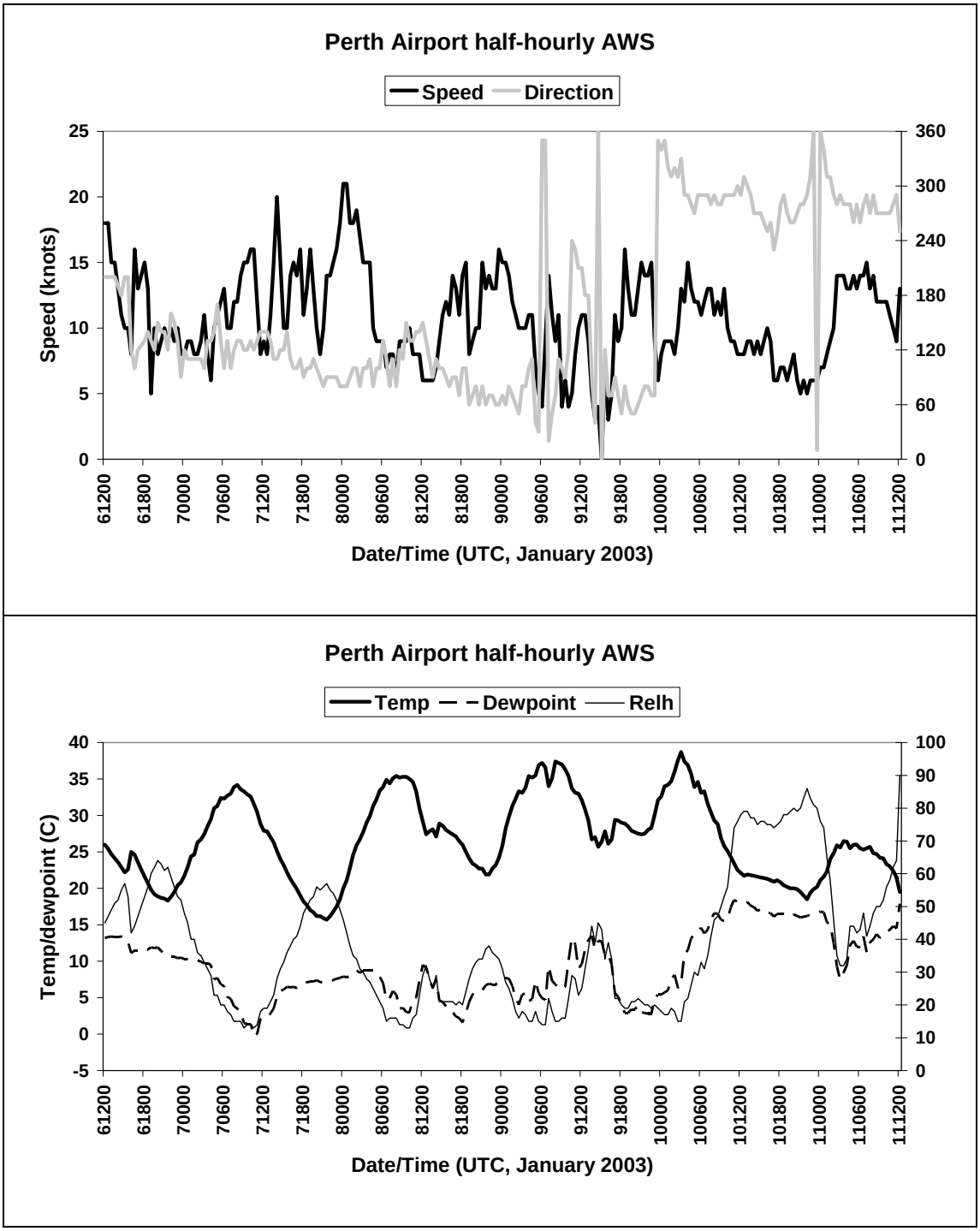

Figure A12.6. Time-series of AWS observations from Perth Airport for the period 1200 UTC 6 January to 1200 UTC 11 January 2003. Upper panel shows wind speed (knots, black) and wind direction (grey, degrees). Lower panel shows temperature and dewpoint (C), and relative humidity (%).

Figure A12.7 shows the C-HAINES fields over WA for the ignition day, overnight, and on the day of the fire activity on 10 January, with the MSLP and wind fields at the same time for comparison. A large area of very high C-HAINES is present through this period, with high values extending west of the axis of the surface trough/change, but decreasing from the west as the trough moves inland. The eastward movement of the wind change can be compared with the change of wind direction from north-easterly to west-north-westerly at both Perth and Bickley on the morning of 10 January. The fact that this change had moved through the fire area before the photo shown in Fig. A12.1 was taken suggests that the fire was interacting with a layer of air

considerably deeper than that represented by the post-frontal air, as temperatures decreased and humidities increased at these stations after the passage of the change.

Finally, Fig. A12.8 shows the temperature lapse and dewpoint depression ingredient fields that contribute to the C-HAINES. The lapse field is very broad, but largely aligned with the warm side of the trough. The humidity pattern shows a large area of very dry air aligned with the region of steeper lapse rate, but there is also an axis of drier air extending from the north-north-west over Carnarvon and southwards along the coast.

The FFDI was extra-ordinarily high before the change on the day of pyrocumulus development.

The pyrocumulus development occurred in a period of declining FFDI following a trough passage/wind change, but during which C-HAINES remained high.

C-HAINES peaks before the FFDI peaks.

A period of very high C-HAINES coincides with a period of low overnight relative humidity recovery, and also a period of active overnight fire behaviour.

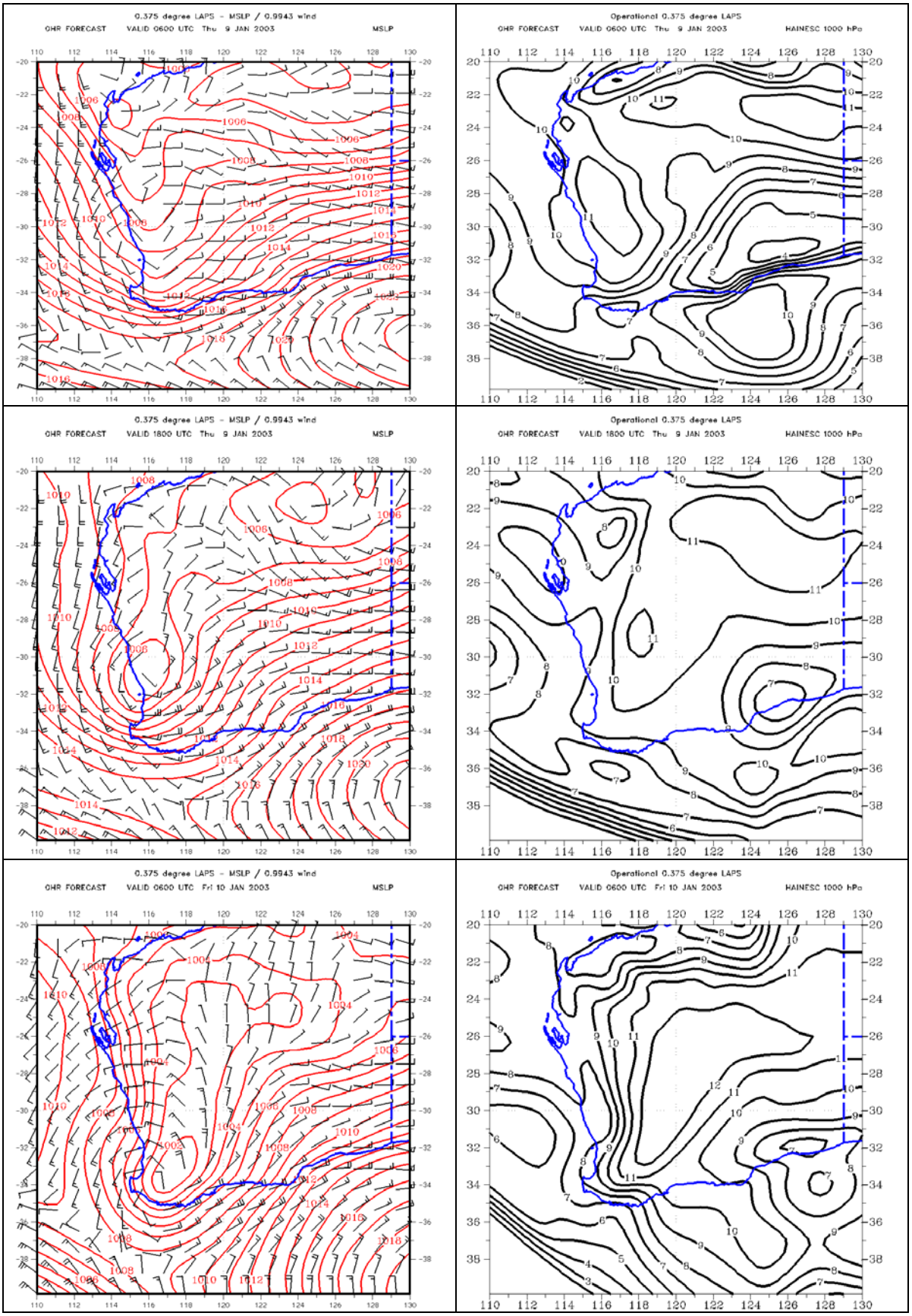

Figure A12.7. LAPS analysis fields of MSLP overlaid with 70m wind barbs (left) and C-HAINES (right), for 0600 and 1800 UTC 9,, and 0600 UTC 10 January 2003.

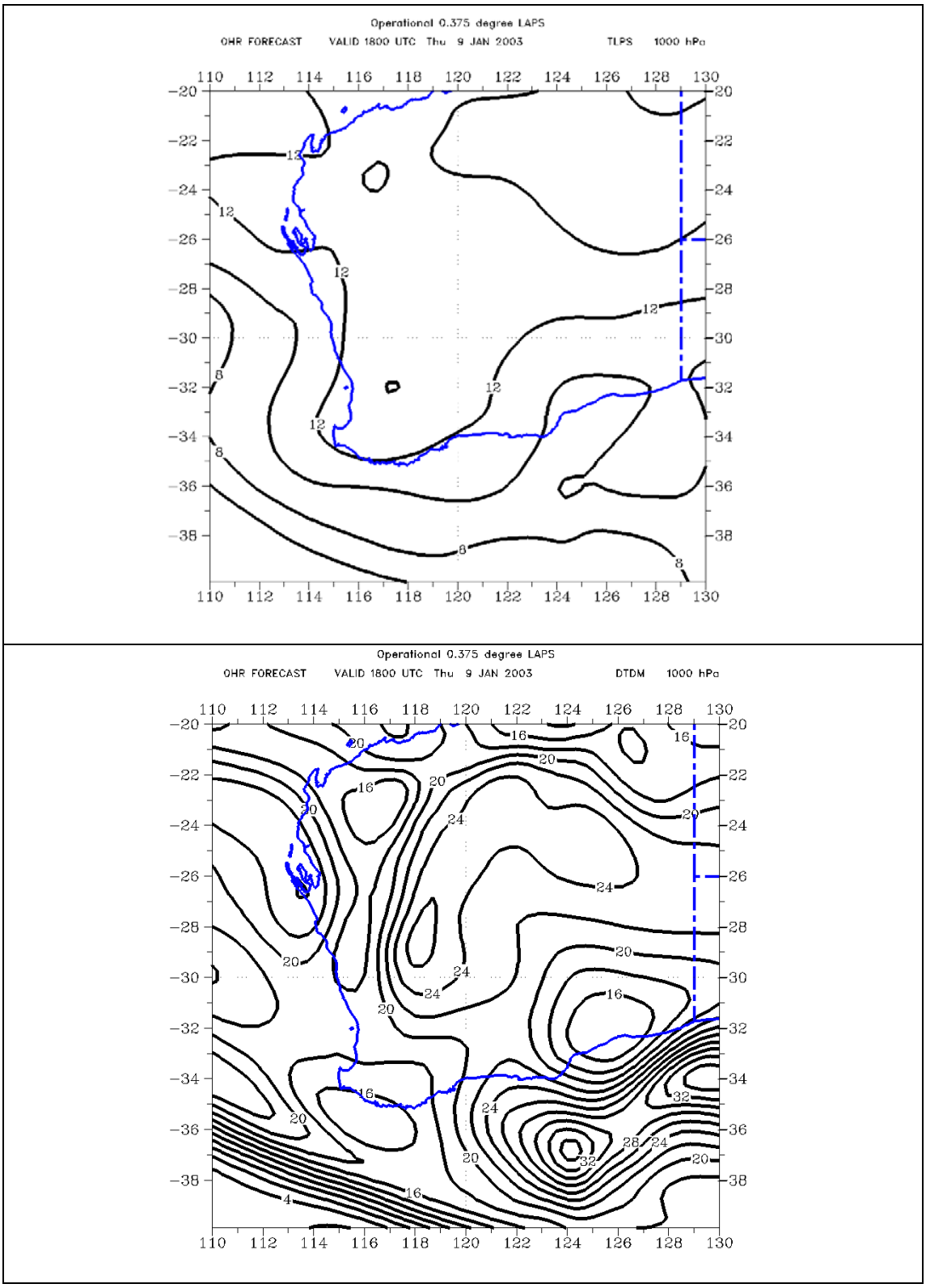

Figure A12.8. Fields of 850-700 hPa temperature lapse (K) and 850 hPa dewpoint depression from the LAPS objective analyses at 1800 UTC 9 January 2009.

A.13 Cobaw State Forest Prescribed Burn

OUT-OF-CONTROL BUSH BURN-OFF THREATENS HOMES

By Andra Jackson
April 8 2003

The CFA was monitoring a forest fire last night after a planned burn-off went wrong and became a 1000-hectare blaze, earlier coming as close as 200 metres to homes.

The fire in the Cobaw state forest between Kyneton and Kilmore, 60 kilometres north of Melbourne, was started on Friday night. The Department of Sustainability and Environment had planned to burn 600 hectares, CFA spokesman Ian Major said, but a hot northerly yesterday blew it out of control.

By yesterday afternoon the fire had consumed an extra 400 hectares and had spread to private land, Mr Major said.

The CFA took control of fighting the fire once it reached private land, sending in 300 CFA and Department of Sustainability and Environment firefighters, 75 tankers and seven planes. A northerly wind pushed the fire south. It jumped the Kyneton-Lancefield Road near Twin Bridges, at one stage forcing its closure.

The strong northerly carried smoke as far as Melbourne.
Residents in scattered housing close to Croziers Road off the Kyneton-Lancefield Road were told to watch out for flying embers and to put their fire protection plans into operation.

Last night the fire was still burning in the forest and casting embers 200 to 250 metres ahead. It had been brought within containment lines but was still not under control, Mr Major said.

CFA units were to stay on the job in case the wind picked up.

Department of Sustainability and Environment chief fire officer Gary Morgan said "no one is to blame" and residents who had suffered losses might be able to claim compensation.

The fire has angered residents. Chris Litchfield, who manages the Cobaw Country House bed and breakfast, said it was too early to be burning off. "It's foolish, to say the least," she said. "People are angry about it. The Cobaw forest has never been so dry in white history."

Alan Cooper, of the Cobaw Ridge Winery, complained about a "lack of communication" with residents. with AAP

This story was found at: ***http://www.theage.com.au/articles/2003/04/07/1049567621691.html***

The text box heading this case study comes from The Age report of a prescribed burn ignited in 6 April 2003, which spread rapidly under worsening fire weather conditions during 7 April. Not mentioned in this web-page were reports at the time that the fire flared up overnight, breaking containment during this time, and this exacerbated difficulty of control when conditions worsened on the 7th.

The scatterplot of 0600 UTC FFDI and C-HAINES for a point just north of point 19 in Fig. 1 (Fig. A13.1) does not indicate that 6 April was particularly statistically extreme, but does show that conditions were considerably more extreme on the 7th, with the FFDI approaching its 95th percentile, and the C-HAINES being above that percentile value, although as not as notably as for many of the other case studies in this report. However, the significance of these values is greater

when the time of year is considered: in the 8-year data set, FFDI only exceeded the 7 April 2003 value on 4 occasions in April, while the C-HAINES value of 10.1 was the highest April value.

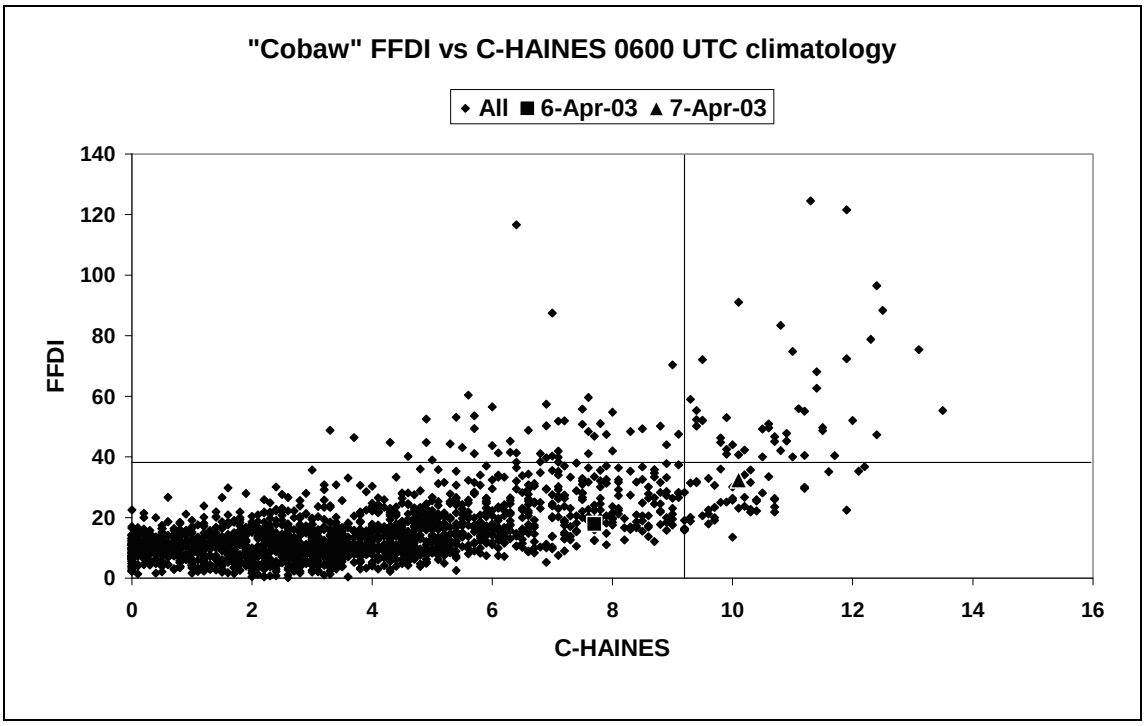

Figure A13.1. Scatterplot of FFDI vs C-HAINES for the "Cobaw" gridpoint at 0600 UTC for the 8-year climatology in this report. The lines show the 95th percentile values of C-HAINES and FFDI respectively, and the highlighted points are those of 6 and 7 April 2003.

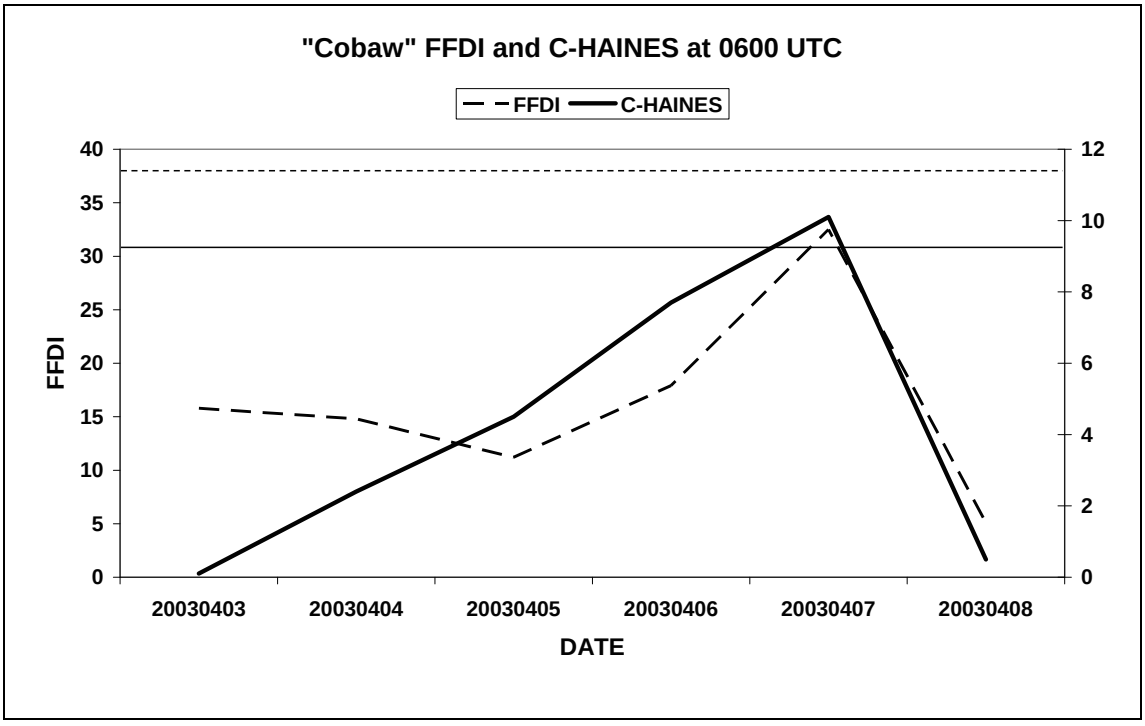

Figure A13.2. Time series of daily FFDI (dashed) and 0600 UTC C-HAINES (solid) from 3 to 8 April 2003 at the "Cobaw" gridpoint. The horizontal lines indicate the 95th percentile values for the two parameters.

Figure A13.2 shows the daily time-series of 0600 UTC C-HAINES and FFDI, and both indices peak on the afternoon of 7 April, but with the C-HAINES being statistically relatively higher than the FFDI on the afternoon of 6 April. The 6-hourly time-series (Fig. A13.3) shows the values of C-HAINES rapidly increasing after 0000 UTC on 6 April, remaining high during the overnight period, and only declining markedly after 1200 UTC 7 April.

There are no AWS data close to Cobaw Ridge and in similar terrain, so the meteograms at Melbourne Airport are shown Fig. A13.4. There is a rapid decline in dewpoint and relative humidity on the morning of 6 April, and comparing this with Fig. A13.3 it is seen that this coincides with the period when the C-HAINES increased significantly. In addition, the dewpoint continued to decline until around 0500 UTC 7 April, while overnight temperatures were higher than the previous several nights, meaning that overnight relative humidity recovery was much lower on the night of 6-7 April, coinciding with the period of unusually high C-HAINES index.

The wind speed also increased overnight on 6-7 April (lower panel of Fig. A13.4), to around 10 knots (18.5 km hr^{-1}), and then further increased during the morning to around 25 knots (~46 km hr^{-1}). (From a change-structure perspective it is interesting to note that the dewpoint increases at around the same time as the wind speed decreases, around 0500 UTC, but the temperature decrease and wind direction change occur around 0800 UTC.)

Mean-sea-level pressure and low level wind analyses, and C-HAINES fields are shown at 12-hour intervals from 0600 UTC 6 April in Fig. A13.5. At the first time a trough lying west-east through south-western Victoria extends north-westwards through central South Australia. The Victorian section of this trough initially moves south-westwards to be offshore by 1800 UTC, but then moves eastwards to bring a cool change to south-western Victoria by 0600 UTC 7 April as a southern ocean front moves eastwards south of the continent. The C-HAINES field shows a maximum extending north-westwards from north-western Victoria at 0600 UTC 6 April, and this subsequently extends southwards and then moves east ahead of the cool change.

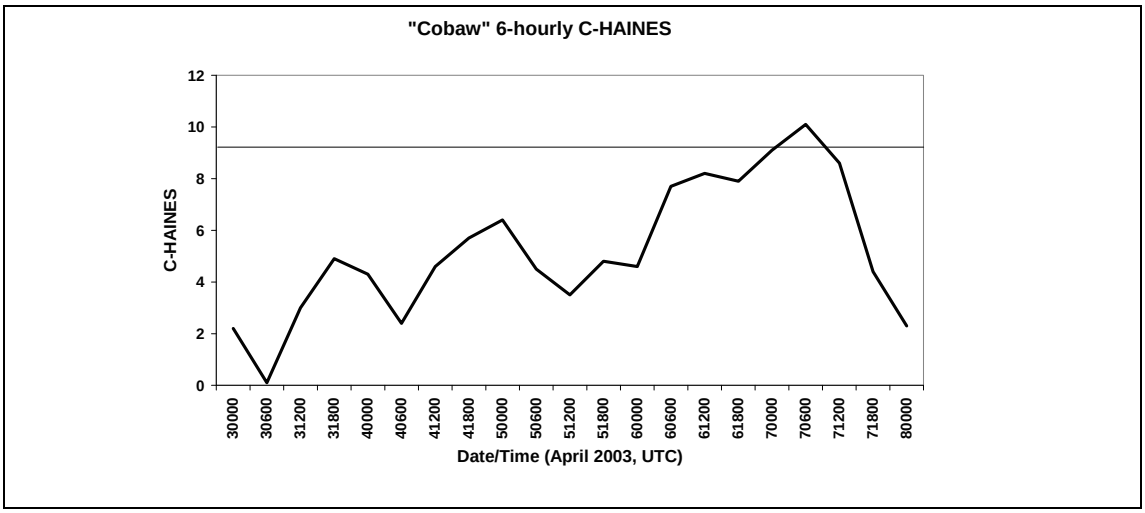

Figure A13.3. Time-series of 6-hourly C-HAINES from the "Cobaw' gridpoint from 0000 UTC 3 April to 0000 UTC 8 April 2003. The horizontal line shows the 95th percentile of the 0600 UTC C-HAINES.

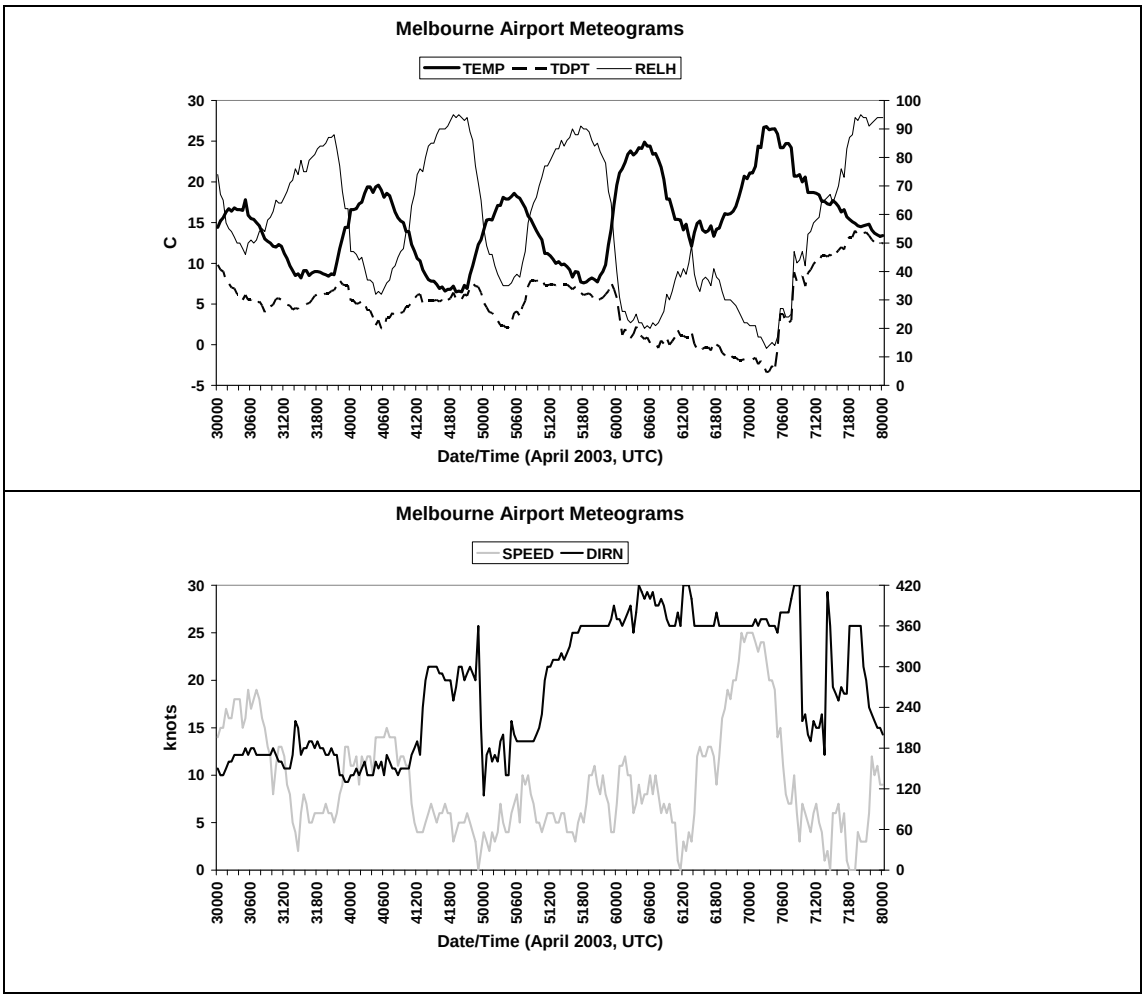

Figure A13.4. Melbourne Airport AWS observation times series from 0000 UTC 3 April to 0000 UTC 8 April 2003. Upper panel shows temperature and dewpoint (C), and relative humidity (%). Lower panel shows direction (black, degrees) and speed (grey, knots).

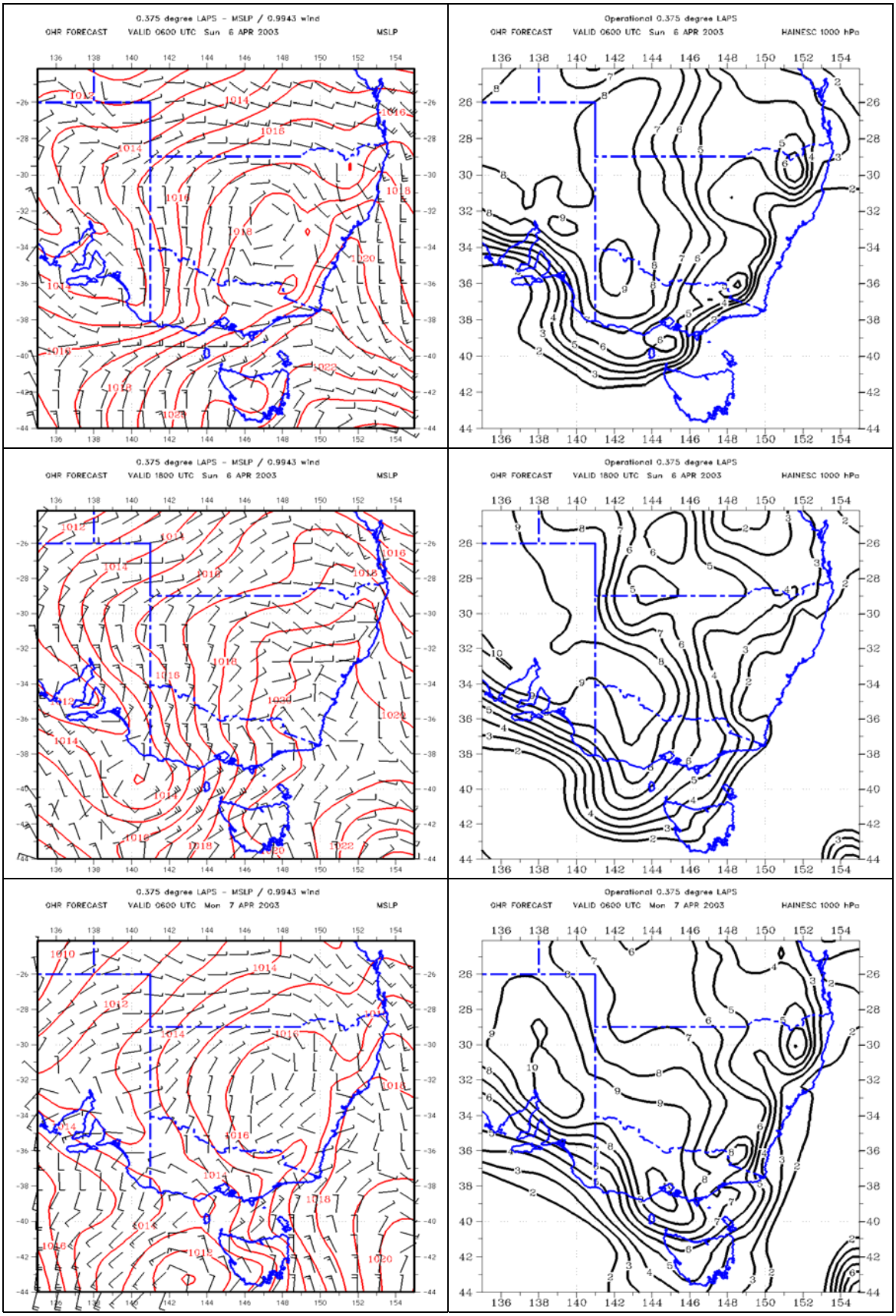

Figure A13.5. LAPS analyses of mean-sea-level pressure and overlaid 70m wind barbs (left panels) and C-HAINES (right panels). Analyses are valid at 0600 UTC (top) and 1800 UTC (middle) 6 April, and 0600 UTC 7 April 2003 (bottom).

The temperature lapse and dewpoint depression ingredients of the C-HAINES (Fig. A13.6) shows that at 0600 UTC 6 April the lapse rate maximum lies in a north-west-south-east band through South Australia and into western Victoria, while the dewpoint depression maximum is oriented north-south and extends from south-western Queensland towards the central highlands of Victoria, with the C-HAINES maximum at this time marking the overlap of these two zones. An alternative perspective of this is shown in the radiosonde soundings from Melbourne Airport at 0000 and 1200 UTC 6 April (Fig. A13.7), where it is seen that the dewpoint through the mixed layer remains around 0C, while the mixed layer becomes much deeper due to low-level warming and a small amount of low-mid level cooling.

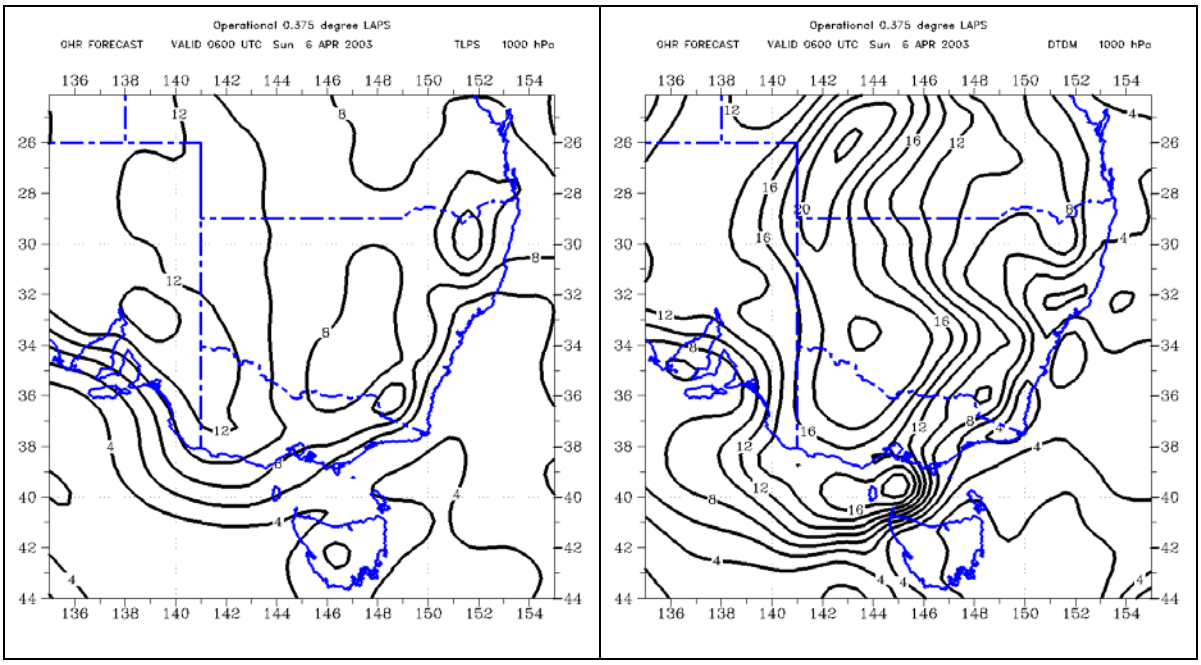

Figure A13.6. LAPS analyses of 850-700 hPa temperature lapse (left) and 850 hPa dewpoint depression (right) at 0600 UTC 6 April 2003.

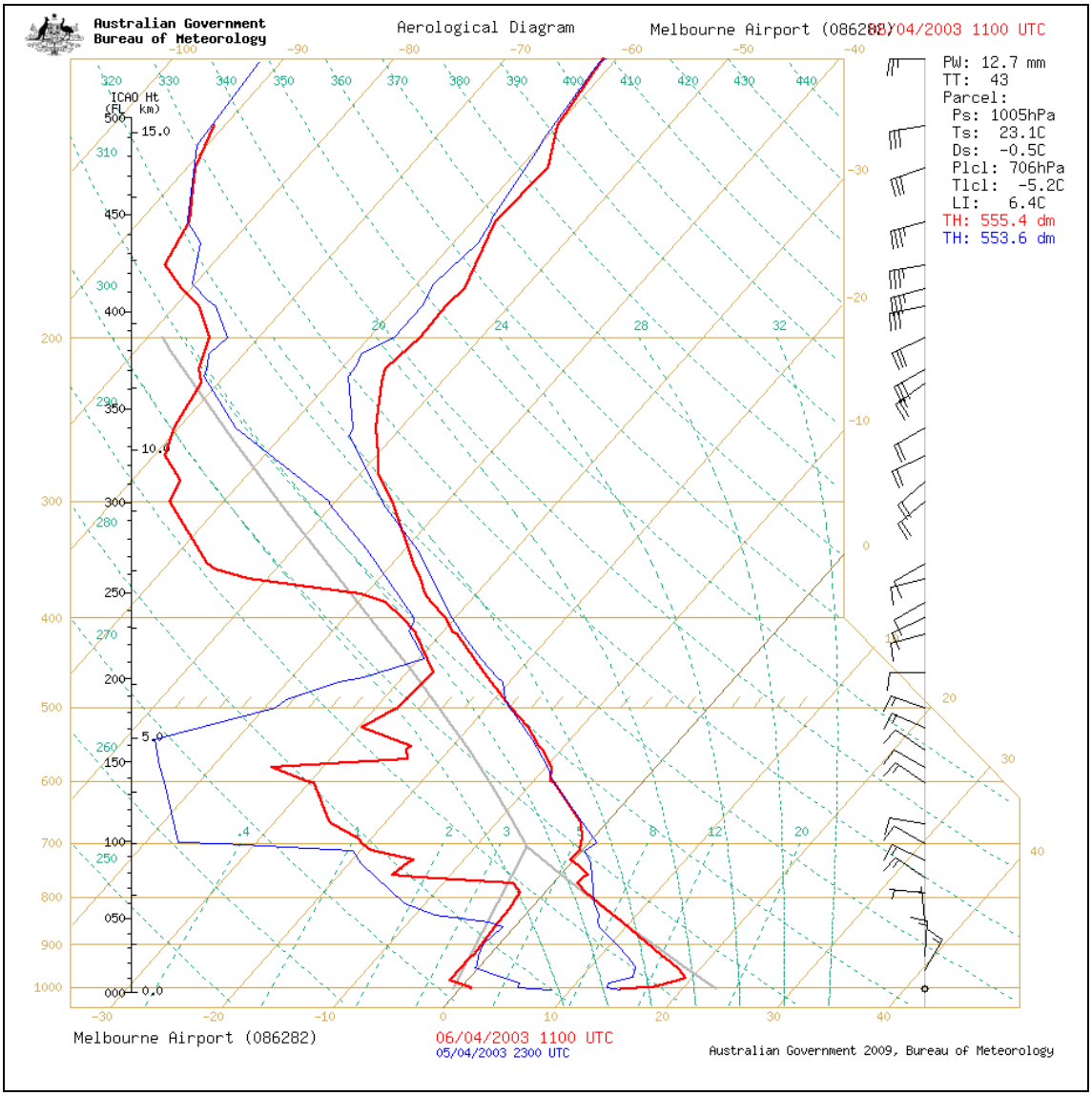

Figure A13.7. Radiosonde data from Melbourne Airport at 0000 (blue) and 1200 UTC (red) 6 April 2003.

An association between unexpected night-time fire activity, low overnight relative humidity recovery, and high values of C-HAINES is seen in this case.

On the 7th April, while FFDI was statistically extreme, particularly given the time of year, the C-HAINES was even more statistically extreme.

The cool change structure was complex, with the highest FFDI occurring 2-3 hours earlier than the wind change and temperature decrease. This was caused by a wind speed decrease and humidity increase well before the "cool change" time.

The Centre for Australian Weather and Climate Research is a partnership between CSIRO and the Bureau of Meteorology.